The Energy Consumption Mechanisms of a Power-Split Hybrid Electric Vehicle in Real-World Driving

by

Matthew A. Lintern

A Doctoral Thesis

Submitted in partial fulfilment of the requirements
for the award of
Doctor of Philosophy of Loughborough University

June 2015

In memory of my grandma

Abstract

With increasing costs of fossil fuels and intensified environmental awareness, low carbon vehicles, including hybrid electric vehicles (HEVs), are becoming more popular for car buyers due to their lower running costs. HEVs are sensitive to the driving conditions under which they are used however, and real-world driving can be very different to the legislative test cycles. On the road there are higher speeds, faster accelerations and more changes in speed, plus additional factors that are not taken into account in laboratory tests, all leading to poorer fuel economy. Future trends in the automotive industry are predicted to include a large focus on increased hybridisation of passenger cars in the coming years, so this is an important current research area. The aims of this project were to determine the energy consumption of a HEV in real-world driving, and investigate the differences in this compared to other standard drive cycles, and also compared to testing in laboratory conditions.

A second generation Toyota Prius equipped with a GPS (Global Positioning System) data logging system collected driving data while in use by Loughborough University Security over a period of 9 months. The journey data was used for the development of a drive cycle, the Loughborough University Urban Drive Cycle 2 (LUUDC2), representing urban driving around the university campus and local town roads. It will also have a likeness to other similar driving routines.

Vehicle testing was carried out on a chassis dynamometer on the real-world LUUDC2 and other existing drive cycles for comparison, including ECE-15, UDDS (Urban Dynamometer Driving Schedule) and Artemis Urban. Comparisons were made between real-world driving test results and chassis dynamometer real-world cycle test results. Comparison was also made with a pure electric vehicle (EV) that was tested in a similar way. To verify the test results and investigate the energy consumption inside the system, a Prius model in Autonomie vehicle simulation software was used.

There were two main areas of results outcomes; the first of which was higher fuel consumption on the LUUDC2 compared to other cycles due to cycle effects, with the former having greater accelerations and a more transient speed profile. In a drive cycle acceleration effect study, for the cycle with 80% higher average acceleration than the other the difference in fuel consumption was about 32%, of which around half of this was discovered to be as a result of an increased average acceleration and deceleration rate. Compared to the standard ECE-15 urban drive cycle, fuel consumption was 20% higher on the LUUDC2.

The second main area of outcomes is the factors that give greater energy consumption in real-world driving compared to in a laboratory and in simulations being determined and quantified. There was found to be a significant difference in fuel consumption for the HEV of over a third between on-road real-world driving and chassis dynamometer testing on the developed real-world cycle. Contributors to the difference were identified and explored further to quantify their impact. Firstly, validation of the drive cycle accuracy by statistical comparison to the original dataset using acceleration magnitude distributions highlighted that the cycle could be better matched. Chassis dynamometer testing of a new refined cycle showed that this had a significant impact, contributing approximately 16% of the difference to the real-world driving, bringing this gap down to 21%. This showed how important accurate cycle production from the data set is to give a representative and meaningful output.

Road gradient was investigated as a possible contributor to the difference. The Prius was driven on repeated circuits of the campus to produce a simplified real-world driving cycle that could be directly linked with the corresponding gradients, which were obtained by surveying the land. This cycle was run on the chassis dynamometer and Autonomie was also used to simulate driving this cycle with and without its gradients. This study showed that gradient had a negligible contribution to fuel consumption of the HEV in the case of a circular route where returning to the start point.

A main factor in the difference to real-world driving was found to be the use of climate control auxiliaries with associated ambient temperature. Investigation found this element is estimated to contribute over 15% to the difference in real-world fuel consumption, by running the heater in low temperatures and the air conditioning in high temperatures. This leaves a 6% remainder made up of a collection of other small real-world factors.

Equivalent tests carried out in simulations to those carried out on the chassis dynamometer gave 20% lower fuel consumption. This is accounted for by degradation of the test vehicle at approximately 7%, and the other part by inaccuracy of the simulation model. Laboratory testing of the high voltage battery pack found it constituted around 2% of the vehicle degradation factor, plus an additional 5% due to imbalance of the battery cell voltages, on top of the 7% stated above.

From this investigation it can be concluded that the driving cycle and environment have a substantial impact of the energy use of a HEV. Therefore they could be better designed by incorporating real-world driving into the development process, for example by basing control strategies on real-world drive cycles. Vehicles would also benefit from being developed for use in a particular application to improve their fuel consumption. Alternatively, factors for each of the contributing elements of real-world driving could be included in published fuel economy figures to give prospective users more representative values.

Acknowledgements

I would like to express my appreciation to all that have made the completion of this thesis possible. Firstly I would like to thank Professor Rui Chen for offering me the opportunity of the PhD position and for all his help and constructive guidance throughout the course of this project.

I would also like to take this opportunity to thank Kathryn Taylor and Stuart Chubbock of Romax Technology for their advice and support during the project, and Kathryn additionally for her help with proof reading this document. Thank you to Steve Carroll from Cenex for the use of their software for creating drive cycles and his help and advice regarding this, and for the loan of the *Smart electric drive* for testing.

My thanks go to Steve Horner and Adrian Broster for their technical support with instrumenting the test vehicles and giving my chassis dynamometer training. Thank you to my colleagues and friends in the Aeronautical and Automotive Engineering Department that have made the last four years an enjoyable time. I would also like to thank David McCarthy from the School of Civil and Building Engineering for his assistance carrying out surveying of the university campus.

Thank you to the EPSRC (Engineering and Physical Sciences Research Council) for providing the funding for my studies and Barry James and his colleagues at

Romax Technology for their sponsorship of the project to cover the operational costs.

Special thanks go to my parents for all their continuous care and support over the years which has helped me significantly in getting to where I am today. Finally, I would like to thank my girlfriend Jo for putting up with me spending the amount of time that I have working on this PhD over the last couple of years, limiting the time we have been able to spend together, and also for proof reading this thesis.

Table of Contents

List of Tables

List of Figures

List of Abbreviations

accel	acceleration
amb.	ambient
ADVISOR	Advanced Vehicle Simulator
APRF	Advanced Powertrain Research Facility
ARTEMIS	Assessment and Reliability of Transport Emission Models and Inventory Systems
aux	auxiliaries
avg	average
BMS	battery management system
CAN	controller area network
chg.	charge
CO_2	carbon dioxide
cons.	consumption
cum.	cumulative
CS	cold start
CSV	comma-separated values
CVT	continuously variable transmission
DAQ	data acquisition
decel	deceleration
diff.	difference
disch.	discharge
dist	distance

ECU	electronic control unit
eff.	efficiency
EOT	end of test
EPA	Environmental Protection Agency (U.S.)
EU	European Union
EUDC	Extra-Urban Driving Cycle
EV	electric vehicle
E-W	east to west
FC	fuel consumption
FCRT	Fleet Carbon Reduction Tool
FTP	Federal Test Procedure
GHG	greenhouse gas
GPRS	general packet radio service
GPS	global positioning system
grad	gradient
GUI	graphical user interface
HEV	hybrid electric vehicle
HHDDT	Heavy Heavy-Duty Diesel Truck
HS	hot start
HSD	Hybrid Synergy Drive
HV	high voltage
HWFET	Highway Fuel Economy Test
ICE	internal combustion engine
inc.	increase
interp.	interpolated
inv.	inverse
IPCC	Intergovernmental Panel on Climate Change
LUUDC	Loughborough University Urban Drive Cycle
LUUDC2	Loughborough University Urban Drive Cycle 2
LU15-UDC	Loughborough University 15 mph Urban Drive Cycle
max	maximum
MG1	Motor-Generator 1
MG2	Motor-Generator 2

MPG	miles per gallon
NEC	net energy change
NEDC	New European Driving Cycle
Ni-MH	nickel-metal hydride
No	number
NREL	National Renewable Energy Laboratory
OBDII	on-board diagnostics II
ORNL	Oak Ridge National Labroratory
PCB	printed circuit board
PID	parameter identification data
PSAT	Powertrain System Analysis Toolbox
PSD	Power-Split Device
REEV	range-extended electric vehicle
R-W	real-world
SAE	Society of Automotive Engineers
SAFD	speed/acceleration frequency distribution
SFTP	Supplemental Federal Test Procedures
SI	spark ignition
SOC	state of charge
SOT	start of test
temp	temperature
THS	Toyota Hybrid System
TRAFIX	Traffic Flow Index
UDC	Urban Driving Cycle
UDDS	Urban Dynamometer Driving Schedule
US	United States (of America)
USA	United States of America
US DOE	United States Department of Energy
VSP	vehicle specific power
V-T	Velocity-Time
VVT-i	Intelligent Variable Valve Timing
2WD	2 wheel drive
4WD	4 wheel drive

w/	with
W-E	west to east
WLTP	World Harmonised Light Vehicles Test Procedure
w/o	without

Nomenclature

a	Acceleration
A_f	Frontal area
Ah	Capacity, Ampere-hours
Ah_{max}	Maximum capacity, Ampere-hours
$Ah_{initial}$	Capacity stored at the start of test, Ampere-hours
Ah_{final}	Capacity stored at the end of test, Ampere-hours
C_d	Aerodynamic drag coefficient
C_p	Specific heat capacity
CO	Carbon monoxide
CO_2	Carbon dioxide
$engmap_{cold}$	Cold engine map
$engmap_{hot}$	Hot engine map
Eff	Efficiency
$Emission_{cat}$	Catalytic converter emissions
$Emission_{eng}$	Engine emissions
Eng_{on}	Engine-on
fuelrate	Fuel flow rate
$fuelrate_{max}$	Maximum fuel flow rate
F	Force
F_{in}	Force in
F_{loss}	Loss forces
FCR_{eng}	Engine fuel carbon ratio

g	Gravitational acceleration
HC	Hydrocarbons
I	Current
I_{max}	Maximum current
I_{in}	Input current
I_{out}	Output current
J	Inertia
J_{in}	Input inertia
J_{out}	Output inertia
J_{compo}	Inertia of component(s)
J_{tx}	Inertia transferred
J_{wheel}	Wheel inertia
K_{temp}	Warm up factor
m	Mass
m_{static}	Static mass
$m_{dynamic}$	Dynamic mass
min	Minimum
No_{cells}	Number of cells
P	Power
P_{acc}	Accessories power
P_{mech}	Mechanical power
P_{loss}	Power loss
$P_{max\ dis}$	Maximum discharge power
$P_{max\ chg}$	Maximum charge power
PWM	Pulse width modulation
PWM_{eng}	Engine pulse width modulation
Q	Heat energy
$Q_{ess\ gen}$	Heat energy generated by the battery (energy storage system)
$Q_{ess\ case}$	Heat energy transferred to the battery (energy storage system) case
r_{wheel}	Wheel radius
R	Resistance
R_{int}	Internal resistance
SOC	State of charge

ΔSOC	Change in state of charge
SOC_{min}	Minimum state of charge
SOC_{max}	Maximum state of charge
SOC_{abs}	Absolute state of charge
SOC_{usb}	State of charge, relative, 0 -> 1
t	Time
t_{max}	Maximum time
t_{warmup}	Warm-up time
$t_{cooldown}$	Cool-down time
T	Torque
T_{max}	Maximum torque
$T_{max\ peak}$	Peak maximum torque
$T_{max\ cont}$	Continuous maximum torque
T_{in}	Torque input
T_{out}	Torque output
T_{loss}	Torque loss
T_{act}	Actual torque
T_{eng}	Engine torque
T_{ct}	Closed throttle torque,
T_{wot}	Wide open throttle torque
T_{brake}	Brake torque
v	Linear velocity
V	Voltage
V_{system}	System nominal voltage
V_{max}	Maximum voltage
V_{min}	Minimum voltage
V_{in}	Input voltage
V_{out}	Output voltage
V_{OC}	Open circuit voltage

Greek

α	Angle alpha
ρ	Density of air
τ_{hot}	Hot temperature
τ_{cold}	Cold temperature
$\tau_{engblock}$	Engine block temperature
τ_{cat}	Catalytic converter temperature
ω	Rotational speed
ω_{in}	Input rotational speed
ω_{out}	Output rotational speed
ω_{eng}	Engine rotational speed
ω_{idle}	Rotational speed at idle

1 Introduction

1.1 Motivation

It is widely known that oil reserves have a finite quantity of oil remaining which from the known reserves available is predicted to last another 53 years [1] if we continue at the current level of consumption. However demand for oil continues to grow from countries with growing economies, notably China and India, particularly in the transport sector [2] where over 75% of transport energy use is by road vehicles [3]. Over half of global greenhouse gas emissions (GHG) are made up of carbon dioxide from fossil fuel use [4], of which transport plays a significant part contributing 23% of world GHG emissions in 2006 [3].

There has been an increased public awareness of environmental issues and aspects such as your "carbon footprint" are common knowledge today. Coupled with this, fuel prices have increased significantly over recent years, from 82.1 pence per litre in June 2004 rising to 130.5 pence per litre in June 2014 for unleaded petrol in the UK [5]. This has meant that more people are buying more fuel efficient low carbon vehicles and there is a large focus on this in the automotive industry. One such area included in this is hybrid electric vehicles (HEVs), the most popular of which to date is the Toyota Prius. After its introduction in 1997, sales were initially slow, but following the introduction of the second generation 2004 model Prius II, sales

increased rapidly. They passed the 3 million mark in 2013, making up just over half of Toyota's total worldwide hybrid vehicle sales [6,7].

A big issue currently is that drivers are finding that their vehicles when driven in the real-world are not performing as well as the manufacturers figures quote for fuel consumption. This is a problem particularly with HEVs due to extra sensitivity of their powertrain to how they are driven [8-10].

EU fleet average CO_2 emissions targets are becoming much tighter from 130 g/km in 2015 reducing to 95 g/km in 2021 which will be phased in from 2020 [11]. This is driving car manufactures to design more fuel efficient vehicles. Predictions in the automotive industry are for an increased level of hybridisation of cars over the next 25 years [12]. Figure 1.1 shows the UK Automotive Council's automotive low carbon technology roadmap that was presented in 2013, which shows that hybrid vehicles have a significant contribution.

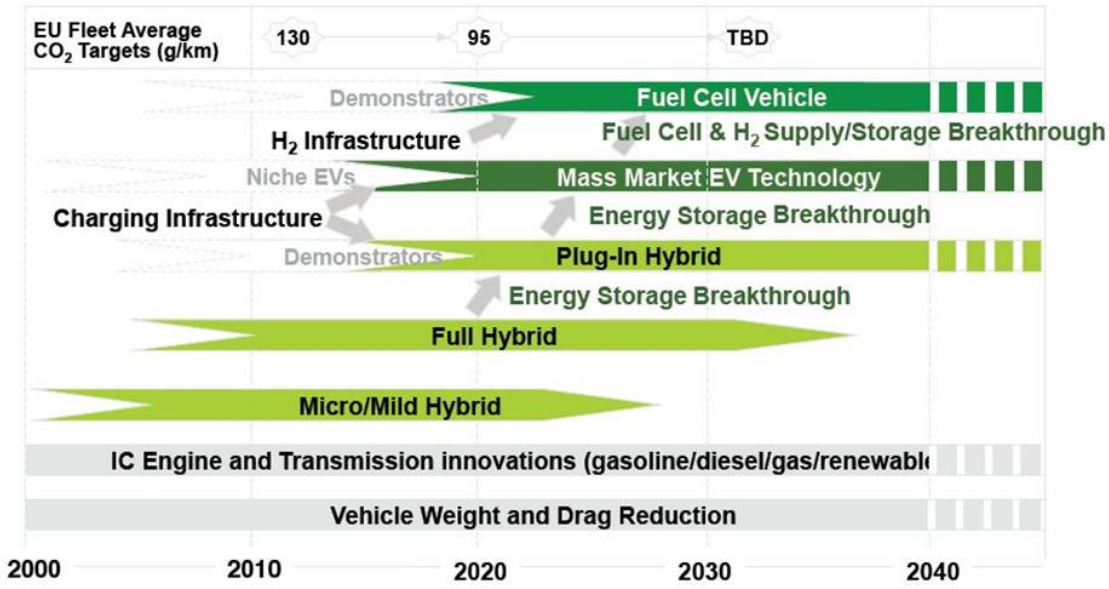

Figure 1.1: UK Automotive Council's automotive low carbon technology roadmap [12]

1.2 Aims and Objectives

This project aims to establish the energy consumption of a HEV under different driving conditions, comparing real-world driving to standard drive cycles. A real-world drive cycle is aimed to be developed to use for carrying out laboratory testing. The energy use of the powertrain of a HEV should be analysed at a component level, and the operation of the system, including:

- Storage – Hybrid vehicle high voltage battery
- Electrical – Electric machines
- Mechanical – Internal combustion engine (ICE)

The objectives of this project are to:

- Produce real-world drive cycles through data collection from a test vehicle
- Establish differences between the real-world drive cycle and the standard test cycles, for example ECE-15
- Investigate the effects of different drive cycles on HEV fuel economy
- Use a simulation model of a Toyota Prius for component level investigation
- Gain a greater understanding of the fuel efficiency of a HEV in real-world driving
- Establish and investigate factors that affect real-world energy consumption

1.3 Thesis Outline

After this introductory chapter, Chapter 2 covers a background to the research area with a review of literature in the field to set the context and provide understanding of others' work that has already been done. Chapter 2 consists of three main parts; an introduction to hybrid vehicles in 2.1, discussion of drive cycles and their development in 2.2 to 2.3, and then vehicle testing and fuel consumption with a focus on HEVs in 2.4 to 2.6.

Chapter 3 covers the methodology of all aspects this project, starting with the tools used including the test vehicles and simulation software, detailing the vehicles that were used and their instrumentation. In 3.2 the real-world use road testing is described along with the associated data processing involved. This leads into the drive cycle development process based on the data being presented. Sections 3.5 and 3.6 discuss the laboratory testing on the chassis dynamometer and the resulting data processing. The following three sections are linked, incorporating campus testing on a specific route, mapping of the gradients along this route, and merging these together to form another drive cycle. The final section of the chapter covers the high voltage hybrid traction battery testing process that was carried out as part of the investigation of some results.

Chapters 4 to 6 constitute the experimental investigations and analysis carried out in the project. Each of these is structured around one of the main contributions of this thesis. Chapter 4 investigates the effect of different drive cycles and leads into the effect of gradient on a HEV. It starts with an initial comparison of drive cycle fuel consumption results to determine the differences between different cycles and to compare results from the chassis dynamometer, simulation and real-world testing. This study highlighted all the factors to be investigated throughout the rest of the project, and emphasised that battery energy usage had to be accounted for along with the fuel consumption. Leading on from this, a more detailed drive cycle comparison is carried out with additional testing on the campus route and with an electric vehicle for comparison to the HEV. The final section brings together the

results that relate to the road gradient, and reinforces these with simulation results to determine the effect that gradient has on energy consumption of a HEV.

In Chapter 5 the drive cycle effects are studied starting with looking at how accurately the developed drive cycle statistically matches the input dataset. From this it is determined that the cycle could be better matched so a replacement is derived, and then the statistics of it are compared to those of existing standard test cycles. In the last section of the chapter, a study on how the average acceleration of a cycle affects fuel consumption is presented.

Chapter 6 details the factors that contribute to the energy consumption of a HEV. There are three parts; the first looks at how different battery initial state of charge (SOC) levels influence the fuel and battery energy use. Section 6.2 investigates differences seen between chassis dynamometer and simulation results. The simulation model accuracy and degradation of the vehicle are covered here. In the third part to the chapter, factors in real-world driving are discussed. Following on from the earlier investigation of gradients, the use of climate control auxiliaries in low and high ambient temperatures is studied, followed by a brief discussion of other small potential factors.

Finally, Chapter 7 concludes the findings of the project, with a summary of the results and suggested ways that the work could usefully be developed further.

1.4 Outline of Contributions

In summary, the key original contributions that have come from this work are as follows:

- Establishing and quantifying the key factors in the difference in fuel consumption between chassis dynamometer testing and real-world driving on the road
- Determining the effect that gradient has on the fuel consumption for a HEV by using precise elevation mapping of a specific route and a test vehicle
- Measuring the resulting improvement in fuel consumption due to rebalancing HEV battery cells through battery charge and discharge testing of all modules individually from a Prius high voltage (HV) battery pack
- Accelerations in drive cycles
    - Deriving an alternative method of calculating acceleration periods in a speed-time trace which is more-representative of the vehicles' dynamic behaviour than accelerations between time steps, for use in statistical analysis or drive cycle production
    - Using this method to produce acceleration magnitude distributions, and during the drive cycle development process matching those of the cycles to that of the driving dataset that they are derived from. From this, finding that drive cycles can more closely represent the dataset in both their statistics and energy consumption results by refining them in this way
    - Highlighting that a drive cycle should be matched in detail to the original dataset to give an output that gives accurate and meaningful results

2 Background – Literature Review

In this chapter a literature review is carried out that focusses on covering the subject areas of hybrid vehicles, drive cycles and real-world driving to give a background to the work covered.

2.1 Hybrid Vehicles

A hybrid vehicle is defined by the Society of Automotive Engineering (SAE) as "a vehicle with two or more energy storage systems both of which must provide propulsion power – either together or independently" [13]. The term is commonly used to refer to HEVs, which combine an internal combustion engine (ICE) with one or more electric machines. In this report from this point forward the use of hybrid vehicle will be with this meaning unless detailed otherwise.

Hybrid vehicles are one solution to reducing fuel consumption and CO_2 emissions of a vehicle due to several key features that are normally utilised:

- Downsized ICE due to the electric motor(s) supplementing propulsion power
- Engine operation independent of vehicle speed, so can be ran in higher efficiency operating regions, for series or power-split architecture
- Engine-off periods while stationary, during low speed driving and while coasting or braking

- Energy recovery through regenerative braking

2.1.1 Types of Hybrid Vehicle

A mild hybrid vehicle generally uses a small electric motor to provide some of the benefits of a full hybrid vehicle. Features can include auto stop-start, additional power assistance for acceleration and regenerative braking under deceleration.

A full hybrid vehicle as defined above can be one of three main configurations as follows:
Parallel Hybrid – The ICE and electric motor are connected to one transmission and can power the vehicle simultaneously, or each power source can provide power independently. The batteries are charged by a generator.

Series Hybrid – The vehicle is driven only by the electric motor which is powered by the hybrid vehicle battery, there is no mechanical connection of the ICE to the final drive. The ICE operates independently of vehicle speed to charge the battery when required. This format is now being used for vehicles referred to as range-extended electric vehicles (REEVs).

Series-Parallel Hybrid – Also called a power-split hybrid, the power output from the engine and electric motor are connected to a power split device (PSD), a planetary gear set, to provide an infinitely variable ratio of power distribution from each of the two sources. The electric motor can operate as a generator to charge the battery, using either the ICE or brake energy recuperation.

2.1.2 Hybrid Vehicle Control System

The control system is very important in a HEV as it defines the entire operating strategy of the powertrain. Key functions for example include managing when the ICE is switched on and off, the charging and discharging of the HV battery and power distribution. The control strategy is crucial in the energy use of a HEV's drivetrain. Part of the control includes a battery management system (BMS) for the battery aspects, which in the Prius has a separate ECU (electronic control unit) for this purpose as part of the electronics located in the battery pack. The control

strategy can be influenced by legislative drive cycles, which is covered further in Section 2.2.1.

2.1.3 Toyota Prius

2.1.3.1 Prius Overview

The first mass produced and most well-known hybrid vehicle is the Toyota Prius [14]. It was first introduced in Japan in 1997, followed by the USA and Europe in 2000. After the launch of the completely redesigned second generation Prius II in 2003 sales increased rapidly, hitting 1 million in 2008, 2 million in 2010 and 3 million in 2013 [6,7].

The Prius is a power-split HEV with the main components of the system including a petrol ICE, two motor-generators, a high voltage battery pack and an electrical inverter. The system is called Hybrid Synergy Drive (HSD), or THS (Toyota Hybrid System). The motor-generators can both operate in either direction hence this term. Motor-generator 1 (MG1), which is sometimes called the generator, generates electrical power to recharge the traction battery or drive motor-generator 2 (MG2), and acts as the starter motor for the ICE. MG2, which is sometimes referred to as the electric motor, provides drive to the vehicle wheels and during regenerative braking charges the battery. This is achieved through the PSD which has a planetary gear set connecting the ICE, MG1 and MG2, and adjusts the amount of torque to or from each component. The PSD removes the need for a conventional gearbox as it acts as a continuously variable transmission (CVT). The planetary carrier is connected to the ICE, the ring gear is connected to MG2 which transfers drive power to the vehicle's wheels, and the sun gear is connected to MG1 which converts engine power to electrical energy. Reduction gears reduce the high revolution speed of MG2 to transfer power to the wheels. An AC-DC inverter converts between AC current from the motor-generators and DC current from the HV battery. The arrangement of the components in the engine bay of a Prius II can be seen in Figure 2.1.

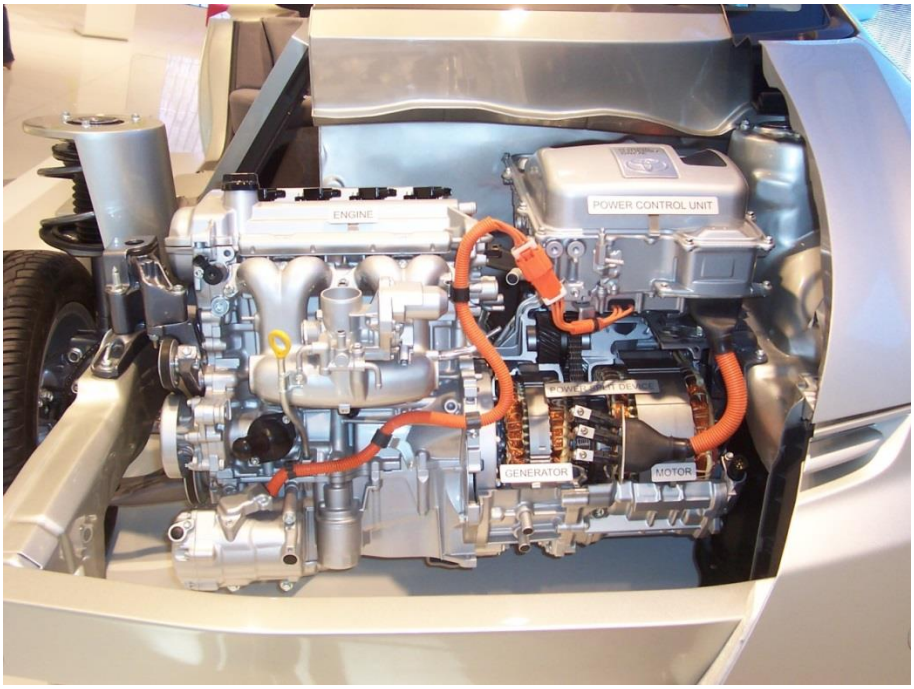

Figure 2.1: Prius II cutaway showing engine bay configuration [15]

The Prius battery cooling consists of an electric fan that draws air from the cabin across the battery pack. The battery modules have protruding features on the side faces to provide an air gap between them when stacked in the pack, and the faces are metal to transfer the heat from the surface. Testing of a Prius I battery under different temperatures on drive cycles to analyse the thermal performance found the thermal management system to perform well controlling temperatures of the pack [16].

2.1.3.2 Prius II

The ICE in the Prius II is a 1.5 litre inline 4-cylinder petrol spark ignition (SI) engine with intelligent variable valve timing (VVT-i) and operates on the high expansion Atkinson cycle. The intake valves are held open for a long period into the compression stroke allowing some of the cycle volume to be pushed back into the inlet manifold, effectively creating a reduction in engine displacement and improving fuel economy. Using the VVT-i system the engine continuously changes between running on the Atkinson cycle and the conventional Otto cycle for optimum efficiency and power when required [17].

The Prius II has a 6.5 Ah nickel-metal hydride (Ni-MH) HV battery pack consisting of 28 modules that each contain six 1.2 V cells, giving a total rated

voltage of 201.6 V. This is located under the boot floor with a BMS ECU and other associated electronics alongside. Ni-MH batteries are used due to their relatively low cost and safer charging process than lithium-ion, although they have a lower energy density. The battery is shown in Figure 2.2 with the cover removed, viewed from the rear of the car. The battery ECU has a target SOC level of 60% and usually operates within a 20% window from this, but can go beyond this to operate between 40-80% SOC [18,19]. Testing of a Prius I battery pack by Kelly et al. [20] confirmed that the battery usage was limited to 40% of its capacity. Chassis dynamometer testing on several drive cycles with different initial SOCs found the battery was forced towards a target 56% SOC for their particular car.

Figure 2.2: Prius HV battery pack in situe in the car with the cover removed

The main traction motor MG2 is a 50 kW permanent magnet motor with 400 Nm maximum torque [21]. A specification table for the Prius II can be seen in Table 2.1.

Table 2.1: Prius II specifications. Content from Toyota GB [21]

Engine	
Type	4-cylinder in-line, high expansion cycle
Valve mechanism	16-valve DOHC VVT-i
Fuel system	Electronic Fuel Injection
Fuel type	95 octane petrol (or higher)
Bore x Stroke (mm)	75.0 x 84.7
Displacement (cc)	1,497
Compression ratio	13.0:1
Max. power (bhp/rpm)	76 @ 5,000
Max. torque (Nm/rpm)	115 @ 4,000
Motor	
Type	Synchronous, permanent magnet
Rated voltage (V)	500
Max. power (bhp/rpm)	67 @1,200-1,540
Max. torque (Nm/rpm)	400 @ 0-1,200
Battery	
Type	Sealed nickel-metal hydride
Nominal voltage (V)	201.6
Modules	28 modules with 6 cells joined together
Linkage	Series
Capacity Ah (hrs)	6.5 (3h)
Hybrid Powertrain	
Type	Series-parallel
Torque transfer type	Planetary gear unit
Combined max. power (bhp/mph)	112 / more than 52mph
Combined max. torque (Nm/mph)	478 / below 22mph
Performance	
0-62mph (sec)	10.9
Max.speed (mph)	106
Fuel Consumption and Emissions	
Combined (mpg)	65.7
Extra Urban (mpg)	67.3
Urban (mpg)	56.5
Emission Compliance Level	Euro 4
CO_2 (g/km)	104

2.1.3.3 Prius Operating Modes

The Prius has five main operating modes that are used dependent on the driving conditions, as detailed below.

Acceleration from stationary and driving at low speeds – Power is generated by the electric motor, supplied by the battery. The ICE is off so that it is not running in a poor-efficiency range. Figure 2.3.

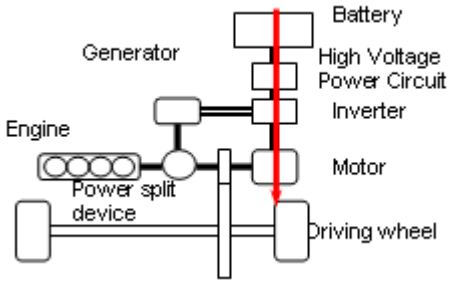

Figure 2.3: Prius operation under acceleration from stationary and at low speed [21]

Driving under normal conditions – Power is generated by the ICE and distributed by the power split device to directly drive the wheels, and also to drive the generator which drives the motor. The distribution of these power streams is controlled to give maximum efficiency at any time. Figure 2.4.

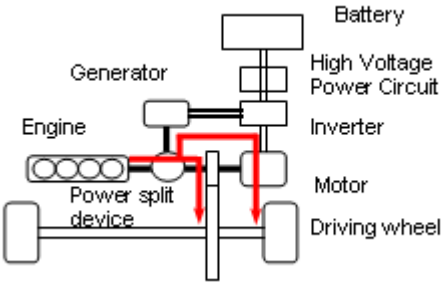

Figure 2.4: Prius operation under normal conditions [21]

Sudden acceleration – Extra power is supplied to the motor from the battery while the ICE adds drive to the motor. Figure 2.5.

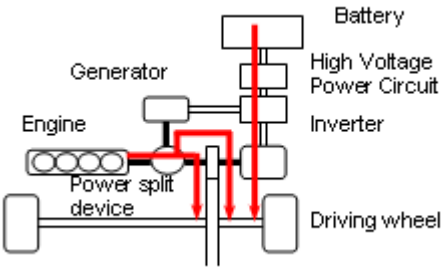

Figure 2.5: Prius operation under sudden acceleration [21]

Deceleration – The motor functions as a large capacity generator, controlling power to the wheels. Under regenerative braking, kinetic energy is recovered as electrical energy which is stored in the battery for use later. Figure 2.6.

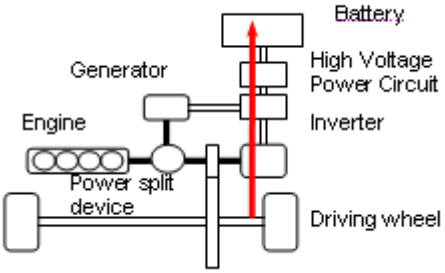

Figure 2.6: Prius operation under deceleration [21]

Battery recharging – As the battery has a target state of charge level to maintain, if the level becomes too low, power from the ICE to the generator recharges it. This can occur at the same time as other operating modes, particularly driving under normal conditions. Figure 2.7.

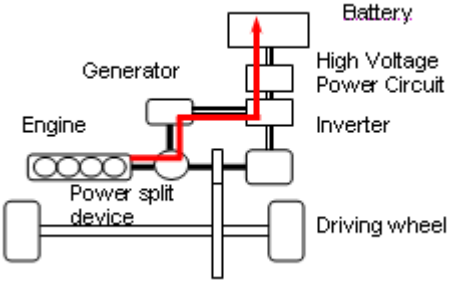

Figure 2.7: Prius operation under battery recharging [21]

2.1.3.4 Prius Developments

In the second generation Prius II significant improvements were made to the vehicle over the first generation, with many to increase efficiency. The paper from Toyota by Muta et al. [14] details the changes made in THS II. The volume and weight of the Ni-MH battery pack were reduced by approximately 15% and 25% respectively due to reduced internal resistance which leads to an improved output density. The high-voltage power circuit maximum voltage was almost doubled from 274 V to 500 V, meaning that the current required to provide a given power is halved. Using an AC synchronous permanent magnet brushless motor with the magnets arranged into a V-shape for MG2 in THS II increased the drive torque and output. With the increased voltage combined with improved motor control giving increased output in the medium-speed range, the electric motor has around 1.5 times more power output than the previous version, going from 33 kW to 50 kW. The AC synchronous MG1 is rotated at high speed to provide the required power to MG2, improvements including to the rotor strength have increased this from 6,500 to 10,000 rpm (revolutions per minute). Changes were made to engine components and engine operating strategy to improve engine efficiency. All of these improvements have helped increase acceleration performance, and reduced fuel consumption by approximately 14%. Additionally, the air conditioning compressor was changed from mechanical drive to electric drive to remove the need for the ICE to be running during low load and stationary periods. Toyota state that with taking into account air conditioning use, the fuel consumption reduction is approximately 20% on their drive cycle.

Key changes in the latest third generation Prius III included upsizing the ICE from 1.5 l to 1.8 l capacity and adding an additional reduction gear to the transmission between the ring gear and the MG2 output. The upsized engine means that the engine speed can be run lower at high cruising speeds, improving fuel consumption, which Toyota quote can be about a 10% reduction [22]. The reduction gear reduces the final drive ratio allowing a lower PSD ring gear output speed. This enables the conversion between electrical and mechanical power flow to be reduced due to the lower MG1 generator speed converting less power, therefore reducing conversion losses. The benefit is experienced particularly for high speed driving [23].

2.1.3.5 Prius Hybrid System Efficiency

Research into the efficiency of the hybrid system of the Prius II has been carried out by Staunton et al. [24] at Oak Ridge National Laboratory (ORNL) with their objectives being to characterise the electrical and mechanical performance, map the performance of the inverter to motor system over the full design speed and load ranges, determine the operating characteristics and quantify the efficiencies of the hybrid electric drive system. Vehicle level tests and subsystem level tests were carried out. To acquire electrical data all accessible power flow points were instrumented to measure voltage and current, which included between the motor-generators, inverter and battery.

Power measurements were taken against vehicle speed, and voltage boost converter response measurements were taken. Motor and generator voltage measurements against motor speed were recorded, plus hybrid drive system power loss across motor speed range measurements were taken.

The motor and inverter were removed and tested out of the vehicle with current, voltage, torque, temperatures and coolant flow measured. Findings from the research were that inverter efficiency was found to be as high as 99%, and motor efficiency was found to peak at 93-94% in the 1750-3000 rpm range at 50-150 Nm torque. Boost converter efficiency decreases as output voltage increases and was at a minimum of 96.7% when maximum boost and power is required. The inverter design was modified by the researchers then tested again and showed improvements in efficiency after the changes.

2.2 Drive Cycles

A drive cycle, or driving cycle, is a speed verses time demand that represents a driving routine, used for testing a vehicle on. They can consist of sections of acceleration or deceleration, constant speeds and stationary periods. There are many cycles available which differ greatly; these include legislative ones for vehicle certification, and non-legislative ones developed by researchers or organisations for other uses. The reason for this is due to drive cycles being specific to certain driving conditions. In some cases, in addition to their designed region they are also used in developing countries that do not have their own drive cycle [25], such as Vietnam using the New European Drive Cycle (NEDC) [26]. Drive cycles are frequently used to drive a vehicle on to take measurements, commonly fuel consumption or exhaust emissions. Drive cycles are used for certification fuel economy and emissions testing for all production vehicles in Europe and the USA.

2.2.1 Certification Cycles

As all vehicles have to go through certification tests it can lead to cars for a particular market being engineered around the relevant drive cycle in order to produce beneficial fuel consumption and CO_2 emissions figures that are published for consumers to see. Some cars are programmed for their ECUs to detect when it is being driven on a test cycle so that the engine management switches into a test mode to optimise the results. The downside of this is that the operation of a vehicle can be more suited to the synthetic driving cycle than real-world driving on the road.

There are many different drive cycles available; here the most well-known ones will be discussed, from Europe, the USA and Japan. The data used to plot Figure 2.8 to Figure 2.16 in this section were obtained from the EPA [27].

2.2.1.1 European Certification Cycles

Within Europe the New European Driving Cycle (NEDC) is used on a chassis dynamometer for legislative testing. It consists of four repeats of the ECE-15 cycle, also referred to as urban driving cycle (UDC), which represents urban fuel economy, followed by the extra-urban driving cycle (EUDC) for extra-urban fuel

economy. The NEDC gives the overall combined fuel economy. Fuel consumption is quoted for each of the two parts, and for the total combined cycle. The EU (European Union) cycles are linear synthetic cycles with constant rate accelerations and decelerations, and a large proportion of stationary time. The cycles are shown in Figure 2.8, Figure 2.9 and Figure 2.10, and a summary of the drive cycle statistics is in Table 2.2.

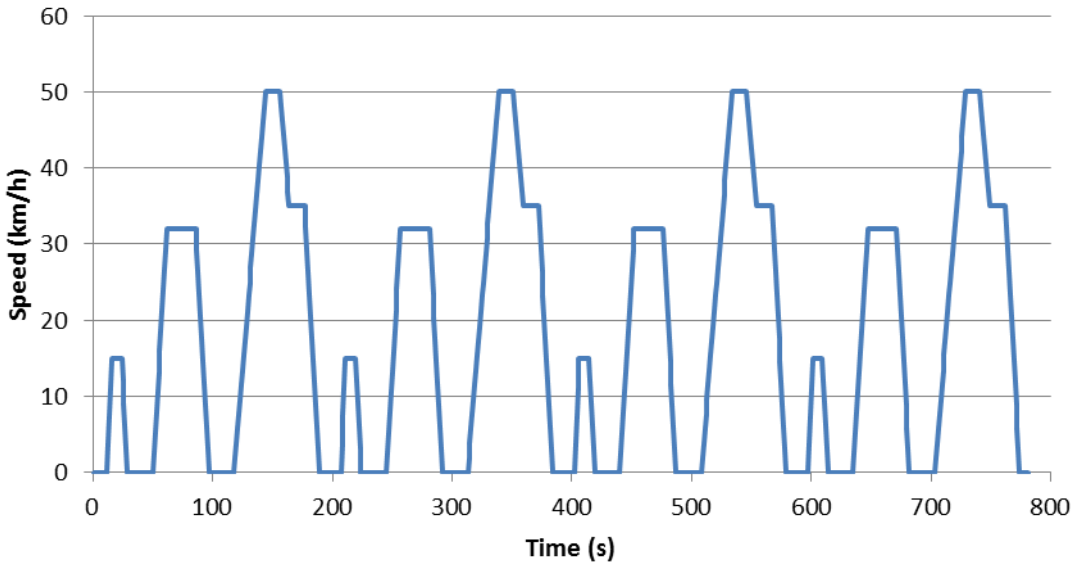

Figure 2.8: ECE-15 cycle

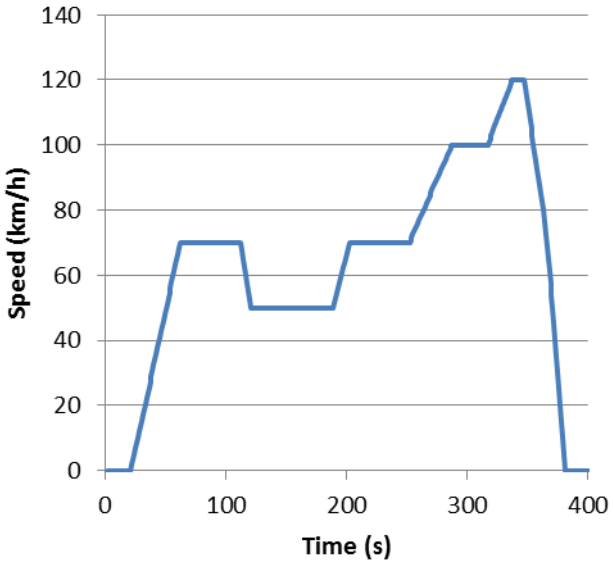

Figure 2.9: EUDC

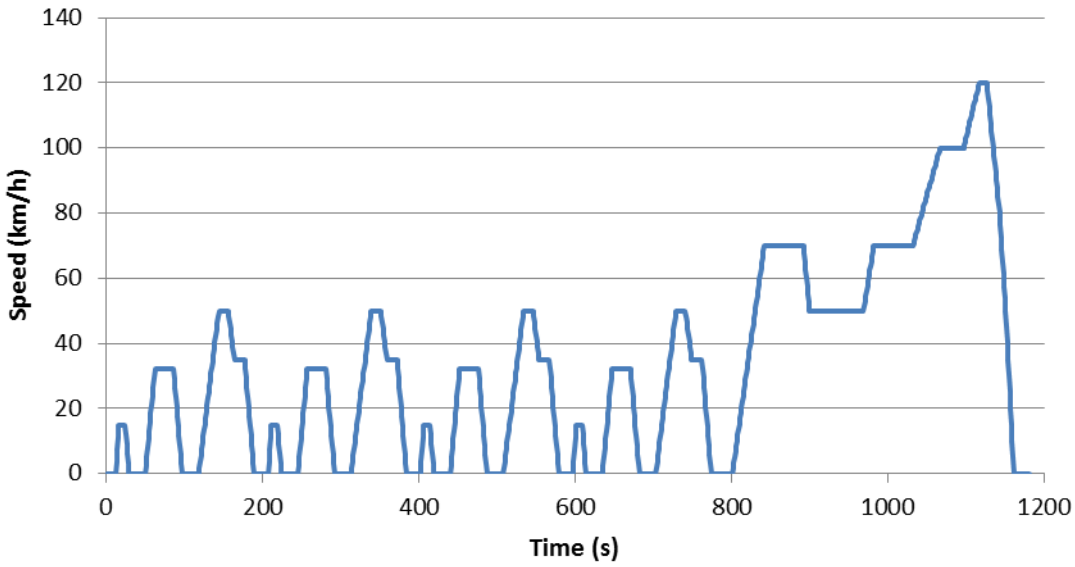

Figure 2.10: NEDC

Table 2.2: European drive cycle statistics. Data from DieselNet.com [28]

	Drive Cycle		
Statistic	**ECE-15**	**EUDC**	**NEDC**
Duration (s)	195	400	1180
Distance (km)	0.99	6.95	10.93
Idle time (s)	57	39	267
Average speed (km/h)	18.35	62.59	33.35
Maximum speed (km/h)	50	120	120
Average acceleration (m/s^2)	0.599	0.354	0.506
Maximum acceleration (m/s^2)	1.042	0.833	1.042

The style of the EU cycles leads to vehicle fuel consumption results being an inaccurate representation of real-world driving. As far back as 1978, a study by Volkswagen found that the ECE cycle was not representative of European urban driving [29]. Data was logged in several cars in different European cities, for which statistics were compared to European, US and Japanese cycles. The authors concluded that the US FTP-72 was a better match, and proposed minor changes to improve it further.

In order to have a worldwide standard and to try to overcome the inaccuracy of existing drive cycles including the NEDC, a new drive cycle is under development. This transient cycle is planned to replace the NEDC in Europe for type approval testing. The World Harmonised Light Vehicles Test Procedure (WLTP) is being developed by a United Nations group consisting of representatives from Europe, Japan and India. There are three classes of cycle to cover vehicles within different

power-to-mass ratio bands, and deviations of each cycle dependant on the vehicle's maximum speed.

2.2.1.2 US Certification Cycles

The US FTP-72, or Urban Dynamometer Driving Schedule (UDDS) is a low speed urban drive cycle. It consists of two parts, the first lasting 505 seconds, and the second lasting 867 seconds. Usually the first part is run with a cold start and the second part with a hot start. The cycle trace is shown in Figure 2.11 and the cycle statistics are in Table 2.3.

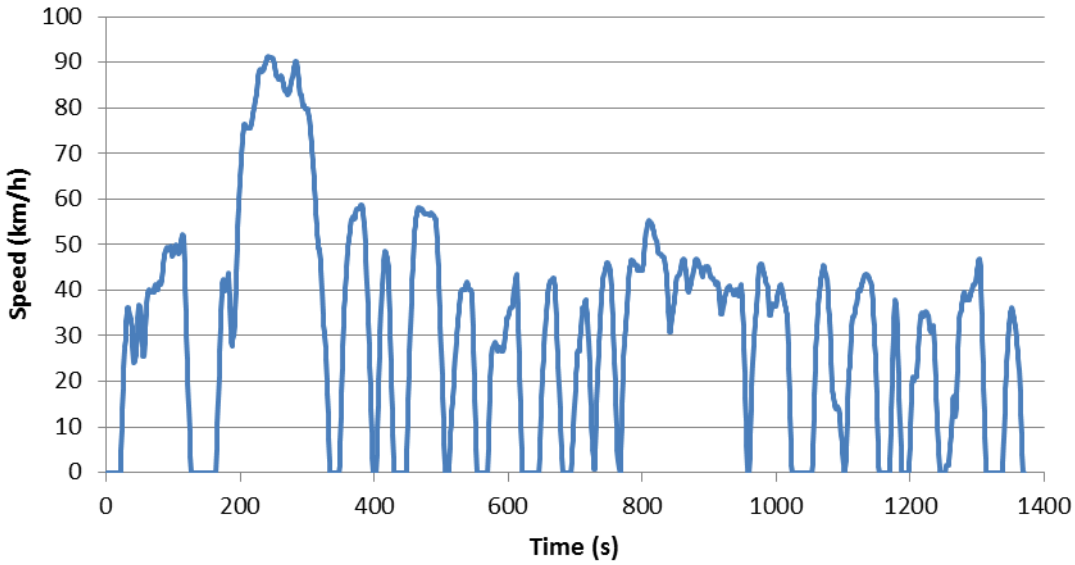

Figure 2.11: UDDS/FTP-72 cycle

The FTP-75, which is sometimes referred to just as FTP (Federal Test Procedure), is the FTP-72 cycle with an additional phase added, which is a repeat of the first 505 second section. This time it is run with a hot start after the engine is stopped for 10 minutes. The cycle is shown in Figure 2.12. The FTP-75 was used for certification testing, and from 2000 two additional Supplemental Federal Test Procedures (SFTP) were used in addition. These are the US06 (Figure 2.13) for representing high speed more aggressive driving, and the SC03 (Figure 2.14) to represent the use of air conditioning. The US cycle statistics are given in Table 2.3.

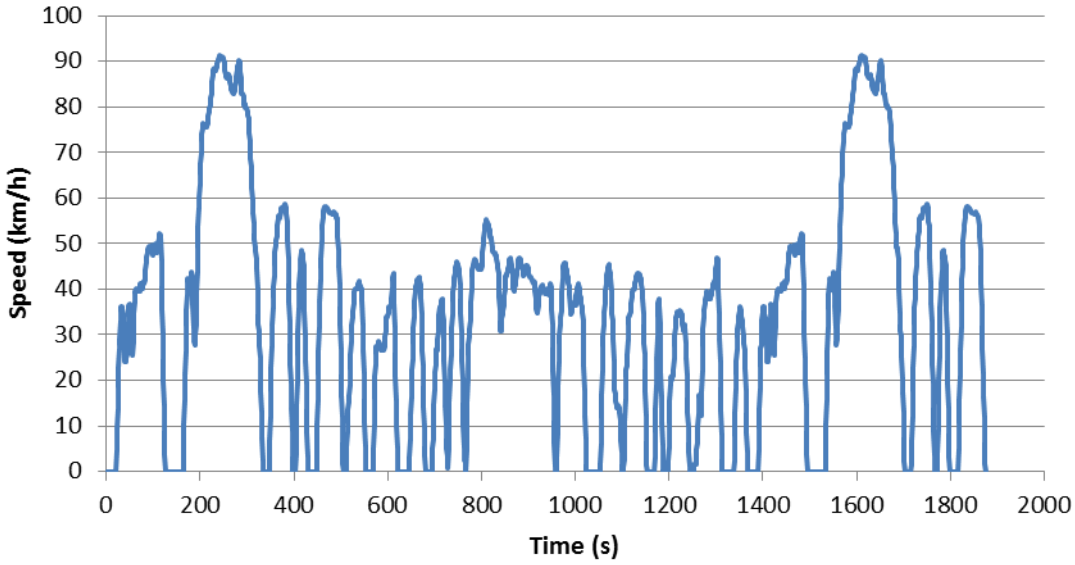

Figure 2.12: FTP-75 cycle

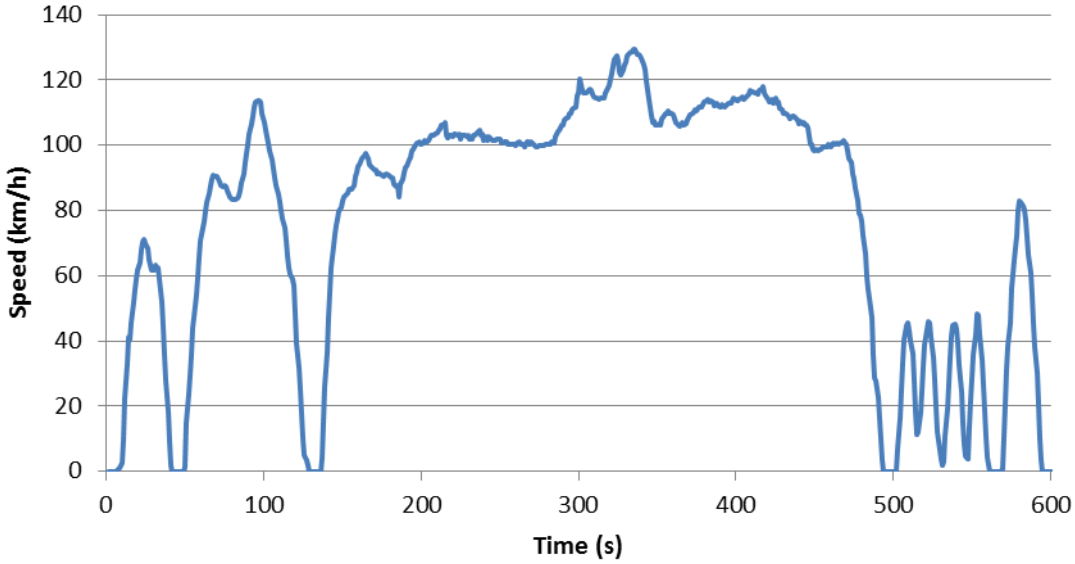

Figure 2.13: US06 cycle

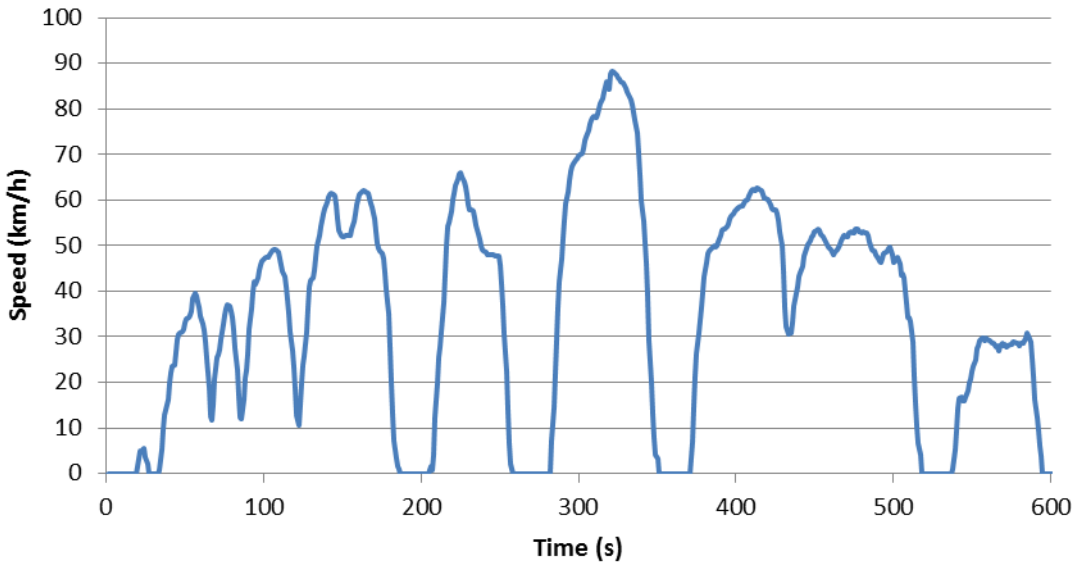

Figure 2.14: SC03 cycle

In the US, the Environmetal Protection Agency (EPA) replaced their previous fuel consumption and CO_2 emissions regulations in 2008 with a new five-cycle test procedure in order to produce results that are nearer to real-world driving [30]. The FTP is still included in this for urban driving, run at regular and low temperatures, along with the US06, SC03 and HWFET (Highway Fuel Economy Test Cycle). The HWFET, shown in Figure 2.15, is used for the highway fuel economy test.

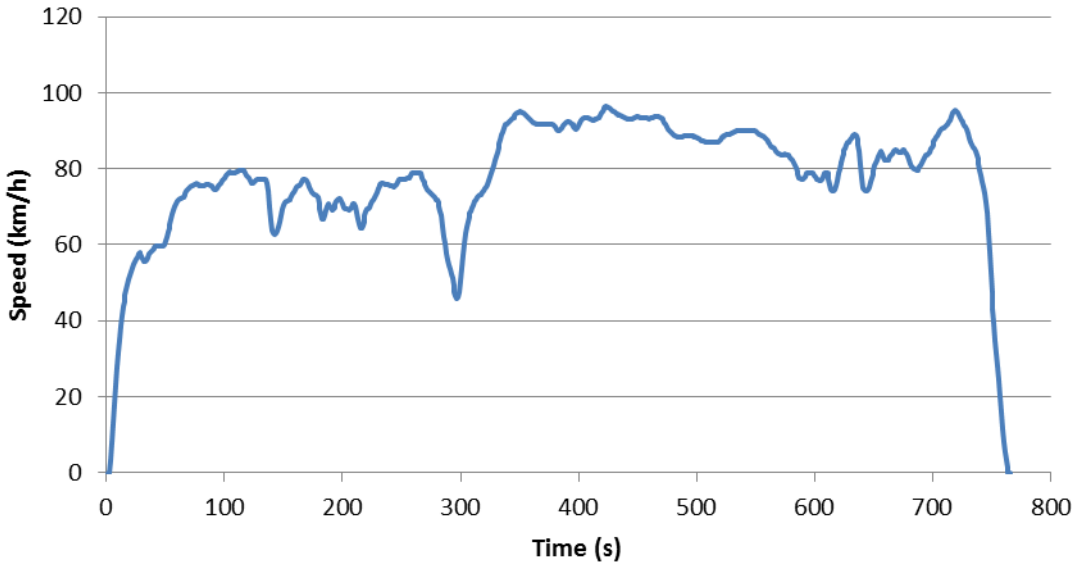

Figure 2.15: HWFET cycle

Table 2.3: US drive cycle statistics. Data from DieselNet.com [28]

	Drive Cycle				
Statistic	**UDDS**	**FTP-75**	**US06**	**SC03**	**HWFET**
Duration (s)	1372	1877	596	596	765
Distance (km)	12.07	17.77	12.80	5.80	16.45
Average speed (km/h)	31.50	34.12	77.90	34.80	77.70
Maximum speed (km/h)	91.25	91.25	129.20	88.20	96.40

2.2.1.3 Japanese Certification Cycles

In Japan the 10-15 mode cycle replaced the previous 10-mode cycle in 1991 [31]. It was derived from the 10-mode cycle, using three 10-mode segments followed by a 15-mode segment at the end as shown in Figure 2.16. The entire cycle features an additional 15-mode segment as part of the warm up before the emissions measurement starts.

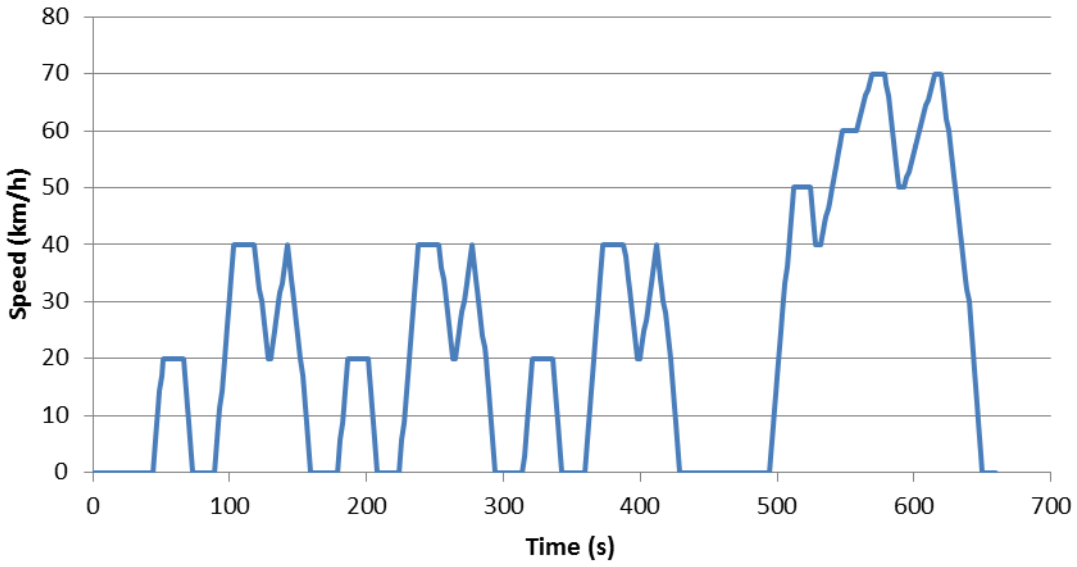

Figure 2.16: 10-15 Mode cycle

Between 2005 and 2011 a new Japanese regulation test cycle representing congested city driving, the JC08, was gradually phased in to replace the 10-15 Mode. It can be seen in Figure 2.17 and the cycle statistics with those of the 10-15 mode cycle are in Table 2.4.

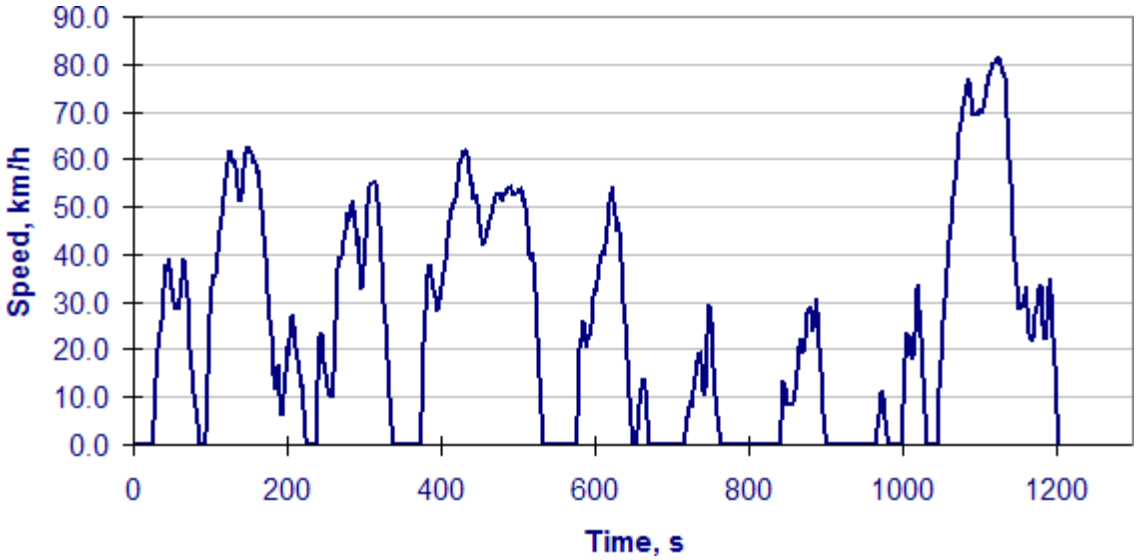

Figure 2.17: JC08 cycle. Source DieselNet.com [28]

Table 2.4: Japanese drive cycle statistics. Data from DieselNet.com [28]

	Drive Cycle	
Statistic	**10-15 Mode**	**JC08**
Duration (s)	660	1204
Distance (km)	4.16	8.17
Average speed (km/h)	22.7	24.4
Maximum speed (km/h)	70.0	81.6

2.2.2 Artemis Driving Cycles

The European ARTEMIS (Assessment and Reliability of Transport Emission Models and Inventory Systems) project was intended to define European methods and tools for measuring pollutant emissions from transport. An objective of this was to derive a set of reference real-world drive cycles to be used within the project, and also in other areas to give consistency between European emissions data. Existing data was used for the development of three cycles, urban, rural, and motorway, to cover the diversity of driving conditions observed [32]. An alternative version of the motorway cycle with a lower maximum speed of around 130 km/h rather than 150 km/h was also produced for facilities with lower maximum test speed. All the cycles are shown below in Figure 2.18, Figure 2.19 and Figure 2.20, and the cycle statistics in Table 2.5. The figures were produced with data from INRETS [33].

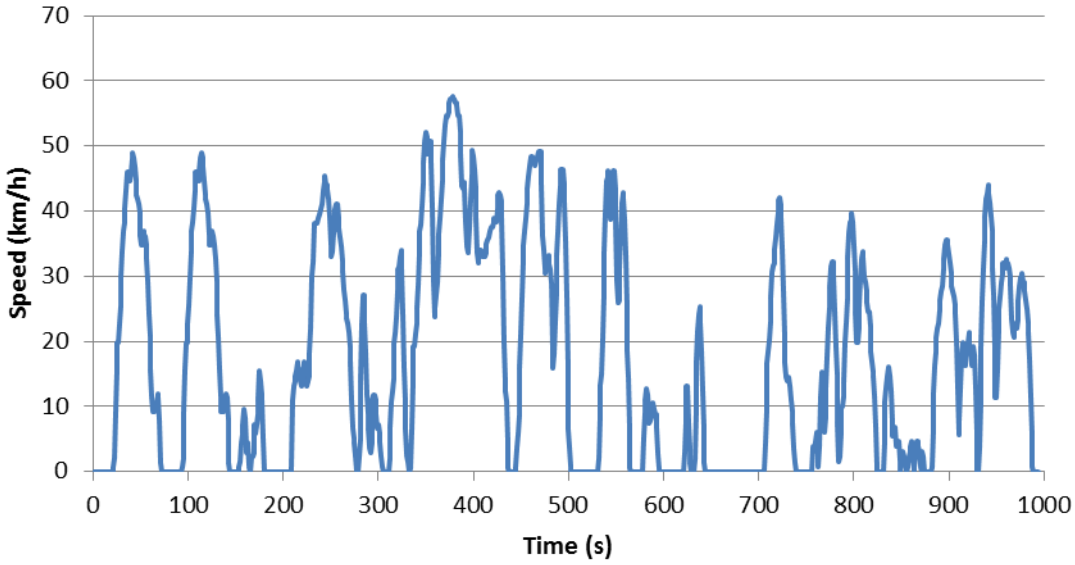

Figure 2.18: Artemis Urban cycle

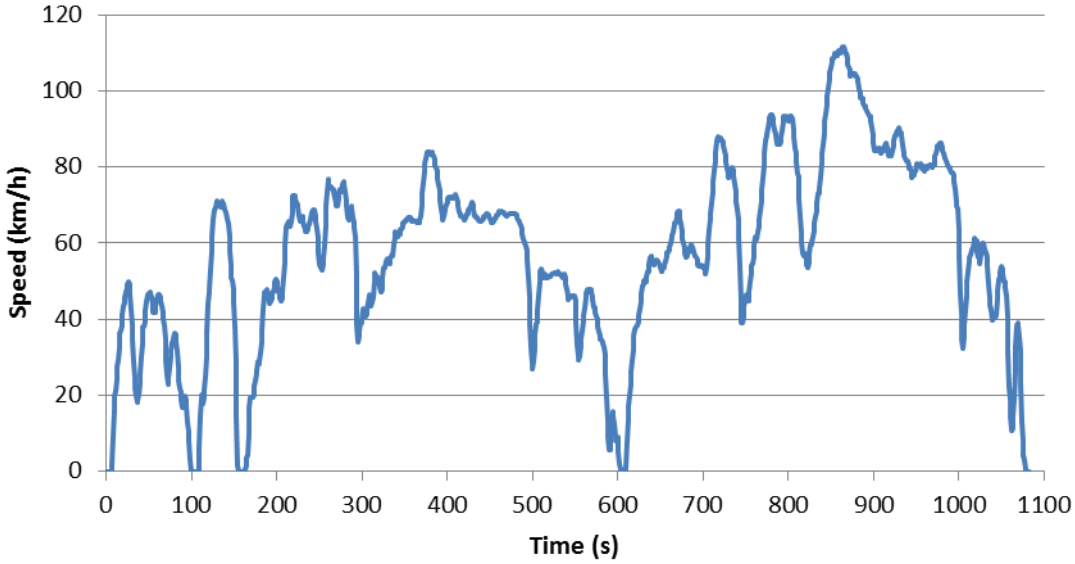

Figure 2.19: Artemis Road cycle

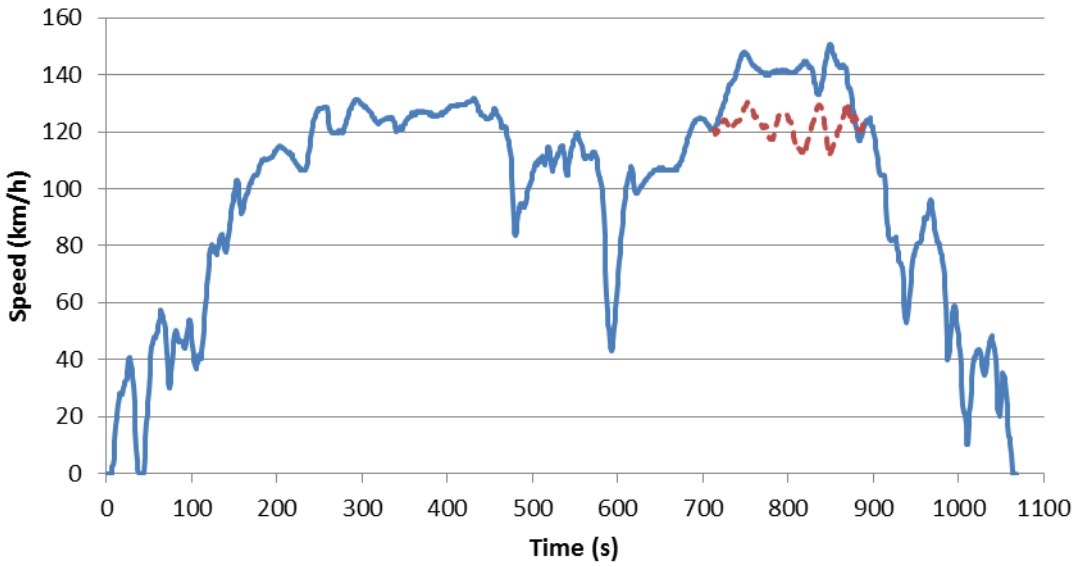

Figure 2.20: Artemis Motorway cycle including 130km/h version shown with dashed line

Table 2.5: Artemis cycle statistics. Data from DieselNet.com and André [28,34]

	Drive Cycle			
Statistic	**Urban**	**Road**	**Motorway (130)**	**Motorway (150)**
Duration (s)	920	1081	1067	1067
Distance (km)	4.47	17.27	28.74	29.55
Idle time (s)	260	33	16	16
Average speed (km/h)	17.5	57.5	97.0	99.7
Maximum speed (km/h)	58	112	132	150
Average acceleration (m/s^2)	0.75	0.58	0.52	0.52

2.3 Drive Cycle Development

2.3.1 Types of Drive Cycle

There are two general types of drive cycle:

1. Transient – Developed from on-road driving data, such as the US FTP
2. Modal, or polygonal – Developed from statistics and comprised of a sequence of steady-state modes, such as the EU and Japanese cycles

For collecting driving data to use in the production of a drive cycle, two main methods are used; the chase car technique, and on-board measurement [35]. In the chase car technique a driver would follow a selected target vehicle on a pre-defined route. The other method involves using instrumented test vehicles to collect data directly.

A review of 101 drive cycles covering both light-duty and heavy-duty vehicles by Tong and Hung provides a good summary of the differences and the ways in which cycles can be developed [35]. A clear trend is shown in drive cycles developed for different driving conditions; with urban drive cycles generally having lower average speed but higher positive kinetic energy and acceleration rates. Conversely, motorway drive cycles have higher average speed but smaller positive kinetic energy and acceleration rates. There is some overlap seen between drive cycles developed for different driving conditions, probably due to a combination of other factors including vehicle type, driving environment and driver behaviour in different geographical areas. When comparing average acceleration to average speed, light-duty and heavy-duty vehicle driving patterns differ so drive cycles are developed for these specific vehicle types.

Comparisons showed differences between drive cycles for different regions, comparing Europe, the USA, Australia and Asia. Motorway driving is generally smoother in the USA, Europe and Australia than Asian cities such as Hong Kong where there is low speed congested driving. Urban and suburban driving commonly has lower speed and features more transient changes. The differences between the three conditions for the Asian cities are less distinctive than for Europe,

the USA, and Australia, due to the generally lower speed congested driving. Weighted average values in relation to the drive cycle duration show in Asia average accelerations are higher than the others and speeds are much lower.

2.3.2 Cycle Construction Methods

There are two main methods of drive cycle construction: the simulation approach and the matching approach. The simulation method has not been used a lot recently; matching is much more widely used so will be focussed on here.

2.3.2.1 Simulation Approach

The 'Knight's Tour' theory considers the driving dynamics at each second to generate a cycle using understanding of how a vehicle moves in a traffic stream, rather than matching to assessment criteria [36]. The name comes from an analogy with how a knight may move around a chessboard. A speed-acceleration matrix with related frequencies of events is used. Using an understanding of how a vehicle moves in traffic implies a path through the matrix using the frequency of events in each cell. The speed profile is generated from this, combined with probability distributions of starting acceleration and length of idling period to define the stops. The cycle does not have to meet statistics of the overall dataset, but results showed that it could do.

The 'Knight's Tour' approach has also been applied in the matching approach to define how driving conditions and modes follow each other [37,38].

2.3.2.1.1 Cycles Developed Using Simulation Approach

The Perth driving cycle was developed based on the 'Knights Tour' concept [36]. An interesting finding from this study was that the rate of acceleration from one second to the next tends to zero, implying that there is a strong inclination for a vehicle to maintain constant acceleration or deceleration rates.

2.3.2.2 Matching Approach

Regularly assessment criteria are used and measured against the total driving dataset. A drive cycle produced with the matching method can constitute a single logged trip or a sequence of microtrips that are considered to be the most representative of the dataset. A microtrip is the speed data between two consecutive stops. An advantage of segment matching approaches is checking the statistical agreement with the dataset. On the other hand a disadvantage is that the criteria may tend to include microtrips with statistics closer to targets, rather than trips with extreme driving behaviour in, meaning that this can get excluded.

Trip-based cycle construction is a simple method where multiple test runs of the route are carried out to collect speed-time data and the one that best matches the target statistics is chosen. For the UDDS [39] the run that had the time closest to the average was chosen and then shortened to make it closer to the average journey length for the area, by removing segments whilst maintaining statistics for the drive cycle. Another example of using the trip-based method is the FTP75. With this method there are no artificial manipulations so it gives reasonable representativeness when there are enough samples to choose from. Driving characteristics recorded in other runs are not included so some important driving behaviour may not be incorporated in the drive cycle.

Microtrip based cycle construction produces a more representative cycle and has additional flexibility. Variations of the method allow for cycles for specific purposes to be produced such as for a region, a specific route or facility-based. Different variations of this approach are the most frequently used for developing a drive cycle. The data is split into microtrips or data segments, which can be defined as the speed data between set points, classified by statistical methods or partitioned by length or type.

The simplest way to develop a drive cycle is to select random microtrips, or find microtrips that incrementally improve the match to the target statistics. One example is the Unified cycle (LA92), which used a ‘quasi-random’ approach, selecting microtrips that incrementally improved the sample speed/acceleration

frequency distribution (SAFD) [37]. An SAFD is a distribution showing the frequency of acceleration rates at a given speed, which is usually displayed as a 3D surface plot. Other examples that use microtrips include the Indian Pune drive cycle [40], Hong Kong cycle [31], Chennai bus cycle [41], Bangkok cycle [25] and Vietnam cycles [26].

Alternatively, to ensure data representing each driving condition is included, the microtrips are first grouped by driving condition. A pre-defined number of microtrips are selected from each group in accordance with the succession probability. Different variations of this approach are the most frequently used. The Heavy Heavy-Duty Diesel Truck (HHDDT) cycle randomly selected microtrips and combined them to form sub-cycles for each operating mode, then joined them together to form the final cycle [42]. Another example is the Artemis cycles [32]. The Edinburgh cycle was produced using the TRAFIX (TRAffic Flow IndeX) method, which generates speed codes for driving segments. The speed at each second is identified and assigned to the relevant pre-defined speed interval. The codes are then compared to codes for the whole dataset [43].

2.3.2.2.1 Modal Segmentation Method

The modal data segmentation method assumes driving consists of a sequence of different driving modes in order to include emission sensitive driving characteristics in the derived cycle. A drive cycle is modelled using Markov theory where the occurrence of a modal event is dependent on the previous modal event [37,38]. The dataset is split into sections that are grouped into modal groups, and then a transition probability matrix is developed and used along with an SAFD to select sections from the groups to construct the drive cycle. Further improvement to this method has been made by considering the intensity and duration of vehicle speed and acceleration events [38].

2.3.2.2.2 Cycles Developed Using Matching Approach

The following are descriptions of the development processes for a selection of drive cycles using different methods.

EPA Urban Dynamometer Driving Schedule (UDDS)

Kruse and Huls [39]

A complete test trip was chosen with the most representative speed-time profile. The development process was as follows:

- 6 drivers drove the same route once each with their speed recorded
- 5 of the 6 speed traces were very similar, from these the one with the time closest to the average was chosen
- A shorter trip length was wanted to be closer to the average trip length for the region
- The speed profile was split into segments between idle points (effectively microtrips), the maximum speed, average speed, time and distance were calculated for each and profiles that were alike were grouped
- In any of these groups 1 in 3 profiles were deleted
- For the long continuous motorway profile, sections were cut out whilst maintaining the average speed of the segment
- Cycle parameters for the shortened cycle were compared to the complete route
- Several combinations were tried before the final version was found
- The original sequence that the segments were recorded in was maintained
- The target number of idle periods was used in the profile section selection process
- The average number of idle periods in all the road runs was multiplied by the proportion of the shortened route distance to the complete route distance to obtain the expected number of idle periods
- To distribute the idle time, all idle periods recorded during all trips were ordered by duration, split into the same number of groups as the number of idle periods, and the average of each group calculated
- The sum of these average times was too large so they were all slightly shortened to produce the idle periods used in the cycle
- The idle periods were distributed between the driving segments using the original recorded trip as a guide

Unified Cycle (LA92)

Lin and Niemeier [37]

The Unified Cycle was designed to address the lack of high speed and high accelerations in the FTP. The development process was as follows:

- Based on the LA92 data collected by the chase car technique on roads in Los Angeles in 1992
- The data was divided into microtrips; there was a total of 833 of them
- The first "seed" microtrip was selected at random
- Subsequent microtrip selection was by a "quasi-random" approach, it is not completely random as the microtrips were selected to incrementally improve the match to an SAFD plot
- After a microtrip was selected it was removed from the set
- The process was repeated until a pre-determined cycle time was met, of approximately 20 minutes
- 18,000 cycles were produced in total
- The final cycle matched the SAFD of the dataset within 22% of the sum of the differences
- The Unified Cycle average speed, maximum speed and maximum acceleration are 13-15% lower than the dataset, and there is 4.6% more idle time
- SAFD plots showed the cycle has 2.5% more occurrences of speeds and accelerations close to zero that the sample data, the difference in other areas is less than 0.8%

Heavy Heavy-Duty Diesel Truck (HHDDT)

Gautam et al. [42]

Randomly selected microtrips were combined to form sub-cycles for each operating mode then joined to form the final cycle. The development process was as follows:

- Trips and microtrips were used as defining parameters and for statistical evaluation, with a trip being an ignition key-on to key-off event
- Microtrips were defined as a "stop-to-stop" including the preceding idle period

- Four operating speed modes were identified – Idle, Creep, Transient & Cruise
- For the Idle Mode no processing was required to create a representative test mode
- For the Creep and Transient Modes, microtrips were selected randomly through an iterative process to construct candidate cycles that matched target parameters, with the one that best met the criteria selected
- Average speed, stops per mile and total kinetic energy were the measures used
- Microtrips were appended until the desired cycle time duration was met
- A different approach was used for Cruise mode due to their long trip durations
- The cruise trips consisted of a variety of intermediate speed operation so individual trip statistics were compared to the targets
- This gave good matches to the targets so a single trip was used in the cycle that was representative of the total dataset for the Cruise mode
- An Idle Mode was added at the beginning of the cycle to represent "idle trips" where the engine was started but the vehicle does not travel any distance
- The developed cycle was too aggressive to be used on a chassis dynamometer due to excessively high accelerations and decelerations, so a filtering method was applied to reduce high frequency speed fluctuations, and also limit deceleration rates

Edinburgh Driving Cycle (EDC)

Esteves-Booth et al. [43]

The TRAFIX (TRAffic Flow IndeX) method which generated speed codes for driving segments and compared them to the whole dataset was used. The development process was as follows:

- 6 routes were driven at 4 different times of day on all 7 days
- There were 840 measured datasets
- The full range of speed was grouped by 5 groups

- TRAFIX generates a code for each measured dataset, in which it identifies the speed at each second and assigns it to the relevant speed interval
- Codes are also generated for acceleration rates
- Statistical analysis of the codes is used to produce the drive cycle
- Method validity based on the speed at a moment in time is of minor importance in calculating the total emissions, the important factors are the speed and acceleration in total in the time period
- After analysis of patterns seen, data was grouped into 3 groups: weekdays, Saturdays and Sundays
- Outlier analysis was used to confirm it was statistically correct to combine the weekdays into one group
- 72 codes were obtained – For each of the 6 routes, for each of the 4 times of day and each of the 3 day groups
- Weighted averages in proportion to recorded traffic flows on the specific routes were used to produce the final code
- The EDC was plotted by comparing the cycle code against the codes for each individual route, finding a close match
- Comparison was made to ECE-15 urban cycle – Average speed, time and distance are closely matched, but operating modes differ significantly due to ECE-15 being artificially formed, whereas realistic transient patterns form the EDC

Artemis Driving Cycles

André [32]

For the Artemis cycles that were discussed earlier in Section 2.2.2, existing data was used to develop the urban, rural, and motorway cycles. The development process was as follows:

- Data from the DRIVE-MODEM[1] and HYZEM[2] projects was used, which came from 77 vehicles monitored for a total of 88,000 km and 2200 hours of driving
- Equal sized segments of driving data were defined
- Segments were grouped by driving conditions according to speed and acceleration statistics
- 12 typical driving conditions were identified
- Drive cycles were derived by combining a sequence of driving segments based on observed probabilities of successive driving sections

2.3.3 Assessment Criteria

To verify if a drive cycle is representative of the dataset on which it is based, or of particular driving conditions, assessment criteria are usually used to compare against and match to. Statistics of the input data provides targets for the same measures on the produced cycle to match. How close they should match will be defined by the developers of the cycle, possibly as a range from the target or by producing a series of candidate cycles and choosing the best from them. They also determine the assessment statistics used and these can vary in what is used and how many are.

The most frequently used criteria in the cycles assessed by Tong and Hung in [35] are average speed, idle time, acceleration parameters and SAFDs, as these have an important influence on vehicle emissions estimation [38,44]. In modal distributions, vehicle operating modes are commonly defined as idling, acceleration, cruising and deceleration. Continuous low speed creeping mode which describes vehicle motion

[1] MODEM (Modelling of Emissions and Fuel Consumption in Urban Areas): A research project within the DRIVE (Dedicated Road Infrastructure for Vehicle Safety in Europe) initiative

[2] HYZEM: European Development of Hybrid Vehicle Technology approaching efficient Zero Emission Mobility

in congested traffic with frequent stop-and-start is commonly ignored in the literature. This operating mode has a significant effect on emissions so is important to be included in cycles based on urban and congested environments.

The methods using succession probabilities use fewer criteria than the matching approach which is in line with the principles behind them. Using a speed/acceleration distribution could implicitly reflect the effect of speed and acceleration based criteria.

A summary of the assessment criteria used in a number of existing drive cycles can be seen in Table 2.6.

Table 2.6: Summary of assessment criteria used in drive cycle production. Reproduced with content from Tong and Hung [35]

	Drive Cycle																					
Assessment Criteria	FTP72/FTP75	LA92/Unified Cycle	LA01	HHDDT Cycle	Arterial Cycles	Edinburgh Cycle	IEC	ARTEMIS Cycle	TRL Cycle	Sydney Cycle	Melbourne Peak Cycle	CUEDC Cycles	Perth Cycle	TMDC	KHM	China Cycles	Beijing Cycles	HK and Zhulai Cycles	Pune Cycle	Metro Manila Cycle	BDC Cycle
Average speed	✓		✓	✓			✓	✓	✓	✓	✓	✓	✓		✓	✓	✓	✓	✓	✓	✓
Average running speed							✓	✓						✓	✓	✓	✓	✓			✓
Average acceleration							✓	✓	✓					✓	✓	✓	✓	✓			✓
Average deceleration							✓	✓						✓	✓	✓	✓	✓			✓
Mean length of microtrips							✓		✓					✓	✓			✓			
Average no. of accel/decel changes							✓								✓	✓		✓			
Average number of stops	✓						✓	✓					✓					✓			✓
% Idling				✓	✓		✓	✓		✓	✓	✓	✓	✓	✓	✓	✓	✓	✓		✓
% Creeping				✓														✓			
% Acceleration				✓	✓		✓					✓		✓	✓	✓	✓	✓	✓		✓
% Cruising				✓	✓		✓								✓	✓	✓	✓	✓		✓
% Deceleration				✓	✓		✓								✓	✓	✓	✓	✓		✓
RMS speed											✓										
RMS acceleration										✓	✓		✓		✓			✓			
Positive kinetic energy (PKE)											✓		✓			✓		✓			✓
Rate of change of acceleration													✓								
Speed/acceleration distribution		✓	✓		✓	✓		✓		✓	✓		✓	✓				✓	✓	✓	
Vehicle specific power					✓												✓				
Maximum speed	✓		✓	✓				✓	✓			✓					✓	✓		✓	
Minimum speed			✓						✓											✓	

2.3.4 Drive Cycle Length

The literature does not show a common approach to defining the length of cycle, or have detailed studies on it. The microtrip based matching method usually chooses a pre-defined number of microtrips to use which loses control of the cycle duration [31]. Some studies controlled the cycle duration when selecting microtrips, eg. Artemis, mainly based on common practices or experience of a reasonable cycle length. Cycles were derived with lengths close to the average trip length, or similar to that of other drive cycles. Some other studies determined cycle length based on cost of carrying out chassis dynamometer testing [38,45]. In these cases the length or duration may not give sufficient representativeness. Cycles should be long enough to give representativeness of the local driving characteristics [25].

2.4 Drive Cycle Testing

2.4.1 Chassis Dynamometer Testing

Chassis dynamometers are commonly used to carry out vehicle testing in controlled laboratory conditions. The driven wheels of the test vehicle are positioned on rollers connected to the dynamometer, which are programmed with a road load model for the particular vehicle to be tested. The vehicle can then be driven through drive cycles displayed to the driver on a screen, or by using an automated robot driver, to take measurements of interest.

Dynamometers can be 2WD (2 wheel drive) which the front or rear wheels sit on as necessary, or 4WD (4 wheel drive) with rollers for both axles. For testing a HEV with regenerative braking on a 2WD chassis dynamometer it could be thought that this may have an effect on the regenerative operation due to the rear wheels being stationary. It was confirmed in Duoba et al. [46] that using a 2WD dynamometer does not have an effect on the regenerative braking though so fuel consumption results are not affected.

2.4.2 Drive Cycle Fuel Consumption

Many tests have been done with different types of vehicles to compare fuel consumption differences between drive cycles, or between different vehicles on the same drive cycle. Burton et al. [47] found when comparing a hybrid heavy-duty truck to a conventional diesel one that the difference in fuel consumption between the two vehicles differed significantly between different drive cycles tested. For two of the cycles the HEV was 25-31% lower, but in another it was 4% higher.

Drive cycles can also be carried out on-road to represent specific journeys or routes. Li et al. [48] investigated the effect of two driving routes with different traffic conditions in Leeds, one in a quiet area with little traffic that they named WP, and another in a busy area with more road traffic influence called HPL. The WP route had a lower average speed than the HPL route, and higher average acceleration and deceleration. The time spent accelerating or decelerating was also higher and the cruising time was lower. The WP route had no idle time and the HPL had a

small amount of idle time consisting 2.9% of the duration. In comparison to the ECE-15 they both had higher average accelerations, maximum accelerations, higher acceleration and deceleration time, and significantly less idle time than the 28.6% in the ECE-15. An ICE car with a 2.0 SI engine was driven on the two routes with the resulting fuel consumption being 60% higher on the WP route which the authors associated to having more acceleration time. There was found to be less variation in repeated test runs for the WP cycle than the HPL, indicating more variables such as traffic and pedestrian crossings were interfering.

Transient driving modes (accelerations and decelerations) have been proven to consume a greater amount of fuel than steady-speeds [49], so are a significant factor in the fuel consumption of a drive cycle.

2.4.3 Prius II Drive Cycle Testing Comparisons

The Toyota Prius performs best for fuel economy in driving that consists of low to medium speeds so that the electric drive can be used, and also with periods of deceleration, to benefit from regenerative braking and engine-off time. From Lenaers' [50] testing of the Prius II on different driving routes, rural driving was found to have the lowest fuel consumption, followed by urban driving, and then motorway. Similar size conventionally powered cars were tested in comparison which included a Peugeot 307 1.6 petrol and 1.6 HDI diesel. The Prius delivered better fuel economy on all driving routes, except on the motorway driving where the diesel performed 6.2% better. The average fuel consumption of the diesel was only 7.6% higher than the 5.53 l/100km recorded for the Prius, and the petrol's fuel consumption was found to be much higher with a 49% increase.

The fuel economy and emissions of two HEVs, a Toyota Prius II and Honda Civic IMA, were tested by Fontaras et al. [51]. The NEDC, plus the ECE-15 and EUDC sections separately, and Artemis driving cycles were tested. The Civic IMA is a mild hybrid so allowed comparison between levels of hybridisation. The Prius II gave better fuel economy than the Civic IMA, particularly on the urban cycles, which supports the effect of the hybridisation levels of the two cars. The results were used for comparison with average speed-dependant emission factors of

conventional vehicles from existing data. Both cars showed lower fuel consumption than conventional petrol cars, and for mean speeds below 90 km/h also were better than conventional diesel. For urban driving at around 20 km/h the Prius fuel consumption was 50% and 60% lower than conventional diesel and petrol cars respectively. Additionally, the full hybrid fuel consumption was 40% less than the mild hybrid. This difference becomes smaller as the mean speed increases, and above 60 km/h they are almost the same. The Prius reaches the fuel consumption level of the conventional petrol and diesel cars at 120 km/h and 95 km/h respectively.

Battery and ICE operation in the Prius was monitored for steady state driving at three speeds, 35 km/h, 50 km/h and 60 km/h. A repeating operational cycle was observed for the engine-on periods for which the duration increases, and ratio of electrical and ICE drive changes with vehicle speed. In Kelly et al. [20], on the FTP drive cycle the amount of battery energy used for driving was nearly 10% of the fuel energy used by the ICE.

Sharer et al. [52] investigated the effect of a drive cycle aggressiveness and speed on a HEVs fuel consumption sensitivity using a Prius II in comparison with a conventionally powered Ford Focus. In this they scaled the UDDS and HWFET drive cycles to produce versions with differing acceleration rates and speeds. A measure of fuel consumption sensitivity was defined and calculated for results for each vehicle. The sensitivity for the Prius was higher than the Focus on both cycles, with a significant difference on the UDDS, and a smaller difference on the HWFET. For the Prius the sensitivity was higher on the UDDS than the HWFET. The main reason explaining this was that on the UDDS the engine is used more often as the cycle becomes more aggressive, therefore increasing energy losses which gives more variation. For the Focus there is less sensitivity due to increasing load giving increased engine efficiency, counteracting the increase in consumption. With the Prius however, this effect is not seen because the operating strategy of its engine is already efficient so less improvement is seen as load increases. Another reason was due to energy recuperation. Looking at regenerative energy sensitivity

to vehicle load, it was much higher for the UDDS, this means the energy captured by regenerative braking increases faster on the UDDS than the HWFET.

2.4.4 Effect of Drive Cycle Conclusions

In summary, the drive cycle has a very significant impact on the energy consumption of a vehicle, and also on how much the energy consumption of a HEV differs to that of a conventional ICE vehicle. Testing has found acceleration, in both count and magnitude, to be an important factor affecting energy consumption of a cycle. The sensitivity of a Prius' fuel consumption to aggressiveness of a cycle has been found to be greater than that of a conventional car.

The Prius performs best for fuel consumption in lower speed driving with coasting and deceleration periods, particularly on rural roads followed second by urban areas. In this environment the full hybrid Prius has been found to perform more economically than mild hybrid and also conventional petrol and diesel competitors. For a Prius the engine-on time is increased with vehicle speed.

2.5 Real-World Driving

2.5.1 Real-World Fuel Consumption

As discussed earlier, fuel consumption in real-world driving can be very different to published official figures for vehicles. An example of a study in existing literature of higher fuel consumption in real-world driving compared to legislative tests can be seen in Zhang et al. [53].

The difference has increased quickly in recent years. In Mock et al. [54-56] data from several sources around Europe of real-world driving is collated and analysed to look at how the difference between legislative test results and real-world driving fuel consumption and CO_2 emissions varies with time. A clear trend of an increasing gap is seen, as shown in Figure 2.21, with the difference in emissions being about 8% in 2001, increasing to approximately 25% in 2011, and quickly rising further to 38% in 2013. This increase was particularly noticeable from 2007, which corresponds with when EU CO_2 regulations for new cars were introduced, and when some EU countries introduced CO_2-based vehicle taxation. The reasons given to explain the increase are:

- Increase in technologies such as auto stop-start, that show a higher benefit in certification tests than real-world driving
- Increased exploitation of permitted variation in test procedure regulations for improved results, such as for inertia bands used for dynamometer testing
- Increased standard fitment and use of air conditioning in cars

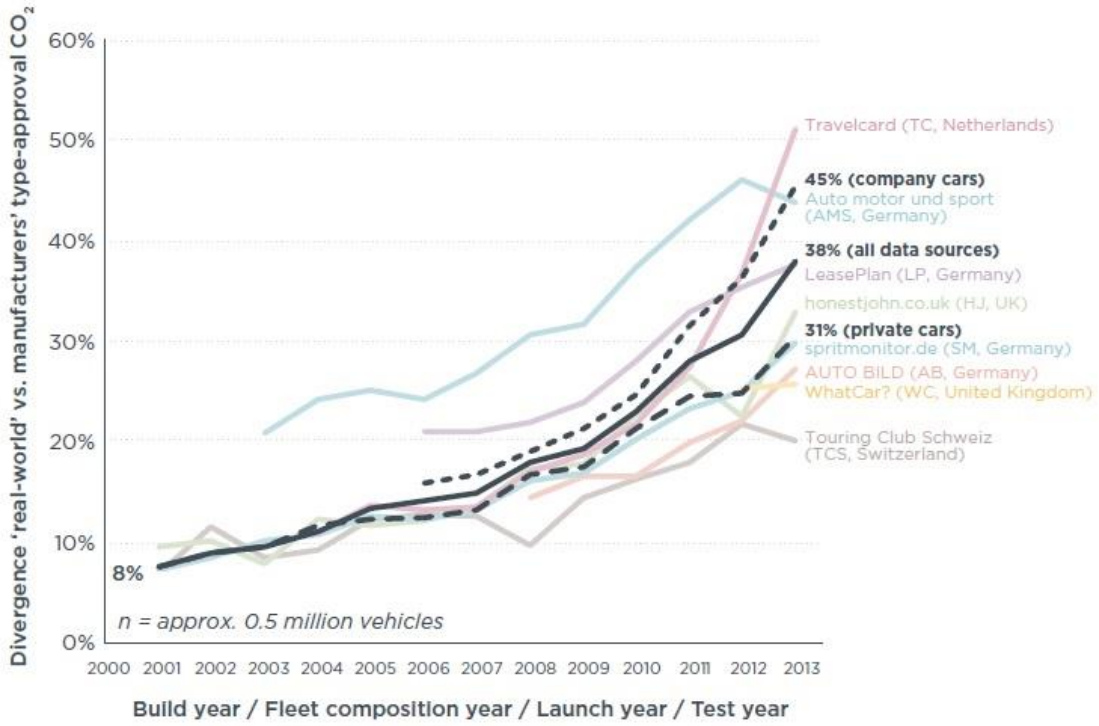

Figure 2.21: Increasing gap between manufacturers' CO_2 emissions and real-world driving. Source the ICCT [56]

2.5.2 HEV Real-World Fuel Consumption

In Zahabi et al. [57] during real-world driving HEVs performed better than conventional petrol vehicles by 28%, particularly at low urban speeds, while for motorway driving they were similar. Ambient temperature was found to have a larger impact on HEVs than conventional cars with a 26% fuel consumption increase in winter compared to spring due to reduced battery performance at low temperatures. Again, this was especially at low speeds. A 2% increase from spring to summer was explained by the increase in temperature being beneficial for the battery and therefore improving fuel consumption, but increased use of air conditioning at the same time reducing fuel consumption.

Howey et al. [58] measured the energy consumption of 51 fuel efficient vehicles over a 57 mile urban and extra-urban route. They found that of the three categories of vehicles tested, the hybrid vehicles on average had energy consumption higher than the electric vehicles and lower than the conventional ICE vehicles.

In Karner and Francfort [59], two Prius II's tested over 160,000 miles each in fleet use real-world driving averaged fuel consumption of 44.4 MPG US, which is only 3.5% below the quoted 46 MPG US fuel consumption [60].

In six months use of real-world testing of heavy-duty trucks Burton et al. [47] concluded that the hybrid truck had 15-17% better fuel economy than the conventional truck tested.

2.6 Effects on Real-World Fuel Consumption

2.6.1 State of Charge Level

The state of charge of the HV battery in a HEV at the start of a test will always have a huge effect on the fuel consumption or emissions results recorded. With a high initial SOC the vehicle will utilise the electrical power for driving, with less ICE use so therefore less fuel used. On the other hand, if the initial SOC is low the ICE will have to be used more for driving power and for recharging the battery leading to higher fuel use. The effect of different battery SOC levels on fuel consumption was investigated in Duarte et al. [61]. On-road testing of a Prius III was carried out under varying driving conditions, and the data analysed using the vehicle specific power (VSP) method. This gives the estimated power per unit mass required to drive the vehicle at a given moment in time, using vehicle dynamics and road gradient. The results can then be grouped into bands or modes of driving behaviour. The estimated fuel consumption of the NEDC was calculated using the on-road fuel consumption measured in each VSP mode, in combination with a distribution of time spent in each VSP mode for the drive cycle. The results showed that as SOC level was increased the ICE off time was increased, leading to lower fuel consumption. Compared to the average of the results, fuel consumption when at between 40-50% SOC was 57% higher, at 50-60% SOC was 10% higher, at 60-70% was 3% lower, and at 70-80% was 38% lower. These results obtained here are very much dependant on the control system philosophy.

2.6.2 Road Gradient

Gradient is one of the main factors not accounted for in dynamometer testing that occurs in real-world driving and can effect fuel consumption. Li et al. [62] tested a petrol 1.8 litre ICE car on a 700 metre length of urban road in Leeds that has a 4.7% gradient in both directions, and compared it to a flat road. Compared to the flat road, the fuel consumption was found to be 18% lower on the downhill, and the uphill was 3.5 times greater. On a round trip going downhill and uphill the average fuel consumption was just over double that of the flat road, showing that fuel consumption can be significantly increased by driving on hilly roads.

There is very limited existing work in this area related to HEVs. In a very recent study from 2014, Wood et al. [63] investigated the contribution of road gradient to energy consumption by linking elevation profiles from a United States Geological Survey digital elevation model to GPS speed traces from over 6000 vehicles in the US. Drive cycles were produced that simulations were run on, with and without the gradients applied. Models included a mid-size conventional petrol car and a mid-size HEV. The tests were grouped based on geographical area. The conventional vehicle experienced a 25% to 73% larger increase in fuel consumption due to gradients than the HEV. For the conventional vehicle increases ranged from 0.2% to 4.1%, and for the HEV 0.1% to 3.0%. Analysis was also carried out based on individual trips with their average gradients, which showed double digit percentage increases and decreases in fuel consumption for both powertrain types. Again, the HEV was less sensitive to road gradient than the conventional model, expected to be due to the HEV being able capture energy on the downhill parts.

2.6.3 Ambient Temperature and Auxiliaries Effect

The use of auxiliaries, particularly air conditioning, is known to add to fuel consumption and in HEVs can have a more pronounced effect due to causing changes in the operation between their electrical and mechanical systems. In Karner and Francfort [59], 11 HEVs were tested with and without air conditioning and the results showed increases in fuel consumption with air conditioning in the range of 15 to 28%. The fuel consumption for the Prius II tested had a 22% increase.

El Khoury and Clodic [64] tested a Prius II and recorded fuel consumption of 3.6 l/100km on the NEDC. At 28°C they tested with the air conditioning on set at a controlled temperature of 20°C, and also set to the maximum cooling temperature and air flow setting "Max Cold". They found that the fuel consumption was increased by 0.7 l/100km, a 19.4% increase in the first case and in the second case this difference doubled to 1.4 l/100km and 38.9%.

Another study in Christenson et al. [65] used a dramatic temperature difference of -18°C compared to 20°C to look at the effect of ambient temperature. In this it was

found that cold temperature had a more detrimental effect on hybrid vehicles than conventional petrol vehicles. There was over 100% increase in fuel consumption on the UDDS at the lower temperature, showing that the Prius is very sensitive to ambient temperature. The engine operation is one reason contributing to this, on the New York City Cycle the engine-off time went from 66% to 20% with the reduced temperature.

2.6.4 Battery Degradation

One concern of the public with HEVs, particularly so a few years ago, is how long the batteries would last. From consumers' experience of mobile phone and laptop computer batteries severely deteriorating in performance or failing completely in just a few years, there was the perception of this happening with hybrid vehicle batteries with a large expense.

Testing of two Prius I battery packs was carried out in Karner and Francfort [59], after 160,000 miles use in the cars. Their capacities were measured as 2.5 Ah and 2.6 Ah, an average 61% reduction. Charge and discharge pulse current tests were carried out to check the capability of the battery pack to meet the short high load demands experienced in typical driving. Ten second pulses were applied at 10% SOC decrements starting from 90%, with the lower the battery is able to go the better it is at meeting the power demands. The batteries tested were all able to absorb the charge pulses without reaching their voltage limits, implying that the battery's ability to absorb energy from regenerative braking was not reduced. For the discharge pulses there was variation in the two Prius I batteries tested with the limit of one being 60% and the other 10%. This shows that the degradation of the batteries can vary, possibly due to different usage patterns of the vehicles.

The US Department of Energy Advanced Vehicle Testing Activity Programme has carried out battery tests on packs in several Toyota Prii after they have been in use for 160,000 miles of real-world driving. Reports have been published with the results for two Prius II and two Prius III vehicles that were tested [66-69]. For the Prius II batteries, one was measured at 5.34 Ah average capacity and 1130 Wh average energy capacity, and the other at 5.25 Ah and 1090 Wh. These results

show a 17.8% and 19.2% reduction in capacity for the two battery packs against the rated capacity. The Prius III batteries were also tested at the start of the testing to establish the actual original battery performance, to use for comparing the end of test results against. For the first car the measured capacity went from 6.24 Ah to 4.99 Ah, a 20.0% decrease, and the measured energy capacity went from 1340 Wh to 1040 Wh, a 22.4% decrease. The results for the second car were from 6.09 Ah at start of test (SOT) and 4.94 Ah at end of test (EOT), a reduction of 18.9%, and 1310 Wh at SOT and 1050 Wh at EOT, a 19.8% reduction. These results show quite consistent degradations of battery capacity across all of the vehicles tested which could be indicative that the driving patterns of the vehicles were similar.

2.7 Vehicle Simulation Software

Many vehicle simulation software packages are available, and they can be categorised into two main types: forward simulation and backward simulation. With forward simulation the operating strategy and power flows in the system are used to produce the output effect, which is velocity in a vehicle. A backward simulation on the other hand uses the drive cycle and works in the reverse direction to derive the required energy input to match the speed. Backward simulations have fast runtimes but they cannot accurately simulate power-split hybrid architectures due to the different energy paths to the wheels that exist. With a conventional vehicle a certain vehicle speed and gear ratio will relate to a specific engine speed, which is the principle that backward simulations use, whereas this is not true for power-split HEVs.

Possible software that was considered that could have been employed includes AVL CRUISE, Argonne National Laboratory's Autonomie or ADVISOR (Advanced Vehicle Simulator). CRUISE models are comprised of separate components that can be modified or interchanged independently. Advanced powertrains including electric and hybrid are incorporated making it suitable, although it would require a vehicle model to be built and validated. There are detailed analysis tools including graphical energy and power flow display which would be a useful benefit for energy analysis, and reports can be generated in the post-processing. CRUISE which is a forward simulation package also has the benefit of interfacing with other AVL software such as BOOST or FIRE if required.

ADVISOR is a systems analysis tool developed by the U.S. Department of Energy (DOE) and the National Renewable Energy Laboratory (NREL). It is a model based on MATLAB and Simulink that can be used for conventional and hybrid vehicles. For a drive cycle it calculates predicted torque, speed, voltage, current and power passed from one component to another. Its key use is for making changes to components or adding or replacing them to analyse the effects of doing so. A combination of backward and forward simulation is used. Backward simulation is used for high level requirements while forward simulation is used to modify

individual component control commands to minimise the error between the driver demand and the response of the system.

The U.S. DOE Argonne National Laboratory's Autonomie is a tool for automotive control system design, simulation and analysis. It is developed from its predecessor, Powertrain System Analysis Toolbox (PSAT). Autonomie is mathematically-based forward simulation software based on MATLAB, with MATLAB data and configuration files and models built in Simulink. Vehicle models are built from individual components either from those built-in or by importing others. It uses a plug-and-play architecture with the flexibility to import models and components from other software packages. A driver model is included to give inputs in the form of accelerator and brake inputs to the vehicle model which then responds to these. Vehicle energy use and performance can be evaluated.

The Autonomie software was chosen due to having an in-built 2004 model year Toyota Prius vehicle model, and the forward simulation approach is suited to the power-split HEV powertrain that is used here. Having an existing model saved many hours of work that would be involved if a model had to be built. Obtaining all the necessary operating maps and efficiency maps for a production vehicle would be very difficult and probably not possible in some cases without testing individual components to generate the data. This is beyond the budget constraints of this project, therefore meaning that estimations and assumptions would have to be incorporated thereby bringing inaccuracy into the model. On the other hand there is confidence in the model provided in Autonomie as it has been developed by teams that have tested the powertrain components, and validated the model against a physical vehicle at Argonne National Laboratory.

3 Methodology

This chapter describes the methodology used in all aspects of investigations carried out within this project. This includes the test vehicles and their data logging instrumentation that was used for the experimental testing, and the software used for vehicle simulations and for drive cycle development. The testing processes are covered along with the associated data processing that is involved, including vehicle tests on the road and in the laboratory, and the Prius HV battery testing. The drive cycle development process is detailed, and included within this is the surveying of one of the drive cycle routes to incorporate gradients.

3.1 Test Vehicles

3.1.1 Toyota Prius

The primary test vehicle used for this research project is a 2004 model second generation Toyota Prius. Details of this vehicle can be seen in Chapter 1. The original idea for this research project was to remove the powertrain from a hybrid vehicle and set it up in a laboratory on a test rig. As the body shell was not required, an accident damaged salvage car was purchased which had rear end damage that did not intrude on any powertrain or mechanical components of the car. It was then determined that the specialist technical labour required, the available budget and timeframe involved meant it was not viable for this project. As the vehicle had

already been obtained it was repaired to be used as a mobile test vehicle for use on the road or chassis dynamometer. The initial phase of repairs involved the minimum required to be made road legal but still with some cosmetic damage. When the test plan was confirmed for the vehicle to be used in service with Loughborough University Security more comprehensive repairs were carried out so that the vehicle looked presentable. At this point vinyl signwriting and graphics were designed and applied to the car as shown in Figure 3.1.

Figure 3.1: Toyota Prius test car with signwriting applied

3.1.1.1 Toyota Prius Instrumentation

The Prius is equipped with added sensors and data logging equipment that were installed for monitoring the vehicle during testing. A schematic diagram of the instrumentation, of which the contents will be discussed in this section, is shown in Figure 3.2. The outline represents the car with the front to the left, in which the items are located in the approximate position that they are installed in the car. In this diagram blue lines represent power connections and orange lines represent signal or data connections. Connections to the left hand side of items are inputs and connections on the right hand side are outputs.

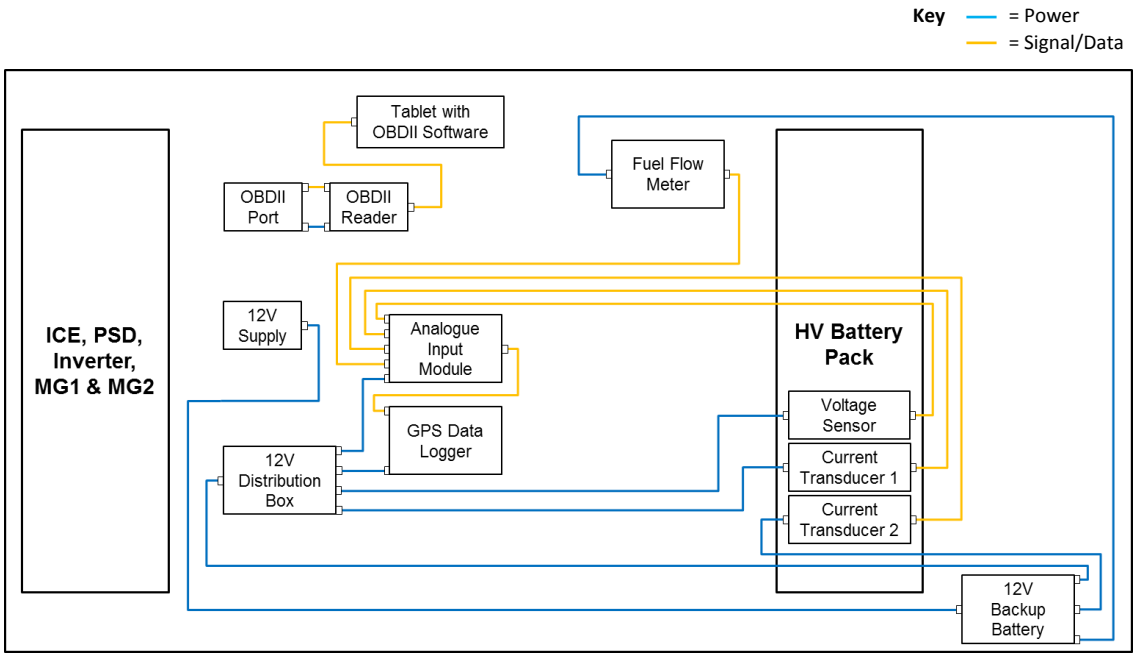

Figure 3.2: Prius instrumentation schematic diagram

An ICP DAS GT-540 GPS data logger is installed with an ICP DAS M-7017 analogue input module connected with 8 inputs. This logger was chosen as it met the key criteria required which included:

- 1 Hz logging frequency
- 0-5 V Voltage input signal
- GPS
- 4+ Analogue inputs
- Functionality to send the data by email using a GPRS connection
- Cost within the limited budget available

The function to remotely send the data was wanted so that when the vehicle was in use it did not require regular access with a computer to download the data in person. Once the data collection had started it became apparent that this function was not required though as the inbuilt 2GB memory on the micro SD card could store enough data for downloads to be only carried out every 2 to 3 weeks.

Figure 3.3: HV battery electronics with Isaac current and voltage sensors installed

Sensors produced by Isaac installed on the high voltage battery pack are connected to the data logging system, as shown in Figure 3.3. A SENVDC-251 250v voltage sensor and SENADC-301 +/-300A current transducer measured the voltage and current in and out of the battery respectively. These sensors were specified based on the same ones already being installed in a similar departmental hybrid test vehicle. Later, as discussed in Chapter 4, a lower current range LEM HAIS 50P current transducer was also installed. This is a low cost PCB-mounted sensor that we produced the necessary circuit board for to output a 0-5 V signal to connect into the existing system.

In order to measure fuel consumption, quick-release inline fuel connections were installed in the vehicle cabin to connect a fuel flow meter. A Corrsys Datron DFL 1x-5bar fuel flow meter was temporarily installed during chassis dynamometer testing.

Figure 3.4: Data logger, input module and 12V supply distribution box installed in glovebox

The instrumentation system was installed unobtrusively in the vehicle keeping the appearance tidy and like that of a standard car. This is to avoid drivers changing the way they drive, which they may have done if they had a constant reminder that it is a research test vehicle, and to prevent any damage to or tampering with the installation. The data logger and analogue input module were installed in the glovebox in the dashboard, as shown in Figure 3.4, as there was sufficient space here and it is close to a switched 12 V supply. The Prius has a 12 V power supply point in the centre console compartment so a feed was split from this and led under the dashboard into the glovebox to power the data acquisition (DAQ) system. This is powered on and off with the vehicle ignition. A distribution box provides 12 V supplies to the data logger and input module, and to each of the sensors in the HV battery pack along wires traced along the side of the car on the path of the vehicle's existing wiring loom under the trim. Signal wires were laid in the same way from the front to rear of the vehicle connecting the sensors to the analogue input module. The current drawn from the DAQ system is milliamps so will have negligible effect on the vehicle energy use. The interior of the Prius partially disassembled during the instrumentation installation can be seen in Figure 3.5.

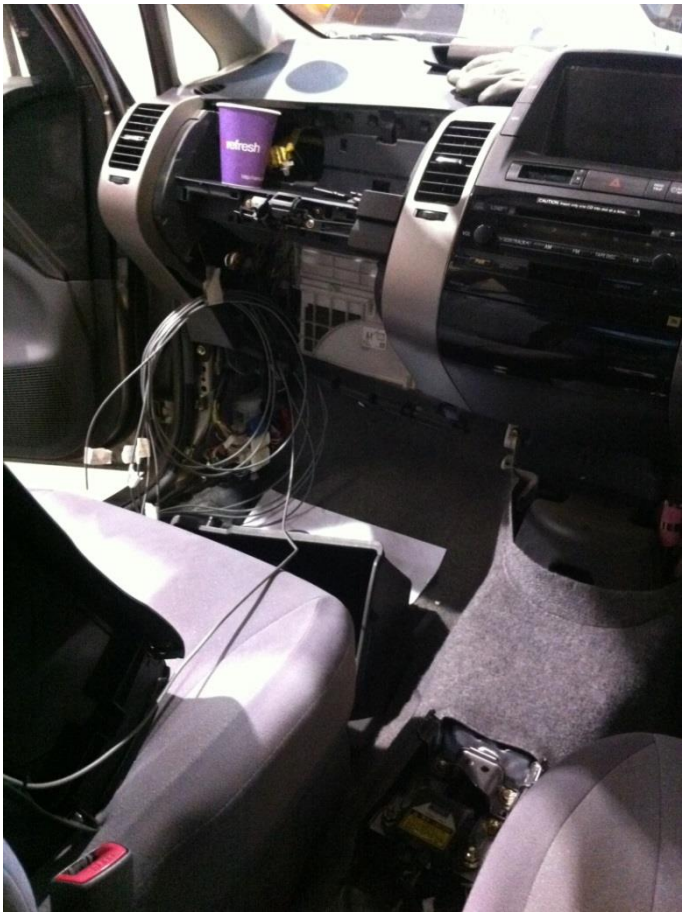

Figure 3.5: Prius during instrumentation installation

Later it was noticed with another test vehicle that occasionally data would not be logged. This was determined to be due to at the ignition-on point the vehicle would sometimes draw enough current that it would pull its 12 V battery supply down to below the 10 V minimum required to power the data logger. This meant that the logger would not switch on so would not record any data until the next time the ignition had been cycled. To resolve this, a small backup battery unit was produced to power the DAQ system to ensure that it always had enough voltage to operate. This was connected to the switched 12 V supply so that when the ignition is switched on it becomes live and powers the DAQ system. Whilst the vehicle is running it is charged, and when the ignition is switched off a 30 second delay timer keeps the supply on to ensure that the data logging is not cut off too abruptly at the end. This unit was installed in a corner compartment under the boot floor with the switched 12 V supply re-routed to pass into this backup unit before the distribution box in the glove box, as shown in Figure 3.2.

To monitor the battery SOC an OBDLink MX reader to monitor and record CAN (Controller Area Network) data was used, linked by Bluetooth to an Android tablet computer. This OBDII reader was chosen due to it being high speed with good reliability reported, and having a power saving function that means it can be left plugged into the cars' diagnostic port permanently without draining the 12V battery. On the tablet the Torque Pro application was used with custom parameter IDs (PIDs) imported specifically for the Prius II that were obtained from a Prius online forum [70]. This meant that that many extra signals were available including battery SOC, battery current, voltages for pairs of battery modules, and MG1/MG2 motor speeds.

3.1.2 Smart Electric Drive

A pure electric vehicle (EV) was tested as a comparison to the HEV to compare the energy consumption for the two different types of low carbon vehicle powertrains. A 2010 model *Smart ForTwo electric drive* was used for this purpose. The *Smart* is a significantly smaller and lighter car than the Prius but was chosen due to accessibility of an instrumented test vehicle. To compensate for the extra weight, results can be normalised by mass to enable more equal comparison of the vehicles.

The car tested was one of the pre-series production evaluation models with a Zytek developed powertrain, shown in Figure 3.6.

Figure 3.6: *Smart electric drive*

This pure electric vehicle has a 30 kW electric motor which operates usually up to 20 kW with a kick down boost function to the full 30 kW for up to 2 minutes when the accelerator pedal is fully applied. The battery is a 16.5 kWh lithium-ion pack that gives a quoted range on the NEDC of 84 miles, and from first-hand experience gives 60 to 70 miles in real-world driving. Maximum speed is electronically limited to 100 km/h (62 mph) to conserve battery range. There is regenerative braking energy recovery when the vehicle is coasting or braking. The battery is charged from a mains electricity 13 amp supply using an on-board 3 kW charger. Charging takes approximately 8 hours for a full charge from 0-100% of the available battery capacity or 4 hours for a "quick-charge" from 20-80%. A specification summary is shown in Table 3.1.

Table 3.1: *Smart electric drive* specification

Battery	
Battery type	Lithium-ion
Battery capacity (Ah)	16.5
Motor	
Motor power (kW)	30
Energy Consumption	
Range on NEDC (km / mi)	135 / 84
Performance	
Maximum speed (km/h / mph)	100 / 62

3.1.2.1 Smart Electric Drive Instrumentation

For data acquisition a Racelogic VBOX II Lite with a CAN02 module was connected to the vehicle's CAN system. Many channels are available through this system such as currents and voltages at different points in the system, vehicle speed and ignition key on/off. The VBOX can be set to log at 1 Hz or higher frequency if desired.

3.2 Vehicle Simulation

Autonomie was used for vehicle simulations as discussed in Section 2.7, with version v1210 used. The purpose for using simulations was for comparison and validation of physical vehicle test results, and for investigating operation inside the vehicle powertrain at a component level for the purposes of explaining vehicle test results obtained.

3.2.1 Autonomie Operation

Autonomie can be used for carrying out drive cycle tests as well as performance tests. Speed against time drive cycles can be run using inbuilt cycles or by importing your own to use, as was necessary in this project. Each time a simulation is run Autonomie builds the vehicle model from its constituent components then runs the programmed simulation, or multiple simulations, using that model.

As mentioned earlier, the Autonomie software was chosen due to it containing an inbuilt second generation Toyota Prius vehicle model that could be used and modified during this project. The overall powertrain model layout can be seen in Figure 3.7. Outside of this model there are also models for the vehicle powertrain controller, a driver and the environment.

Figure 3.7: Autonomie model of Prius II powertrain

Each component within the vehicle model has its own model consisting of Simulink models, operating maps, efficiency maps, calculations and data. These can have more than one component, for example as shown in Figure 3.8 the HV battery has blocks for a controller and the plant. There are various levels to a model made up of sub-models, the top level plant model is shown in Figure 3.9, showing the input and output variables to it. The deeper level battery cell model is shown in Figure 3.10; it consists of blocks for each function with their inputs and outputs.

Figure 3.8: Autonomie HV battery model block diagram

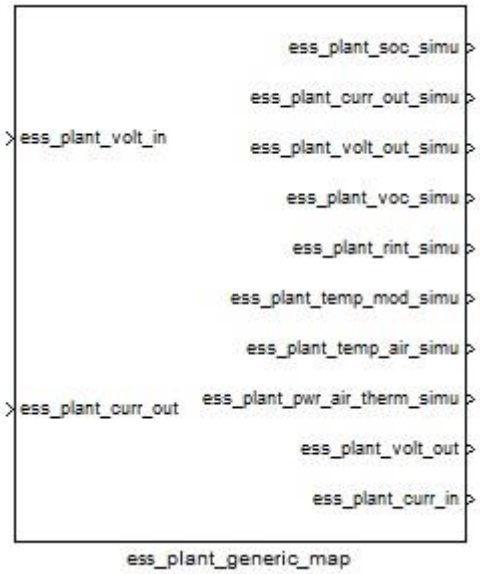

Figure 3.9: Autonomie HV battery plant model

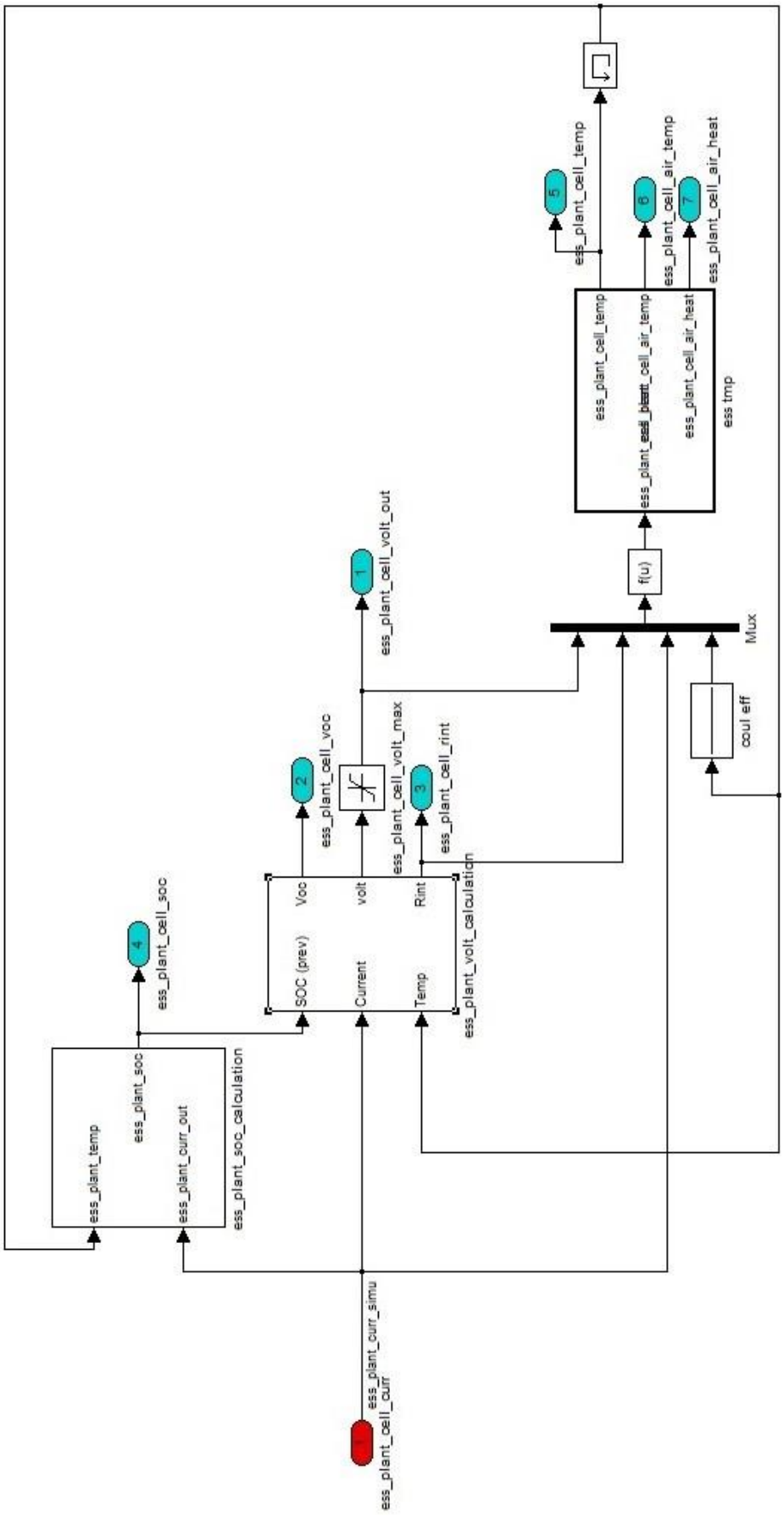

Figure 3.10: Autonomie HV battery cell model

In the following subsections the vehicle model and each of the component models are described and their equations given.

3.2.1.1 Vehicle Model

In the vehicle model a form of the standard equation for longitudinal dynamics, $F = ma$, is utilised, with the forces including aerodynamic drag and the force of gravity to overcome when climbing a gradient. The force provided by the powertrain and the vehicle losses are used to calculate the actual vehicle speed for the output. The equations are:

$$v = \int \frac{F_{in} - F_{loss}}{m_{static} + m_{dynamic}} \tag{3.1}$$

$$F_{loss} = \frac{1}{2}\rho C_d A_f v^2 + mg \sin\alpha \tag{3.2}$$

3.2.1.2 Engine Model

A requested torque is provided by the powertrain controller to the engine model which provides the torque if it is within normal operating conditions. The fuel rate and emissions associated with the torque and speed are determined, and temperature correction factors are incorporated.

The model output is engine torque and its equations are as follows:

$$T_{eng} = (1 - PWM)T_{ct} + PWM * T_{wot} \tag{3.3}$$

$$Fuelrate[kg/s] = f(T, \omega) \tag{3.4}$$

$$Emissions[kg/s] = f(T, \omega) \tag{3.5}$$

The constraint is:

$$T_{max} = f(\omega) \tag{3.6}$$

Hot and cold engine maps are used, and when during a warm up period a factor is used for the cold conditions based on engine block temperature.

$$Cold = K_{temp} * Hot \tag{3.7}$$

$$K_{temp} = 1 + \left(1 - \frac{engmap_{cold}}{engmap_{hot}}\right)\left(\frac{\tau_{hot} - \tau_{engblock}}{\tau_{hot} - \tau_{cold}}\right) \tag{3.8}$$

The model is based on the theory that a proportion of the fuel energy is used to warm-up the engine and this is balanced by the heat loss from the engine which is proportional to the warm-up state of the engine.

$$K_{temp} = \int \left(\frac{fuelrate}{fuelrate_{max}} * \frac{1}{t_{warmup}} - \frac{K_{temp_{n-1}}}{t_{cooldown}} \right) \tag{3.9}$$

3.2.1.3 Exhaust Model

The catalyst temperature is computed using an asymmetric first order linear model and exhaust emissions are calculated using efficiency maps. The equations for these are as follows:

$$Emission_{cat} = (1 - Eff) Emission_{eng} \tag{3.10}$$

$$Eff = f(\tau_{cat}, Equivalent\ ratio) \tag{3.11}$$

$$\tau_{cat} = \int \left[\frac{1}{\tau_{hot}} PWM_{eng} (\tau_{hot} - \tau_{cat}) + \frac{1}{\tau_{cold}} \left(1 - PWM_{eng}\right) (\tau_{hot} - \tau_{cat}) \right] \tag{3.12}$$

$$CO_2 = \frac{44}{12} \left[FCR_{eng} (fuelrate - HC) - \frac{12}{28} CO \right] \tag{3.13}$$

3.2.1.4 Electric Motor and Generator Model

The motor controller provides the demanded torque from the powertrain controller. The effect of losses and rotor inertia are taken into account when calculating the current corresponding to the produced torque. The temperature is taken into account by limiting the time allowed to run above continuous torque. The model outputs are torque and current, the equations are:

$$T_{out} = PWM * T_{max} \tag{3.14}$$

$$I = \frac{P_{mech} - P_{loss}}{V} \tag{3.15}$$

$$P_{loss} = f(\omega, T) \tag{3.16}$$

The constraints are:

$$T_{max} = min\big[-K_{temp} * T_{max\,peak} + K_{temp} * T_{max\,cont}\ ,\ T_{max\ allowed\ by\ I_{max}\ at\ actual\ V}\big] \tag{3.17}$$

$$K_{temp} = \int \frac{1}{t_{max}\ at\ overtorque} \left(1 - \frac{T_{act}}{T_{max\,cont}}\right) \tag{3.18}$$

The generator controller includes the effects of losses, inertia, the generator's speed-dependant torque capability, and the controller's current limit. Power losses are modelled by a 2D lookup table indexed by rotor speed and input torque. The model outputs are current and rotational speed for which the equations are:

$$I = \frac{P}{V} \tag{3.19}$$

$$\omega = \int \frac{T - T_{loss}}{\sum J} \tag{3.20}$$

The constraint for continuous and peak torque in propelling and regenerative conditions is:

$$T_{max} = f(\omega) \tag{3.21}$$

3.2.1.5 Battery Model

The battery pack is modelled as a charge reservoir and an equivalent circuit with parameters that are a function of the remaining charge in the reservoir. The equivalent circuit accounts for the circuit parameters of the battery pack as though it is a perfect open circuit voltage source in series with an internal resistance. The model output is voltage and its equations are:

$$V = No_{cells}(V_{OC} - I * R_{int}) \tag{3.22}$$

$$V_{OC} = f(SOC\ , \tau) \tag{3.23}$$

$$R_{int} = f(SOC\ , \tau) \tag{3.24}$$

$$\tau = \int \frac{Q_{ess\ gen} - Q_{ess\ case}}{m * C_p} \tag{3.25}$$

$$SOC_{abs} = Ah_{max} - \int \frac{I * Coulomb\ eff.}{3600} \tag{3.26}$$

$$Ah_{max} = f(\tau) \tag{3.27}$$

$$SOC_{usb} = \frac{SOC_{abs} - SOC_{min}}{SOC_{max} - SOC_{min}} \tag{3.28}$$

The constraints of the battery model are:

$$P_{max\ dis} = min\left[\frac{V_{OC}^2}{4 * R_{int}}, \frac{(V_{OC} - V_{min})V_{min}}{R_{int}}\right] \tag{3.29}$$

$$P_{max\ chg} = \frac{(V_{max} - V_{OC})V_{max}}{R_{int}} \tag{3.30}$$

3.2.1.6 Gearbox and Final Drive Models

The gearbox model allows the torque multiplication and speed division based on the ratio command from the powertrain controller. The losses are taken into account using torque losses. The model outputs are torques and rotational speeds. The equations are:

$$T_{out} = Ratio(T_{in} - T_{loss}) \tag{3.31}$$

$$T_{loss} = f(T_{in}, \omega_{in}, Ratio) \tag{3.32}$$

$$\omega_{in} = Ratio * \omega_{out} \tag{3.33}$$

$$J_{out} = \left(J_{in} + J_{tx_{shaft\,1}}\right) Ratio^2 + J_{tx_{shaft\,2}} \tag{3.34}$$

For neutral conditions:

$$\omega_{in} = \int \frac{T_{in} - T_{loss}}{J_{in}} \tag{3.35}$$

$$J_{out} = J_{tx_{shaft\,2}} \tag{3.36}$$

The final drive model's function is to apply a fixed reduction ratio to torque and speed by taking into account the losses. Outputs are torque, rotational speed and inertia. The equations are:

$$T_{out} = Ratio(T_{in} - T_{loss}) \tag{3.37}$$

$$T_{loss} = f(T_{in}, \omega_{in}) \tag{3.38}$$

$$\omega_{in} = Ratio * T_{out} \tag{3.39}$$

$$J_{out} = J_{in} * Ratio^2 + J_{compo} \tag{3.40}$$

3.2.1.7 Accessories Models

The mechanical accessories model takes into account the mechanical losses associated with the powertrain. The torque losses are subtracted from the engine torque. The outputs are rotational speed and torque for which the equations are:

$$\omega_{in} = \omega_{out} \tag{3.41}$$

$$T_{out} = T_{in} - \frac{P_{acc} * Eng_{on} * (\omega_{eng} > \omega_{idle})}{\omega_{in}} \tag{3.42}$$

The electrical accessories model takes into account the electrical losses associated with the powertrain. The current losses are subtracted from the energy storage. The outputs are voltage and current which have the following equations:

$$V_{out} = V_{in} \tag{3.43}$$

$$I_{out} = I_{in} - \frac{P_{acc}}{V_{in}} \tag{3.44}$$

3.2.1.8 Wheel Model

The wheel model converts rotational energy into linear, converting ω into v, and T into F, which are the two outputs. The losses due to mechanical brakes and tyre friction are accounted for, and the equations are:

$$F = \frac{T}{r_{wheel}} \tag{3.45}$$

$$T = T_{in} - T_{brake} * PWM \tag{3.46}$$

$$v = \frac{\omega}{r_{wheel}} \tag{3.47}$$

$$m_{dynamic} = \frac{\sum J + J_{wheel}}{r_{wheel}^2} \tag{3.48}$$

3.2.2 Simulation Tests

In this project a variety of drive cycles were tested in the simulations including existing cycles and newly developed cycles, so drive cycles had to be imported into the software. Although the UDDS and Artemis Urban cycles are built into Autonomie, all cycles that were used were imported to ensure complete consistency with those used for chassis dynamometer testing. To import drive cycles requires some formatting of the speed-time trace in MATLAB to generate the necessary files. This includes assigning to variables the time, speed in m/s, gradient if applicable, ignition key-on array, and a cycle name, which are then saved into a .mat file. The import cycle function can then be used to load and save the cycle into the software for use.

The built-in Prius model was used for carrying out drive cycle simulation tests. Initially the only changes to the model included setting the mass to 1375 kg which was the measured weight of our test vehicle, and the initial SOC to 60% which is the vehicle's target charge level that it will typically operate at [19]. The original

settings for these are 1449 kg and 70% respectively. Further changes were later made to the model, which are described in the relevant following sections.

A conventional diesel vehicle model similar to a Citroën Berlingo 1.6 HDI was also used for a basic comparison study to the HEV. For this a model was built using inbuilt components by choosing ones closest to the specification of the Berlingo. Default parameter values such as the engine capacity, maximum power, maximum torque, frontal area, wheel and tyre size, etc. were changed to the values for the Berlingo.

3.3 Real-World Vehicle Road Testing

The main on-road real-world testing was carried out by the Loughborough University Security department. The Toyota Prius was put into use as one of their regular patrol vehicles for nine months and was driven on a daily basis across three shifts that covered 24 hours a day. This usage meant that a lot of miles were covered and therefore a large amount of data could be collected. The driving was mainly around the university campus and some use was in the local area, so the driving was all urban. This testing is relevant to various other usages within an urban environment with similar driving patterns, for example a delivery vehicle or commuting.

During the test period Security kept log sheets with the vehicle's mileage whenever it was used and when any fuel was added, which would be used to work out the average fuel consumption. Corresponding CO_2 emissions were estimated using the carbon content of the fuel and the amount of fuel used.

3.3.1 Security Driving Fuel Records Analysis

From the vehicle mileage and fuel records for the 9 months test period the data was split into sections as close to one month duration as possible using selected refuelling points as the separators. This was so that the average fuel consumption over each month could be calculated using all the refuelling data for between these points. A table was constructed with the mileage at the start and end point of each month and the amount of fuel added during this period. From this the monthly fuel consumptions could be calculated and the overall consumption for the whole period. It should be noted that from the vehicle logs it was not possible to distinguish precisely when during a day's use the vehicle was refuelled so there may be a small amount of error in the monthly total mileages and fuel consumptions due to accounting for the miles covered on the day of the start of a new month. For consistency in the data processing, all refuelling logs against the first vehicle use of the day were assumed to be carried out at the start of a day, and all refuelling logs against the last vehicle use of the day were assumed to be carried out at the end of a day.

3.3.2 Driving Data Processing

GPS data logged while the Prius was in use was processed to develop a drive cycle representative of urban driving. The raw CSV (comma-separated values) data files from the data logger were generated with poor formatting with all the GPS data stored in the same column, so an Excel macro was produced to format the data into a usable form. An example of the raw data is shown in Appendix 1. The macro splits the GPS data into separate columns in order to use the speed from it. For the rows that the GPS status is active, the speed, which is logged in knots, is converted to km/h. Similarly the time is separated from the date, and then the time and speed columns are copied and pasted into a new workbook which is saved. A sample of some output data can be seen in Appendix 2 (a).

A MATLAB programme was written, using MATLAB R2010a, to process these CSV files and output them in the two-column format required for use in the Cenex Fleet Carbon Reduction Tool (FCRT) software, which will be discussed in Section 3.4. An example of the output data is shown in Appendix 2 (b). The functions of the programme are as follows:

- Round down small fluctuations in speed below 1 km/h that were logged when the vehicle was stationary, by replacing the values with zero
- Cut down zero-speed periods that are longer than a predefined length reducing the maximum idle times to this limit
- Check first and last speed values are zero, if not inserts them as necessary
- Edit sections with a large jump in speed caused by the vehicle setting off before a GPS fix is found, meaning that logging started mid-journey, or due to loss and regaining of GPS signal
- Save speed and time data as a CSV file

In the first version of this programme that was used initially, for any of the speed jumps the data were smoothed by inserting a linear gradual change in speed between the two speed points. Instead of this, as an improvement in a later version of the programme which is described in more detail in Chapter 5, the section of data from the jump continuing until the next stop occurs is removed. The

programme process is shown in the flow chart in Figure 3.11 and a copy of the programme code is in Appendix 3.

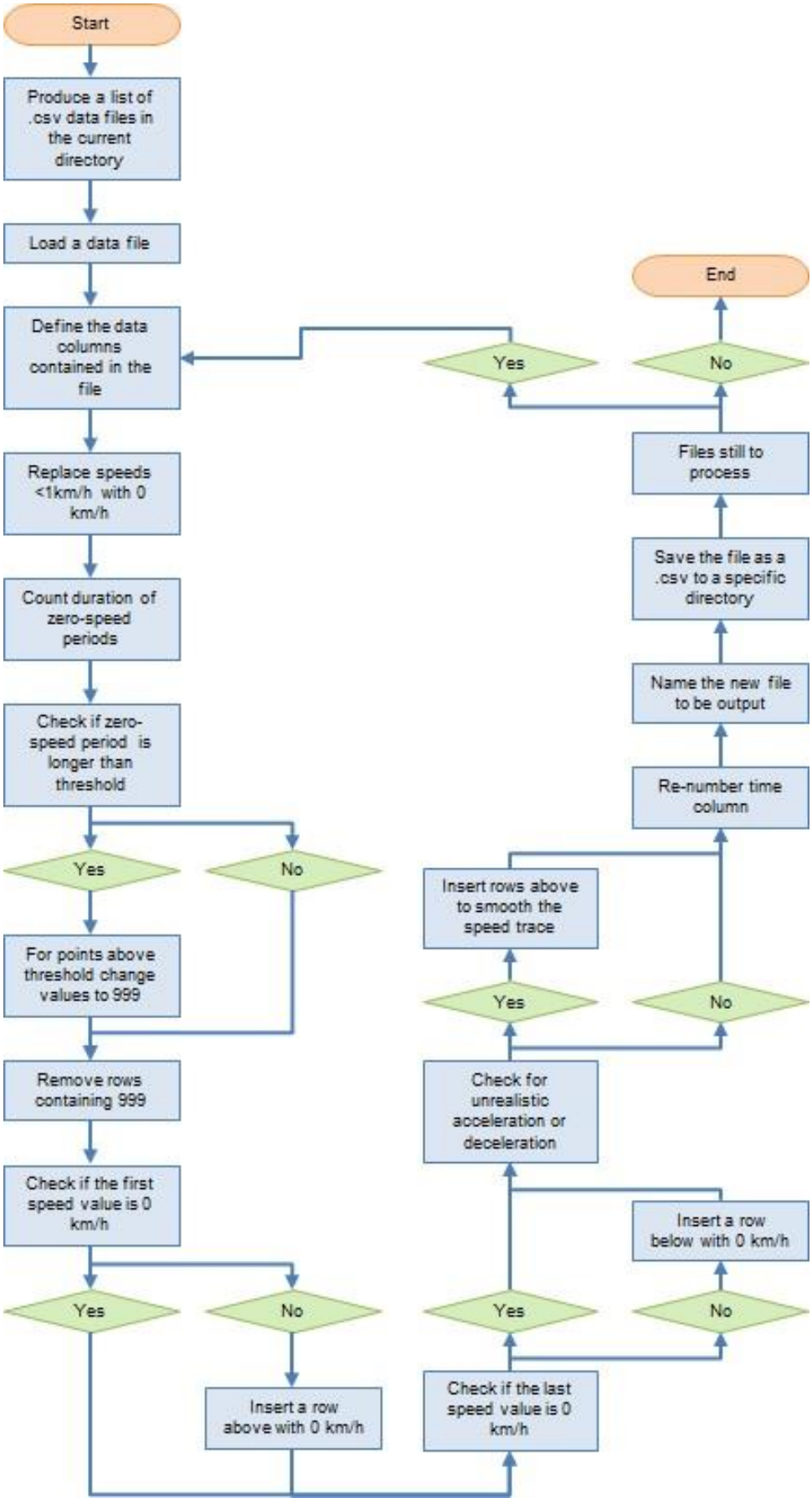

Figure 3.11: Driving data processing MATLAB programme flow chart

3.4 LUUDC Drive Cycle Development

A considerable amount of time was spent on the development of the real-world Loughborough University Urban Drive Cycle (LUUDC), for which the processes involved will be discussed in this section.

3.4.1 Cenex FCRT Software

The drive cycle construction function within Cenex's Fleet Carbon Reduction Tool (FCRT) was used to generate the drive cycle from the logged data. This software was used as access to it was available due to doing other work in partnership with Cenex, and saved time compared to developing our own programme.

The FCRT cycle construction operation process is as follows. The CSV driving data files are loaded into the software and statistics for each one are calculated. The statistics are aggregated to give a single set of target values for the generated cycle to meet. The data in each input file is split into segments; a segment is a continuous length of driving data. These short fixed length segments are matched to the software's inbuilt criteria of speed thresholds to be designated as a specific driving type, which is either urban, road (A-/B-road), or motorway. Adjacent segments with the same designation are merged and the segment boundaries moved to the nearest point of minimum speed. All segments are entered into a pool from which segments are selected at random when constructing a drive cycle. Based on a target cycle duration input by the user, a selection of segments consisting of equivalent proportions of each road type as the full dataset has, are joined together. After each segment has been selected and added to the new cycle, any segments in the pool that would be too long, too fast or too transient that they would cause the cycle statistics to become irretrievably far from the target parameters for them to be met are removed from the pool. Finally the selected segments are shuffled randomly and appropriate idle periods added to form the constructed cycle. This drive cycle is created to be statistically representative of the larger set of driving data.

The FCRT is bespoke software produced for Cenex so there was limited detail available about the operation of the programme, and also no existing validated

results from it available to verify the use of this tool. Initial trial work using the FCRT was carried out, which indicated that short duration cycles gave less accurate fuel consumption results in the inbuilt simulation element of the software compared to longer cycles. Therefore a validation process, discussed in Sections 3.4.2 to 3.4.3, was carried out to determine the shortest duration of cycle that could be created whilst still being accurate. A relatively short cycle in the region of 30 minutes duration was desired for dynamometer test purposes.

In later studies detailed in Section 5.1 it was established that the drive cycle produced in the FCRT was not as representative of the full dataset as it could be. The FCRT was continued to be used at this point due to experience gained of the effect of the cycle and segment duration input settings, which could be expanded upon to potentially produce an improved drive cycle. This was found to be successful. The alternative option considered was to write a MATLAB programme from scratch to produce drive cycles but time constraints made this unviable.

3.4.2 Initial Drive Cycle Length Validation

Using three sets of a week's duration and a set of a month's duration of data, over 50 cycles of differing lengths from 0.5 hours to 6 hours were created. It should be noted that these were the input requested cycle durations but the output cycles were not necessarily precisely this length. Any cycle lengths given in this section, unless otherwise stated, refer to the input cycle length. Cycles with two different maximum stop durations were tested, 300 seconds (5 minutes) and 600 seconds (10 minutes) to check for variability. This stop time was set in the driving data processing programme, and the two sets of data produced.

The FCRT software has a vehicle simulation feature that gives fuel consumption and CO_2 emissions results for a drive cycle using built in vehicle models. Each cycle was run in the FCRT simulation to use the fuel consumption as a comparison measure, then for each set of cycles the mean fuel consumption and the squared difference from it for each cycle was calculated. It was found that the simulation results were generally stable for cycles of at least 2 hours and for all cases the 2 hour cycles were consistent with low squared differences. Therefore 2 hours was

the selected duration for the production of initial drive cycles. The drive cycle statistics given in the graphical user interface (GUI) for each cycle produced were also recorded and analysed but there were no clear trends seen.

Cycles with a 2 hour input cycle length were produced for each of the 38 weeks and each of the 9 months of the test period, before an overall cycle using the total 9 months' dataset was produced. Each of these 47 cycles was again run in the FCRT simulation. All the cycles showed similar fuel consumptions and the squared differences between them were small, showing that the driving dataset is consistent over the time period. The statistics for the overall cycle are shown in Table 3.2 and the cycle can be seen in Figure 3.12.

Table 3.2: Initial 2 hour drive cycle FCRT statistics

Input Duration (h)	Cycle Duration (h)	Fuel Cons. (l/100km)	CO2 Emissions (g/km)
2.0	1.61	6.10	165.02

Distance (km)	Mean Speed (km/h)	Max Speed (km/h)	Town (%)	Road (%)	Motorway (%)
22.87	14.18	58.67	97.20	2.80	0.00

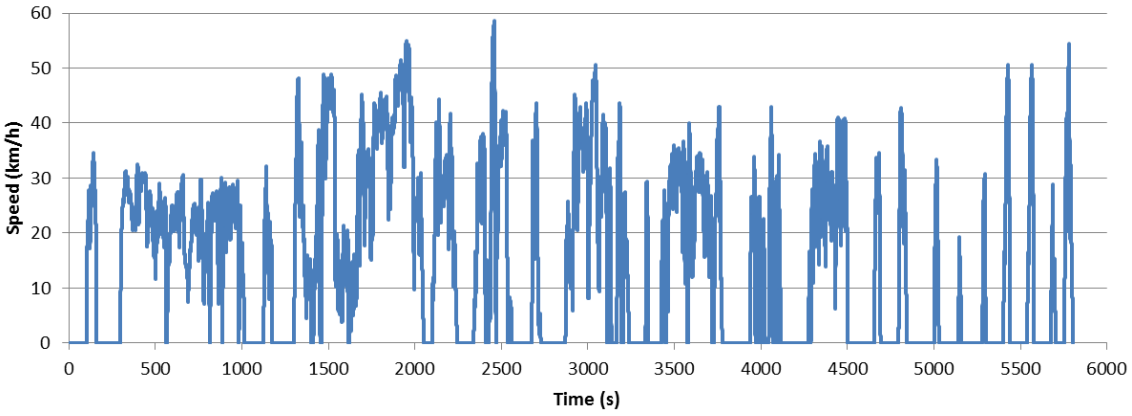

Figure 3.12: Initial 2 hour drive cycle

A shorter cycle of approximately half hour duration was required for chassis dynamometer testing purposes. Therefore from the 2 hour cycle, sections of approximately 0.5 hour length were cut out to use as candidate cycles and compared to the 2 hour cycle. However, during this process after having earlier highlighted the issues being faced in producing short drive cycles, the FCRT

software developers produced an update that meant one of these cut down cycles would not be needed. They determined that when producing short drive cycles the software could be constructing them from a small number of large segments of the input driving data, potentially only one or two, so may not be very representative of the total dataset. The FCRT software update added the functionality to specify the maximum segment length that could be used in the construction. This enabled shorter cycles to be generated with a representative number of shorter segments.

3.4.3 Revised Cycle Settings Validation

Using the updated software, cycles could now be produced with different maximum segment sizes. Similarly to previously covered in Section 3.4.2, validation was conducted by producing cycles with varying cycle lengths and then with varying segment lengths to compare the outputs of each. This was done using three sets of a week's data and three sets of a month's data. Cycle lengths of 0.5 to 4 hours were produced with a maximum segment duration as close as possible to 33% of the cycle duration, which was a suggested segment length from the developers of the FCRT software. The cycle results can be seen in Appendix 4.

The FCRT simulation fuel consumption results were consistent across the cycle length range down to the shorter sub-2 hour cycles. An exception was the 0.5 hour cycles for the weekly datasets and the third monthly set which gave significantly higher fuel consumption results than the rest of the range, particularly in the weekly cycles. The weekly cycles all had a squared difference less than 0.44, with the 0.7 hour and 0.8 hour cycles being at the low end of the range. The monthly cycles appeared to have an anomaly with the 3 hour cycles for months 2 and 3 and the 4 hour cycle for month 1, which all have low fuel consumption. Aside from these and the previously mentioned 0.5 hour month 3 cycle, the squared differences are 0.48 or lower.

To investigate the maximum segment length, a range of 0.5 hour cycles each with a different maximum segment duration within the range of 4-50% of the cycle duration were constructed. With the weekly cycles the segment length did not appear to have a significant effect on the simulated fuel consumption for 10-40%

maximum segments, with the fuel consumptions being consistent. The 20% maximum segment cycles for week 2 and 3 looked like anomalies due to higher squared differences. Increasing to 50% maximum segment length, the fuel consumption results were high compared to those with the smaller maximum segments. With the smallest 4% maximum segment length the fuel consumptions were also higher with larger squared differences.

Starting the same analysis on monthly datasets brought up a problem with the updated software; it was causing cycle creation to run very slowly with the larger dataset being used. Several days were taken to generate two cycles, so due to time constraints on access to the FCRT software the choice of settings that would be used had to be based on the weekly dataset cycle results already obtained. From experience of the first validation exercise with the old software version it was expected that similar trends would be seen for the monthly cycles.

3.4.4 LUUDC Production

Based on the above findings, for the final overall drive cycle based on the whole 9 months' driving data the target cycle length used was 0.7 hours and a 10% maximum segment length of 0.07 hours was chosen. These settings should avoid the irregularities seen in the validation process and allow the cycle to be made up of a reasonable number of segments, so should be well representative of the original data. It is also a practical length for chassis dynamometer testing. The cycle produced gave the results shown in Table 3.3 and can be seen in Figure 3.13. This cycle was named the Loughborough University Urban Drive Cycle (LUUDC).

Table 3.3: LUUDC FCRT statistics

Input Duration (h)	Input Max Segment (h)	Max Segment % of Duration	Cycle Duration (h)	Fuel consumption (l/100km)	CO2 Emissions (g/km)
0.7	0.07	10%	0.70	6.62	178.95

Distance (km)	Mean Speed (km/h)	Max Speed (km/h)	Town (%)	Road (%)	Motorway (%)
8.74	12.54	77.15	97.36	2.64	0.00

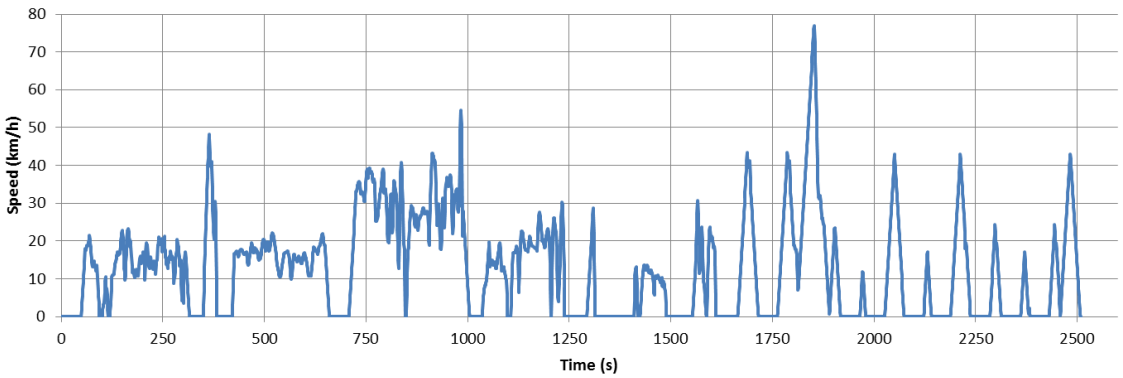

Figure 3.13: LUUDC

3.4.5 FCRT Drive Cycle Formatting

The drive cycles are output from the FCRT with 10 Hz frequency, so to use the cycles a MATLAB programme was written to convert them to 1 Hz frequency. This loads a drive cycle CSV file and defines the columns. A "for" loop uses a counter to take every tenth row from the input cycle and add it to a new array. A new output filename is defined based on the input filename, then the modified cycle is output to a CSV file. The programme code is shown in Appendix 5.

3.5 Chassis Dynamometer Testing

3.5.1 Vehicle Coastdown Tests

In order to model the Toyota Prius for the chassis dynamometer, coastdown tests were carried out at MIRA Proving Ground. Ten runs were driven in each direction on the parallel straights starting from 100 km/h, putting the transmission into neutral and allowing the vehicle to slow down to 0 km/h without driver assistance.

The data for each of the runs was identified and copied out of the data log file into individual CSV files. A velocity-time (V-T) plot of runs 1-10 can be seen in Figure 3.14 which shows very good repeatability between runs. Only half of the runs are used so that the lines can be distinguished on the graph. A MATLAB programme was written to convert the data into the necessary form. It loads a run data file and switches the data from time steps to speed steps, interpolating at 5 km/h decrements. The corresponding gatetimes, which are the measured times taken between the speed points, are then calculated. Finally the new gatetime data is output to a new CSV file.

After combining all the formatted data into a single spreadsheet, pairs of runs in opposite directions were averaged. These ten datasets were then averaged to give overall gatetimes to use in the dynamometer coastdown model. For some runs the speed did not get all the way down to zero due to approaching faster and running out of track during testing. In these cases if one or both runs of a pair did not have a gatetime those data points were not used, so they were not included in the overall average. For the last gatetime for 5 to 0 km/h there was still four data points available to include in the average. The gatetimes are shown in Table 3.4.

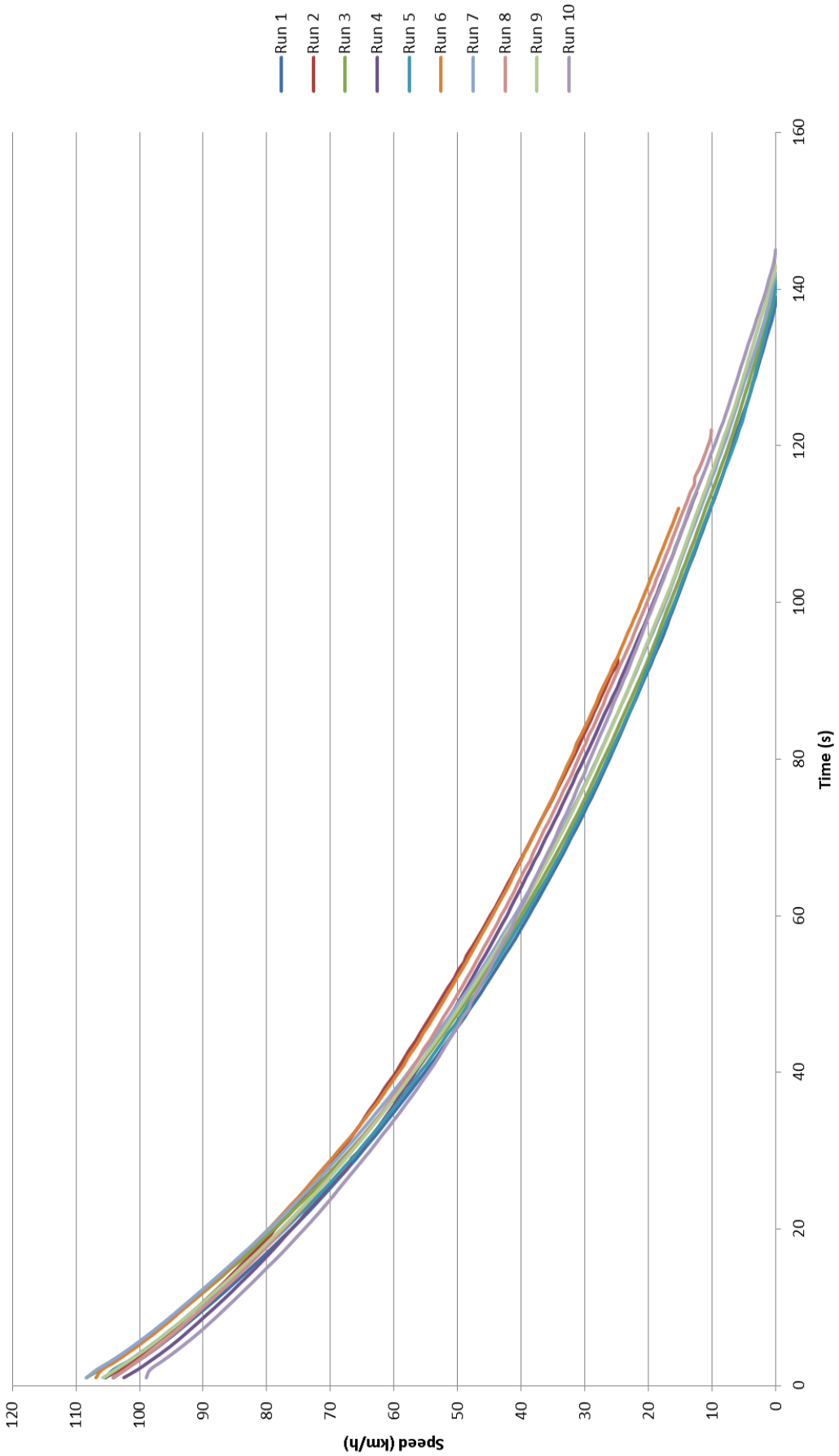

Figure 3.14: Prius coastdown V-T curves

Table 3.4: Prius coastdown gatetimes

End Speed (km/h)	Time (secs)
100	0.00
95	3.09
90	3.44
85	3.78
80	3.97
75	4.29
70	4.46
65	4.87
60	5.25
55	5.77
50	6.23
45	6.71
40	7.35
35	7.78
30	8.53
25	8.93
20	9.71
15	10.19
10	11.05
5	12.07
0	13.38

3.5.2 Chassis Dynamometer Setup

The gatetimes were entered into the Dynamotive Vehicle Manager software which uses them to generate a speed-time curve, and the corresponding coefficients of the line. The coefficients were then loaded into the Dynamotive dynamometer control software.

Before doing any testing several calibrations have to be carried out. At the beginning of a test period, i.e. when starting a week's testing, a dynamometer calibration is carried out. This calibrates for parasitic losses in the system between the torque transducer and the rollers, and the inertia of the dynamometer, so that they are accounted for in the applied force to give an accurate force at the rollers' surface.

Each time the vehicle was re-sited onto the dynamometer rollers a vehicle calibration, also known as a forced coastdown, was carried out. This involves the dynamometer running to a high speed then forcing the vehicle wheels to decelerate

following the road load coastdown curve. The motor force to do this is recorded over the speed range, to be applied to the vehicle model.

Following a vehicle calibration, vehicle coastdowns are carried out to check that the times match up accurately to the modelled times. These tests simulate those carried out on a test track. It involves the rollers driving the vehicle wheels up to a speed above the coastdown starting speed, then is left to decelerate under the resistance of the vehicle coastdown model with gatetimes recorded in the process.

To set up the vehicle on the dynamometer it is positioned with the front wheels square to the rollers and parked on the wheel supports. Straps to stop lateral movement are attached to the front towing eye and the other ends to eye bolts on the lab floor leaving them slack. A longitudinal strap is attached to the car's rear tow eye, again with some slack to allow for movement. Safety guards are fitted around the rollers and the exhaust gas extraction pipe is connected to the vehicle exhaust pipe. A cooling fan is positioned in front of the vehicle aligned with its cooling intake. The vehicle is put into neutral and the handbrake applied. The dynamometer is then run slowly at 5 km/h to allow the vehicle to centralise itself on the rollers with a driver to deal with any steering input required. The ratchet straps are then tightened but without applying pressure on the vehicle to allow for any small movements during testing, whilst avoiding any additional pressure being applied onto the rollers which could affect the recorded results. The setup is shown below in the diagram in Figure 3.15.

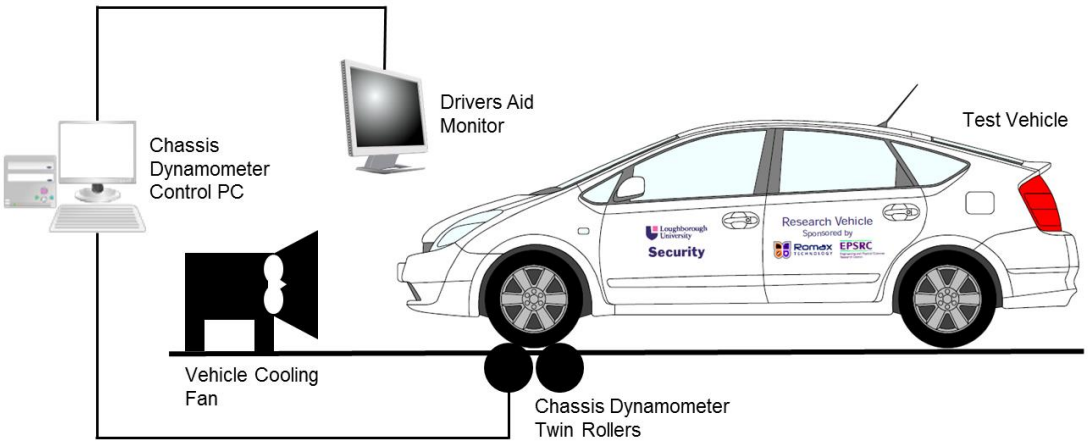

Figure 3.15: Diagram of chassis dynamometer setup

For drive cycle testing a PC with an NI LabVIEW VI is used to read drive cycle files and display them to the driver on a driver's aid monitor. For this the drive cycles have to be saved in text files with extra columns containing limits for the duration of the cycle and for the y-axis to cover the maximum speed range that it contains.

3.5.3 Chassis Dynamometer Test Procedure

A chassis dynamometer operating guide was written including the setup procedure from the previous Section 3.5.2 and the operating procedure, it can be found in Appendix 6. Contents of the guide are summarised below.

For chassis dynamometer testing the following procedure was carried out:

1. Check tyre pressures & adjust if necessary
2. Warm up dynamometer rollers at 80 km/h for 45 minutes
3. Carry out dynamometer calibration if necessary (only at the start of a test period)
4. Position and strap vehicle in place on rollers
5. Disable vehicle traction control to allow the front wheels to be driven without the traction control interfering due to the rear wheels not turning
6. Warm up vehicle engine, tyres and transmission on rollers by driving at a constant 80 km/h for 30 minutes
7. Carry out vehicle calibration
8. Carry out vehicle coastdown
9. Condition HV battery
10. Run drive cycle tests

Figure 3.16 shows the Prius test car set up on the chassis dynamometer.

Figure 3.16: Toyota Prius II test car on Loughborough University chassis dynamometer

To measure the fuel consumed, a fuel flow meter was installed in the car. To do this an extension was added to the fuel line out of the fuel tank that passes into the car's interior with inline quick release connectors. These are disconnected and connected to either side of the fuel flow meter. An additional wiring loom connects the fuel meter to a 12 V supply from the DAQ system battery, and connects the data signal outputs to spare channels on the analogue input module. The fuel flow instrumentation set up in the car is shown in Figure 3.17.

Figure 3.17: Fuel flow instrumentation set up for chassis dynamometer testing

As vehicle speed is usually measured by GPS it could not be used whilst being static inside a building during testing on the chassis dynamometer. Therefore as it could not be recorded by the vehicle, the chassis dynamometer logged speed from the rollers within the dynamometer software. This meant that there were two simultaneous data files that had to be combined. Log sheets were produced which were used for each test run to record information including the test start and finish times, start and end SOC, start and end odometer reading, and temperature, to be used in the data processing.

3.5.3.1 Smart Electric Drive Chassis Dynamometer Testing

Testing of the *Smart electric drive* was done using the same process as above with a few differences. Coastdown gatetime data was provided by Cenex so this could be loaded straight into the software. For the vehicle set up, with it being rear wheel drive, the rear wheels were positioned onto the rollers, the lateral straps were fitted to the rear towing eyes of the car and the handbrake was left off. For the vehicle warm-up in most cases it was done by leaving the vehicle in neutral and driving the wheels by the dynamometer to preserve the battery range, although sometimes the vehicle was driven. It was done at a lower speed of 50 km/h for 30 minutes to stay within the manufacturer's guidelines given for towing the car to avoid damage to

the electric motor. The *Smart* set up on the chassis dynamometer is shown in Figure 3.18.

Figure 3.18: *Smart electric drive* on Loughborough University chassis dynamometer

3.6 Vehicle Test Data Processing

3.6.1 Prius Test Data Processing

For Prius chassis dynamometer test results analysis two data files have to be merged, the one from the vehicle data logger containing the HV battery data, and one from the dynamometer PC with the vehicle speed data. This was done by finding the correct time period in the vehicle file and matching the initial increase in current drawn from the HV battery as the vehicle starts to move, to the first acceleration at the start of the speed trace. This data was copied into a new Excel worksheet for each test run and column headings were added. Additional columns were added as follows:

- Fuel flow correction which subtracts the offset at zero from the fuel reading
- Fuel flow conversion to litres per hour from the scaled logged value
- Fuel flow conversion to litres per second
- Sum of the total fuel used in litres
- Conversion of the total fuel used into gallons
- Conversion of the speed from km/h to mph
- Conversion of the speed from mph to mi/s
- Sum of the total distance covered in miles
- Calculation of average fuel consumption in miles per gallon
- Conversion of the speed from km/h to km/s
- Sum of the total distance covered in kilometres
- Calculation of average fuel consumption in l/100km
- Calculation of energy consumption from fuel used in kWh, kWh/km, MJ and MJ/km
- Conversion of battery current from logged value into Amps
- Calculation from current of Ampere-hours charged or discharged
- Sum of the total Ampere-hours charged or discharged
- Calculation of the change in SOC from the total Ampere-hours as a proportion of the total battery capacity

The energy consumption was calculated using the amount of fuel used in litres, multiplied by 31.8 MJ/litre [71] the energy content of petrol, then all divided by 3.6 giving the result in kWh.

3.6.2 Smart Electric Drive Test Data Processing

To process the data recorded by the VBOX in the *Smart* the individual test sections were found in the full data files by plotting the vehicle speed to identify the drive cycles. Similarly to the Prius data it was copied into a new Excel worksheet and additional columns were added. The columns are as follows:

- Calculation of battery power in Watts by multiplying voltage by current
- Power into the battery using an IF statement to check if the value on each row in the power column is positive
- Power out of the battery using an IF statement to check if the value on each row in the power column is negative
- Calculation of energy in Watt-hours from power
- Calculation of energy into the battery in Watt-hours from power into the battery
- Calculation of energy out of the battery in Watt-hours from power out of the battery
- Speed in km/h copied from the chassis dynamometer software logfile, matched to the CAN vehicle speed column
- Conversion of the speed from km/h to km/s

In cells at the top of the spreadsheet, totals of the energy, energy in, energy out and distance travelled are calculated. From these by dividing the energy by the distance, energy consumption in Wh/km is then calculated.

3.7 Campus Driving Testing

Tests were carried out driving across Loughborough University campus to get repeats of real-world driving on exactly the same route. This route was driven as close as possible to the ideal case of sticking to the 15 mph speed limit maintaining a constant speed when able and using light acceleration and deceleration. The route used was the main road, University Road, which runs across the campus from south-west to north-east as shown in Figure 3.19. The campus is the brown area on the map bounded by the A512 and A6004. There are university main entrances at each end of this road known as the west entrance and the east entrance, so the points for the ends of the routes will be referred to as west and east from here on.

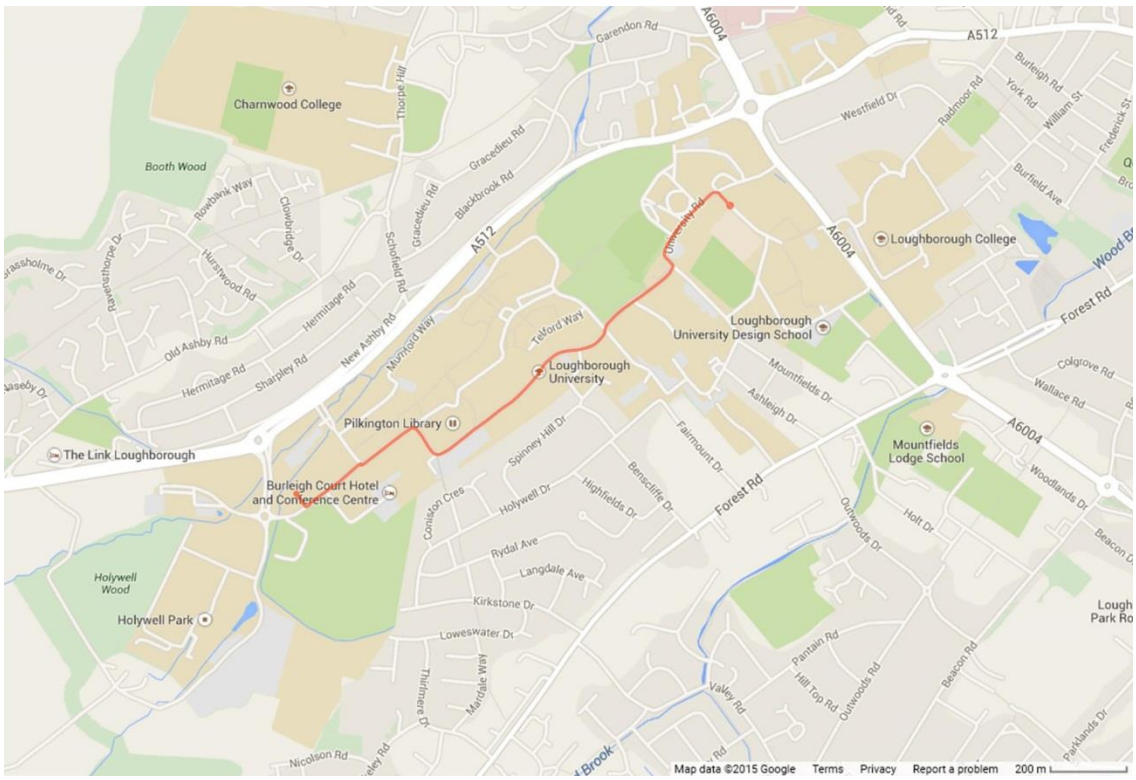

Figure 3.19: Map of Loughborough University campus showing route [72]

The tests were carried out setting off from the west edge of the campus, driving to the east edge of the campus, stopping for 2 minutes so that this point could be distinguished in the recorded data, and driving back to the west edge. The driving consisted of many small fluctuations in speed, some larger fluctuations in speed due to corners and speed bumps, and some stops due to pedestrian crossings or

road junctions. Like with the chassis dynamometer tests, log sheets were used, and these were filled in for each of the two legs of a complete test. Tests were repeated ten times and carried out in both the Prius and *Smart electric drive*. The fuel flow meter was installed in the Prius and the VBOX and CAN module were installed in the *Smart* to collect the necessary data.

As described in Section 3.3.2 the raw data files from the Prius data logger have to go through some formatting to get them into a form that can be used for analysis when the GPS data is used. They were then processed in the same way as with the chassis dynamometer test data except the speed was converted from the GPS logged speed in one of the first columns in this case. The *Smart* data files were processed in the same way as for the chassis dynamometer tests, other than the speed in km/h column was taken from the CAN vehicle speed for this on-road testing.

3.8 Campus Gradients Mapping

To investigate the effect of road gradient on fuel consumption, the gradients on the campus route used in the campus driving tests were measured and applied to the drive cycle for use in simulations. Gradient profile data was attempted to be obtained from Loughborough University Civil Engineering department, from the university Facilities Management and from ordnance survey maps, but complete data to cover the whole route could not be found. Therefore the area across the campus of interest was surveyed using a total station, similar to the one shown in Figure 3.20, and a pole mounted prism reflector. The total station uses an infrared laser to measure horizontal distances and height differences between two points from the time taken for the light to be sent to and returned by the reflector, which can be used to calculate gradients from.

Figure 3.20: Surveying using total station [73]

Measurements were taken at points along the road, working from one end to the other in sections. This involves setting up a tripod with total station mid-way along a section of road where it is in line of sight with the first measurement point and with at least one more point. One person goes to the first measurement point with the reflector and positions it here while a second person points the total station lens at the reflector and takes a reading. The position of the point is measured in east,

north and vertical (height) directions. The reflector is then moved to the next measurement point which may be nearer the camera in the same direction as the first point if there is a noticeable change of gradient to record, or alternatively somewhere in the opposite direction from the camera. Another reading is taken before the reflector is moved to another position if there is another point in sight of the camera. When all the readings with the total station in this location have been taken the total station is moved to a new location. In this position another set of readings are taken where the first measurement point for the reflector should be the same as the previous point recorded to reference it to the new station location. This process was repeated until the whole route was covered.

The differences in measurements between consecutive points were calculated which the horizontal distance could be found from using Pythagoras' theorem for the change in E and N measurements. Using Pythagoras' theorem again with the horizontal distance and the change in height, the road distance was calculated. The profile of the route in one direction from east to west can be seen in Figure 3.21 which shows the cumulative distance against height.

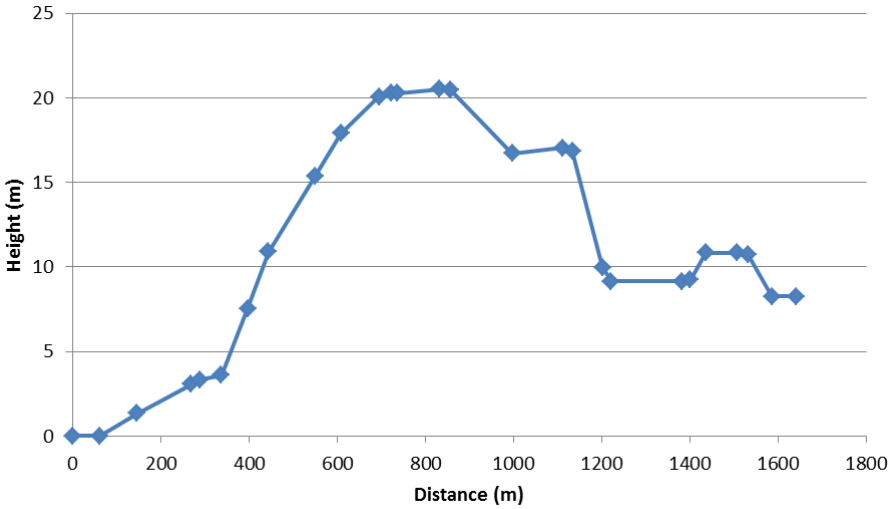

Figure 3.21: Loughborough University campus route east to west measured height profile

The route was grouped into fourteen main sections of approximately constant gradient to simplify it. Summing the distances and heights of points within each section gave totals to calculate the gradients from. The gradients were calculated from the inverse tan of the change in height divided by the distance. The new

profile can be seen in Figure 3.22, which as can be seen is very similar to the previous profile in Figure 3.21 showing that little of the definition has been lost.

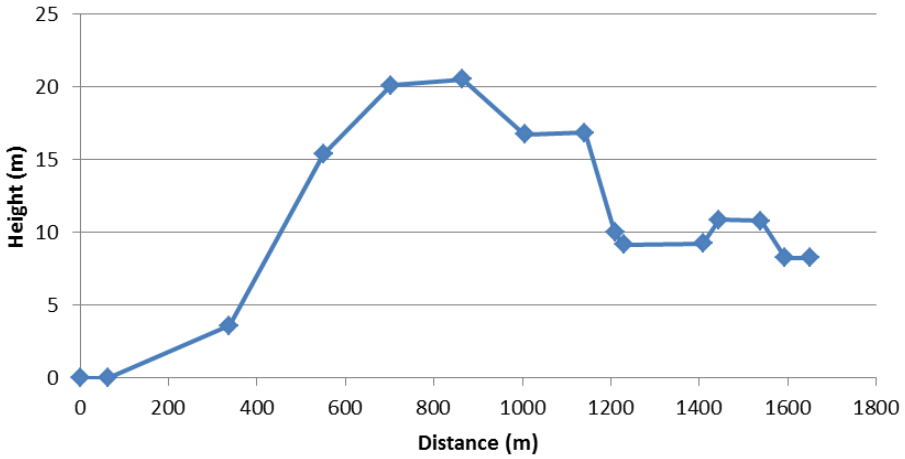

Figure 3.22: Loughborough University campus route east to west simplified height profile

This profile represents the length of the road running east to west of the campus, so to form the west to east leg of the journey this profile was reversed. The complete driving circuit route profile was then formed, as shown in Figure 3.23, by joining the two together.

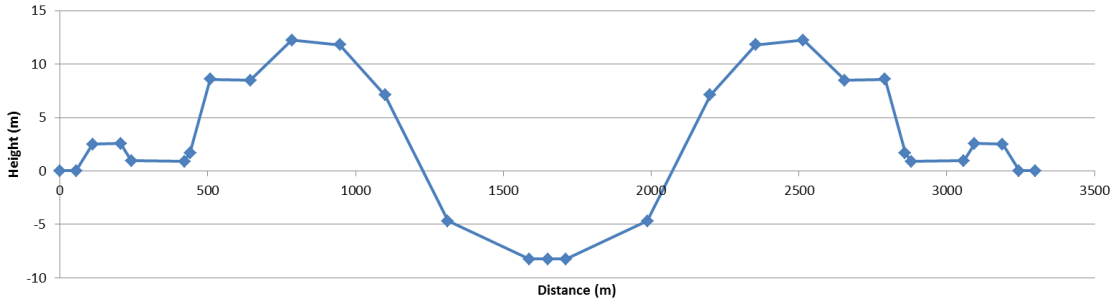

Figure 3.23: Loughborough University campus complete circuit route east to west to east height profile

3.9 LU15-UDC Drive Cycle Development

To produce a drive cycle that the gradient mapping from the previous section could be applied to, a campus driving test run logged in the Prius, as described in Section 3.7, was selected. This was done by referring to the notes recorded on the test log sheets and visually looking at the data to choose one that represented a typical average run without any irregular factors involved, such as being held up following a slow-moving grounds maintenance vehicle, or waiting in traffic.

To apply gradients in Autonomie simulations the imported drive cycle requires a gradient column after the usual time and speed columns, with a gradient value for each row of data. To do this, cumulative distance for the drive cycle was calculated from the speed, which could then be used to associate with the distance from the campus profile to find the corresponding gradient. Gradient was then assigned to each second of the cycle with the gradient changing at the relevant cumulative distance points. The resulting Loughborough University 15 mph Urban Drive Cycle (LU15-UDC) is shown in Figure 3.24. The drive cycle contains many small fluctuations in speed along with some larger spikes of deceleration and subsequent acceleration caused by corners and speed bumps on the route, and a brief 5 second stop at 289 seconds due to waiting at a mini-roundabout. A 10 second stop at 321 seconds defines the end of the first direction of travel before the start of the return leg along the same route.

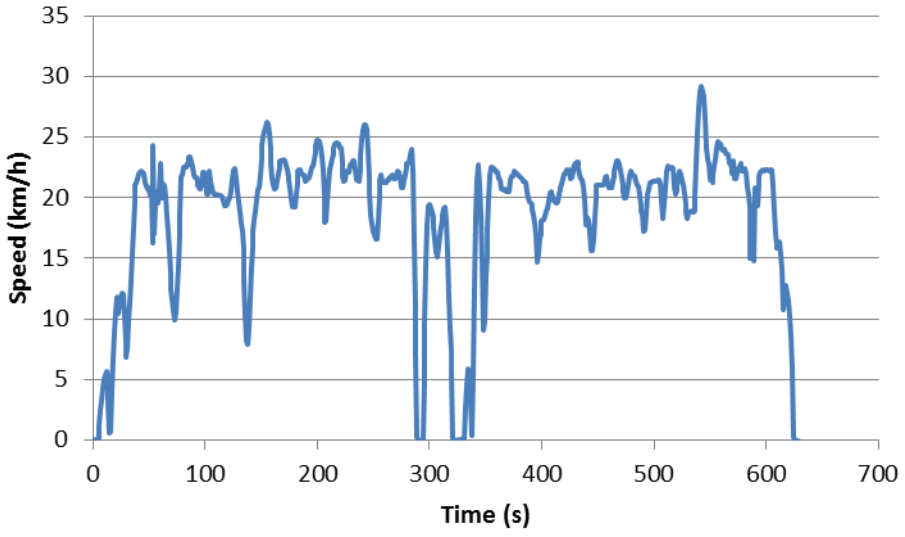

Figure 3.24: LU15-UDC

3.10 High Voltage Battery Testing

3.10.1 Battery Testing Procedure

To investigate the degradation of our vehicle's battery it was tested on the battery tester based in a laboratory at Loughborough University. The test bench built by ATE Systems consists of two independent channels, each with a power supply and electronic load to facilitate charging and discharging tests. It is connected to a host PC and programmed and operated through National Instruments Veristand software. Data from the tests is logged by a National Instruments PXIe-1073 data acquisition system. The currents and voltages are recorded along with temperature from four thermocouple wires. The battery tester and fume cupboard for the batteries to be sited in during testing are shown in Figure 3.25.

Figure 3.25: Loughborough University Battery Tester

The 28 modules were tested separately because it was expected that the modules would perform differently to each other due to their individual charge levels becoming imbalanced over time. The parameters for charging and discharging currents and voltage limits were found from Panasonic's industrial Ni-MH battery product details [74].

This indicated the values as follows:

- Minimum voltage – 1.0 V
- Maximum voltage – 1.5 V
- Maximum charge current – 0.5C
- Maximum discharge current – 1C

As the modules consist of six cells the voltage values above were multiplied by six to give a minimum limit of 6.0 V and a maximum limit of 9.0 V. A charging test programme was written which was the same for both channels. This logged the data starting with a 30 second neutral period before charging commenced at 3.25 A. If the maximum voltage was reached the charging current would be cut to zero, but during the testing the modules did not reach this voltage before they plateaued and started to decrease. Therefore the tests were monitored to identify when the module voltages peaked so that the charging could be stopped as the voltage started to decrease, which was done when the voltage had reduced by 0.02 V. This was done separately for each channel and then when charging had stopped on both channels the batteries were left to rest for 30 minutes before the logging stopped. By slightly overcharging the modules going beyond the voltage plateau ensures that all cells within it are fully charged. Due to the cells having different initial SOCs, whilst the ones that started higher start to overcharge, the lower ones have chance to catch up and reach full charge. If the modules were only charged to the peak voltage there could be some cells that have not reached their full charge. A similar discharging programme was written with a 6.5 A discharge commencing 30 seconds after the test start. When the measured voltage reached 6.0 V the current was cut off to zero (again this was independent for each channel), and then there was a 30 minute rest period.

The battery pack was removed from the vehicle to be tested. The modules are connected with bus bars which had to be removed to test them individually. The connection to the BMS was also removed so that it would not be damaged, or have any influence on the tests carried out. Each module was numbered from 1 to 28 to identify them during testing. With having 28 modules, two were tested simultaneously to reduce the time taken. Test pairs were spaced half the pack away

from each other to eliminate heat or expansion interference between the modules. A thermocouple was put at each end of each module to monitor the temperature to ensure they did not get too high. If the temperature was to go above 50°C the stability of the results could be affected and it could indicate a problem. The setup of the battery pack in the fume cupboard with two modules connected to the two channels of the battery tester is shown in Figure 3.26.

Figure 3.26: Prius HV battery during testing

The test procedure involved initially charging the module from its starting SOC to a full charge before being discharged to minimum charge level which established the capacity of it. Following this a second cycle was carried out with a full charge and full discharge to work out the charge efficiency and establish any improvement in capacity. A final cycle was carried out to identify if there was any further significant increase and to complete the module cell balancing process. This test process equated to a duration of approximately 3 hours per test for the first set, increasing to 5 hours each for the full charge and discharge cycles, and 8 hours for the third set due to an extra charge to full capacity at the end.

Upon completion of testing all the batteries, it was found that one of them had a significantly reduced capacity so required replacement. New modules are not available individually so a used one was purchased from a car being dismantled.

This was tested using the same process as the other modules. The modules are held together in the pack under compression, so to replace the faulty module that was midway along the line the pack had to be dismantled. The clamping end plate was taken off and all the modules to one side of the one to be replaced were separated and moved apart to give room for movement. The bad battery was taken out and its replacement put into the same location. The pack could then be compressed back together and reassembled ready to be refitted back into the car.

After running the tests the modules will have been left at slightly different voltages, so to balance the voltage across the modules they were all connected together in parallel. They were left like this overnight to stabilise before being disconnected. The voltages of all modules were measured and found to be exactly equal.

3.10.2 Battery Test Data Processing

To process the test data a MATLAB programme was written, which can be seen in Appendix 7. This loads the data from a test file and applies smoothing using the inbuilt "lowess" method to remove small high frequency fluctuations recorded in the measured voltage. The result of different smoothing methods was looked at by applying them to a sample data file, to find which gave the nearest result to the original data when plotted. An example plot is shown in Figure 3.27 with the original test data plotted as a black line and the smoothed data plotted as a green line. The plot shows that the smoothed data is a very accurate representation of the raw data with the lines being on top of each other, apart from the point at which the charging current is cut off and the voltage drops. This is not relevant though as the data used in the analysis is up to the maximum point of charge which is before this point. Additionally, the features of the plot are labelled in Figure 3.27.

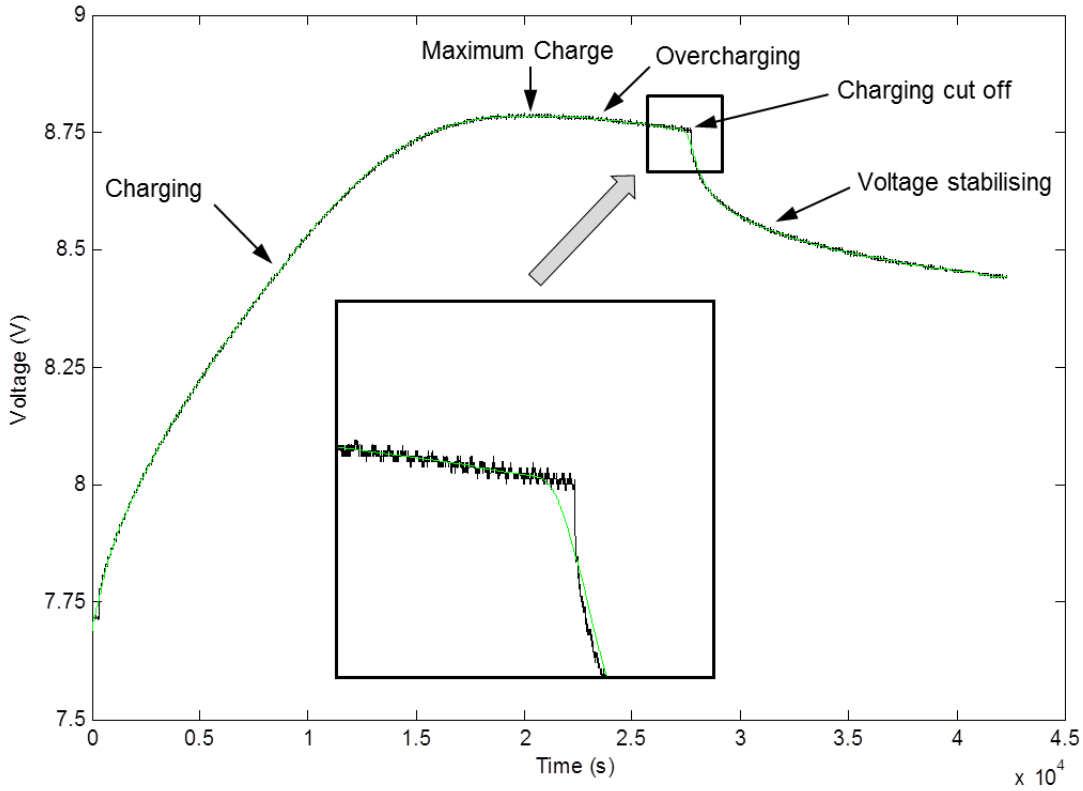

Figure 3.27: Battery module charge graph with raw data and smoothed data plotted

The maximum value of the voltage trace is found, to be used in the later processing of a charging test. The data in the requested current column are checked to determine if they are positive and therefore a charging test, or negative and therefore a discharging test. For a discharge, the current across the period where there is negative current is summed. For a charge, the current is integrated from the start of the positive current output from the power supply to the point corresponding to the maximum voltage. These summed 10 Hz currents are then converted to capacities in Ampere-hours by dividing by 10 then dividing by 3600. The change in capacity against the rated value is calculated and then the results are constructed in an array which is output as a CSV file.

3.11 Chapter Conclusions

The equipment, processes and testing within this project have been detailed in this chapter. There are some key points from this to highlight. There were several reasons for the new LUUDC and LU15-UDC drive cycles being developed rather than using existing cycles. The motivation was that they enabled the confines of test boundaries to be defined for establishing results within. It also enabled factors within drive cycle development to be studied, as discussed in Chapter 5, which highlighted how important accurate and detailed cycle development is to the output's representativeness of the original data. The LU15-UDC was required in order to be able link a drive cycle with a gradient profile to test the vehicle in real-world driving, to investigate the effect of gradient on energy consumption.

4 Effect of Gradient on a Hybrid Electric Vehicle

The detrimental effect on fuel consumption that driving on uphill and downhill gradients has compared to driving on a flat road may not be the same for a HEV as for a conventional diesel or petrol ICE vehicle. One may naturally assume that the extra energy consumed by going uphill would outweigh the saving by going downhill, resulting in higher fuel consumption than driving on a flat road. With a power-split HEV though, due to features of its powertrain this may not be the case, so in fact the gradient has negligible effect on fuel use and is a second order effect compared to vehicle mass for instance. In comparison to on the flat, when driving uphill the ICE will use more fuel although it will also be operating close to its most efficient operating region due to the control system. On the downhill though the engine will be switched off as opposed to being switched on part of the time on the flat, and also on the downhill there will be some energy recovery through the regenerative braking that operates when coasting and braking. This is therefore investigated later in this chapter to determine the effect. Firstly, the real-world driving is compared to the LUUDC, which should be equivalent, to establish how close they are. Comparisons are also made with other existing drive cycles to determine the differences that occur due to the drive cycle effect.

4.1 Initial Drive Cycle Fuel Consumption Comparison

This study formed the initial comparisons of fuel consumption over different drive cycles and derived the further areas to investigate for later work. The real-world Security department driving data was processed to determine the fuel consumption. Drive cycle tests were carried out on the chassis dynamometer, and drive cycle simulations done using Autonomie. The cycles used were the LUUDC, NEDC, ECE-15 and Artemis Urban to analyse the fuel consumption differences.

4.1.1 Real-World Security Driving Results

The monthly fuel consumption shows month-on-month variation as seen in Figure 4.1, with a range of 5.35 to 8.53 l/100km. The variation is likely to be due to different usage styles for the vehicle, of where and how it was driven. Where the highest fuel consumption occurred in month 7 the car covered a low mileage suggesting that it had been used differently to other months. The records table can be seen in Appendix 8. It should be noted that the lowest mileage in month 3 was mainly due to the car being taken off test for a week to be brought into the workshop to carry out work on the data logging system. The overall average fuel consumption over the total 11330 miles (18233 km) covered over a period of 242 days was 6.61 l/100km, or 42.7 MPG.

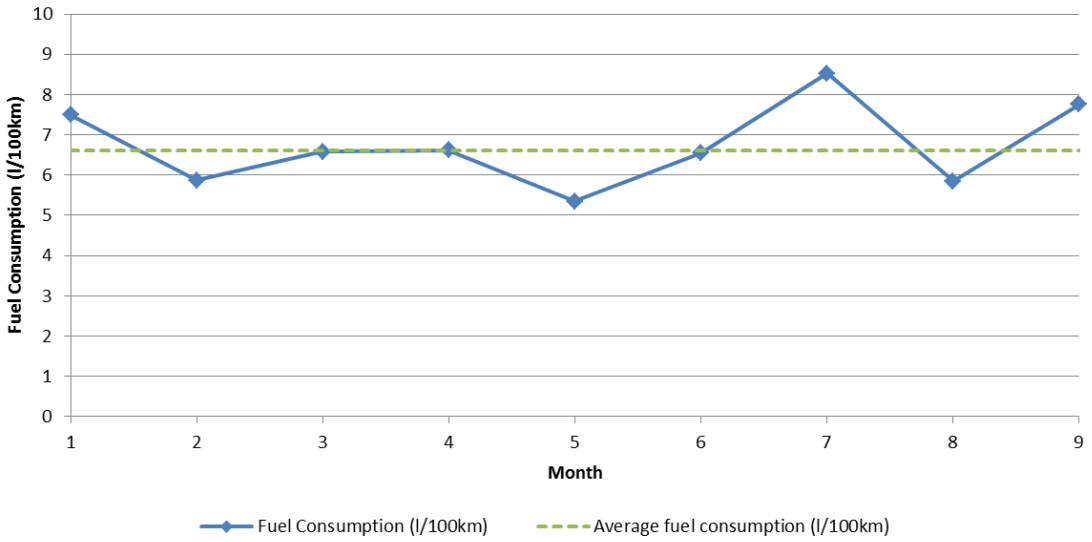

Figure 4.1: Security real-world driving monthly fuel consumption

4.1.2 Chassis Dynamometer Testing Process

During testing the HV battery current and voltage, and fuel flow were logged by the vehicle instrumentation as described in Section 3.1.1. As CO_2 emissions measurement equipment was not available, this was estimated from the fuel consumption as described later in this section. SOC measurement equipment was not available at this time so estimated SOC levels were calculated for each drive cycle test using the voltage method. This method was used as it was possible with the facilities and data available. For this, a battery discharge curve of voltage against SOC is used to find the SOC corresponding to a particular HV battery voltage. The weakness of this method is that the voltage is affected by the battery current and temperature. Additionally, as a battery degrades its discharge pattern will change, therefore not following the same curve. The results from these experiments did not appear meaningful so were not used, as described later in Section 4.1.3.

As battery SOC measuring instrumentation was not available, before running a drive cycle the vehicle was driven for 15 minutes at a constant 115 km/h, in order to condition the battery so that it would be at a similar level at the start of each different drive cycle test. This speed, equivalent to motorway cruising speed, was used as it allowed the HV battery to be charged to provide a high SOC starting point. For each cycle four runs were carried out back-to-back to be averaged to account for any experimental differences.

For the test results the corresponding CO_2 emissions were estimated from the amount of fuel consumed. The carbon content of the fuel was multiplied by an oxidation factor which accounts for the small proportion of fuel that was not oxidised into CO_2, and by the ratio of the molecular mass of CO_2 to the molecular mass of carbon. These parameters are as follows:

- Carbon content of a US gallon of gasoline – 2421 g [75]
- Carbon content of a litre of gasoline – 639.6 g
- Oxidation factor for oil products – 0.99 [75]
- Molecular mass of CO_2 – 44

- Molecular mass of carbon – 12

$$CO_2\ emissions\ [g/litre] = 639.56 \times 0.99 \times \frac{44}{12} = 2321.6\ g/litre \quad (4.1)$$

The CO_2 emissions in the standard form of g/km were then calculated using the result of this equation as follows:

$$CO_2\ emissions\ [g/km] = \frac{Fuel\ cons.\ [l/100km]}{100} \times 2321.6 \quad (4.2)$$

In the simulations the Prius model was used with the initial SOC set at 60%, the target level that the Prius BMS aims to maintain [19]. Tests were run on the same set of drive cycles as for the chassis dynamometer tests, but just one run was carried out as due to the nature of the simulations they are repeatable every time.

4.1.3 Test Results

4.1.3.1 Chassis Dynamometer Test Results

Figure 4.2 shows the fuel consumption results from the chassis dynamometer testing for each of the drive cycles tested. These fuel consumption results are in miles per gallon (MPG), where higher MPG equals lower fuel consumption. It can be seen that the fuel consumption of the first run is lower than the subsequent runs, particularly in the case of the ECE-15, and the fuel consumption for run 2 to run 4 is quite stable. The lower fuel consumption for run 1 will be due to the higher initial SOC level attained by doing the pre-conditioning. This will have changed the control strategy, allowing the vehicle to be driven by the electric motors for more of the drive cycle and using the ICE less. The change in fuel consumption between the first run and the following runs is much greater for the ECE-15 due to its linear cycle profile leading to a larger benefit from the high initial state of charge. The stability of the results of the subsequent runs indicates that after the first run the SOC is at a similar level at the start of each of these tests. From this finding, the average of runs 2, 3 and 4 were taken as the final results for the chassis dynamometer tests.

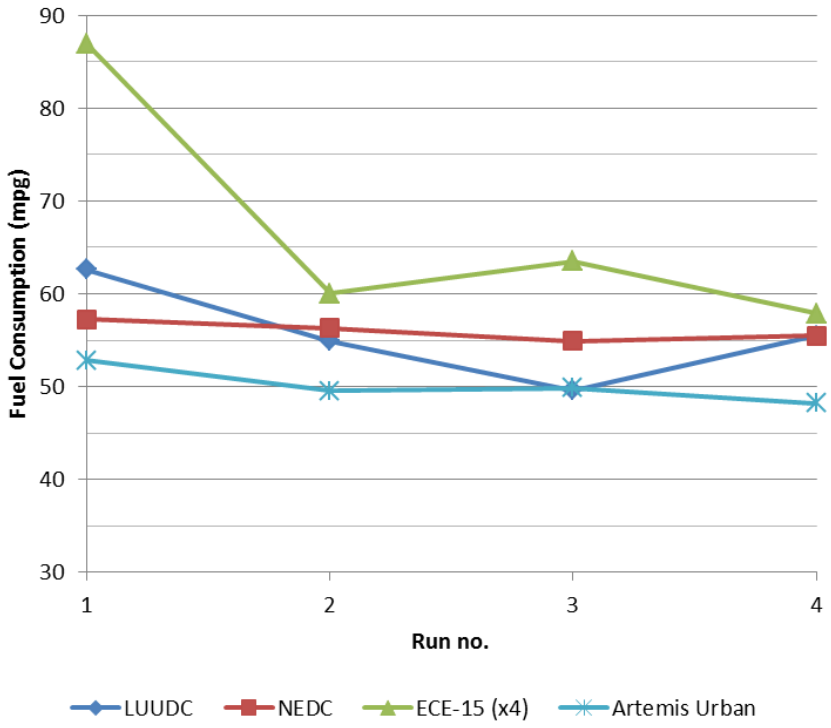

Figure 4.2: Chassis dynamometer initial drive cycle fuel consumption individual run results

The estimated CO_2 emissions were calculated and the percentage difference in fuel consumption between each cycle and the LUUDC is shown in Table 4.1. The values show the results for the LUUDC are similar to the NEDC with only a 4.1% increase in fuel consumption. The LUUDC does not contain high speed driving like the NEDC so is more comparable to the ECE-15 urban drive cycle, making it a more useful comparison for results. There is a more significant difference with 11.8% greater fuel consumption than the ECE-15. This difference will be due to the transient nature of the LUUDC with its high frequency of changes in speed, plus the accelerations are more aggressive. Having constant speed periods in the ECE-15 allows the vehicle to run in a more efficient operating mode. The gradual linear accelerations on the ECE-15 mean that the vehicle can be driven electrically more so than on the LUUDC, where the harsher accelerations require the ICE to provide more propulsion power. In contrast, the LUUDC was 8.4% better than the Artemis Urban cycle which gave the largest consumption of the tests.

Table 4.1: Chassis dynamometer initial drive cycle fuel consumption and estimated CO_2 emissions results

Drive Cycle	Fuel Consumption		CO2 Emissions	Difference to
	MPG	l/100km	(g/km)	LUUDC
LUUDC	53.3	5.30	123	0.0%
NEDC	55.6	5.08	118	-4.1%
ECE-15	60.5	4.67	108	-11.8%
Artemis Urban	49.2	5.74	133	8.4%

The fuel consumption for the duration of the vehicle's road test period was 42.7 MPG (6.61 l/100km), as discussed in Section 4.1.1, which means that the result recorded during the chassis dynamometer testing on the LUUDC is 19.9% lower, which should in theory be equivalent. There are several factors not accounted for in the generation of the drive cycle that could account for this difference, including tyre pressures, vehicle loading, gradients and use of auxiliaries. Since the vehicle only usually carries a driver and sometimes one passenger, and as the speeds travelled at are low, loading and tyre pressures should not be significant in this case. Gradient could be important as there are several across Loughborough University campus including two long gradual slopes and a short steep hill, therefore these could be a significant contributor. On a flat road at low speed the vehicle could run in electric only mode, whereas on an incline the ICE could be required to drive the vehicle at the same speed or acceleration rate, leading to increased fuel use. The use of auxiliaries is not accounted for in the chassis dynamometer tests but air conditioning, heater, radio, lights etc. will have been used throughout the course of the real-world driving. Use of air conditioning particularly is known to increase fuel consumption so auxiliary use is likely to be a contributor. Additionally, the drive cycle produced may not be as accurate a representation of the driving dataset on which it is based as it could potentially be.

The SOC levels were calculated using the voltage method, as described in the previous section, for the start and end of each run of a drive cycle. However these appeared not to be accurate. Many were in the 20-40% region which is below the usual 50-70% operating range of the Prius [19] and some values were as high as 92%, again outside this region. Additionally, for some tests there was a significant difference of up to 34% between the level at the end of a run compared to at the start of the following successive run. There should not have been a significant

change as the vehicle was switched off during this time. Due to the apparent inaccuracy of the values they were not used in the analysis. It is likely to be due to the disadvantages of this method mentioned earlier including the test vehicle's battery being likely to have degraded due to the number of cycles it has undergone due to its age and mileage, so the discharge curve used from Autonomie will not reflect the battery in its current state.

4.1.3.2 Simulation Test Results Comparison

The results of simulations run over the same drive cycles as for the chassis dynamometer tests are shown in Table 4.2, and Figure 4.3 shows the results next to the chassis dynamometer test results. The results follow the same trend but there are differences in the values with the simulations giving fuel consumption values 13-29% lower than the chassis dynamometer testing. For illustration the average fuel consumption over the duration of the real-world driving test is shown in Figure 4.3 next to the test results for the LUUDC.

Table 4.2: Simulation initial drive cycle fuel consumption and CO_2 emissions results

Drive Cycle	Fuel Consumption		CO2 Emissions
	MPG	l/100km	(g/km)
LUUDC	74.9	3.77	119
NEDC	72.8	3.88	122
ECE-15	76.1	3.71	117
Artemis Urban	56.8	4.97	157

There are several likely reasons for the difference between dynamometer and simulation results, one of which is because there could have been a difference in SOC levels between those at the start of the chassis dynamometer tests, compared to the 60% used in the simulations being higher. Another possible reason for the difference is degradation of the HV battery on the test vehicle as previously mentioned. This could mean that the SOC depletes more quickly so requires more charging, or that the SOC operating range is lower giving less available electrical power before charging occurs. This would reduce the amount of electric drive assistance provided, meaning the ICE has to be utilised more. Another factor that could be involved is the simulation model may not be a completely accurate representation of the vehicle. For example, operating maps for vehicle components or the control strategy in the software could be different to the real vehicle. This

could be particularly true with our test vehicle being a UK market version and the software model being based on a Japan market car.

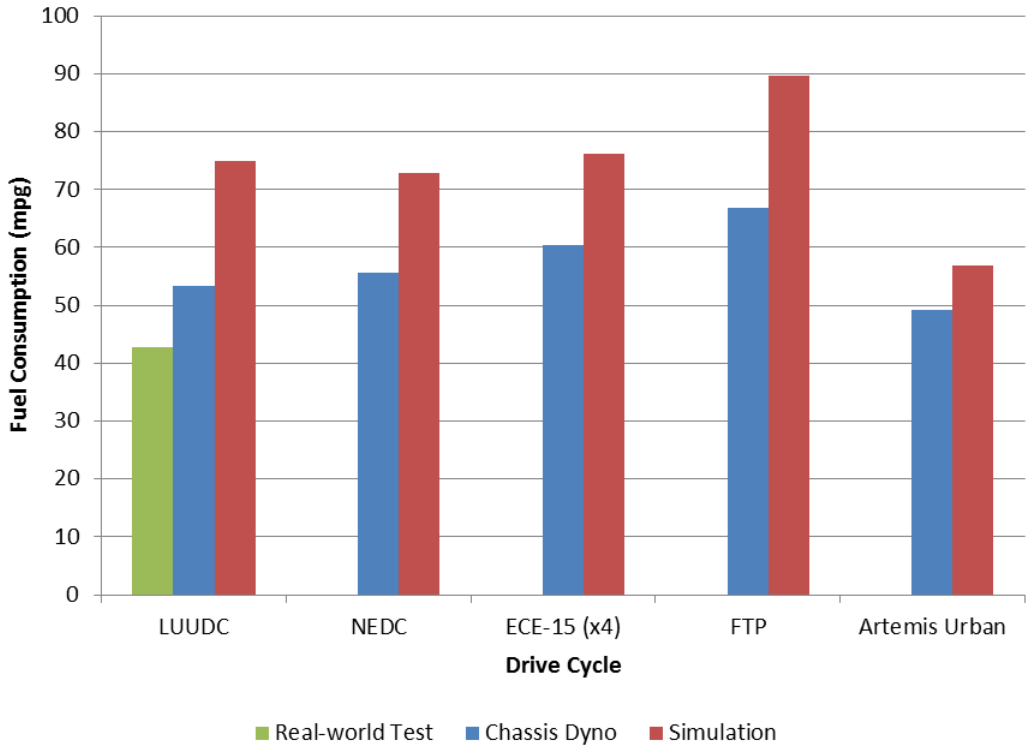

Figure 4.3: Comparison of chassis dynamometer and simulation initial drive cycle fuel consumption results with real-world driving fuel consumption

In the simulation, over each of the drive cycles there was an increase in SOC in the range of 2-7.5%. In the chassis dynamometer tests on runs 2 to 4 the indicated SOC on the vehicle display remained constant at either 5 or 6 bars out of 10, except the last ECE-15 run where it increased from 5 bars to 6 bars. This would imply that the change in SOC is small, so similar to the simulation.

The potential factors in the difference that are given above will be investigated and quantified in the following sections of this chapter and in Chapter 6.

4.1.4 Section Conclusions

Comparison of the LUUDC to other cycles in testing found that the fuel consumption and CO_2 emissions were higher than the equivalent ECE-15 European urban test cycle. This was thought to be due to having many more changes in speed coupled with greater magnitudes of acceleration in the developed cycle. Simulations were conducted to validate the trend and establish any

differences between the testing types. Close trends were shown but with lower fuel consumption than the chassis dynamometer tests, which was by 28.9% on the LUUDC. This was thought to be due to HV battery degradation, lower initial SOCs in the test vehicle and simulation model inaccuracy. Also, from this study the fuel consumption in lab testing was found to be 20% lower than in real-world use, believed to be due to road gradients, use of auxiliaries and the drive cycle accuracy. With these two results referenced to the same point it equates to the real-world driving fuel consumption being 24.7% higher than the chassis dynamometer test.

This therefore produced several areas for further work to investigate the effect on fuel consumption of the factors shown in the diagram in Figure 4.4, which summarises the results from above. In addition to these factors drive cycle accelerations were studied as a contributor to the drive cycle differences. All of these factors were investigated, and discussed and quantified later in this chapter and in Chapters 5 and 6.

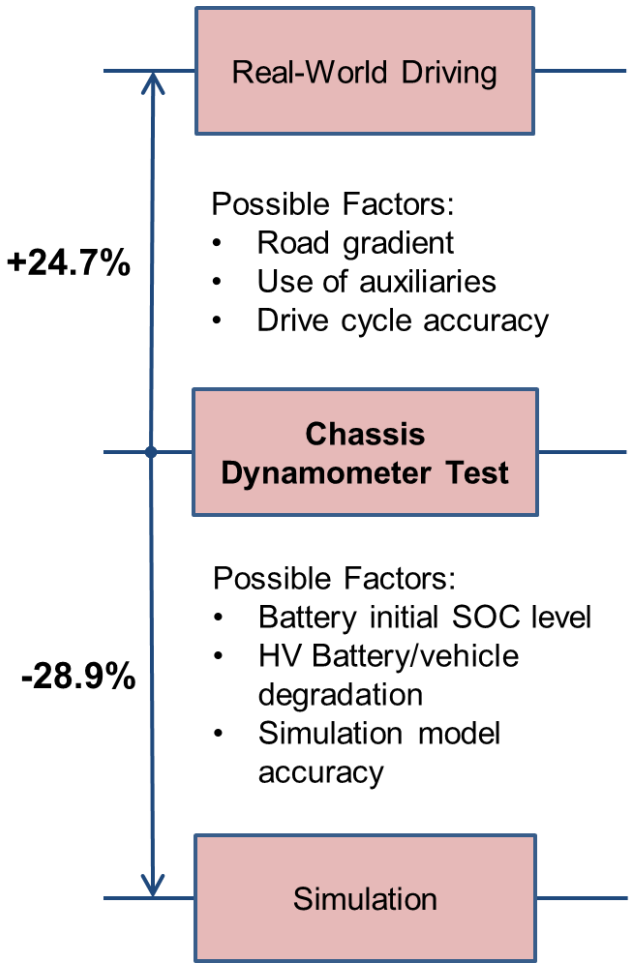

Figure 4.4: Section 4.1 results and conclusions summary diagram

4.2 Drive Cycle Fuel Consumption and Test Differences Investigation

4.2.1 State of Charge Correction

In the process of starting to investigate the results from the previous section in further detail, it was noted that for the short LU15-UDC the energy consumption from simulations differed significantly if three runs were run back-to-back in comparison to a single run, with three runs giving fuel consumption 15.6% lower. This was found to be due to differences in the battery SOC change over the test. It therefore became apparent that it was important for the HV battery energy usage to be accounted for in results in addition to the fuel used.

Methods of accounting for battery SOC across tests were researched and SOC correction from the SAE J1711 Recommended Practice for Measuring the Exhaust Emissions and Fuel Economy of Hybrid-Electric Vehicles, Including Plug-in Hybrid Vehicles [76], the similar SAE J2711 for heavy-duty vehicles [77], and ECE Regulation No 101 Appendix 8 [78] provide a suitable technique.

During a test the Net Energy Change (NEC) of the battery is calculated, which is the difference in the amount of energy stored in the battery. NEC for a battery can be defined as:

$$NEC = \Delta SOC \times V_{system}$$

or

$$NEC = (Ah_{final} - Ah_{initial})V_{system}$$

Where:

ΔSOC = Change in battery SOC

V_{system} = Battery nominal voltage

$Ah_{initial}$ = Battery Ampere-hours stored at the start of test

Ah_{final} = Battery Ampere-hours stored at the end of test

The NEC should be plotted on a chart against the fuel consumption, with fuel consumption on the y-axis and NEC on the x-axis. Multiple points are plotted with each representing a single test. Points representing charge-depleting and charging-increasing tests are recommended to enable interpolation of the data rather than extrapolation. The region to the left hand side of the y-axis with negative NEC represents charging of the battery and the region to the right hand side of the axis with positive NEC represents discharging. A linear regression line can be fitted to the points, and the point at which this line crosses the y-axis where NEC = 0 is the SOC corrected fuel consumption result. This therefore represents a test where the SOC is balanced across the test, being the same at the end as it was at the start.

The above procedure was applied to the existing chassis dynamometer test results using the battery SOC change. This was calculated by integrating the current that had passed in and out of the battery which had been recorded by the current transducer.

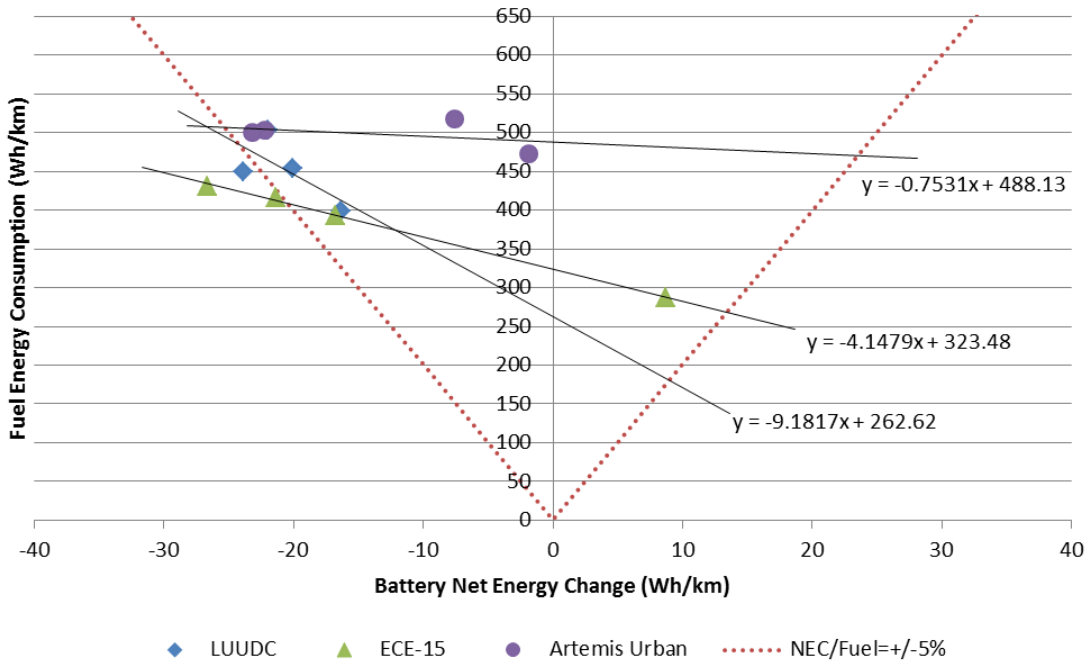

Figure 4.5: SOC correction plot for initial chassis dynamometer drive cycle fuel consumption results

The results, which can be seen in Figure 4.5, showed that the tests for the LUUDC were all net charging runs with no points close to the NEC = 0 line. This meant that the points formed a charge correction line with a steep gradient which appears

could be inaccurate compared to the lines for the other two drive cycles. Having a point in the net charge depleting zone could hugely affect the trendline and therefore the SOC corrected result. Due to this it was decided additional LUUDC tests should be carried out to improve the dataset.

In Figure 4.5 the red dotted lines mark the boundaries of the region above the lines that corresponds to a ratio of battery NEC to fuel energy of less than 5%. These would be used as the limits in which a new test run point can be SOC corrected by using an existing correction trendline from previous tests.

4.2.2 Investigation Preparation

During the new LUUDC chassis dynamometer tests, instrumentation to read SOC from the vehicle CAN was introduced to cross-reference with the current transducer logged data. Processing of the data highlighted a major discrepancy between the two signals with CAN indicating SOC changes of -14% to -20% and calculation from the current transducer giving +7% to +11%. Investigation found several factors that could be contributing to this. Battery operation during the tests was typically only up to approximately 40A, which is in the low range of the 150A current transducer. The resolution equated to approximately 1A which was not good enough for accuracy. Additionally, the zero point of the sensor drifted by a small amount during tests. Also, the background current when the vehicle was in a neutral state with just the ignition switched on had not been included during data processing. With the combination of these factors, by summing the 1 Hz current data the cumulative error became significant.

The above finding meant that a new lower range current transducer would have to be installed and all of the chassis dynamometer tests re-done. A LEM 50A nominal current transducer was specified and installed in the HV battery pack with a circuit board to give a +/-5 V output signal. The sensor installed is shown in Figure 4.6.

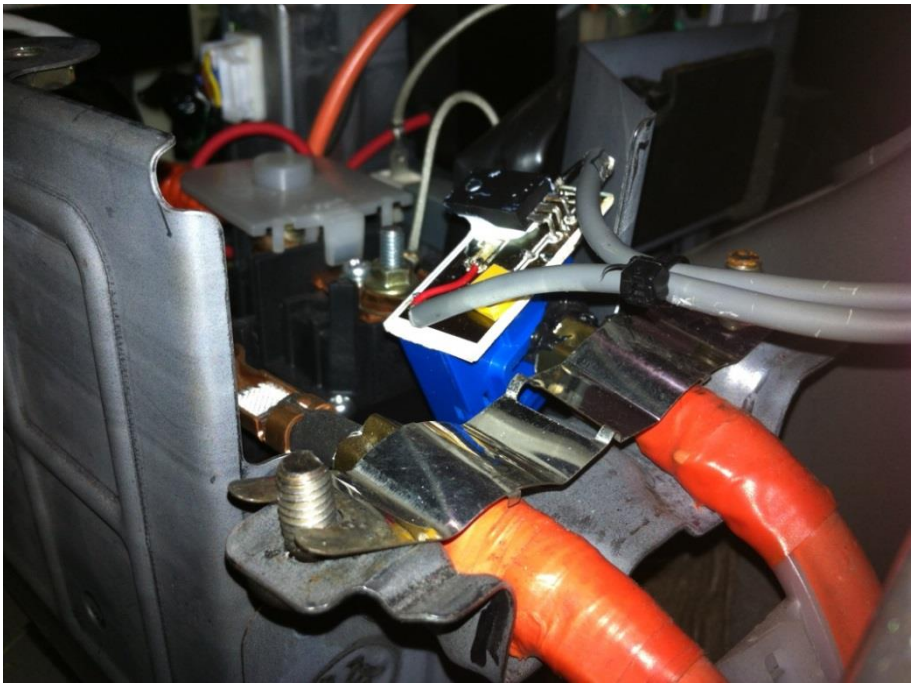

Figure 4.6: LEM current transducer installed on HV battery

4.2.3 Chassis Dynamometer Testing

4.2.3.1 Test Process

The subsequent chassis dynamometer drive cycle tests were completed, this time with pre-conditioning to produce a specific initial SOC. Tests with low, middle and high levels were carried out to ensure that the points distinctly crossed the y-axis, and so that the effect of initial SOC level could be investigated. The target points for this were 40%, 55% and over 75%. This was achieved by running the dynamometer at a constant speed with the car's transmission in drive to provide regenerative charging of the battery, and driving at low speed by electric drive to discharge the battery.

The logged current from the new transducer gave greater precision but did not appear consistent with the CAN data particularly during the tests with a large net discharge. For these the value calculated from the sensor was 8-17% lower than from the CAN reader. The CAN data reflected what the display in the car showed and also what would be expected for how the SOC would change. Due to this it was decided to use the SOC from the CAN data logger for the SOC correction of the results.

Part of the inaccuracy with the sensor value was due to the method of calculating the change in SOC. As mentioned in Section 3.6.1, this involved the current flow in and out of the battery being summed, converted into Ah and divided by the rated battery capacity. Because the test car's battery was likely to have a lower capacity than it did originally, which was later determined to be true as discussed in Section 6.2.2, the calculated SOC value would be skewed. With a lower measured battery capacity substituted into the calculations instead, the results were closer but still had differences of up to -14% for the high initial SOC tests.

4.2.3.2 Test Results

The test results for each of the drive cycles can be seen below in Figure 4.7.

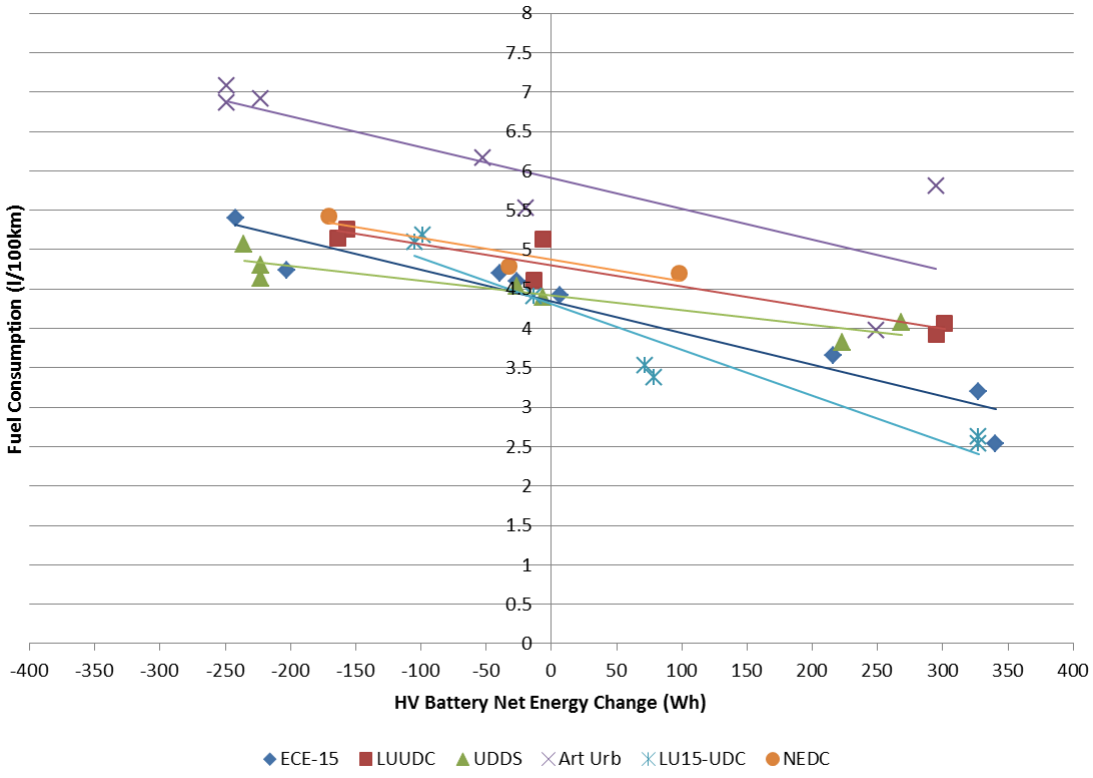

Figure 4.7: Chassis dynamometer drive cycle fuel consumption results SOC correction plot with Artemis test anomaly point

As previously mentioned, on charge correction plots the left hand side of the y-axis in the negative NEC region represents charging of the battery and the right hand side of the axis in the positive region represents discharging. As expected, all the points show the same trend with higher fuel consumption linked to greater levels of battery charging, and lower fuel consumption with greater levels of battery discharging. There is a linear relationship between test points showing that to

power the vehicle the control system operates with a direct relationship between battery and ICE operation dependent on SOC. At any moment in time the battery SOC level will be used to determine the choice of power source to give optimum energy consumption.

The uppermost point on the right hand side for the Artemis Urban appears to be an anomaly in the test results. Looking at the results behind it confirms this, as it does not fit into the relationship of fuel consumed and battery SOC change of the rest of the test runs. Therefore this point was removed from the results to give a more accurate trend line, which gives the results in Figure 4.8 and the corresponding SOC correction trendline equations in Table 4.3. In these equations the gradient of the line signifies the sensitivity of the drive cycle to initial SOC. A cycle with a steeper gradient is more sensitive to initial SOC, so will give more varied fuel consumption results as initial SOC is changed. The intercept as mentioned previously is the charge corrected fuel consumption result where NEC = 0. The overall SOC corrected fuel consumption results are given in Table 4.4.

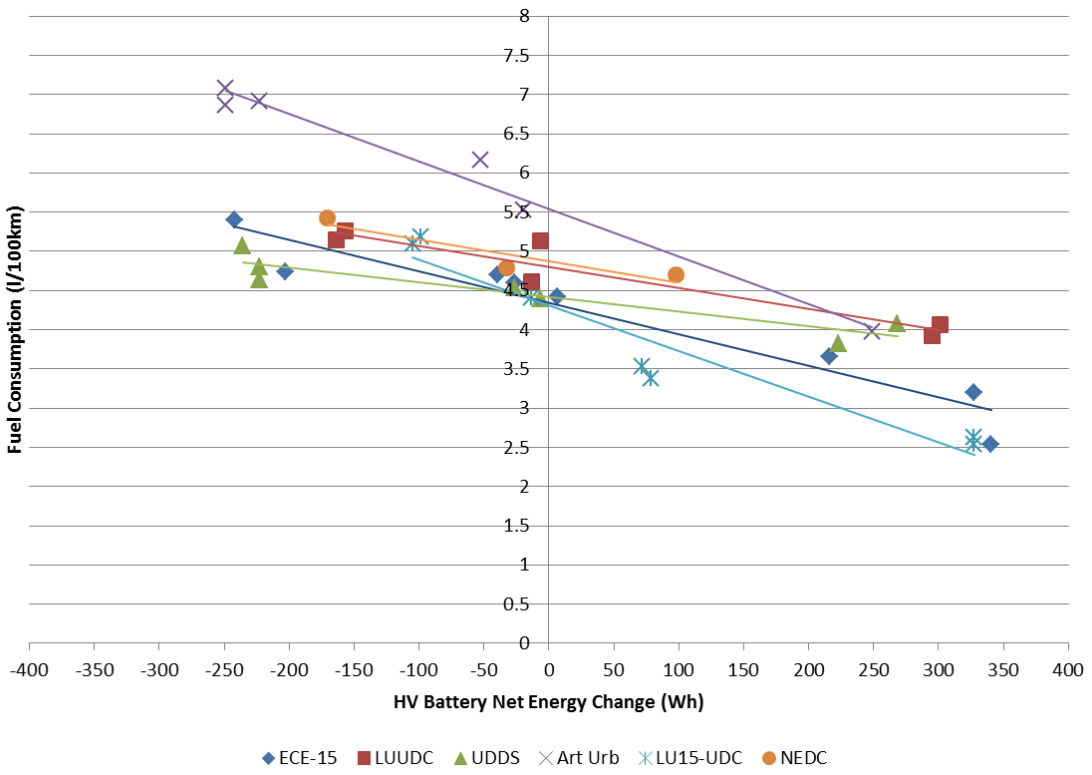

Figure 4.8: Chassis dynamometer drive cycle fuel consumption results SOC correction plot

Table 4.3: Chassis dynamometer drive cycle SOC correction line equations

Drive Cycle	Equation
LUUDC	y = -0.0027x + 4.8022
ECE-15	y = -0.0040x + 4.3468
UDDS	y = -0.0019x + 4.4175
Artemis Urban	y = -0.0060x + 5.5389
LU15-UDC	y = -0.0058x + 4.3112
NEDC	y = -0.0027x + 4.8761

Table 4.4: Chassis dynamometer drive cycle fuel consumption results

Drive Cycle	Fuel Consumption (l/100km)
LUUDC	4.80
ECE-15	4.35
UDDS	4.42
Artemis Urban	5.54
LU15 UDC	4.31
NEDC	4.88

It can be seen that the fuel consumption on the LUUDC is 10.3% higher than the baseline comparison, the ECE-15, with a value of 4.80 l/100km compared to 4.35 l/100km. ECE-15, UDDS and LU15-UDC all have very close charge corrected fuel consumptions in the range of 4.31 – 4.42 l/100km. The NEDC, the only non-urban drive cycle, gave close fuel usage to the LUUDC at 1.5% greater. It can clearly be seen that the highest fuel consumption is on the Artemis Urban cycle at 5.54 l/100km, which is 15% higher than the LUUDC. Looking at the data points for this cycle in Figure 4.8, the result for the high initial SOC fits the trend although it is thought that another valid test point in this region may be higher in the y-direction which would lift the right hand end of the SOC correction line slightly.

A key finding from this testing is that the 6.61 l/100km recorded in the real-world driving upon which the LUUDC is based is 37.7% higher than chassis dynamometer LUUDC fuel consumption, which will be investigated later in Section 4.3, Chapter 5 and Chapter 6.

4.2.4 Simulation Comparison

The same drive cycles were run in simulation using Autonomie to validate the vehicle test results. The SOC correction plot can be seen in Figure 4.9 and the SOC correction line equations in Table 4.5. A comparison of the simulation results to the chassis dynamometer results is shown in Figure 4.10 and Table 4.6.

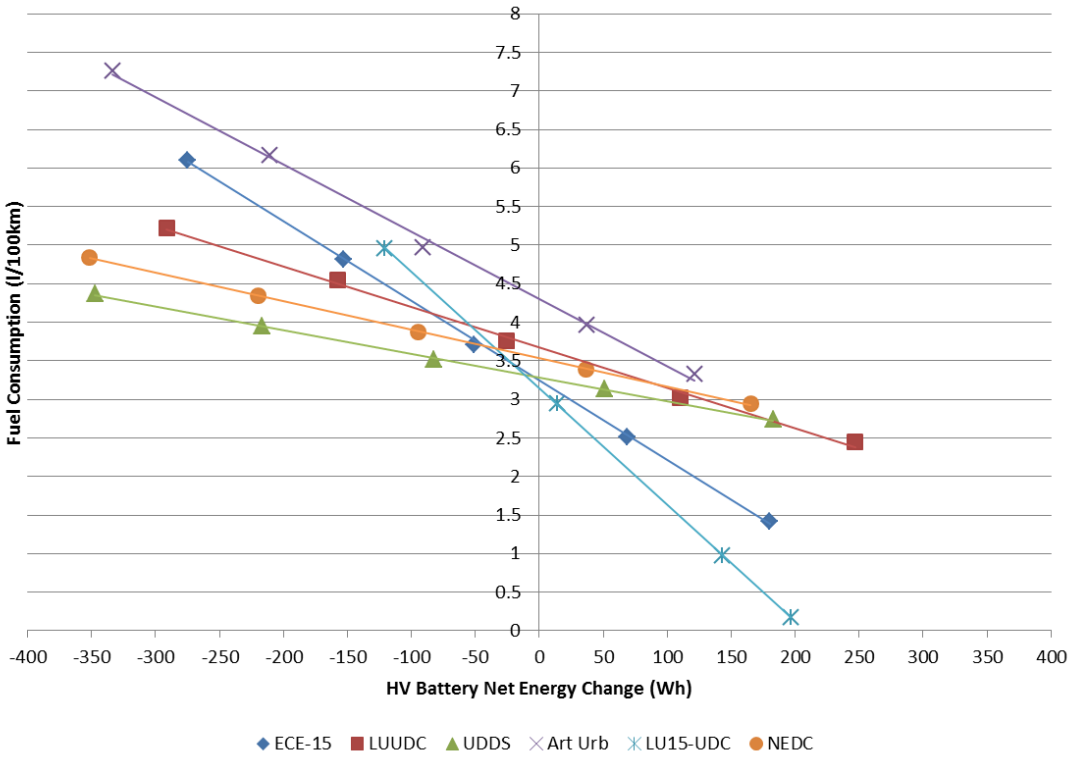

Figure 4.9: Simulation drive cycle fuel consumption results SOC correction plot

Table 4.5: Simulation drive cycle SOC correction line equations

Drive Cycle	Equation
LUUDC	y = -0.0053x + 3.6768
ECE-15	y = -0.0103x + 3.2383
UDDS	y = -0.0031x + 3.2892
Artemis Urban	y = -0.0087x + 4.3040
LU15-UDC	y = -0.0151x + 3.1410
NEDC	y = -0.0037x + 3.5336

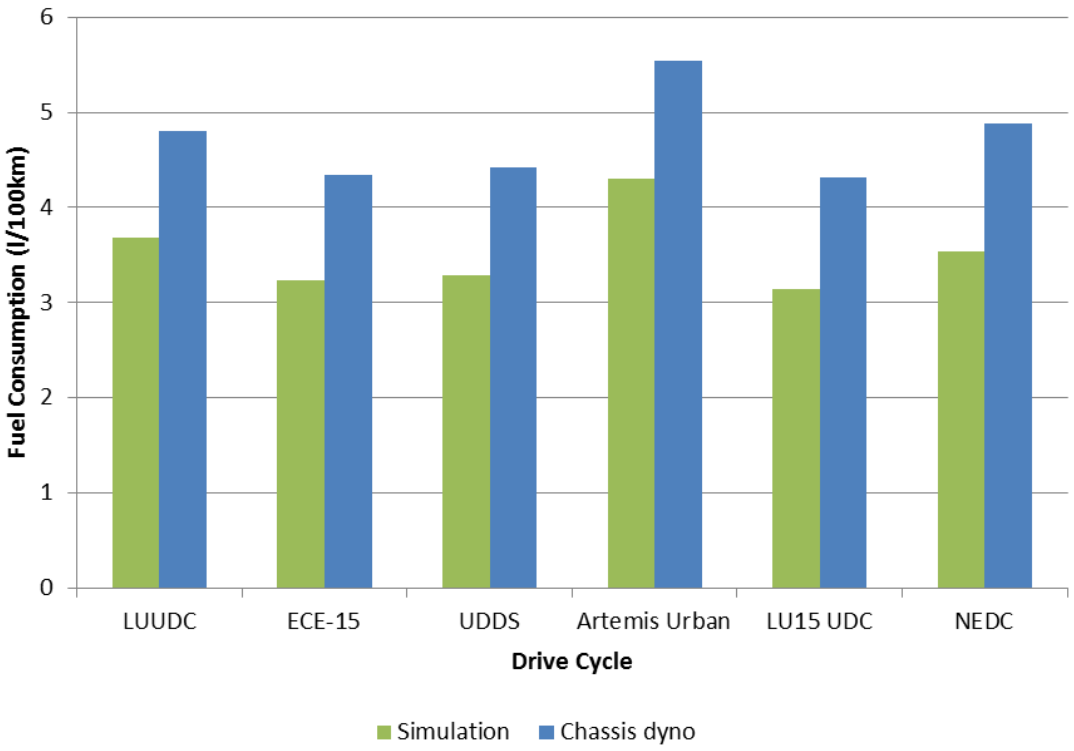

Figure 4.10: Comparison of chassis dynamometer and simulation drive cycle fuel consumption results

Table 4.6: Comparison of chassis dynamometer to simulation drive cycle fuel consumption results

Drive Cycle	Fuel Consumption (l/100km)		Difference
	Chassis dyno	Simulation	
LUUDC	4.80	3.68	-23.4%
ECE-15	4.35	3.24	-25.5%
UDDS	4.42	3.29	-25.5%
Artemis Urban	5.54	4.30	-22.3%
LU15-UDC	4.31	3.14	-27.1%
NEDC	4.88	3.53	-27.5%

The urban cycles show the same fuel consumption trend. The only difference seen is with the NEDC; in the simulation the consumption is lower than the LUUDC and Artemis Urban, whereas on the chassis dynamometer only the Artemis Urban cycle uses more fuel than the NEDC. The simulation results are consistently lower than the chassis dynamometer results with differences in the range of 22-28%. The difference is likely to be due to degradation of the HV battery and the vehicle in general, and also the vehicle model may not be an entirely accurate representation of the real vehicle. This interesting result will be discussed further in Section 6.2, and the possible causes investigated. A summary of the results above is given at the end of this chapter.

4.2.5 Campus Driving Testing

Campus driving tests were carried out for the primary purpose of investigating the effect of gradient on fuel consumption as detailed later in Section 4.3. The data was processed in the same way as for the other tests with SOC correction carried out, as detailed in Section 4.2.1. The plot shown in Figure 4.11 shows the corrected fuel consumption to be 4.20 l/100km. There is not a clear trend to the points like there is with the drive cycle result plots earlier in the chapter because here there was only small differences in the SOC level at the start of runs, meaning all the points are relatively close to the y-axis.

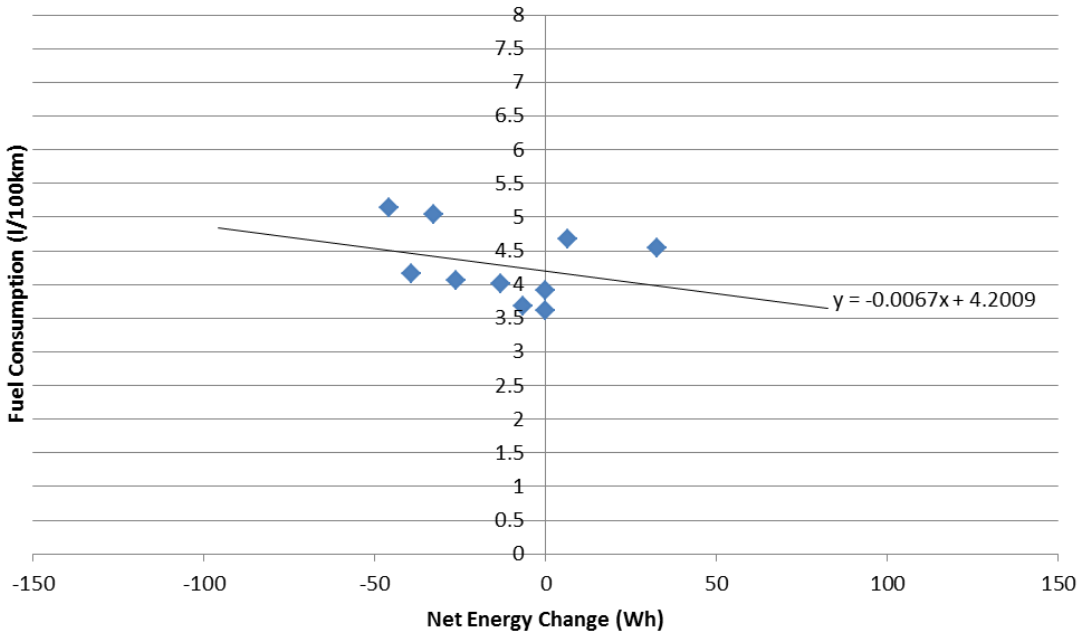

Figure 4.11: Campus driving fuel consumption results SOC correction plot

4.2.6 Electric Vehicle Comparison

4.2.6.1 EV Chassis Dynamometer Testing

A *Smart electric drive* was used as a comparison electric vehicle to test for analysis against the hybrid Prius on the chassis dynamometer and for campus driving tests. Chassis dynamometer tests were carried out on the LUUDC, ECE-15 and Artemis Urban drive cycles. It can be seen in Figure 4.12 that the results for the test repeats were consistent apart from run 2 for the LUUDC with its higher fuel consumption.

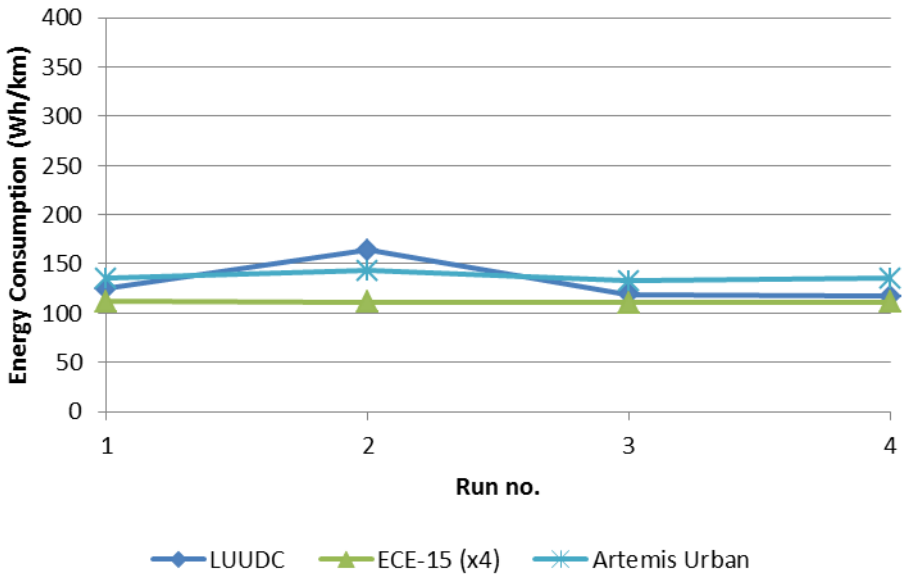

Figure 4.12: *Smart electric drive* chassis dynamometer drive cycle energy consumption individual run results

Electrical energy consumption follows the same order in size as the Prius fuel consumption, showing that the cycle profiles have a consistent effect on energy consumption for the different powertrains. The sizes of the cycle to cycle differences vary though; Table 4.7 shows that the ECE-15 produced 15% lower energy consumption than the LUUDC and the Artemis Urban 4% higher energy consumption. This is a larger difference than for the Prius (-9.5%) on the ECE-15 and a much smaller difference on the Artemis Urban (+15.3%). This result indicates that for the EV, differences in real-world drive cycles have a lesser effect on the energy usage than they do with the HEV.

Table 4.7: *Smart electric drive* chassis dynamometer drive cycle energy consumption results

Drive Cycle	Average Energy Cons. (Wh/km)	Diff. from LUUDC
LUUDC	131.16	0.0%
ECE-15	111.20	-15.2%
Artemis Urban	136.79	4.3%

4.2.6.2 EV Campus Driving Testing

As with the chassis dynamometer tests, the campus driving tests in the *Smart electric drive* showed consistent repeatability as shown in Figure 4.13, and had an average energy consumption of 103.2 Wh/km.

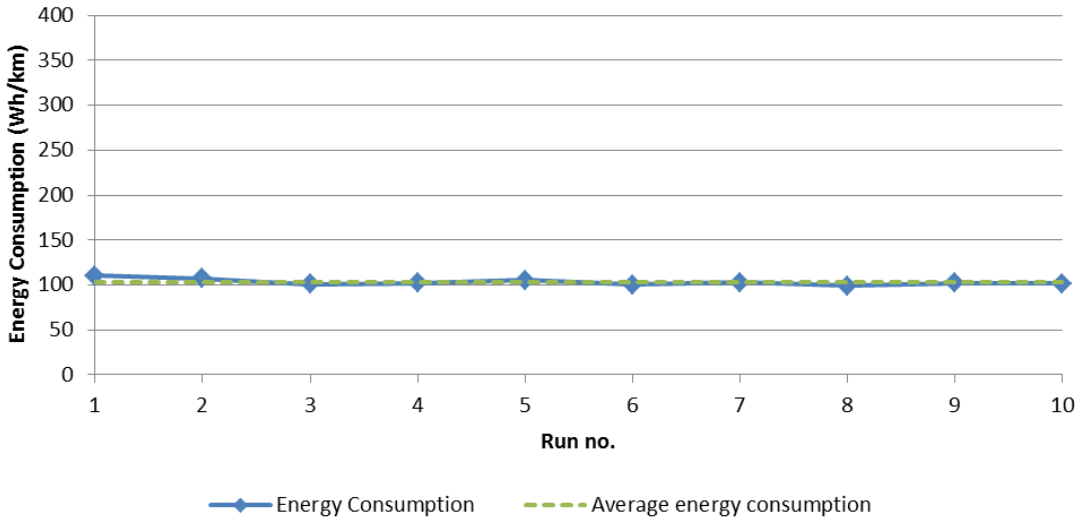

Figure 4.13: *Smart electric drive* campus driving individual run energy consumption results

4.2.6.3 Comparison of HEV to EV

For comparison of the two vehicles the Prius fuel consumption was converted into energy consumption in Wh/km to be directly comparable to the *Smart electric drive*. The results shown in Table 4.8 show a very large difference between the two vehicles, which is consistent, in the range of 69-72% across all of the tests.

Table 4.8: Comparison of Prius to *Smart electric drive* energy consumption results

Drive Cycle/Test	Energy Consumption (Wh/km)		Difference
	Prius	smart	
LUUDC	424.19	131.16	-69.1%
ECE-15	383.96	111.20	-71.0%
UDDS	390.21	-	-
Artemis Urban	489.27	136.79	-72.0%
LU15-UDC	380.82	-	-
Campus R-W driving	371.05	103.22	-72.2%
Security R-W driving	584.03	-	-

The *Smart* and Prius are significantly different cars, with the *Smart* being a compact 2-seater city car and the Prius a 5-seater family hatchback which means there is a corresponding difference in mass. At 1375 kg the Prius weighs a third more than the 1036 kg *Smart*. Due to this, the energy consumption results were normalised by mass to produce a fairer comparison, which can be seen in Table 4.9 and Figure 4.14. Despite this there is clearly still a large difference of 59-63% between results for each vehicle, showing that the electric vehicle is much more energy efficient. This will be due to ICE's having efficiencies of typically 30-35% and

electric motors typically around 90%, which leads to the fully electric powered vehicle being significantly more energy efficient.

Table 4.9: Comparison of Prius to *Smart electric drive* energy consumption results normalised by mass

Drive Cycle/Test	Energy Consumption (Wh/km/tonne)		Difference
	Prius	smart	
LUUDC	308.50	126.60	-59.0%
ECE-15	279.24	107.33	-61.6%
UDDS	283.79	-	-
Artemis Urban	355.83	132.04	-62.9%
LU15-UDC	276.96	-	-
Campus R-W driving	269.85	99.64	-63.1%
Security R-W driving	424.75	-	-

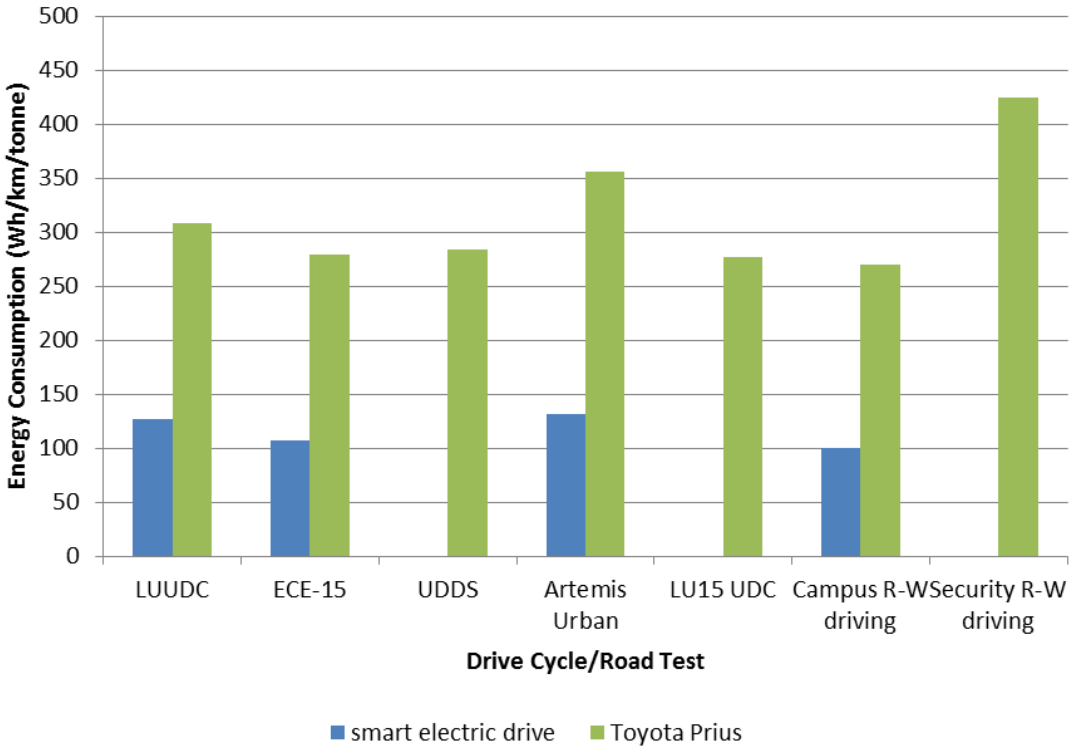

Figure 4.14: Comparison of Prius to *Smart electric drive* energy consumption results normalised by mass

4.3 The Effect of Road Gradient

4.3.1 Gradient Vehicle Tests

As mentioned earlier in the chapter in Section 4.2, there is a large difference of 37.7% between the chassis dynamometer LUUDC fuel consumption of 4.80 l/100km and the Security real world driving fuel consumption of 6.61 l/100km, which could be due the gradients faced on the road.

The LU15-UDC which has been used in the preceding sections was developed as discussed in Chapter 3, primarily to investigate the contribution of road gradient on fuel consumption. The first comparison is with the real-world campus driving test results from the results presented in Section 4.2.5. With 4.2 l/100km in the real-world driving with gradients, and 4.3 l/100km in the dynamometer tests without gradients the results are very close, the real-world being 2.6% lower than the dynamometer. This implies that there is insignificant difference between the two cases, and the small difference which is in the opposite direction to what was anticipated, is expected to be due to test accuracy variation.

4.3.2 Circuit Route Gradient Simulations

The above finding was investigated further using simulations of the same drive cycle with and without gradients incorporated. Simulations were carried out at various SOC levels, and SOC correction was carried out in the same way as for the physical vehicle tests as shown in Figure 4.15. Without gradients the fuel consumption was 3.14 l/100km and with gradients it was 3.16 l/100km, only a 0.6% increase. This confirms that there is negligible difference caused by gradients in this scenario.

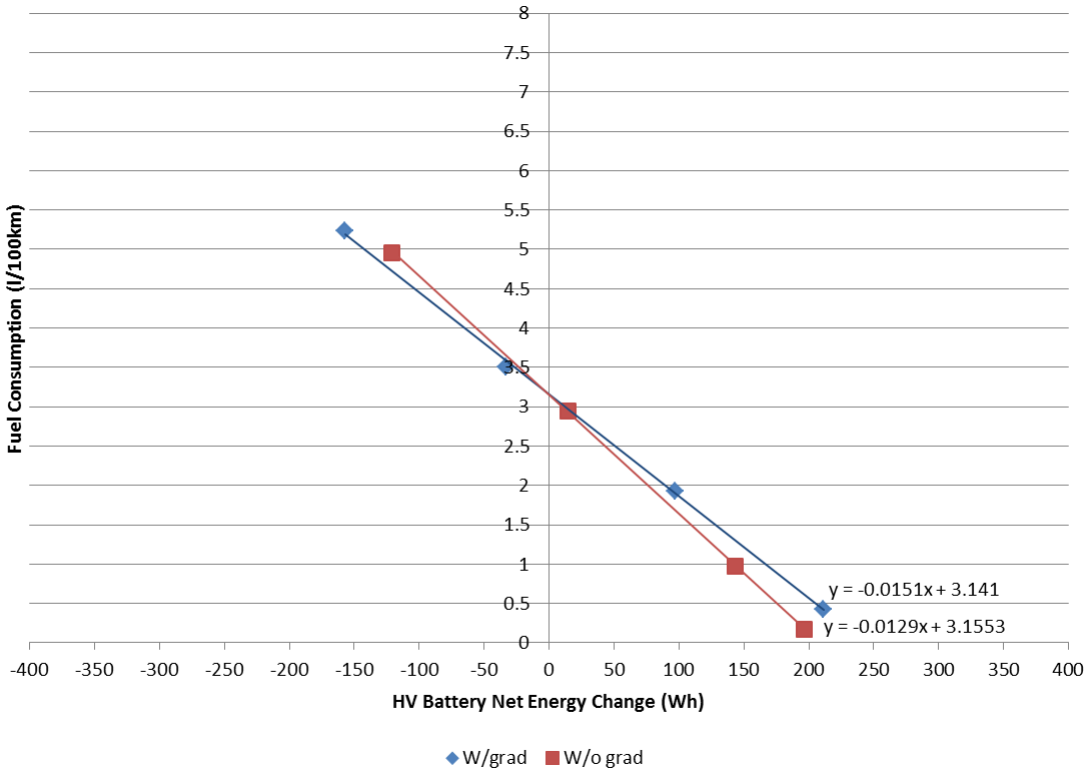

Figure 4.15: LU15-UDC simulations with and without gradient SOC correction plot

The reason for this can be seen by looking at plots of output signals from Autonomie for the cumulative fuel used. Figure 4.16 shows the cumulative fuel used over the drive cycle for cases with and without gradient. Both simulations started with the same SOC at 59% which gives as near as possible to no change in SOC in the no gradient case.

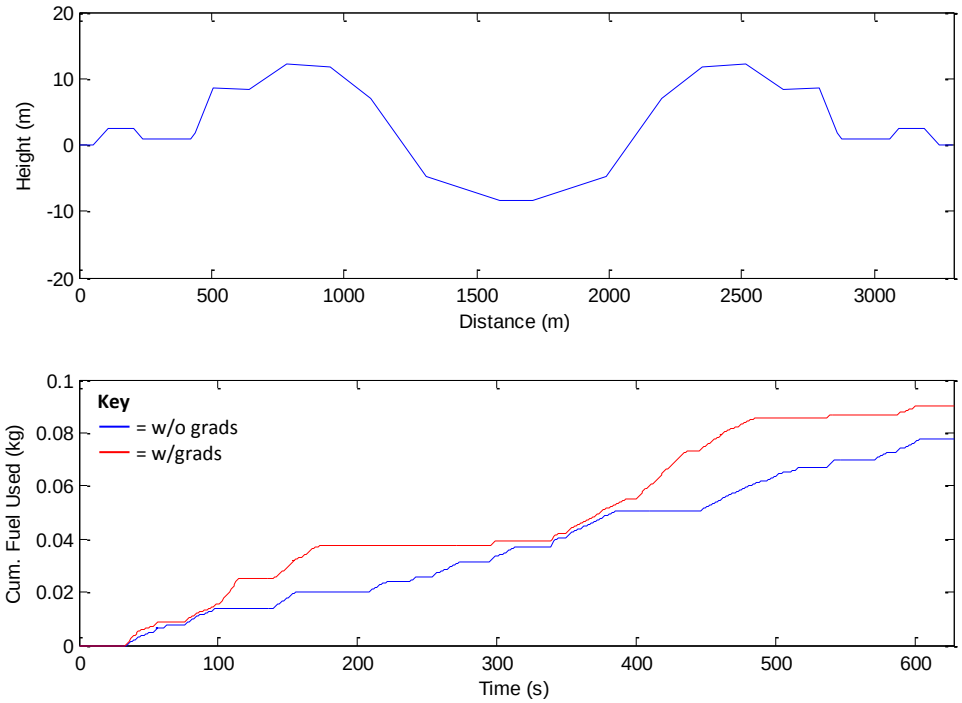

Figure 4.16: LU15-UDC simulation cumulative fuel consumption and cycle gradient profile

It can be seen that with gradients during the downhill sections between 166-388 seconds and 491-628 seconds the fuel graph levels off showing that no fuel is being consumed which will be due to the engine being switched off and the car moving under the force of gravity. In the case of without gradients, the line continues increasing during these periods while the vehicle travels on a level road. This is because the engine continues to be used to propel the vehicle or charge the depleting battery after it has been used to drive the vehicle electrically. This results in the two fuel consumption lines ending close together.

Looking at the SOC level for the same simulations, in Figure 4.17, with gradients there is a greater ending SOC at 62.5% compared to 59.1% without gradients, so although more fuel has been used there is more energy stored in the battery at the end which has to be taken into account, which reduces the difference. The plot highlights two key points at which the with-gradients SOC line increases significantly more than the without-gradients line. The first one of these points starts at approximately 220 seconds which corresponds to the long downhill gradient, and the second from around 540 seconds which is at the short steep

downhill section of the route. This is due to energy being able to be recovered through regenerative braking when travelling on the downhill gradients.

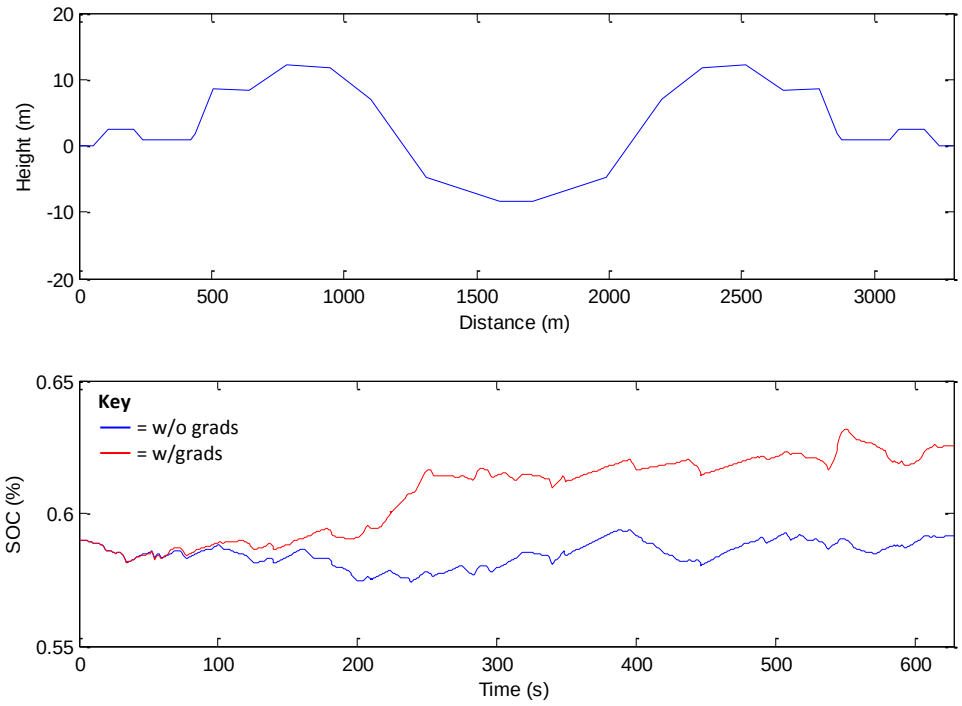

Figure 4.17: LU15-UDC simulation SOC and cycle gradient profile

4.3.3 Circuit Route Energy Flows With and Without Gradients

4.3.3.1 Instantaneous Power Flow

To further verify the above findings the instantaneous power and energy flows at a component level will be studied. Again using the LU15-UDC with the same initial SOC setting of 59%, the instantaneous power for the ICE, HV battery and each motor-generator can be seen in Figure 4.18. In these it is the power at the input to the component, except with the battery where it is the output power. Therefore for the motor-generators positive power represents motoring and negative is generating, and for the battery positive power is discharging with negative being charging. A plot of road gradient is shown on each of the components' graphs to reference the plots against, and additionally the route profile is shown again in Figure 4.19.

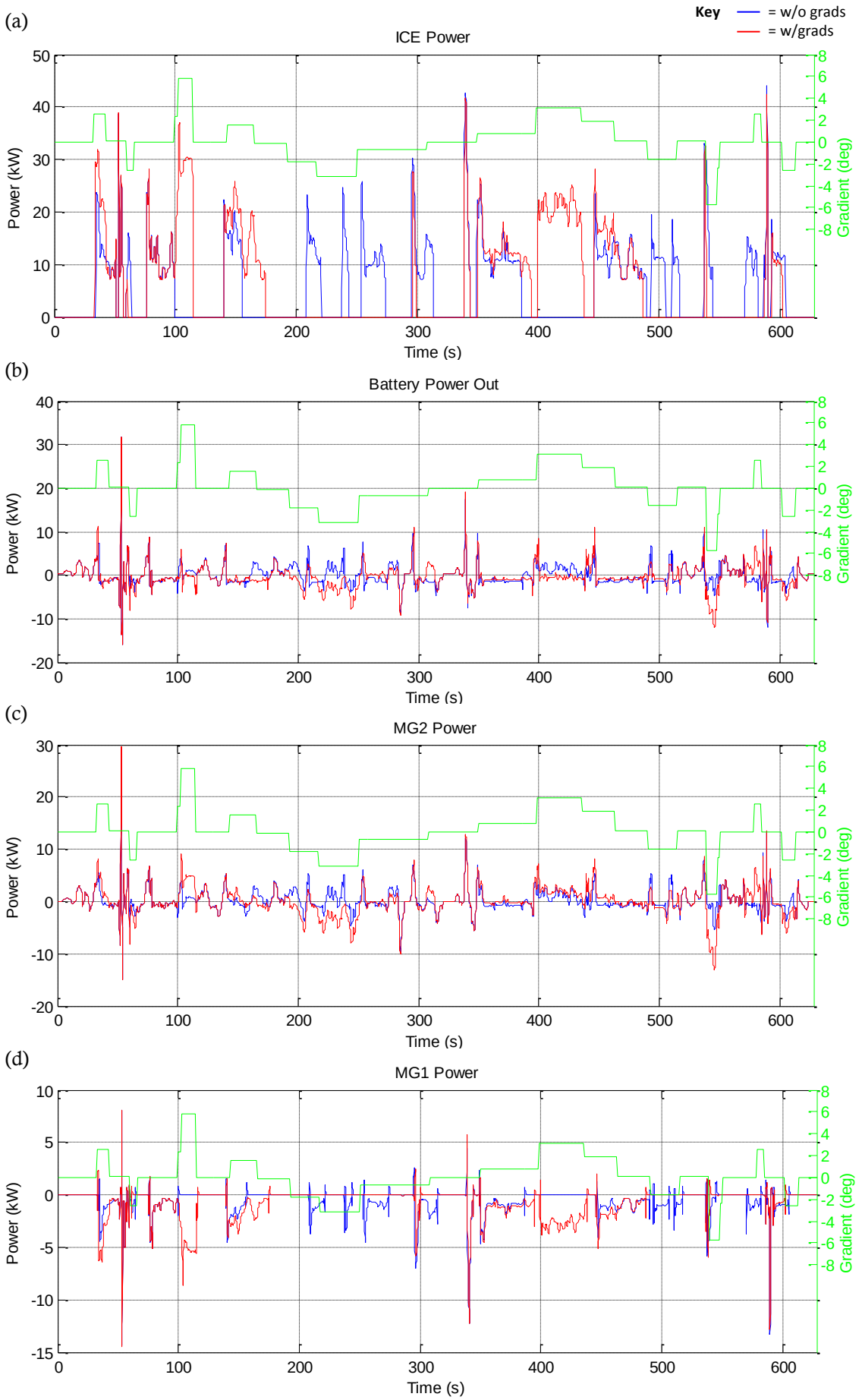

Figure 4.18: Component instantaneous power plots

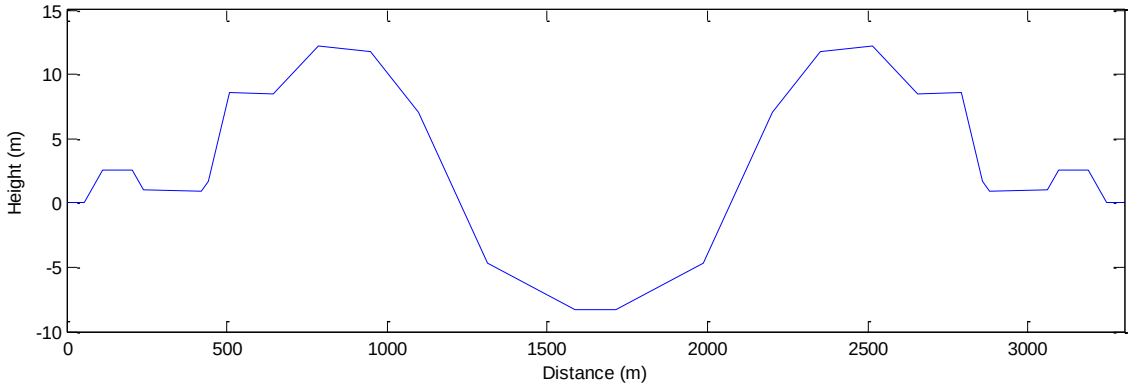

Figure 4.19: LU15-UDC campus route height profile

The plots in Figure 4.18 show some interesting features that reinforce the earlier findings. Looking at the ICE power from the start it can be seen that with gradients the first peak is higher due to greater use of the engine power on the uphill gradient. At the same point there is also a greater peak in battery output and MG2 power showing there is also additional electrical drive with the gradient, along with more power generation by MG1. At approximately 50 seconds there is an unusual spike in the plots for the gradient case whilst there is negligible gradient. As this does not represent the road demand it will be a point that the vehicle control strategy has switched on the ICE to recharge the battery, which can be seen by the negative spikes in the battery and motor-generator charts. The following downhill gradient allows the ICE to be switched off and energy to be recuperated, shown by the larger negative peaks in the battery power and MG2 power when there are gradients. On the other hand without gradients there is an extra period of ICE power supplied where it continues to drive the vehicle due to not having the gravitational advantage.

At just after 100 seconds where the steepest incline on the route occurs when gradients are applied, there is a peak in ICE power that continues for the duration of the incline. It can be seen that the electric drive is used too, from the MG2 plot that is similarly shaped to the ICE plot, along with the corresponding negative MG1 power. The battery power plot shows that it provided energy at the start of the incline to assist the ICE. Without the gradient the ICE is not used in the same period and the battery provides the small amount of power required to drive the vehicle using the electric motor. Similarly, at the next uphill gradient the ICE provides more power and continues to provide power for longer than it does when

there are no gradients. Again, battery power is used to drive MG2 in the case of no gradients, with a larger battery power output this time.

With the gradients, from the start of the downhill section of the route from 193 seconds to the end of the first direction of the journey at 328 seconds there is no ICE power except a brief period just before 300 seconds. During the time that the vehicle is coasting on the downhill with the ICE switched off there is a large amount of electrical energy recuperation seen by the sustained negative battery power and MG2 power. Without gradients the ICE is on for over 50% of the time to power the car and maintain the battery SOC. The battery charging can clearly be seen by the negative MG1 power trace corresponding to the ICE power. Additionally, in the middle of this section there is some electric drive, shown by the positive battery power output and MG2 power.

On the second leg of the journey, for the initial part the two lines on the graphs follow similar trends but with the ICE and MG2 power being slightly higher with the gradients in force. From approximately 390 seconds though, for the uphill gradient until about 440 seconds there is a large amount of ICE power to propel the vehicle, and negative power from MG1 providing electrical power which is being used by MG2 to assist in providing drive. This means the battery output stays stable at close to zero. Without the gradient in this same period there is no ICE usage; the lower power demand is supplied by MG2 with the power being drawn from the battery.

From 491 seconds for the start of the downhill section there is no power from the ICE and the battery and MG2 powers are lower than when there are no gradients. Without gradients there is power provided by the ICE for a significant amount of this time to propel the vehicle and also provide charging through MG1. At the end of the following almost zero gradient part, the ICE provides power for just a few seconds before the steepest downhill section. On this negative gradient there is a large amount of regenerative braking shown in the MG2 and battery power plots by the negative peaks. Without gradients this energy is much smaller. After this point until the end of the drive cycle there is a period where the ICE operates

without the gradients applied, where it does not when the gradients are applied. At approximately 590 seconds there is another very large spike in the ICE power similar to the earlier one, which gives a large negative spike in MG1 power and a significant battery charging, plus high MG2 power.

Overall, although there are points at which the ICE power is higher when the gradients are applied compared to when there are no gradients there is clearly more of the time that fuel energy is being used by the ICE over the drive cycle. The battery power output is generally lower with the gradients applied and there is more battery charging. In the next section the total energy flow in each component will be studied.

4.3.3.2 Cumulative Energy with Equal Initial SOC

To look at the total energy flow over the drive cycle for each of the components used in the previous section, cumulative plots are shown in Figure 4.20. The net total energy for each component has then been summed and these are presented in powertrain layout diagrams in Figure 4.21. Additionally, the positive and negative energies have been summed separately and are summarised in Table 4.10.

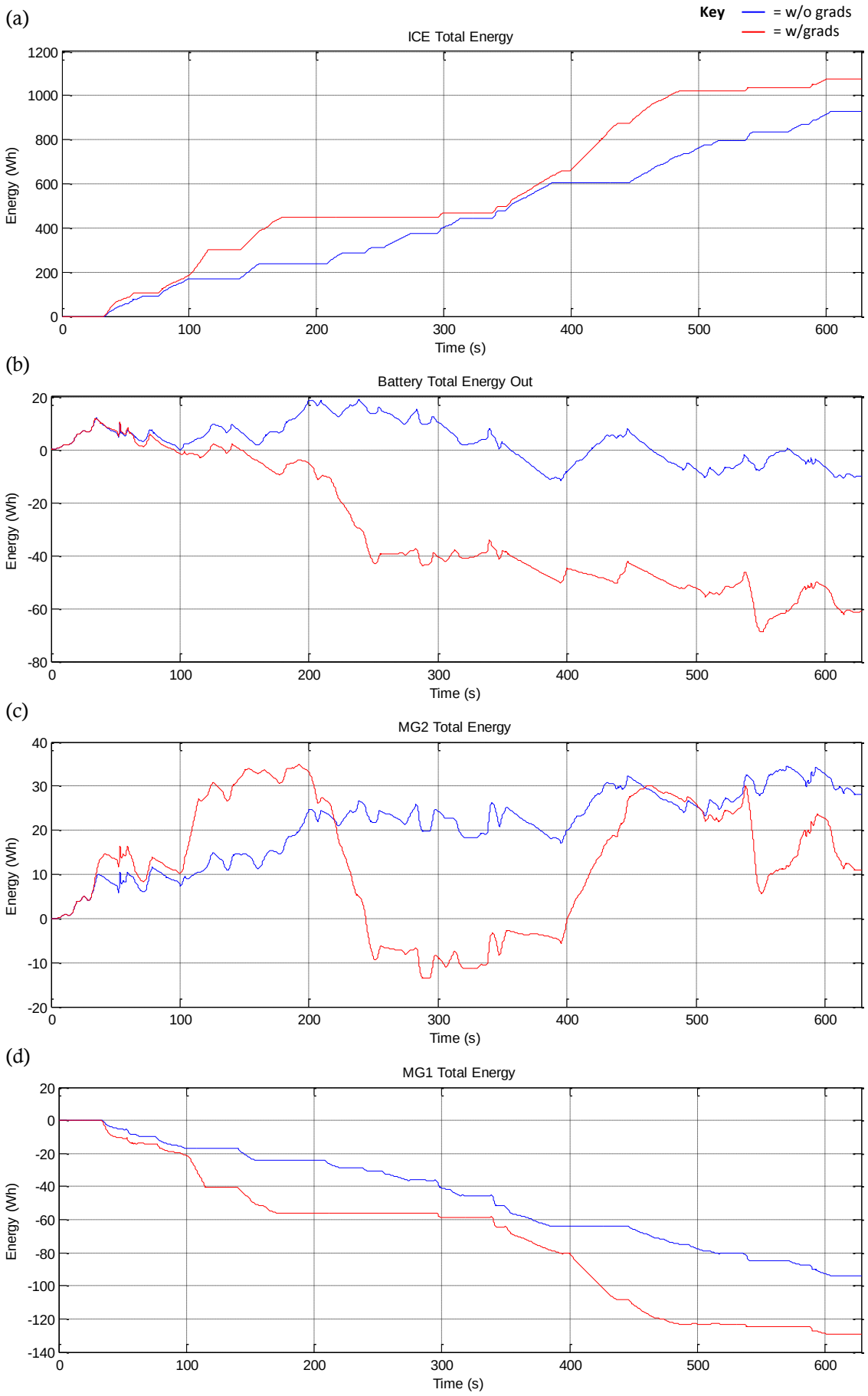

Figure 4.20: Component cumulative energy plots with equal initial SOC

The ICE total energy, Figure 4.20 (a), is essentially the same as that shown earlier in Figure 4.16 but with the units now being energy in Wh. With a total of 1075.5 Wh with the gradients applied, the ICE energy is 16.0% higher than the 927.4 Wh without gradients. As mentioned earlier it is the electrical energy usage that causes the overall energy consumption to be much closer, so that will be analysed here.

Looking at the battery energy, there is net charging in both cases with -9.9 Wh without gradients, but over six times more with gradients at -61.2 Wh. This plot shows features that reflect what was seen earlier in Figure 4.17, there are two clear points that contribute significantly to the charging, one at approximately 220 seconds and one at approximately 540 seconds, corresponding to the downhill sections where brake energy is recuperated. This highlights that having downhill gradients allows significantly more electrical energy to be recovered.

The MG2 total energy shows a much more variable range of energy usage when gradients are applied, with four key parts at which there is a large difference between the two simulations. At approximately 100 seconds and 400 seconds there are large increases in energy output due to the two most significant uphill sections of the route requiring a large energy demand to drive the vehicle. The same sections of gradient when travelling in the opposite direction (downhill) have the opposite effect, with drops in the total energy at approximately 200 seconds and 540 seconds where MG2 is acting as a generator. The profile of the plot when with gradients follows a similar shape to the height against distance profile, Figure 4.19.

The uphill sections starting at approximately 100 seconds and 400 seconds are reflected in the plot of MG1 total power by increased charging due to some power from the ICE being routed through MG1 to provide drive through MG2.

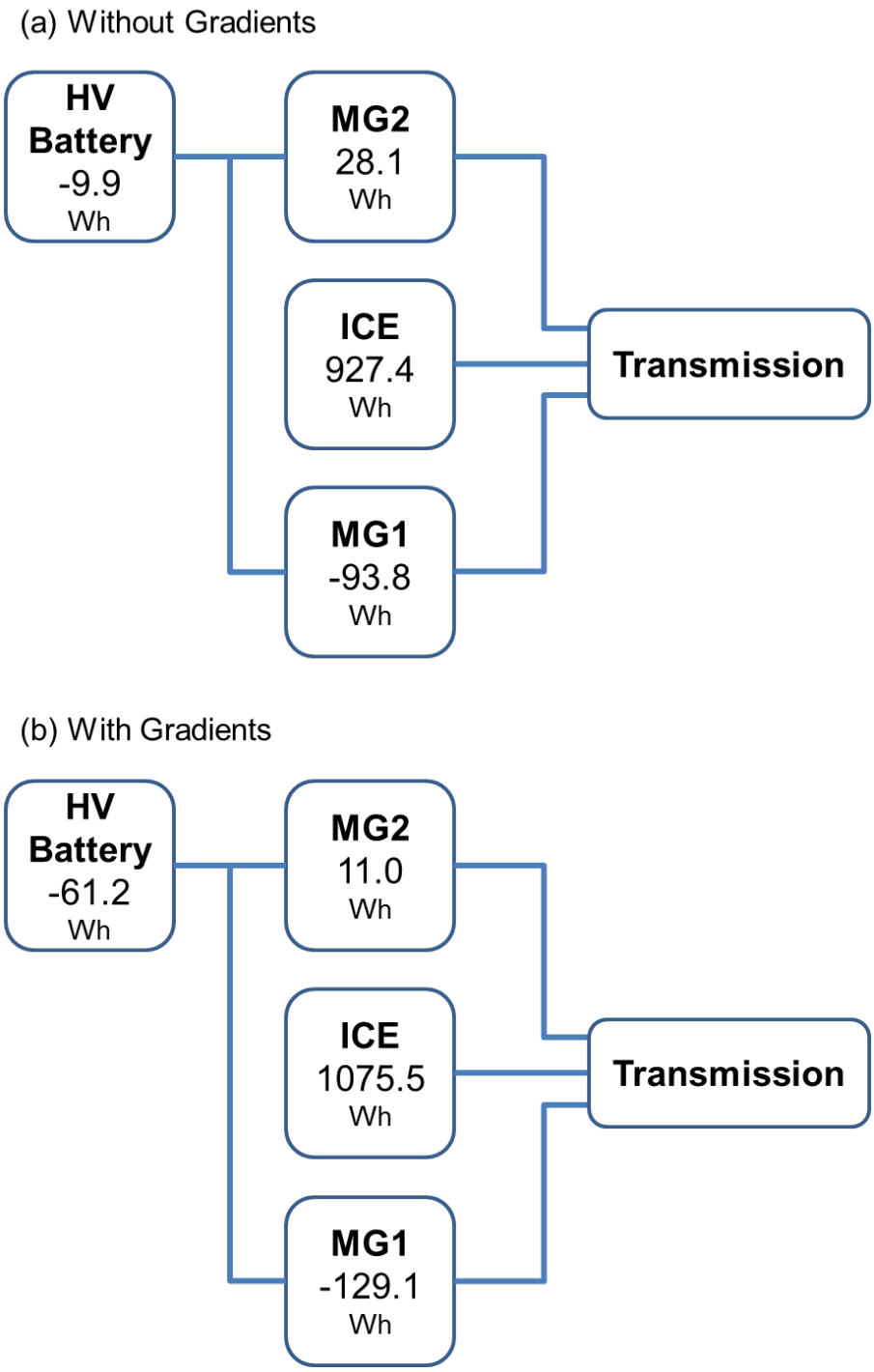

Figure 4.21: Component net energy flow with and without gradients powertrain diagrams

Table 4.10: Component energy flow with and without gradients results summary

Component	Case	Energy Out (Wh)	Energy In (Wh)	Net Energy (Wh)
ICE	W/o Gradients	927.40	0	927.40
	W/ Gradients	1075.49	0	1075.49
Battery	W/o Gradients	139.70	-149.55	-9.85
	W/ Gradients	122.55	-183.76	-61.21
MG2	W/o Gradients	134.33	-106.24	28.09
	W/ Gradients	164.78	-153.76	11.02
MG1	W/o Gradients	6.82	-100.60	-93.78
	W/ Gradients	5.55	-134.68	-129.13

The diagrams in Figure 4.21 show notable differences in the total component energies. The results reiterate the trends seen earlier with the ICE using more energy overall when the gradients are applied, at 1075.5 Wh against 927.4 Wh. However, the battery charged by 61.2 Wh which is significantly more than the 9.9 Wh without gradients, so there is more electrical energy stored at the end of the test. Linked to this, MG2 uses less energy, and MG1 provides more charging with the gradients compared to when they are not present.

Looking at the energies separated into energy in and energy out in Table 4.10, the greater battery charging with gradients is due to both lower energy output and more energy recovery. The higher energy-in with gradients for MG2 fits with this, and higher MG2 energy-out plus higher energy-in for MG1 indicates that there is more energy from the ICE providing electrical energy for driving through the motor-generators.

4.3.3.3 Cumulative Energy with Different Initial SOCs Set For Charge Balance

In the previous section the total energies for the components cannot be summed to give an overall total due to component efficiencies and non-equivalence of fuel and electrical energy. Therefore to get results that clearly reinforce the finding of gradient not having an effect on the energy consumption of a HEV, it is useful to look at the energy flow when the test is as close as possible to zero net change in charge level, so is therefore balanced. The initial SOCs will therefore be different for with and without gradients. As previously mentioned and used above, this is 59%

for the case of no gradients. For with gradients the initial SOC set to 63% gives negligible change in SOC.

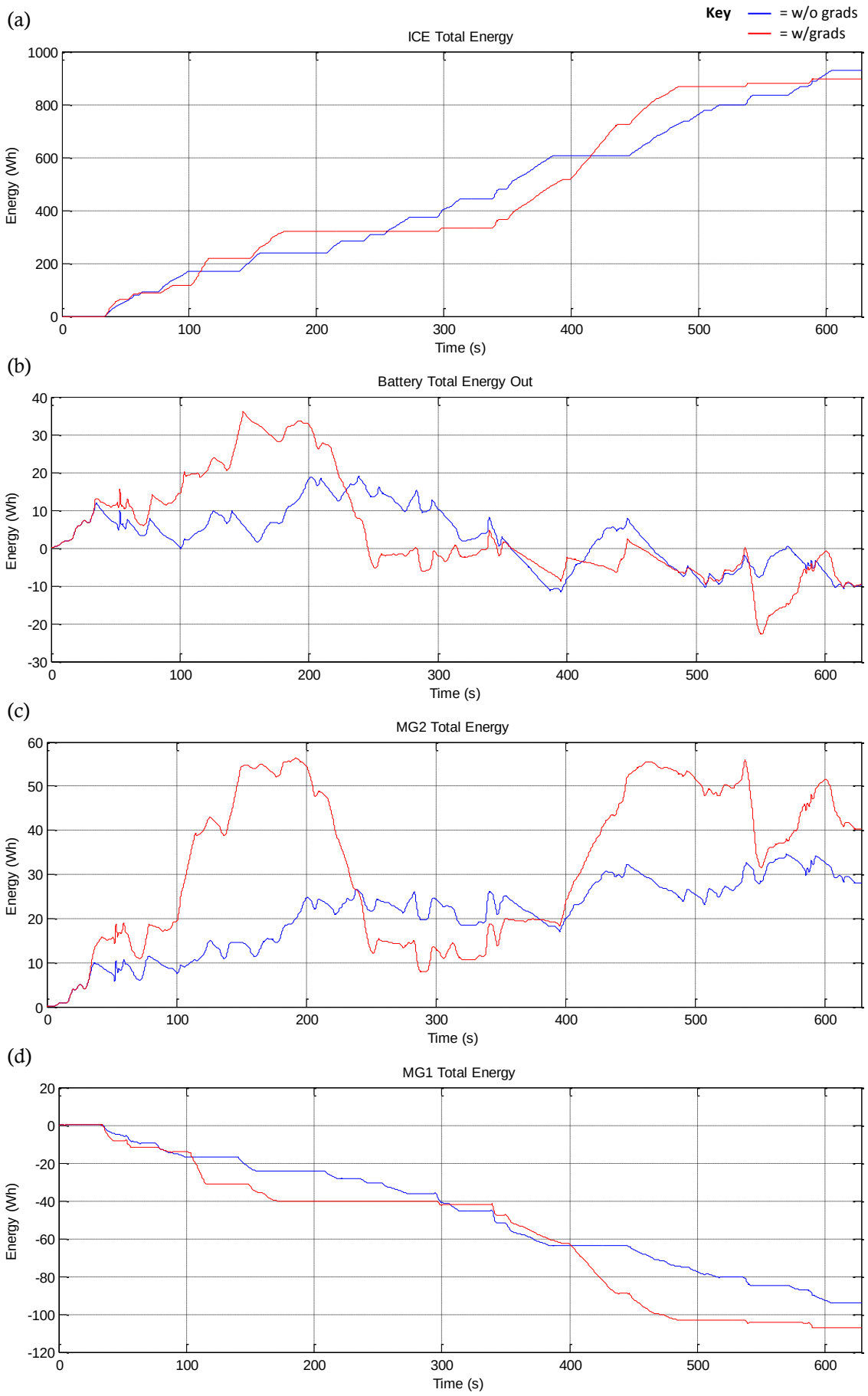

Figure 4.22: Component cumulative energy plots with different initial SOCs giving charge balance

Looking at the total energy plots in Figure 4.22, similarities can be seen with the previous plots in Figure 4.20. With the higher initial SOC with gradients the MG1 and MG2 plots follow very similar profiles to the previous ones, but for MG2 rising to higher positive energies and MG1 not going as far into the negative energies. This shows that less charging energy is produced by MG1, and MG2 provides more energy for driving. There are two clear parts where MG2 provides more energy in this second simulation compared to the first; one is at approximately 70 seconds which corresponds to a flat section, and the other most prominent point is at approximately 140 seconds which is the start of the second stage of the uphill section before reaching the highest point of the route.

The battery energy plot shows that both simulations ended at almost the same level. Looking at the ICE total energy, with a balanced SOC over the test it finishes lower than before (Figure 4.20) due to the utilisation of the additional battery energy rather than having it stored at the end of the test. This means that the total fuel consumption ends 3.5% lower with the gradients applied than without, at 895.2 Wh against 927.4 Wh, reinforcing the finding that gradient has a negligible effect on the HEV.

4.3.4 Single Direction Route Gradient Simulations

To investigate the effect of gradient on a net uphill and net downhill journey the two legs of the round journey that made up the LU15-UDC were used individually in simulations. The two legs were named W-E for the downhill west to east leg, and E-W for the uphill east to west leg. As shown in Figure 3.22 in the previous chapter, there is a gain of 8.25 meters elevation in the E-W route and therefore a decrease of an equal amount in the W-E route.

By again running simulations with differing initial SOCs, a SOC correction plot was produced as shown in Figure 4.23 and the corresponding SOC correction trendline equations are given in Table 4.11. From this plot it can be seen that the two tests without gradients are similar, at less than 0.2 l/100km apart, and there is a clear difference with the gradient cases. For the downhill leg the line is lower in the y-direction, and for the uphill leg the line is higher by a similar proportion. The

results are summarised in Table 4.12 from which it can be seen that the fuel consumption is 23.8% lower with downhill gradients and 28.0% higher with uphill gradients, both with respect to having no gradients.

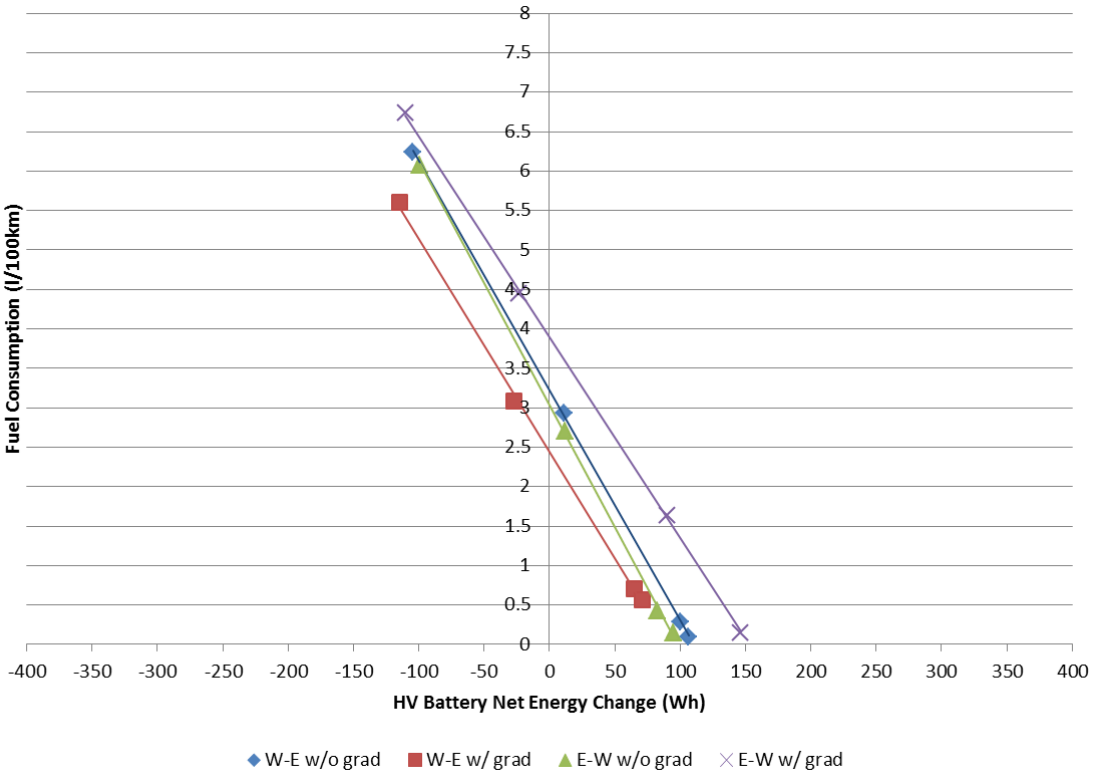

Figure 4.23: Uphill and downhill campus route sections simulation SOC correction plot

Table 4.11: Uphill and downhill campus route sections simulation SOC correction line equations

Route	Equation
W-E w/o gradients	y = -0.0291x + 3.2186
W-E w/gradients	y = -0.0270x + 2.4528
E-W w/o gradients	y = -0.0309x + 3.0409
E-W w/gradients	y = -0.0255x + 3.8918

Table 4.12: Uphill and downhill campus route sections simulation results

Route	Fuel cons. (l/100km)	Diff. to w/o grads
W-E w/o gradients	3.22	-
W-E w/gradients	2.45	-23.8%
E-W w/o gradients	3.04	-
E-W w/gradients	3.89	28.0%

These results show that gradient can have a significant result on the fuel consumption of a hybrid vehicle where there is a net change in elevation. The more important finding though is the earlier one in this chapter, of gradient having

negligible difference for a circular route. This is more relevant to real-world driving because overall journeys are carried out returning to the starting place on the whole.

4.3.5 Diesel Vehicle Simulation Comparison

A simulation model similar to a conventional diesel Citroën Berlingo 1.6 HDI like those typically used by Loughborough University Security was used for comparison to the Prius, to confirm if the results found for gradients are specific to vehicles with hybrid powertrains.

Without gradients the fuel consumption was 7.09 l/100km and with gradients 7.50 l/100km which shows a 5.8% increase due to gradients. As expected this is significantly more than for the Prius, confirming the benefit just for HEV powertrains of not seeing an increase of energy consumption due to gradients. This is due to the engine switching off on the downhill sections so therefore stopping consuming fuel, and also there is some brake energy recovery with the regenerative braking. For the conventional vehicle on the other hand, the engine does not switch off on the downhill sections so therefore continues to consume fuel, and there is no brake energy recovery.

A plot of the cumulative fuel consumption for the diesel vehicle which can be seen in Figure 4.24 can be compared to the equivalent plot for the HEV in Figure 4.16. For the conventional diesel vehicle the cumulative fuel used forms a much straighter line that for the HEV, due to the constant engine running with it being the sole power source. Comparing the two lines in Figure 4.24, there are two clear points at which the fuel consumption with gradients increases significantly compared to without gradients. One is at around 105 seconds where the short steep uphill section occurs, and the other is at approximately 400 to 450 seconds, corresponding to the long uphill stretch starting at 2000 meters. This confirms that the uphill gradients account for the increased energy consumption for the conventional vehicle.

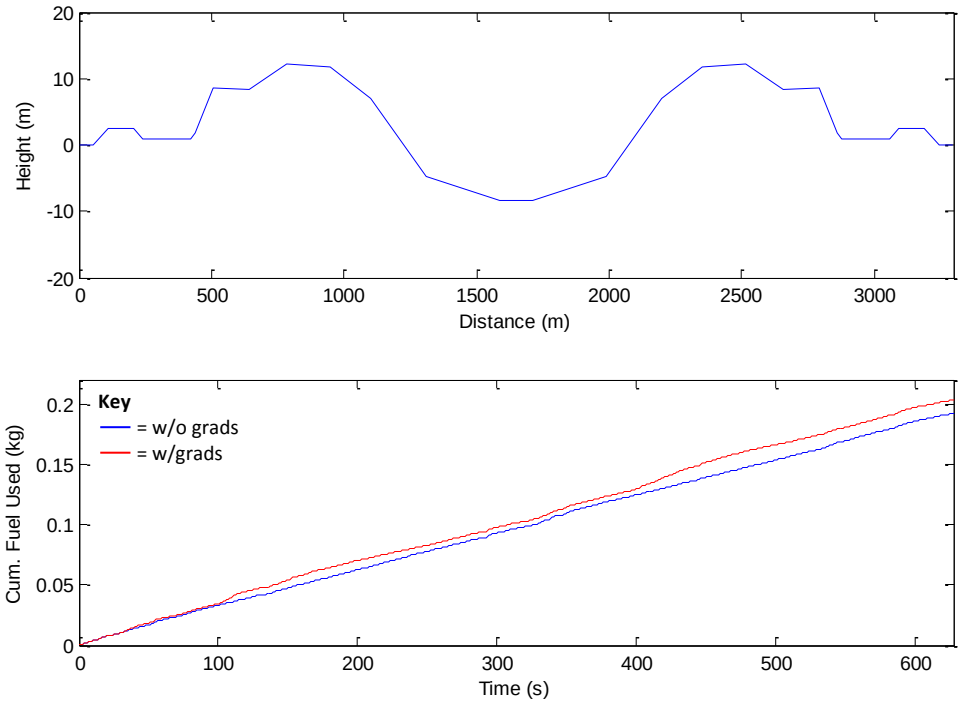

Figure 4.24: Diesel simulation LU15-UDC cumulative fuel consumption and cycle gradient profile

4.4 Chapter Conclusions

After the initial drive cycle comparison tests it was determined that battery energy usage must be included in the energy consumption to get reliable and meaningful results. From the repeated tests carried out with battery SOC measurement included and SOC correction carried out on the fuel consumption, the results were significantly different to the earlier ones. Following on from the conclusions from Section 4.1, the LUUDC fuel consumption was found to be 10.3% higher than the ECE-15 urban drive cycle due to the very different driving cycle profile, with the LUUDC being transient and having many more accelerations. The simulation fuel consumption results compared to the later chassis dynamometer test results were closer than with the original test results but the simulation is still 23.4% lower. After eliminating SOC effects that were present in the original tests, the proposed reasons for this are degradation of our test vehicle, particularly of the HV battery, giving it poorer fuel economy, and inaccuracy in the simulation model giving it fuel consumption lower than reality.

Whilst the chassis dynamometer lab test results became closer to the simulation results in the more accurate tests, the difference to the real-world driving increased by a large amount to 37.7%. It has been concluded that gradient has a negligible effect overall on the fuel consumption for a HEV when carrying out a circuit journey. Through analysing simulation data signals at a component level for power and energy flows, it was found that this is because the decreased fuel usage during engine-off periods when on downhill gradients coupled with increased regenerative braking energy outweighs the additional energy consumption required to power the vehicle uphill compared to on the flat.

However this result is not the case for a conventional diesel vehicle, where a 5.8% increase was seen when gradients are applied. For the HEV, when studying just net uphill and net downhill journeys the difference in fuel consumption compared to having no gradients is +28.0% and -23.8% respectively, showing that gradient can have a notable effect in certain circumstances. The other possible contributing factors to the difference between the chassis dynamometer test and real-world test

results, as suggested earlier, are the use of auxiliaries in low or high temperatures and the drive cycle accuracy.

These results are summarised in Figure 4.25. The remaining factors will be studied in the following chapters to establish their contributions.

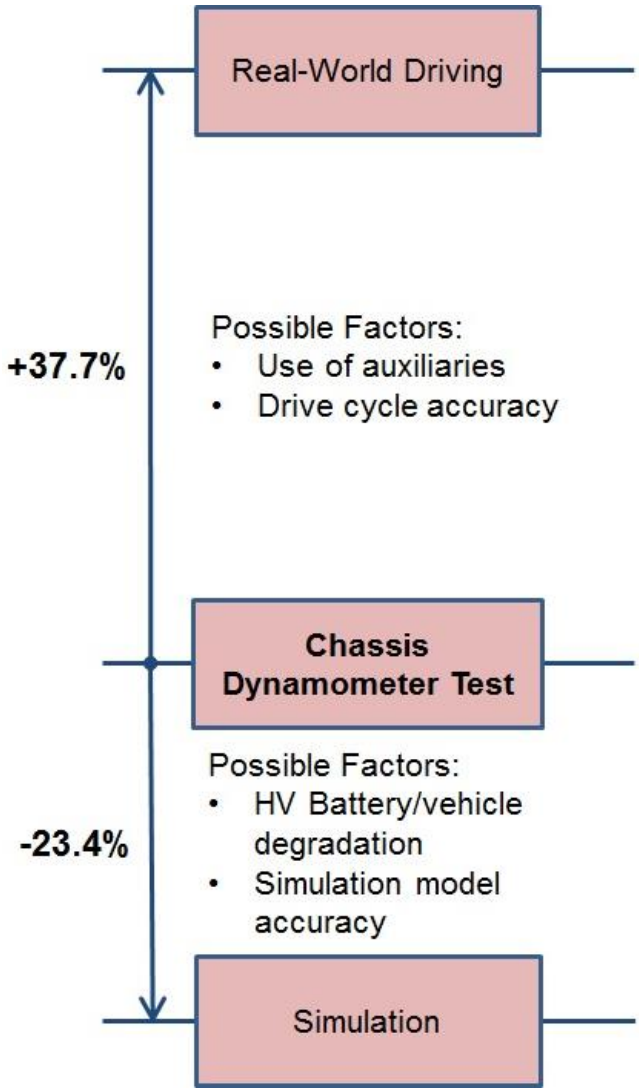

Figure 4.25: Chapter 4 results and conclusions summary diagram

5 Factors in Drive Cycle Development

It was found in Chapter 4 that there was a 37.7% difference in fuel consumption between the LUUDC chassis dynamometer testing and the real-world driving that the cycle is based on, and the gradient did not contribute towards it. A possible contributor from the list given at the end of the chapter could be the accuracy of the generated drive cycle in representing the original dataset being lower than desired. Therefore this will be investigated here.

Additionally, following on from the differences in energy consumption results seen between different drive cycles in Sections 4.1 and 4.2, the cycles are analysed statistically to find reasoning. The direct effect of acceleration in a drive cycle profile on fuel consumption is then studied using the new LUUDC2 and the LU15-UDC.

5.1 Drive Cycle Accuracy

To investigate the accuracy of the cycle, the drive cycle statistics programme that was developed was used on the full dataset to establish the target statistics that the developed cycles should meet as closely as possible. To do this all of the daily driving data files were joined together into one continuous trace then loaded into

the programme to be analysed. This function was incorporated into the beginning of a new version of the driving data formatting MATLAB programme detailed earlier in Section 3.3.2 and also discussed further in Section 5.1.2. A copy can be seen in Appendix 9.

5.1.1 Cycle Statistics Programme

A MATLAB programme was written to calculate drive cycle statistics, including the following list of parameters:

- Total distance
- Maximum speed
- Average speed
- Number of accelerations
- Number of decelerations
- Number of accelerations per km
- Number of decelerations per km
- Maximum acceleration
- Maximum deceleration
- Average acceleration
- Average deceleration

It also produces acceleration and deceleration magnitude distributions which will be described later in this section.

The simple metrics from the list above were defined as follows:

- Total distance – Sum of the speed trace converted into km/s
- Maximum speed – Maximum value of the speed trace
- Average speed – Mean of the speed trace values

The acceleration parameters will be described in the following subsections. The programme code can be seen in Appendix 10.

5.1.1.1 Drive Cycle Accelerations Calculation Method

A study based on data collected from multiple vehicles during real-world driving, analysed driving pattern parameters to determine significant factors that have an effect on fuel consumption and emissions [79]. Nine factors were identified, four of which describe aspects of acceleration and power demand, and two for speed level. This highlights the importance of accelerations in drive cycles, so they should be a focus.

Typically elsewhere in this field accelerations and decelerations are treated as just the change in speed from one time step to the next and statistics are based on these. However when driving a vehicle, the actual accelerations and decelerations encountered are over longer periods of time. As accelerations contribute significantly to a fuel consumption result a different approach was taken here, which finds complete acceleration and decelerations periods across multiple time steps. It is thought that this will give a more accurate representation of the driving statistics.

Accelerations are calculated by firstly identifying the start of an acceleration period by when the speed increases from one time point to the next. An array is formed with the first speed value of this acceleration before checking if the speed continues to rise at the next time step. If the acceleration continues, the speed value is added to the acceleration array. This process continues until the speed ceases to increase, leaving a resulting array of the speed trace for a single acceleration period. Using the change in speed between the first and last values of the array divided by the time duration, the acceleration is calculated and this value added to a new array of overall accelerations.

The above process then continues finding acceleration periods and adding the overall acceleration of each one to the overall accelerations array. The final array can then be used to calculate the number of accelerations by the count of the number of elements, and the number per kilometre by dividing this by the cycle distance. The minimum and maximum accelerations can be found from the

minimum and maximum values from the array, and the total cycle average acceleration from the mean of the values contained in it.

The whole process described above was also duplicated in the same manner for decelerations with the code instead finding decreases in speed over time steps rather than increases.

5.1.1.2 Drive Cycle Acceleration Distributions

The average acceleration and number of accelerations per kilometre give a good guideline comparison between drive cycles, but do not give a full detailed definition of a cycle or dataset. For example, a cycle may have equal numbers of small accelerations and large accelerations, and another may have all medium accelerations, and both would have similar statistics. As a test cycle though the fuel consumption of these is likely to be quite different.

For more detailed analysis, the production of acceleration per kilometre and deceleration per kilometre distributions that categorise them into groups of magnitude was integrated into the cycle statistics programme. This separates acceleration and deceleration into ten bands of increasing magnitude for each. From the accelerations calculated as described above in Section 5.1.1.1, the number within each range that defines a group of magnitude is counted to form a distribution. By dividing the elements of this distribution by the cycle distance then gives the acceleration and deceleration per kilometre distributions.

Existing works have used Speed and Acceleration Frequency Distributions (SAFDs) which capture second-by-second speed and acceleration as discussed in Section 2.3. Matching against these in a cycle development will only guarantee the occurrence frequency of acceleration rates at a moment in time, not necessarily complete acceleration events. Also, SAFDs are usually used as a validation check to confirm a final cycle's statistics are within tolerances, not as a development tool as in the case here, where acceleration distributions are used additionally as a measure to compare candidate cycles.

5.1.2 Drive Cycle Statistics

The statistics calculated for the dataset and for the LUUDC are shown in Table 5.1. It can be seen that the average speed is closely matched, but the other most important statistics for accuracy of the drive cycle, the number of accelerations and decelerations per kilometre, and the average acceleration, are 20-25% lower for the LUUDC than for the dataset. It appears that there is therefore room for improvement of the drive cycle to make it more representative.

Table 5.1: Driving dataset and LUUDC statistics comparison

	Data Set	LUUDC	Difference
Cycle dist (km)	17452	8.74	-
Max speed (km/h)	122.79	77.04	-37.3%
Avg speed (km/h)	11.78	12.53	6.3%
No of accels	413890	156	-
No of decels	414100	155	-
Accels per km	23.72	17.86	-24.7%
Decels per km	23.73	17.74	-25.2%
Max accel (m/s^2)	4.43	1.85	-58.3%
Max decel (m/s^2)	-8.13	-2.12	-74.0%
Avg accel (m/s^2)	0.425	0.333	-21.7%
Avg decel (m/s^2)	-0.434	-0.387	-10.7%

To look at the accelerations in more detail, the acceleration and deceleration distributions for the dataset and the LUUDC are analysed, as shown in Figure 5.1.

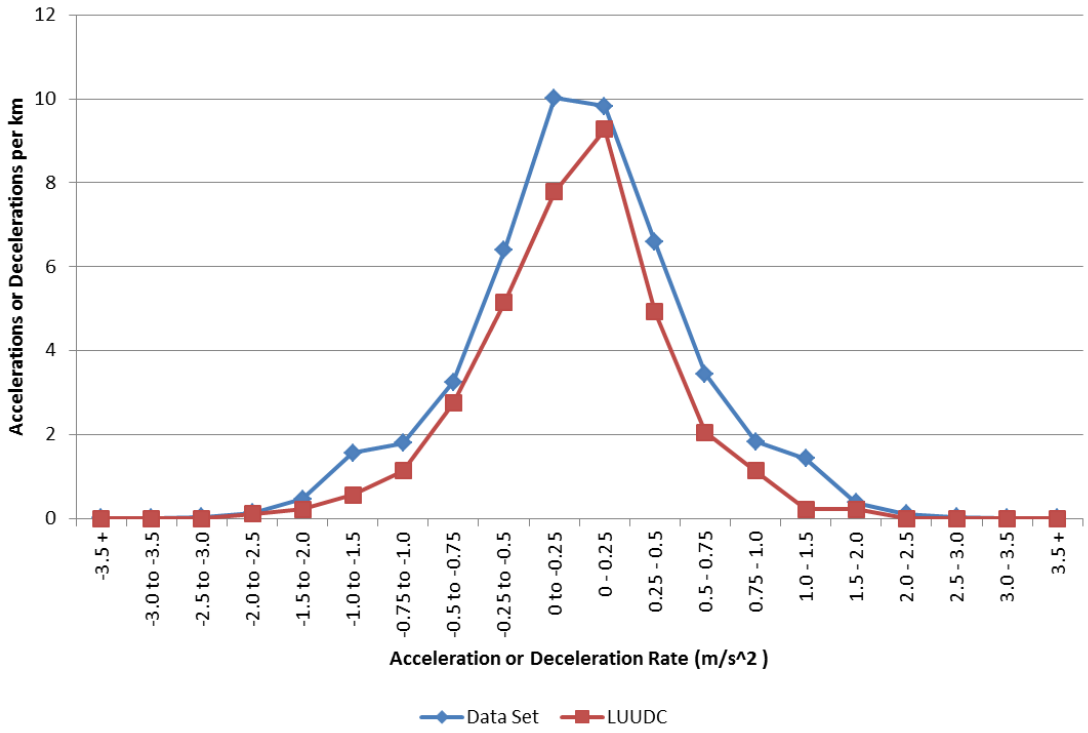

Figure 5.1: Driving dataset and LUUDC acceleration and deceleration distributions

It can be seen that the distributions follow a similar profile but there are differences, the largest of which is with the small decelerations of 0 to -0.25 m/s^2, but the most important differences seen are with the larger accelerations. There is a significant gap between the two lines across the range of accelerations from 0.25 to 1.5 m/s^2, which confirms that there is potential for the drive cycle match to the dataset to be improved. At this stage it is unknown how close would be acceptable or possible. By deriving a new drive cycle with a closer statistical match and testing it in simulation or on the chassis dynamometer to determine the effect on the cycle's energy consumption, the importance of this will be discovered.

In the new version of the driving data processing programme, rather than inserting an acceleration to smooth the speed trace where a jump in speed occurs, the section of data immediately following the jump and continuing until the next stop occurs, is removed. This was done because since the original version was produced it was thought that by inserting artificial accelerations the statistics for the data could be affected, or the artificial accelerations may be selected for use in the construction of a drive cycle. By not manipulating the data in the new version, and instead

removing small defective sections, the data will stay as representative of the real-world driving as possible.

Table 5.2 shows the statistics for the dataset processed in the original programme (v1) and in the new version (v2). The significant difference between average speeds is because the long zero speed stops were not removed in the new version, which brings the average speed down. The maximum acceleration and maximum deceleration are smaller in the old version due to the way the programme inserted accelerations to reduce any sharp accelerations deemed too large. The other key parameter statistics are very similar showing that the processing method does not have a significant effect on the data.

Table 5.2: Dataset original processing method and revised processing method statistics comparison

	Data Set v1	Data Set v2
Cycle dist (km)	17452	16885
Max speed (km/h)	122.79	122.79
Avg speed (km/h)	11.78	6.34
No of accels	413890	404890
No of decels	414100	405070
Accels per km	23.72	23.98
Decels per km	23.73	23.99
Max accel (m/s^2)	4.43	13.27
Max decel (m/s^2)	-8.13	-12.30
Avg accel (m/s^2)	0.425	0.429
Avg decel (m/s^2)	-0.434	-0.432

5.1.3 Drive Cycle Software Settings Validation

5.1.3.1 Sample Dataset Validation

An indicative sensitivity study to analyse the statistics of drive cycles of differing maximum segment durations was carried out on a small dataset consisting of three days' driving data, in order to hugely reduce processing time. Six cycles were produced using the FCRT software with maximum segment lengths ranging from 2.9% to 14.3% of the cycle duration. The important statistics used for comparison of cycles were the accelerations per kilometre, decelerations per kilometre, average acceleration and average deceleration. From the statistics for these cycles shown in Table 5.3 it can be seen that that there is variation in the results and the 0.03 hour 4.3% maximum segment size gave the closest statistics to the dataset used.

Table 5.3: Sample dataset and various settings sample drive cycle statistics comparison

	Data set	Maximum Segment Duration [h] (% of cycle duration)					
		0.02 (2.9%)	0.03 (4.3%)	0.04 (5.7%)	0.06 (8.6%)	0.08 (11.4%)	0.10 (14.3%)
Cycle dist (km)	243.11	3.73	4.13	3.07	3.69	3.18	2.70
Max speed (km/h)	78.6	57.3	46.9	41.9	47.9	54.9	63.9
Avg speed (km/h)	5.91	9.96	10.40	8.56	9.67	8.84	8.03
No of accels	5793	80	102	63	82	59	48
No of decels	5801	80	102	63	83	59	48
Accels per km	23.83	21.46	24.72	20.50	22.22	18.55	17.76
Decels per km	23.86	21.46	24.72	20.50	22.49	18.55	17.76
Max accel (m/s^2)	5.79	1.22	2.40	1.51	2.06	1.86	1.65
Max decel (m/s^2)	-12.30	-1.99	-2.08	-1.85	-1.96	-1.53	-1.51
Avg accel (m/s^2)	0.487	0.413	0.468	0.533	0.399	0.615	0.598
Avg decel (m/s^2)	-0.480	-0.470	-0.502	-0.578	-0.362	-0.716	-0.572

To compare acceleration distributions using numerical values, the difference between the value in each acceleration band of a cycle's distribution and the dataset's distribution was calculated. The sum of the absolute value of these differences gives the total variation from the target values, which was used as the accuracy measure for the drive cycles. These values are shown in Table 5.4 and a plot of the sum of the absolute differences is shown in Figure 5.2.

Table 5.4: Sample dataset and various maximum segment size sample drive cycles acceleration comparison

	No. of Accelerations per km										
	Acceleration (m/s^2)										Total
	0 - 0.25	0.25 - 0.5	0.5 - 0.75	0.75 - 1.0	1.0 - 1.5	1.5 - 2.0	2.0 - 2.5	2.5 - 3.0	3.0 - 3.5	3.5 +	
R-W sample data	8.72	6.15	3.78	2.34	2.04	0.52	0.12	0.07	0.03	0.05	23.83
0.02	5.90	10.19	3.49	0.80	1.07	0.00	0	0	0	0	21.46
Diff. from R-W data	-2.82	4.04	-0.30	-1.54	-0.97	-0.52	-0.12	-0.07	-0.03	-0.05	10.45
0.03	8.48	8.72	2.67	2.67	1.45	0.48465	0.24	0	0	0	24.72
Diff. from R-W data	-0.24	2.57	-1.12	0.32	-0.59	-0.04	0.12	-0.07	-0.03	-0.05	5.14
0.04	4.88	7.16	3.90	2.28	1.95	0.32533	0.00	0	0	0	20.50
Diff. from R-W data	-3.84	1.00	0.12	-0.07	-0.09	-0.20	-0.12	-0.07	-0.03	-0.05	5.58
0.06	7.05	10.84	1.63	1.08	1.36	0	0.27	0	0	0	22.22
Diff. from R-W data	-1.67	4.69	-2.16	-1.26	-0.69	-0.52	0.15	-0.07	-0.03	-0.05	11.28
0.08	4.09	4.72	3.77	3.14	2.52	0.31438	0	0	0	0	18.55
Diff. from R-W data	-4.63	-1.44	-0.01	0.80	0.47	-0.21	-0.12	-0.07	-0.03	-0.05	7.83
0.10	2.96	5.55	2.96	4.07	1.85	0.37009	0	0	0	0	17.76
Diff. from R-W data	-5.76	-0.60	-0.82	1.73	-0.19	-0.15	-0.12	-0.07	-0.03	-0.05	9.52

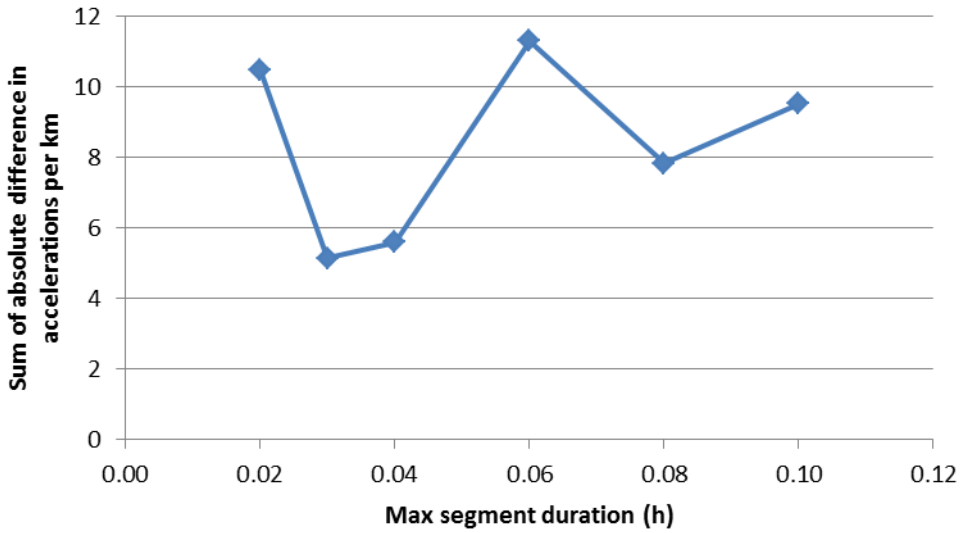

Figure 5.2: Sample dataset drive cycle maximum segment duration sensitivity analysis

From the chart a general trend can be seen with a decrease in maximum segment duration leading to a more accurate distribution match, down to a point at which there is poorer accuracy with the smallest segment duration. This can be interpreted as when a drive cycle is constructed from smaller segments, a larger number are used giving a greater representation of the whole dataset incorporated. For the very small segments there are likely to be very few that have the features able to give a statistical match to the dataset due to their limited length. The most accurate match for the 0.03 hour cycle agrees with the result of the statistics in Table 5.3. The trend appears that it is not entirely conclusive though due to the spike at 0.06 hour maximum segment.

5.1.3.2 Full Dataset Validation

Due to the above relationship not being completely clear because of the spike as mentioned above, using the full dataset a similar series of drive cycles with differing maximum segment lengths were developed to confirm the trend. The statistics for these are shown in Table 5.5. From these results the shortest segment durations have the most accurate match to the statistics of the dataset. The 2.9% is the closest this time which is different to that in the study above with the small sample dataset.

Table 5.5: New drive cycle statistics comparison to driving dataset

	Data Set	Cycle Max Segment Duration [h] (% of cycle duration)				
		0.02 (2.9%)	0.03 (4.3%)	0.04 (5.7%)	0.05 (7.1%)	0.07 (10%)
Cycle dist (km)	16885	4.86	3.65	4.08	4.43	3.60
Max speed (km/h)	122.79	48.04	44.32	52.76	48.56	58.36
Avg speed (km/h)	6.34	11.10	8.54	9.24	10.31	9.24
No of accels	404890	115	81	76	70	65
No of decels	405070	116	79	75	73	66
Accels per km	23.98	23.66	22.21	18.63	15.81	18.06
Decels per km	23.99	23.87	21.66	18.38	16.48	18.33
Max accel (m/s^2)	13.27	2.20	1.69	1.66	1.44	1.65
Max decel (m/s^2)	-12.30	-2.84	-3.53	-3.50	-2.04	-4.33
Avg accel (m/s^2)	0.429	0.460	0.395	0.497	0.373	0.474
Avg decel (m/s^2)	-0.432	-0.457	-0.580	-0.564	-0.456	-0.486

Using the same methodology with acceleration distributions, the plot of the sum of absolute differences can be seen in Figure 5.3. This has the same general trend as the small dataset albeit with a different shape formed by the points for the greater than 0.03 hour maximum segment durations. The point of greatest accuracy is again at 0.03 hour maximum segment, 4.3% of the cycle duration. This time this does not agree with the statistics in Table 5.5, where the statistics for the 0.02 hour maximum segment cycle are closer to those of the dataset. This highlights that it is important to analyse the drive cycle accelerations in this greater level of detail.

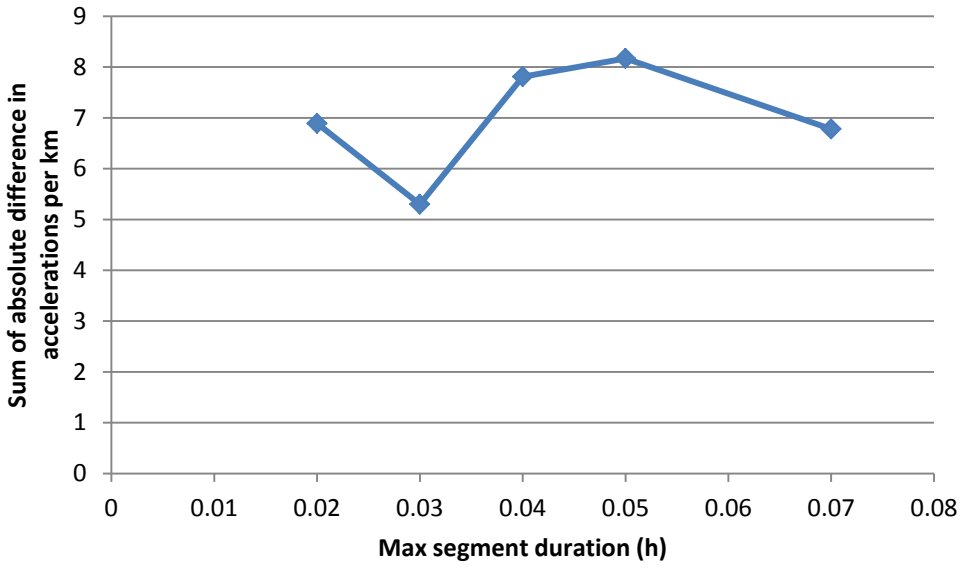

Figure 5.3: New drive cycle maximum segment duration sensitivity analysis

5.1.3.3 New LUUDC2 Cycle Production

The output drive cycles produced for studying the effect of maximum segment duration had cycle durations approximately half that of the input target length. Therefore a final cycle was generated with the target length doubled to make it a similar length to the original LUUDC, and from the findings above a comparable maximum segment duration of 5% was selected. For the acceleration distribution which is shown in Figure 5.5, the sum of the absolute differences measure is the lowest of all the cycles produced at 4.53, indicating it has the most accurate match to the original dataset. As this is significantly lower than the 6.12 difference for the original LUUDC, this new cycle named LUUDC2 was introduced for subsequent work. The LUUDC2 is shown in Figure 5.4.

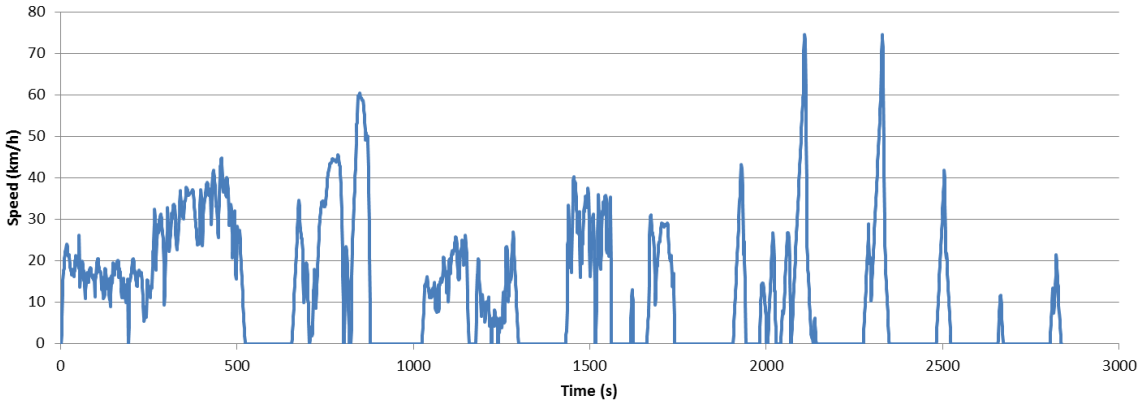

Figure 5.4: LUUDC2

Comparing the statistics of the new LUUDC2 to the driving dataset, it can be seen in Table 5.6 that the acceleration and deceleration statistics are much more closely matched. The accelerations and decelerations per kilometre difference to the dataset is approximately 17%, compared to 25% with the old cycle. The average accelerations and decelerations are now matched to less than 1% difference, rather than 10-22%.

Table 5.6: Comparison of LUUDC2 statistics to driving dataset

	Dataset	LUUDC	LUUDC2	Diff. LUUDC2 from dataset
Cycle dist (km)	16885	8.74	9.48	-
Max speed (km/h)	122.79	77.04	74.63	-39.2%
Avg speed (km/h)	6.34	12.53	12.02	89.6%
No of accels	404890	156	188	-
No of decels	405070	155	189	-
Accels per km	23.98	17.86	19.84	-17.3%
Decels per km	23.99	17.74	19.94	-16.9%
Max accel (m/s^2)	13.27	1.85	2.23	-83.2%
Max decel (m/s^2)	-12.30	-2.12	-2.21	-82.1%
Avg accel (m/s^2)	0.429	0.333	0.426	-0.6%
Avg decel (m/s^2)	-0.432	-0.387	-0.431	-0.4%

Looking at the acceleration and deceleration distributions in Figure 5.5, the LUUDC2 accelerations clearly match the dataset much more closely than the old cycle. The better matching is particularly noticeable for the 0.25-1.5 m/s^2 range, where the lines on the plot are significantly closer together. This cycle is therefore more representative of the original driving data than the previous cycle and should give closer fuel consumption results.

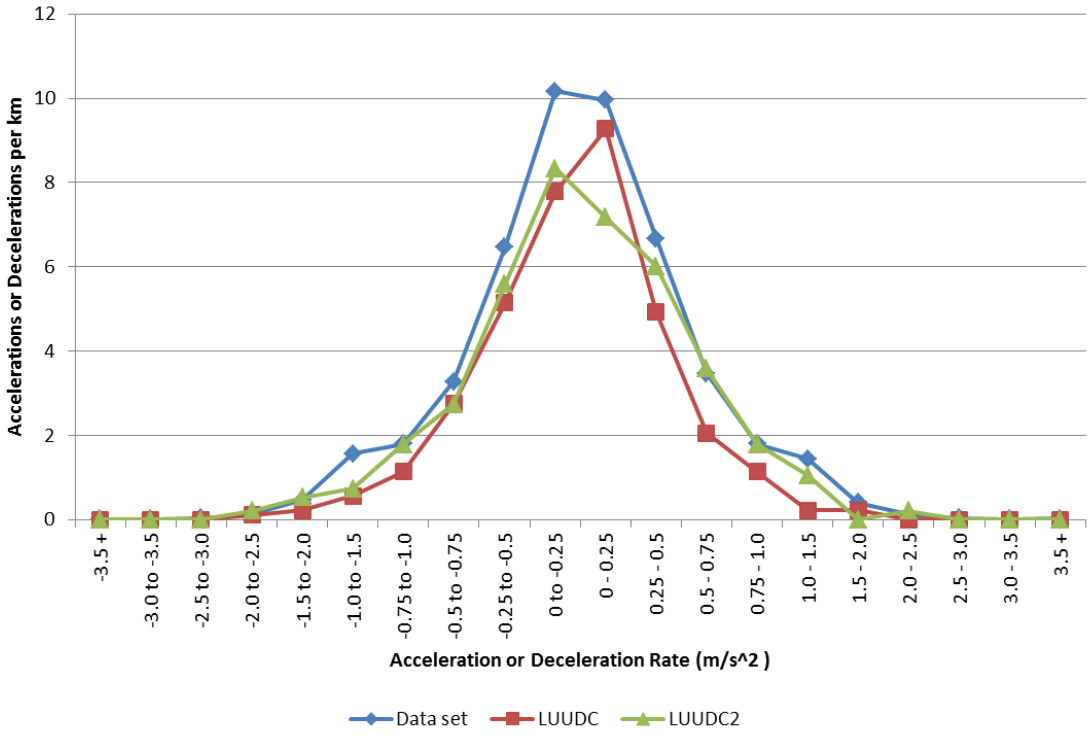

Figure 5.5: Driving dataset, old LUUDC and new LUUDC2 acceleration or deceleration distributions

There is a larger discrepancy with the 0 to 0.25 m/s^2 band but as this represents small speed fluctuations is not significant as these will only have a minor effect on energy consumption. This larger difference for this band in this cycle is likely to be due to the way in which the FCRT generates the drive cycles. There is a degree of variation possible in cycles produced with the same settings and input dataset, due to the nature in which a selection of segments are used which will be different each time, therefore varying the statistics of the cycle. On this occasion it happens that the match for the small accelerations is not as good as the old cycle. A way to obtain the best match including this acceleration range would be to generate a number of cycles with the same settings, calculate the statistics and acceleration distributions for each of them, then select the one with the closest match. This was not feasible for this study due to the previously mentioned issue of these cycle creations taking several days each to run, which there was not time to accommodate.

5.1.3.4 Simulation Testing of New LUUDC2

Carrying out simulations with varying initial SOCs and then producing an SOC correction plot, the new LUUDC2 drive cycle fuel consumption was found to be 4.17 l/100km. This is a 13.3% increase over the 3.68 l/100 km of the old cycle from Section 4.2.4. It can be expected that the same trend will be shown with chassis dynamometer testing of the new cycle, therefore bringing it closer to the real-world result. This will be confirmed later in Chapter 6.

5.2 Drive Cycle Comparison

Using the programme written in Section 5.1, statistical comparison between drive cycles can be made. Here the LUUDC2 will be compared to existing standard cycles.

5.2.1 Comparison of LUUDC2 Statistics to Existing Drive Cycles

Comparing cycle statistics of the LUUDC2 to the ECE-15 shows some very significant differences, see Table 5.7. In the LUUDC the number of accelerations per km is over 6 times greater and the maximum acceleration is more than doubled. The average acceleration is 81.2% larger in the ECE-15 due to its cycle profile consisting of similar constant rate accelerations, so does not provide a useful representation.

Comparing the LUUDC2 to the other urban cycles, the number of accelerations per kilometre is roughly similar to the Artemis Urban which is 18.8% lower and significantly more than the UDDS which is 70.1% lower. The UDDS has 16.4% lower average acceleration while the Artemis Urban's is 48.3% higher. Maximum accelerations are lower in both cycles than the LUUDC2, by 27.7% for the Artemis Urban and 47.0% for the UDDS. Average speed for the LUUDC2 is lower than both due to the long idle time bringing the average speed down. From these statistics there is not a clear link with the fuel consumption results recorded for these cycles in Section 4.2.3.

Table 5.7: Statistics of LUUDC2 and existing drive cycles

	Drive Cycle				
	LUUDC2	**ECE-15**	**Art Urb**	**UDDS**	**NEDC**
Cycle dist (km)	9.48	3.98	4.47	11.99	10.89
Max speed (km/h)	74.63	50.00	57.70	91.20	120.00
Avg speed (km/h)	12.02	18.33	17.48	31.51	33.20
No of accels	188	12	72	71	16
No of decels	189	16	70	81	18
Accels per km	19.84	3.02	16.10	5.92	1.47
Decels per km	19.94	4.02	15.65	6.76	1.65
Max accel (m/s^2)	2.23	1.04	1.61	1.18	1.04
Max decel (m/s^2)	-2.21	-0.83	-1.88	-1.34	-0.98
Avg accel (m/s^2)	0.426	0.772	0.632	0.356	0.668
Avg decel (m/s^2)	-0.431	-0.743	-0.651	-0.341	-0.754

Looking at the acceleration distributions provides a more detailed comparison of the cycle acceleration statistics; a plot of these is shown in Figure 5.6. This shows very different distributions for the cycles. The LUUDC2 and UDDS are similarly shaped, roughly like a normal distribution, with a clear peak at the smallest magnitude accelerations and decelerations, with the frequency decreasing with increasing magnitude. For the Artemis Urban the distribution is much flatter with a more consistent spread of accelerations across the +/-1m/s^2 magnitude range, before reducing beyond this. The synthetic linear profile of the ECE-15 and NEDC leads to a very different distribution to the transient cycles, with 0 or close to 0 accelerations/decelerations in the low magnitudes, and small peaks at 0.5 to 0.75 m/s^2 acceleration and in -0.75 to -1.0 m/s^2 deceleration.

The LUUDC2 has around twice the number of small accelerations under 0.25 m/s^2 compared to the other two transient cycles. Increasing beyond this it has approximately 50% more accelerations in the 0.25 to 0.5 m/s^2 group than the Artemis Urban, and 12 times more than the UDDS. In the 0.5 to 0.75 m/s^2 band the LUUDC2 gets close to the Artemis Urban which is 12.7% lower, before dipping below where it is 50% lower in the next band.

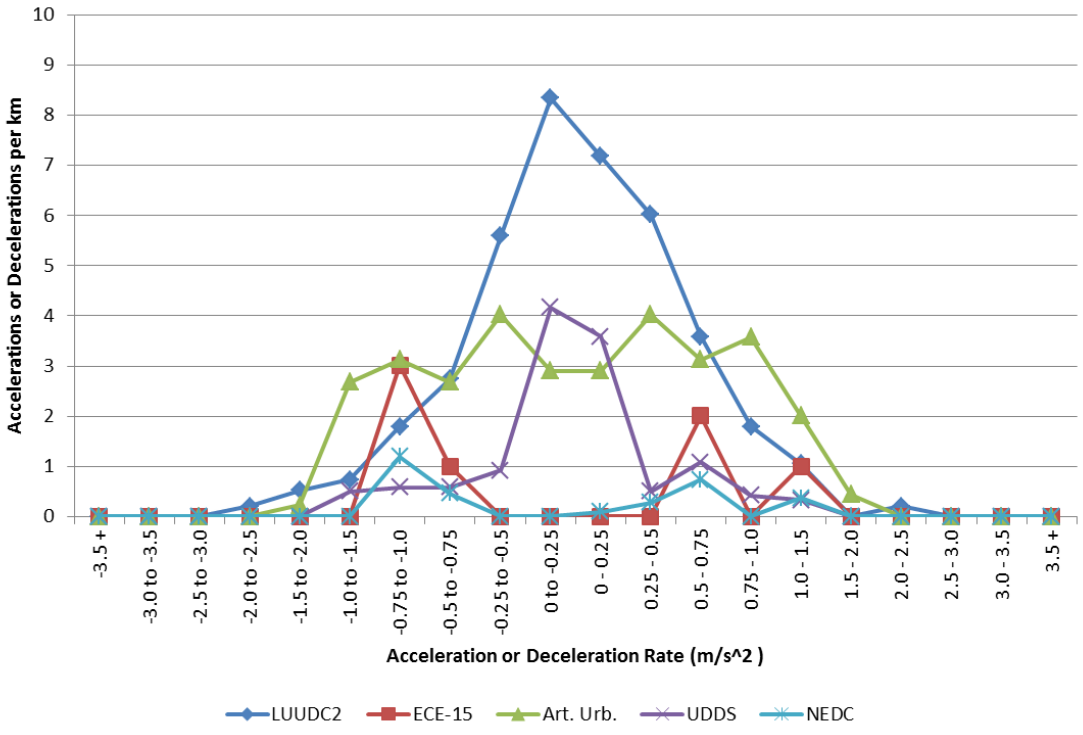

Figure 5.6: Acceleration and deceleration distributions for LUUDC2 and existing drive cycles

These more detailed acceleration statistics can now explain the fuel consumption results seen in Section 4.2.3, and 6.2.4 for the LUUDC2, which the earlier statistics in Table 5.7 could not. The highest fuel consumption was on the Artemis Urban cycle followed closely by the LUUDC2. These two cycles have the highest number of accelerations per km in the higher bands. On the other hand the UDDS and ECE-15 gave the lowest fuel consumption and they have fewer larger magnitude accelerations.

The NEDC is a different case to this trend because it is not an urban cycle, it has a high speed section which has an influence on fuel use. It leads to higher fuel consumption which can be seen in the test results in Section 4.2.3.2 where the NEDC on the chassis dynamometer was 1.7% higher than the result of the LUUDC.

5.3 Drive Cycle Profile Effect on Fuel Consumption

From the later results in Section 6.2.4 for the chassis dynamometer testing, the LUUDC2 gives 31.7% higher fuel consumption than the LU15-UDC at 5.20 l/100km and 3.95 l/100km respectively. Similarly, in simulations 4.17 l/100km on the LUUDC2 is 32.8% higher than the LU15-UDC with 3.14 l/100km. These variations will be down to the cycle profile differences, including accelerations, so statistical analysis of each of the cycles is required.

5.3.1 Comparison of LUUDC2 Statistics to LU15-UDC

Comparing the cycle statistics for the two Loughborough University drive cycles, shown in Table 5.8, the average speed of the LU15-UDC is higher than for the LUUDC2 due to more of its duration being cruising and having very little stop time. There are also more accelerations per kilometre in the LU15-UDC due to the small speed fluctuations in the cycle, while the maximum accelerations are closely matched. The key comparison here is that the average acceleration is 78% higher in the LUUDC2.

Table 5.8: LUUDC2 and LU15-UDC cycle statistics

	Drive Cycle	
	LUUDC2	**LU15-UDC**
Cycle dist (km)	9.48	3.26
Max speed (km/h)	74.63	29.20
Avg speed (km/h)	12.02	18.66
No of accels	188	78
No of decels	189	75
Accels per km	19.84	23.93
Decels per km	19.94	23.01
Max accel (m/s^2)	2.23	2.22
Max decel (m/s^2)	-2.21	-2.03
Avg accel (m/s^2)	0.426	0.240
Avg decel (m/s^2)	-0.431	-0.242

From the acceleration distributions shown in Figure 5.7 it can be seen that the LU15-UDC has a large number of accelerations of less than 0.25 m/s^2 due to the small speed fluctuations as mentioned above, which will not be significant to the fuel use over this drive cycle. The distribution for the LUUDC2 is more widely spread with significantly more accelerations of the larger magnitudes of 0.25 to 1.5

m/s^2, which are the ones that contribute to the higher fuel consumption of this cycle.

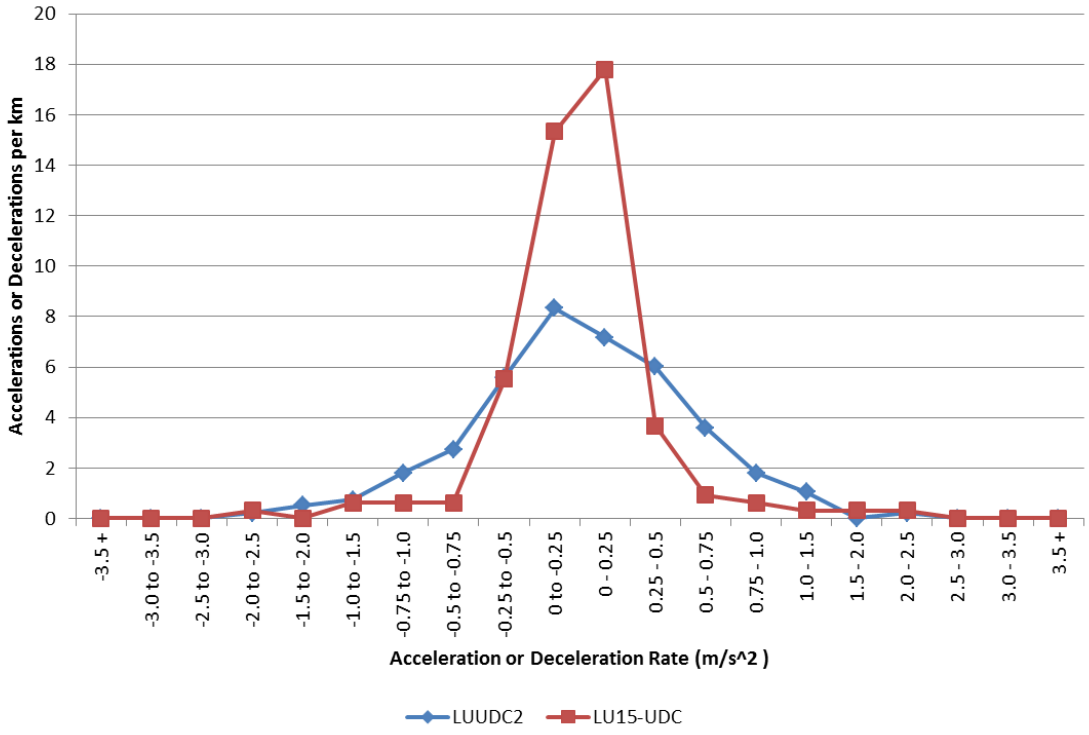

Figure 5.7: LUUDC2 and LU15-UDC acceleration and deceleration distributions

5.3.2 Acceleration Rate Fuel Consumption Comparison

5.3.2.1 Acceleration Rate Cycles

To directly compare the effect acceleration rate has on fuel consumption, a cycle was designed with multiple acceleration features all with the same acceleration rate, and then duplicates of it were made with a different acceleration rate in each one. There are three main aspects to the cycle, accelerations from and decelerations to rest, accelerations from and decelerations to a cruise, and small speed fluctuations.

The first part of the cycle consists of five pairs of peaks, starting after a 5 second stop with an acceleration from 0 to 1 m/s, a deceleration back to 0 m/s, then a repeat of this. Next there are similar pairs of peaks consisting of an acceleration and deceleration with maximums of 3, 6, 9 and 15 m/s, all separated by 5 second stops. There is an acceleration to 6 m/s leading into a 5 second cruise then an acceleration up to 9 m/s and deceleration back to 6 m/s. This acceleration peak is repeated before pairs of peaks with an acceleration and deceleration with

maximums of 12 and 15 m/s, all separated by 5 second 6 m/s cruises. Next after another 5 second cruise are small speed fluctuations with acceleration to 7 m/s, deceleration back to 6 m/s, then a repeat of this peak. After a 5 second cruise there is an acceleration to 15 m/s then deceleration to 13 m/s, an acceleration to 15 m/s, a deceleration to 13 m/s again, then a final acceleration back up to 15 m/s. The cycle is ended with a 5 second cruise at 15 m/s before decelerating back to a standstill and a 5 second stop. The cycle is shown in Figure 5.8.

These cycles were produced with accelerations of 0.25, 0.5 and 1.0 m/s^2 acceleration rates, all of these can be seen in Figure 5.9. These accelerations were chosen as they cover the range of average accelerations calculated for all the drive cycles studied, meaning that the results from this can be linked to those cycles.

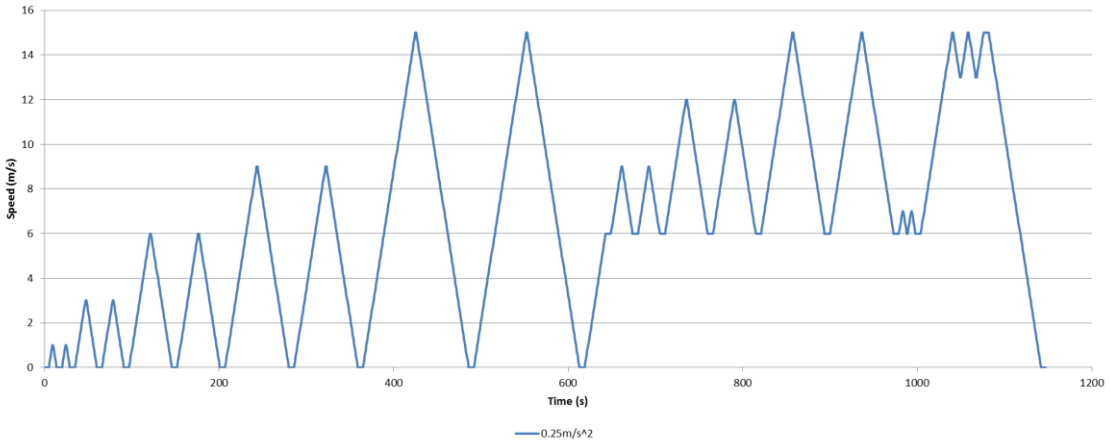

Figure 5.8: Acceleration rate 0.25 m/s^2 drive cycle

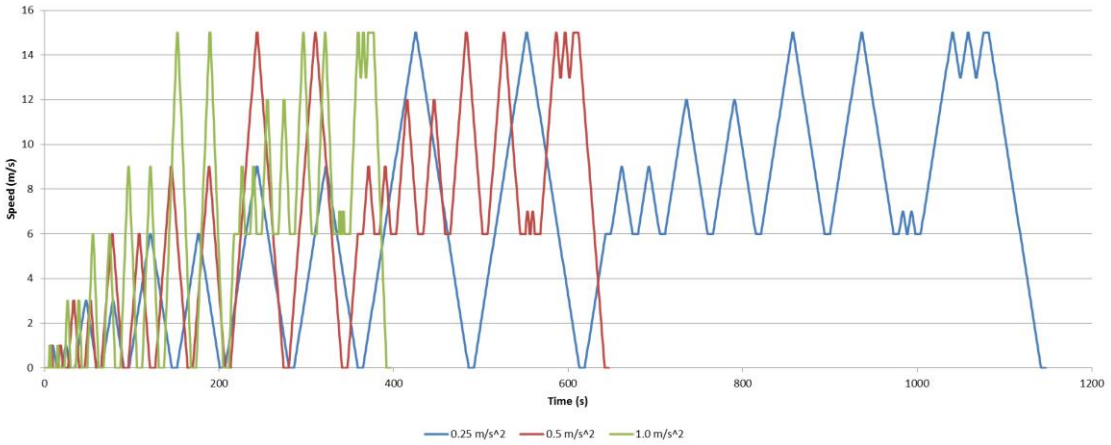

Figure 5.9: Acceleration rate 0.25, 0.5 and 1.0 m/s^2 drive cycles

The increased acceleration rate reduces the cycle distance and duration as can be seen in Figure 5.9. The 1.0 m/s^2 cycle has approximately half the cycle distance of the 0.5 m/s^2 cycle, and it itself has approximately half the cycle distance of the 0.25 m/s^2 cycle. This does not have a significant impact on the results though due to the state of charge correction procedure being applied. To confirm this, the process below was repeated with a version of the 0.5 m/s^2 cycle repeated twice, and of the 1.0 m/s^2 cycle repeated four times so that all the cycles had similar cycle distances, and the results were within 1%.

5.3.2.2 Acceleration Rate Results

Simulations were carried out on each of the three cycles using the Toyota Prius model with the state of charge correction process again followed. The results which can be seen in Figure 5.10 and Table 5.9 show the acceleration rate has a significant effect on fuel consumption. For the 0.5 m/s^2 cycle the fuel consumption of 2.89 l/100km is 17.8% higher than the 0.25 m/s^2 cycle's 2.45 l/100km. With the acceleration rate increased to 1 m/s^2 it leads to a huge 67% increase in fuel consumption to 4.10 l/100km.

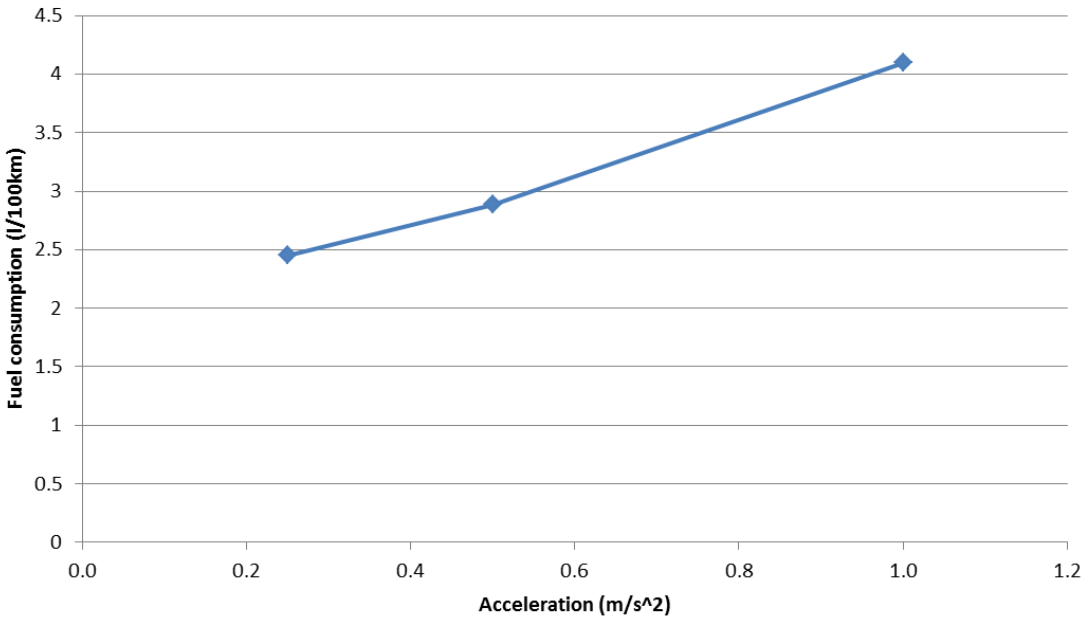

Figure 5.10: Acceleration rate drive cycle fuel consumption results

Table 5.9: Acceleration rate drive cycle fuel consumption results with difference

Acceleration (m/s^2)	Fuel cons. (l/100km)	Inc. over 0.25 m/s^2
0.25	2.45	0.0%
0.5	2.89	17.8%
1.0	4.10	67.1%

A MATLAB programme was written to linearly interpolate and extrapolate from these data points to be used to give an estimated fuel consumption increase for a given increase in average acceleration rate which can be applied to drive cycles.

5.3.2.2.1 Acceleration Rate Results Applied to LU Cycles

The average acceleration of the LUUDC2 at 0.43m/s^2 is higher than the LU15-UDC at 0.24 m/s^2. This difference equates to an estimated increase in fuel consumption of 13.6% due to the increased average acceleration. This confirms that acceleration is a very significant factor in drive cycles.

This analysis accounts for the effect of increasing acceleration rate based on the average acceleration for a cycle, however it is thought that by taking this further using other statistical analysis methods on the accelerations, such as possibly cluster analysis, the contribution to increased fuel consumption would be greater than the 13.6% determined here.

5.4 Chapter Conclusions

A programme was produced to calculate drive cycle statistics with a focus on accelerations due to their importance in defining a cycle. An alternative method of defining accelerations was used that treats a continuous acceleration period as one acceleration rather than taking the acceleration between each time step. Acceleration and deceleration distributions were also used in the programme which counts accelerations and decelerations within groups of magnitude to look at them in more detail than by just using the average.

Using these metrics the LUUDC was compared to the full data set and potential for improvement was observed. Through a cycle refinement process a new cycle, the LUUDC2, was developed and it showed a much closer statistical match to the original data. The difference in accelerations per kilometre to the data set came down from 25% to 17%, and the average acceleration became within 1% rather than 22%. This shows the importance of creating drive cycles with an accurate match to a detailed set of statistics, to give an output that is representative of the data that it is based on in order to get meaningful results from it.

The statistics of the LUUDC2 were compared to those of the ECE-15 and other existing drive cycles. The acceleration distribution profiles differed significantly between cycles and they explain earlier results trends from Sections 4.2.3 and 4.2.4, and the LUUDC2's result in Section 6.2.4. Following this, the direct effect of changing the average acceleration of a cycle was investigated to quantify the fuel consumption difference between the LU15-UDC and the LUUDC2. From the study carried out it was indicated that the difference in their average acceleration equated to a 13.6% increase in energy consumption. This is close to half of the measured difference but it is thought that using further statistical methods the percentage would be higher.

6 Key Contributors to Hybrid Electric Vehicle Fuel Consumption in Real-World Driving

It has been established in Chapter 4 that gradient has a negligible effect on the fuel consumption of a HEV, and in Section 5.1 it was found that cycle production processes are important, leading to a new drive cycle being developed. Here further factors that could also be an influence are investigated.

The effect of differing battery initial SOC levels was eliminated in the experimental work by accounting for the battery energy in the corrected fuel consumption, but it is interesting to determine the amount of influence it has and why, so this is covered at the start of this chapter. There were notable differences in the gradients of the trendlines of the SOC correction plots in Chapter 4, which appeared to be related to the length of the cycles. This relationship is studied in the second part of Section 6.1.

The difference between the fuel consumption results in the chassis dynamometer tests and simulation is investigated by looking into the factors suggested earlier which includes the Autonomie model accuracy and degradation of the test vehicle.

Within the degradation study, the HV battery is focussed on with battery charge and discharge tests carried out.

In the final section of the chapter the higher fuel consumption measured in the real-world driving testing is examined. A study is conducted based on data from the literature into the contribution of using the heater or air conditioning in corresponding low or high temperatures.

6.1 Initial State of Charge Level

6.1.1 Chassis Dynamometer Tests

The chassis dynamometer testing discussed in Chapter 4 was carried out with widely varying initial HV battery SOCs, so that the effect of this on the drive cycle energy consumption could be studied. In Figure 4.8 there is a clear trend of decreasing fuel consumption with increasing net battery energy change. Compared to a mid-level initial SOC, with a low initial SOC the ICE has to operate for more of the time in order to recharge the battery to meet its usual charge sustaining level, therefore increasing the fuel consumed. Conversely, with a high initial SOC the ICE is operated less due to more electrical energy being available to drive the car, whilst still ending with a mid-level SOC at the end of test.

Table 6.1: LUUDC chassis dynamometer test results for various initial battery SOCs

	Run 1	Run 2	Run 3	Run 4	Run 5	Run 6
Initial SOC (%)	42.5	41.5	53.5	53.5	77.0	76.5
End SOC (%)	54.5	54.0	54.5	54.0	54.0	54.0
ΔSOC (%)	12.0	12.5	1.0	0.5	-23.0	-22.5
Fuel Used (l)	0.4613	0.4552	0.4041	0.4214	0.3606	0.3475
Distance (km)	8.778	8.838	8.766	8.207	8.885	8.855
Fuel Consumption (l/100km)	5.26	5.15	4.61	5.13	4.06	3.92
Battery Energy Consumption (Wh)	157.20	163.75	13.10	6.55	-301.30	-294.75
Fuel Energy Consumption (Wh)	4074.82	4020.93	3569.55	3722.37	3185.30	3069.58
Fuel Energy Consumption (Wh/km)	464.21	454.96	407.20	453.56	358.50	346.65

Table 6.2: LUUDC chassis dynamometer average test results for various initial battery SOCs

	Initial SOC Point		
	Low	Mid	High
Initial SOC (%)	42.00	53.50	76.75
End SOC (%)	54.25	54.25	54.00
ΔSOC (%)	12.25	0.75	-22.75
Fuel Used (l)	0.4583	0.4128	0.3541
Distance (km)	8.808	8.487	8.870
Fuel Consumption (l/100km)	5.20	4.87	3.99
Battery Energy Consumption (Wh)	160.48	9.83	-298.03
Fuel Energy Consumption (Wh)	4047.88	3645.96	3127.44
Fuel Energy Consumption (Wh/km)	459.58	430.38	352.58

The results for the LUUDC are shown in Table 6.1, and in Table 6.2 are summarised with average values of the two comparable runs. Compared to the near to charge sustaining tests, with low initial SOC at an average of 42.0% the average fuel consumption was 6.8% higher. Making the same comparison but with the high initial SOC average of 76.75%, the average fuel consumption was 18.1% lower. This is clearly linked to the net change in battery SOC with +12% for the low initial SOC, +0.75% for the medium initial SOC and -23% for the high initial SOC.

6.1.2 Simulation Analysis

6.1.2.1 LUUDC Data Analysis

To investigate the system operation, Autonomie simulations were carried out. In these the same settings were used as previously, but in addition the control system target battery SOC level was set to 55% to reflect that of the real test vehicle. The results can be seen in Table 6.3. Here the changes in SOCs are similar to the chassis dynamometer test, but the fuel consumptions are lower. The change in fuel consumption compared to a medium initial SOC is +23.5% for a low initial SOC, and -41.0% for a high initial SOC, so is greater than in the chassis dynamometer tests.

Table 6.3: LUUDC simulation test results for various initial battery SOCs

	Initial SOC Point		
	Low	**Mid**	**High**
Initial SOC (%)	42.0	55.0	77.0
End SOC (%)	54.93	54.87	54.29
ΔSOC (%)	12.93	-0.13	-22.71
Distance (km)	8.73	8.72	8.72
Fuel Consumption (l/100km)	4.73	3.83	2.26

From the simulations, looking at Figure 6.1 which shows the battery SOC for each of the three initial SOC levels, it can be seen that with the low initial SOC the battery is quickly charged to the same level as the medium initial SOC within the first 400 seconds, after which it follows the same line. The high initial SOC on the other hand discharges gradually over the first 1600 seconds before following the same line as the others. Further on in time however, the line deviates slightly from the other two but follows the same profile. It can be noted also that the high SOC line follows a close profile to the others in the early part of the cycle whilst it converges on them.

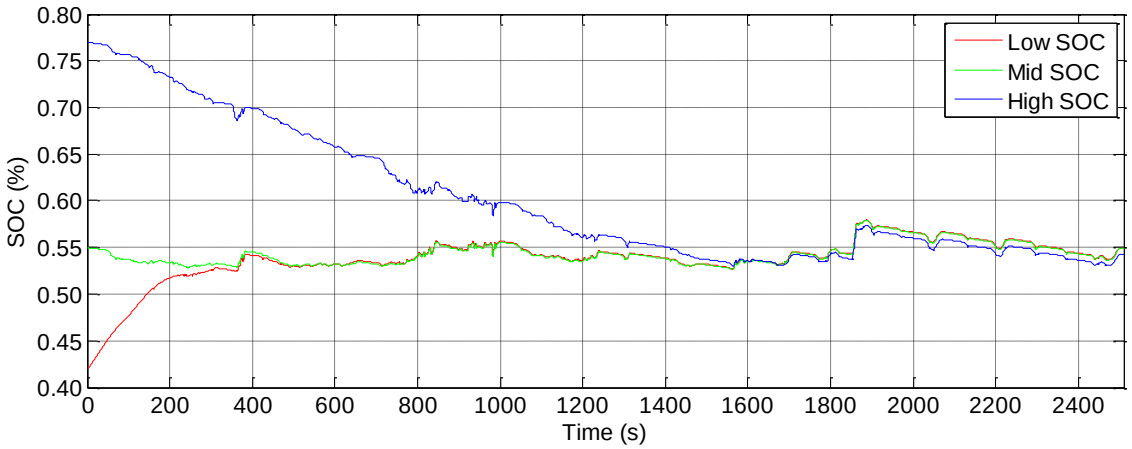

Figure 6.1: LUUDC simulation battery SOC for various initial SOCs

The output battery energy is shown in Figure 6.2 which can be clearly related to the SOC in Figure 6.1. For the low initial SOC the energy out increases negatively during the first 400 seconds, i.e. energy is flowing in because it is charging. With the high initial SOC the energy out increases over the first 1600 seconds before following the same profile as the other two lines.

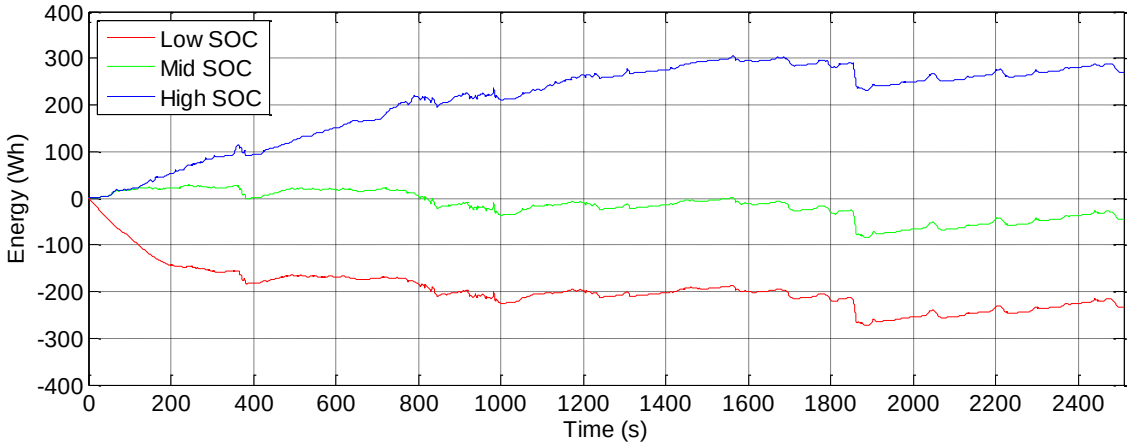

Figure 6.2: LUUDC simulation battery energy out for various initial SOCs

Figure 6.3 shows the energy out for MG2 and Figure 6.4 shows energy out for the ICE. For MG2 the trends correspond with the battery energy output, due to the battery powering MG2. For the low initial SOC the energy out increases negatively from the start of the test and for the high initial SOC it increases positively from the start. Again, later in the cycle from 1200 seconds onwards, the three lines follow a closely matched profile.

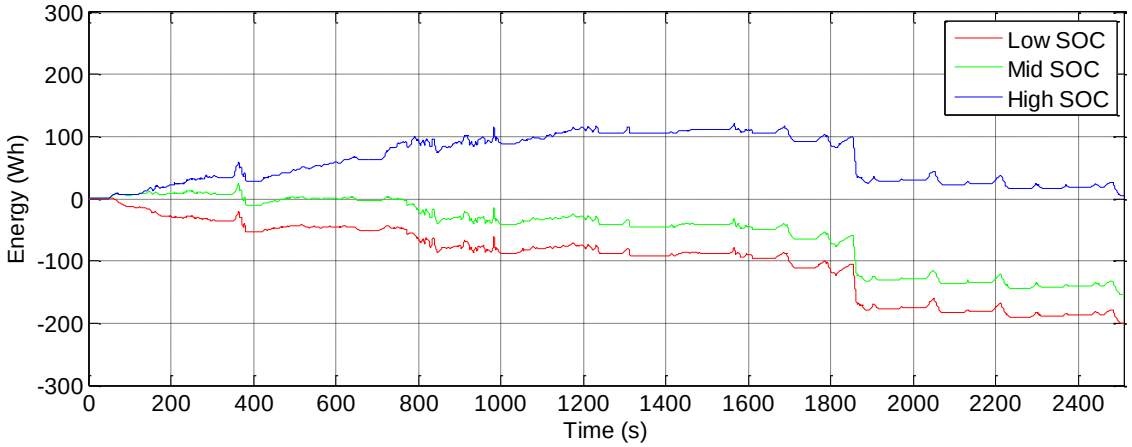

Figure 6.3: LUUDC simulation MG2 energy out for various initial SOCs

Due to having little power available for driving the vehicle and charging of the battery taking place, there is a significant amount of energy output from the ICE during the first 400 seconds of the drive cycle with the low initial SOC. For the medium initial SOC there is no energy output for the first 150 seconds, then a gradual increase to a much lower level than the low initial SOC case. With the high initial SOC there is no energy output from the engine until approximately 360 seconds where there is a small increase, and then a further section of approximately

360 seconds duration where there is no energy output. From around 720 seconds the three lines follow a similar profile to each other.

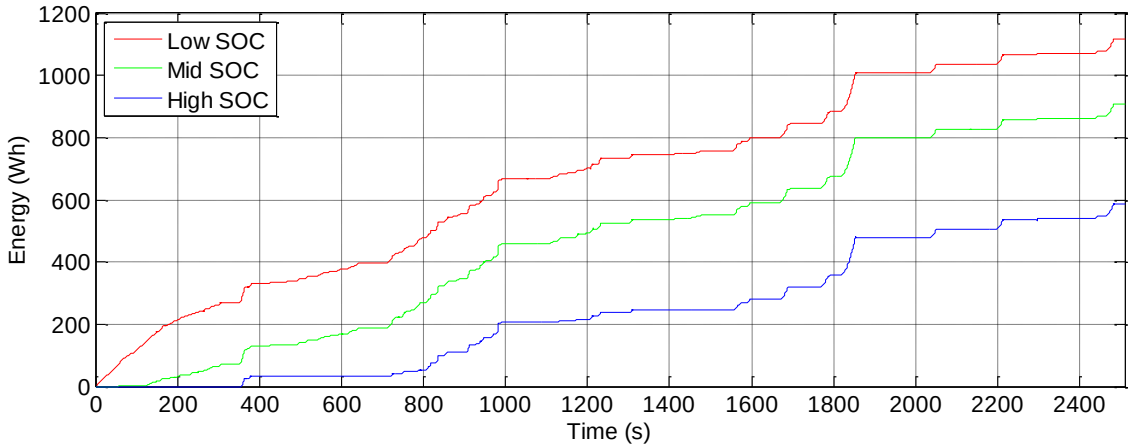

Figure 6.4: LUUDC simulation ICE energy out for various initial SOCs

6.1.2.2 ECE-15 Data Analysis

For comparison to the LUUDC, the chassis dynamometer results for the ECE-15 can be seen in Table 6.4, and summarised average values in Table 6.5. The difference in fuel consumption between medium initial SOC and low or high SOCs is close to double that for the LUUDC, at +12.4% and -36.3% respectively. This shows that energy consumption on the ECE-15 is much more sensitive to the initial SOC level.

Table 6.4: ECE-15 chassis dynamometer test results for various initial battery SOCs

	Run 1	Run 2	Run 3	Run 4	Run 5	Run 6
Initial SOC (%)	38.5	40.0	55.0	53.0	79.0	77.0
End SOC (%)	57.0	55.5	54.5	55.0	53.0	52.0
ΔSOC (%)	18.5	15.5	-0.5	2.0	-26.0	-25.0
Fuel Used (l)	0.2178	0.1914	0.1777	0.1838	0.1022	0.1294
Distance (km)	4.030	4.045	4.025	3.992	4.019	4.041
Fuel Consumption (l/100km)	5.40	4.73	4.41	4.60	2.54	3.20
Battery Energy Consumption (Wh)	242.35	203.05	-6.55	26.20	-340.60	-327.50
Fuel Energy Consumption (Wh)	1923.90	1690.70	1569.68	1623.57	902.77	1143.03
Fuel Energy Consumption (Wh/km)	477.39	417.97	389.98	406.71	224.62	282.86

Table 6.5: ECE-15 chassis dynamometer average test results for various initial battery SOCs

	Initial SOC Point		
	Low	Mid	High
Initial SOC (%)	39.25	54.00	78.00
End SOC (%)	56.25	54.75	52.50
ΔSOC (%)	17.00	0.75	-25.50
Fuel Used (l)	0.2046	0.1808	0.1158
Distance (km)	4.038	4.009	4.030
Fuel Consumption (l/100km)	5.07	4.51	2.87
Battery Energy Consumption (Wh)	222.70	9.83	-334.05
Fuel Energy Consumption (Wh)	1807.30	1596.63	1022.90
Fuel Energy Consumption (Wh/km)	447.68	398.34	253.74

Simulation results for ECE-15 are shown in Table 6.6. Again the change in fuel consumption as a result of changing the initial SOC is much greater in the simulations than the dynamometer tests.

Table 6.6: ECE-15 simulation test results for various initial battery SOCs

	Initial SOC Point		
	Low	Mid	High
Initial SOC (%)	42.0	55.0	77.0
End SOC (%)	54.98	54.95	59.89
ΔSOC (%)	12.98	-0.05	-17.11
Distance (km)	3.98	3.97	3.97
Fuel Consumption (l/100km)	4.93	3.06	0.88

Plots from the simulations of the same signals as for the LUUDC are shown in Figure 6.5 to Figure 6.8. These show generally similar trends as the plots for the LUUDC, with some key details to point out as follows:

- With the high initial SOC, the SOC does not meet the level of the other two lines as due to the shorter cycle duration it does not have enough time for this to happen
- The battery energy out line for the high initial SOC does not follow the same profile as the other lower cases
- The trends of the three MG2 energy out lines again can be linked with the battery energy out plots, however this time the signals are more stable without the high frequency changes seen in the LUUDC plot
- The ICE energy out shows a very similar result fitted into the shorter time period, with the y-axis scale being approximately half the magnitude of that

of the LUUDC, due to the lower fuel consumption of the ECE-15 and the shorter cycle time

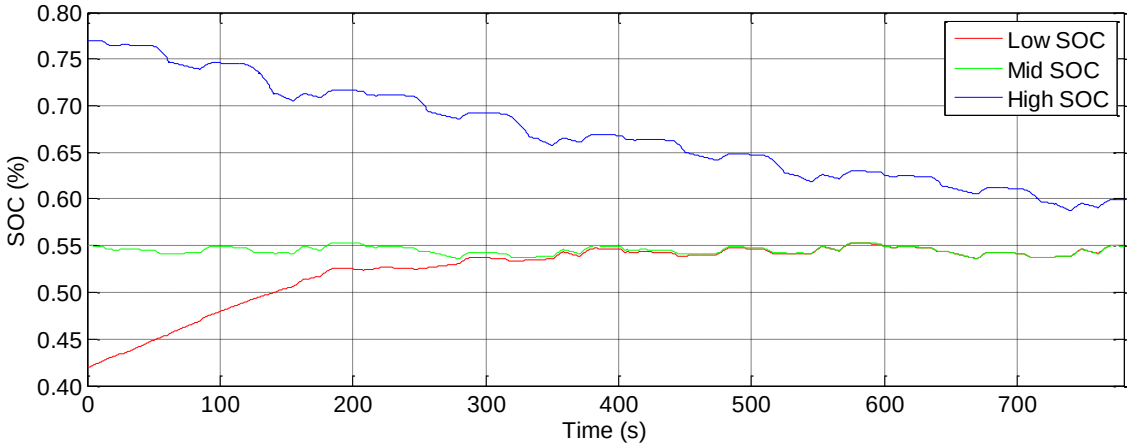

Figure 6.5: ECE-15 simulation battery SOC for various initial SOCs

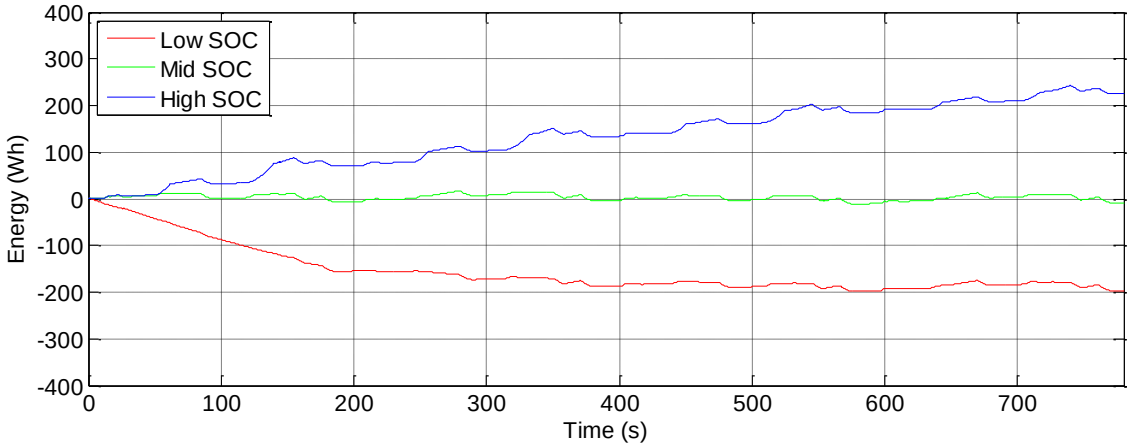

Figure 6.6: ECE-15 simulation battery energy out for various initial SOCs

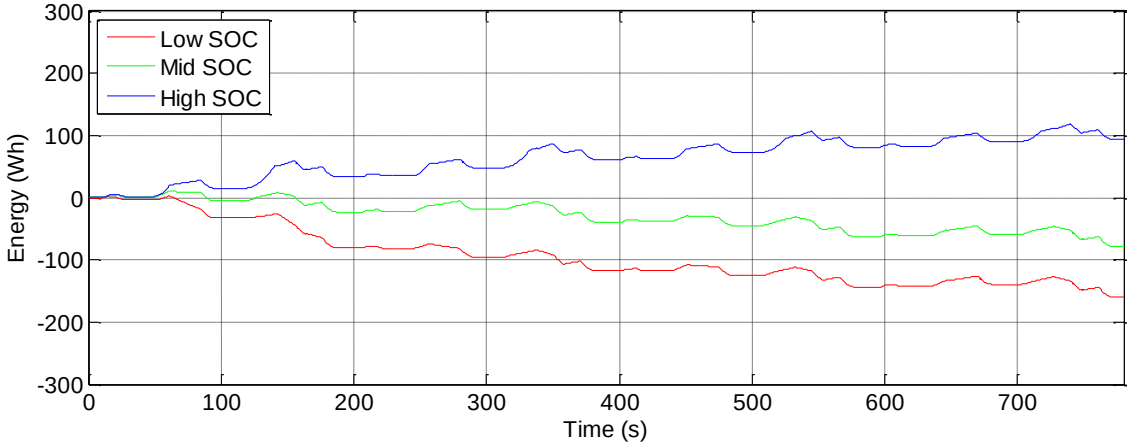

Figure 6.7: ECE-15 simulation MG2 energy out for various initial SOCs

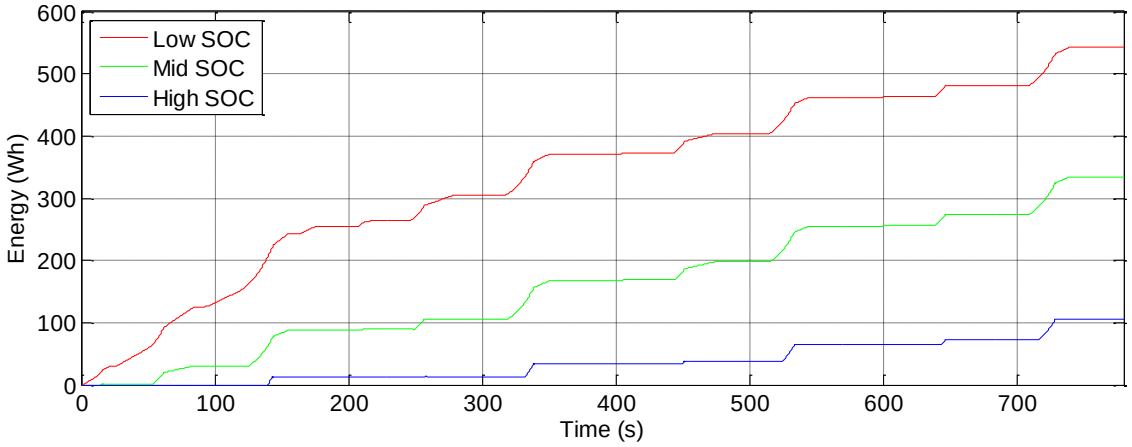

Figure 6.8: ECE-15 simulation ICE energy out for various initial SOCs

6.1.2.3 Simulation Analysis Conclusions

The above conclusions can also be confirmed by looking at the SOC correction plots in Figure 4.8 and Figure 4.9 in Chapter 4. The larger fuel consumption change with varying initial SOC can be seen by the steeper gradient of the ECE-15's correction line compared to the LUUDC's, in both dynamometer tests and simulations. The larger fuel consumption change with varying initial SOC in simulations compared to the chassis dynamometer tests can be seen by the steeper correction lines in the simulation results than those in the dynamometer results.

6.1.3 SOC Correction Trendline Gradient versus Cycle Distance

6.1.3.1 Various Drive Cycle Trendlines

Looking at the SOC correction plots it is clear that there are varying gradients of the correction trendlines. These decrease as the cycle distance increases, illustrating that on shorter cycles the fuel consumption is more sensitive to initial SOC. To look at this relationship, for both dynamometer tests and simulation results, the inverse of the gradient coefficient was plotted against cycle distance. The results are shown in Figure 6.9 and Figure 6.10.

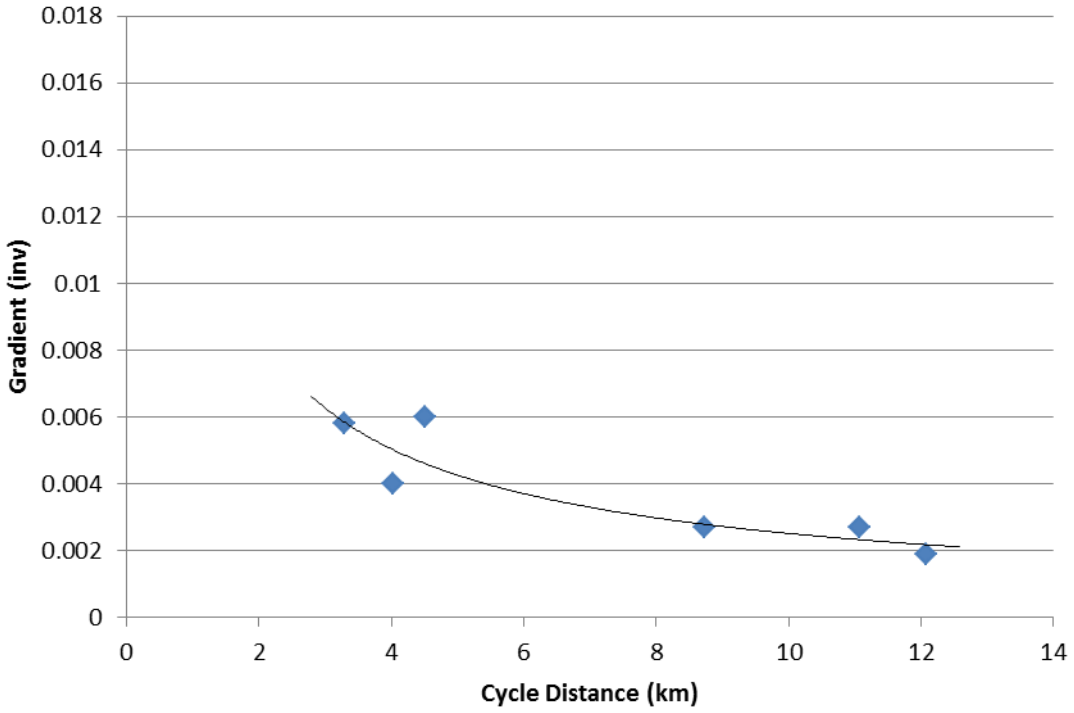

Figure 6.9: Chassis dynamometer test drive cycle distance against SOC correction trendline gradient

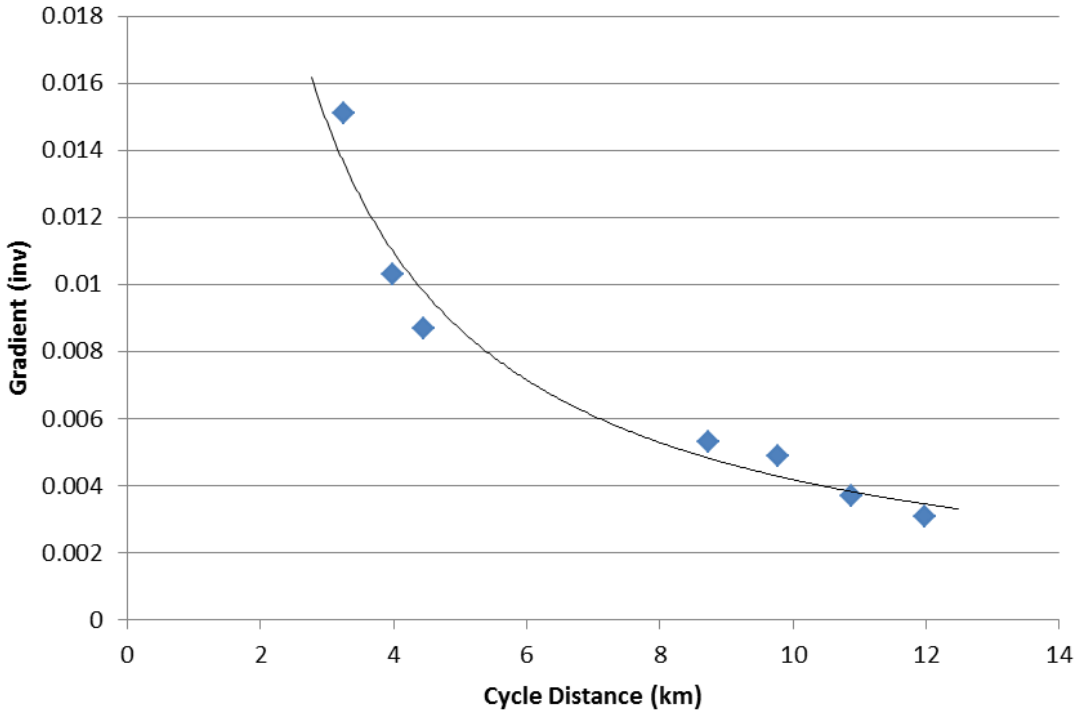

Figure 6.10: Simulation test drive cycle distance against SOC correction trendline gradient

The graphs confirm the trend of increasing cycle length giving a decreasing gradient. A similar trend is seen between both types of test, although for the

simulations the increase in gradient for the short cycles is more severe than that seen for the dynamometer.

6.1.3.2 Repeated Section Cycle Trendlines

Because the cycle profiles differ, to confirm if the same trend would be seen for a repeatable cycle, a 525 second section of the LUUDC2 cycle was used to form drive cycles with varying length by duplicating the cycle section. Cycles with 1, 2, 3, 4, 5, 6, 8, 10 and 12 of the cycle sections were produced and run in simulations with varying initial SOCs.

The results which are shown in Figure 6.11 form charge correction lines that decrease in gradient as the cycle length is increased, with the difference in results between successive cycles reducing with the longest cycles. The fuel consumption with zero net battery energy change values for all cycles are very close with the largest difference being 2% between the '1x' and '12x' cycles. This further confirms the validity of using this charge correction technique for test data.

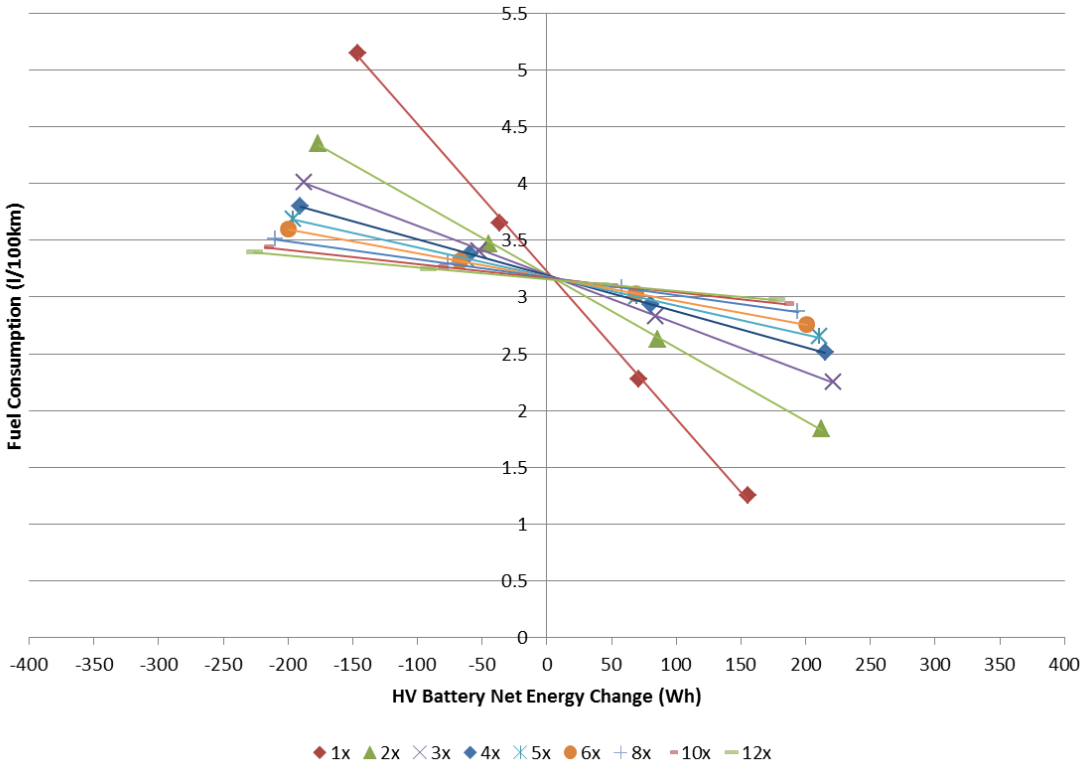

Figure 6.11: Repeated section drive cycle simulation results SOC correction plot

The results are shown in Table 6.7 and the plot of cycle length against gradient in Figure 6.12. This plot shows the same trend as seen in the simulation results in Figure 6.10, but fitting perfectly to the trendline this time due to not having the variation in the cycle profile with the changing length. It can be seen that by extending into much longer cycle distances the trendline is levelling out so there is very little change in angle for the long cycle lengths. It is expected that if the tests were extended, not far beyond 40 km there will be a point at which the cycle length has no effect on the gradient.

Table 6.7: Repeated section drive cycle simulation results

Cycle Section Repeats (No)	Cycle Distance (km)	Grad inv.	Fuel Consumption (l/100km)
1	3.32	0.0129	3.22
2	6.64	0.0064	3.20
3	9.95	0.0043	3.20
4	13.27	0.0032	3.19
5	16.59	0.0026	3.18
6	19.91	0.0021	3.18
8	26.58	0.0016	3.17
10	33.23	0.0012	3.17
12	39.87	0.0010	3.16

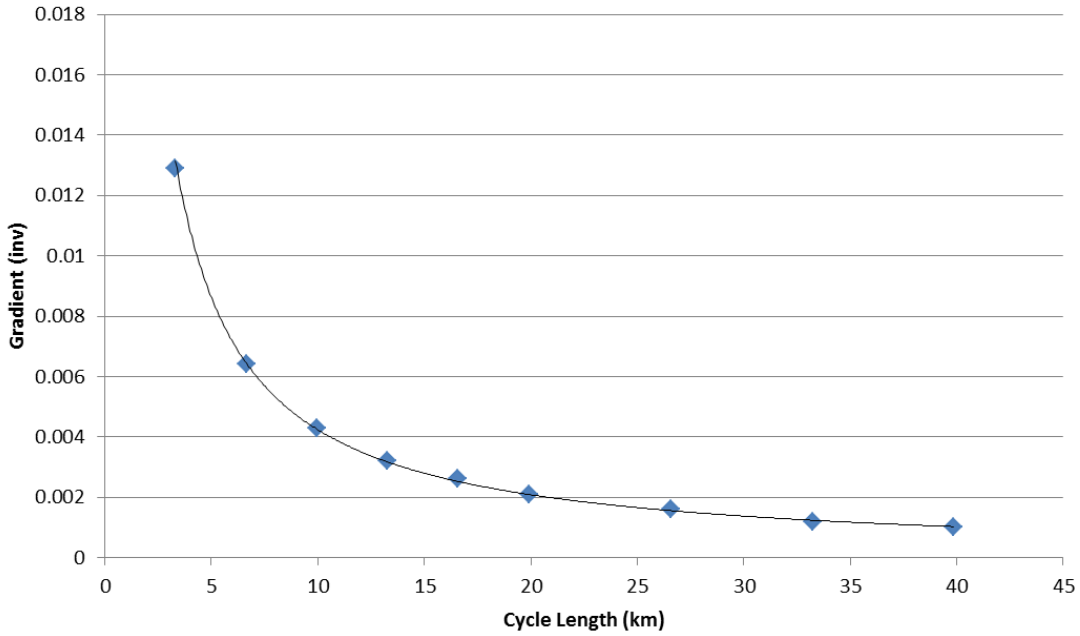

Figure 6.12: Simulation repeated section drive cycle distance against SOC correction trendline gradient

6.2 Factors Affecting HEV Energy Consumption

From the results in Section 6.2.4.2 and Section 5.1.3.4 for the LUUDC2, comparing the chassis dynamometer fuel consumption of 5.20 l/100km and the simulation fuel consumption of 4.17 l/100km, it is 19.8% lower. Making a similar comparison for the LU15-UDC from 3.95 l/100km to 3.14 l/100km there is a very similar 20.5% decrease.

6.2.1 Autonomie Model Inaccuracy

The first reason for the difference is the Autonomie model is not a completely accurate representation of the real vehicle. To establish the size of the difference, a comparison can be made between simulations on the NEDC and the manufacturer's quoted fuel consumption. The result from Chapter 4 for the NEDC simulation is 3.53 l/100km which when compared to the quoted 4.3 l/100km is 17.9% lower.

The 2004 Prius model used in Autonomie was validated in the predecessor software PSAT by Argonne National Laboratory [80] based on a Japanese specification vehicle that was tested [81]. Fuel consumption and battery SOC was found to be within 6% of test results in their validation. Being a different market vehicle could account for some difference in results due to differences in the control strategy to suit different country's drive cycles. However, in El Khoury and Clodic [64] a Prius II was tested and recorded fuel consumption of 3.6 l/100km on the NEDC, only 2% higher than the simulation.

6.2.2 Vehicle Degradation

Due to the test car being 8-9 years old and having been used for approximately 100,000 miles it will have deteriorated to some degree compared to new. Particularly, the HV battery will have been through many charging and discharging cycles and is likely to have faced some degradation. This would give lower battery performance or utilisation, leading to poorer fuel consumption.

A comparison can initially be made again using the manufacturer's quoted combined (NEDC) fuel consumption. On the dynamometer the NEDC fuel consumption was 4.88 l/100km which is a 13.5% increase over the official 4.3 l/100km. This increase represents the effect of all vehicle deterioration factors combined, one of which will be the battery.

Another factor that could also be part of the 13.5% above is reduced fuel consumption due to the type of tyres fitted to the test car. Standard tyres are fitted rather than low rolling resistance tyres that would come as standard original equipment. It is estimated that low rolling resistance tyres improve fuel consumption by approximately 3% in Calwell et al. [82].

Linked to this, although it appeared cosmetic, because the car was accident damaged there is a possibility that the impact has caused the wheel alignment to be shocked out of the correct position, adding to the rolling resistance and therefore increasing fuel consumption. There are no apparent signs of this however, the car drives fine, and there was not any obvious unusual tyre wear. It is therefore unlikely, but something to bear in mind. To confirm this, the vehicle would require a professional full laser geometry alignment.

6.2.3 High Voltage Battery Degradation

Battery tests were carried out as described in Section 3.10 to investigate their condition.

6.2.3.1 Battery Test Results

From the tests, the initial discharge test results showed the modules all had a reduction in their capacity compared to their rated 6.5 Ah. The average was 5.31 Ah which is an 18% decrease; however one module, number 10, was measured at only 4.28 Ah, a large 34% decrease. An example discharge graph is shown in Figure 6.13, including the worst module plotted as a green line and a typical module plotted as a black line. The significant difference in discharge capacity can clearly be seen. As the whole pack can only perform at the level of the worst module this shows that the test vehicle battery had a usable capacity down by 34%

since new. This was proven in Leijen and Scott [83] where a Prius I battery pack in good health was tested, then a module was replaced with one of half the capacity and the electric driving range was halved.

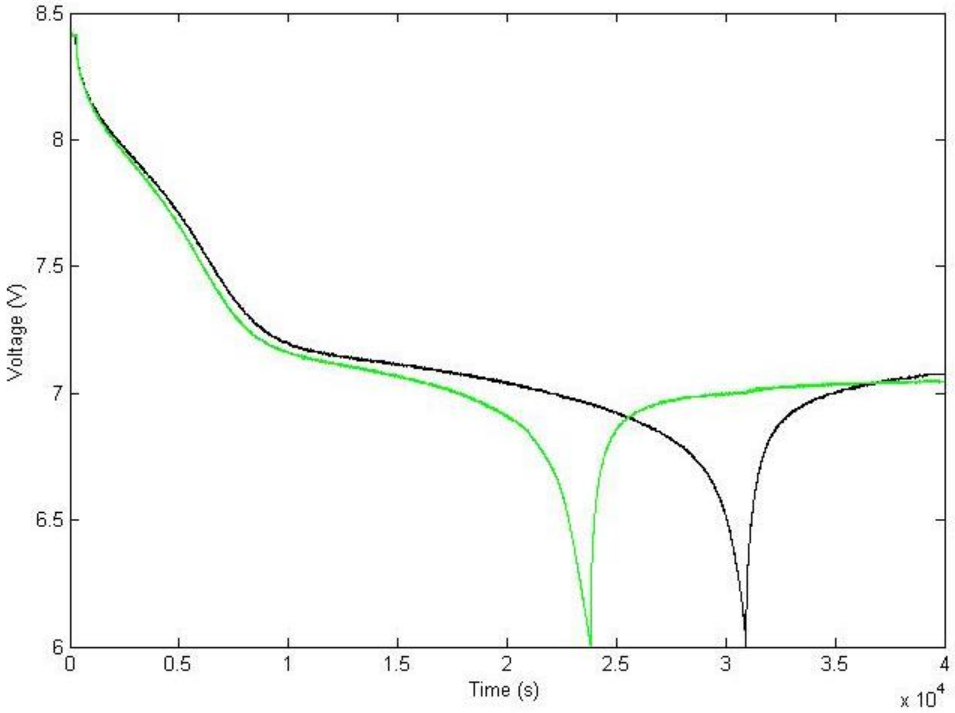

Figure 6.13: Example battery discharge graphs for two modules

In the second tests after a full charge going into the overcharge region, the average capacity measured increased to 6.53 Ah, which is back to their original capacity. This implies that the cells in the battery modules had become imbalanced over time from charging and discharging, causing them to operate within the range of the lowest cell within a module, and for the whole battery pack to operate in the range of the lowest module. With cell voltages being imbalanced the usable battery capacity is reduced, which in a vehicle will lead to more use of the ICE to compensate, so contributing to greater fuel consumption. With this full charging process applied the cells will have become more balanced within the modules at a higher voltage. The poor performing module discharged 5.55 Ah, 15% lower than the rest.

In the final tests that were carried out to see if there was any further improvement there was a small increase across the modules with an average of 6.62 Ah. The number 10 module still only discharged 5.90 Ah, so at more than 9% below the

others it had to be replaced to obtain a higher capacity out of the battery pack. The full set of results is shown in Table 6.8.

Table 6.8: HV battery discharge capacity and charge efficiency test results

Module No.	Capacity (Ah)			Charge Eff.
	Test 1	Test 2	Test 3	in Test 2
1	5.40	6.49	6.56	98.1%
2	5.29	6.42	6.55	98.5%
3	5.40	6.49	6.54	97.1%
4	5.18	6.43	6.58	98.0%
5	5.27	6.46	6.51	96.7%
6	5.22	6.48	6.60	98.3%
7	5.25	6.51	6.61	95.3%
8	5.27	6.42	6.58	97.7%
9	4.99	6.40	6.60	97.4%
10	4.28	5.55	5.90	98.1%
11	5.29	6.44	6.53	97.6%
12	5.11	6.43	6.57	96.5%
13	5.28	6.40	6.53	96.3%
14	5.17	6.31	6.57	91.8%
15	5.42	6.70	6.75	98.3%
16	5.45	6.72	6.75	98.7%
17	5.46	6.66	6.64	99.3%
18	5.37	6.69	6.79	96.8%
19	5.31	6.68	6.75	99.0%
20	5.37	6.68	6.75	98.5%
21	5.35	6.66	6.69	99.8%
22	5.49	6.68	6.72	97.6%
23	5.44	6.69	6.73	97.8%
24	5.45	6.68	6.77	96.6%
25	5.53	6.71	6.55	96.0%
26	5.41	6.72	6.78	95.6%
27	5.56	6.62	6.72	96.0%
28	5.67	6.60	6.74	92.2%
Avg.	5.31	6.53	6.62	97.1%

During the second series of tests with successive full range charges and discharges carried out, charge efficiency could be calculated between them. The efficiencies ranged from 91.8% to 99.8% with an average of 97.1% which was much higher than expected. It was thought that battery degradation may have contributed to lower efficiencies.

To replace the module number 10, another module (number 29) was obtained which was a used part due to the unavailability of individual new ones. This was tested in the same way as the other modules, but it showed a lower initial capacity

than the existing module. The first test recorded 3.73 Ah, increasing to 5.23 Ah in the second test cycle and 5.76 Ah in the third. Due to a significant increase occurring between tests 2 and 3, further cycles were carried out to investigate if the capacity would improve further. A further two tests increased the capacity to 5.92 Ah which is only marginally better than the existing module. Therefore a further replacement module, number 30, was obtained and tested. This one had a similar initial capacity to the rest of our pack at 5.36 Ah but did not increase in capacity as much as they did. Like with the first replacement module, a significant improvement was noted between 5.57 Ah discharged in test 2 and 6.03 Ah in test 3, so further tests were carried out. In the final fifth test the capacity was measured as 6.27 Ah, so although it was not as high as the rest of the pack it was a 6% increase over the original module.

Along with the low capacity, charge efficiency of module 29 that was obtained and later discarded was lower than the rest the modules from our pack. The efficiency varied from 83.1% to 91.5% across tests 2 to 5. The charge efficiency of module 30 was quite consistent at between 92.5% and 96.0% which makes it less efficient than the average of the rest of the pack but not as low as some of the modules.

6.2.3.2 Battery Degradation Simulations

In order to quantify the battery contribution, the lowest measured capacity from the battery test results of 4.3 Ah was incorporated into the Autonomie Prius model, along with the target SOC level changed to 60% to be more representative of our real car. These changes were made by editing the values in the battery and control system model files.

Simulations were run on the LUUDC and SOC correction was again carried out on the results. On this cycle this gave fuel consumption of 3.76 l/100km, a 2.3% increase.

Another battery factor that could be changed in the model files is the charge and discharge resistances. Values for these were not available for our physical battery

pack so various offsets from 20-80% were applied to the SOC-dependant resistance arrays in the battery model to study the effects.

With the other two changes above still included, the resulting fuel consumptions and percentage increases over the original value are shown in Table 6.9. Assuming the charge and discharge resistances have increased by a similar percentage to the capacity change of 34%, this indicates that the battery contributes an approximately 5% increase in fuel consumption.

Table 6.9: HV battery increased charge and discharge resistance, and decreased capacity simulation fuel consumption results

Inc. in chg. & disch. Resistances	Fuel Cons. (l/100km)	Change
20%	3.83	4.1%
40%	3.88	5.5%
80%	3.99	8.6%

6.2.4 Post Battery Balancing Chassis Dynamometer Testing

6.2.4.1 Chassis Dynamometer Test Results

Following the battery pack cell rebalancing, additional chassis dynamometer tests were carried out to study the effect of the battery balancing on fuel consumption on the physical vehicle. Tests were conducted using the same method as for the work done in Chapter 4, although this time the preconditioning and initial SOC points were different. The aim was for tests to be as close to charge sustaining as possible so that only a small amount of SOC correction would be required. To do this a preconditioning run of the drive cycle about to be tested was run, which should produce an end SOC, and therefore an initial SOC for the recorded test, that will lead to being close to charge sustaining. The drive cycle tests were then carried out back-to-back. From looking at the initial and end SOC results as the tests progressed, additional preconditioning was carried out where necessary to slightly increase or decrease the SOC in order to produce SOC correction plots with points crossing the y-axis. This was done by motoring the vehicle in gear using the dynamometer, and driving at low speed by electric drive respectively, as described in Section 4.2.3.

The test results are plotted on a SOC correction plot in the same manner as previously, which is shown in Figure 6.14. The same axis scales are used as on previous plots so that direct comparison can be made. The points are much closer on this plot due to the small change in SOC over the tests. Due to this the results are also shown on a smaller x-axis scale in Figure 6.15 which allows the relationships to be seen much more clearly. The equations of the SOC correction lines are given in Table 6.10.

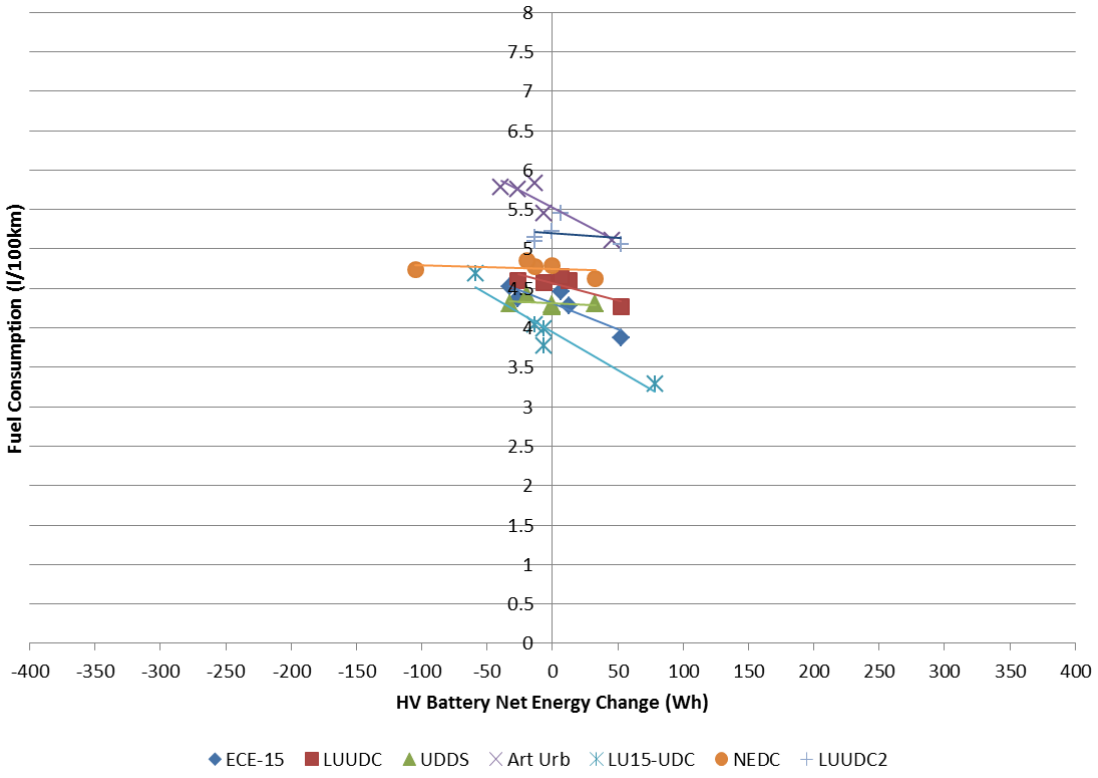

Figure 6.14: Post battery cell balancing chassis dynamometer drive cycle fuel consumption results SOC correction plot

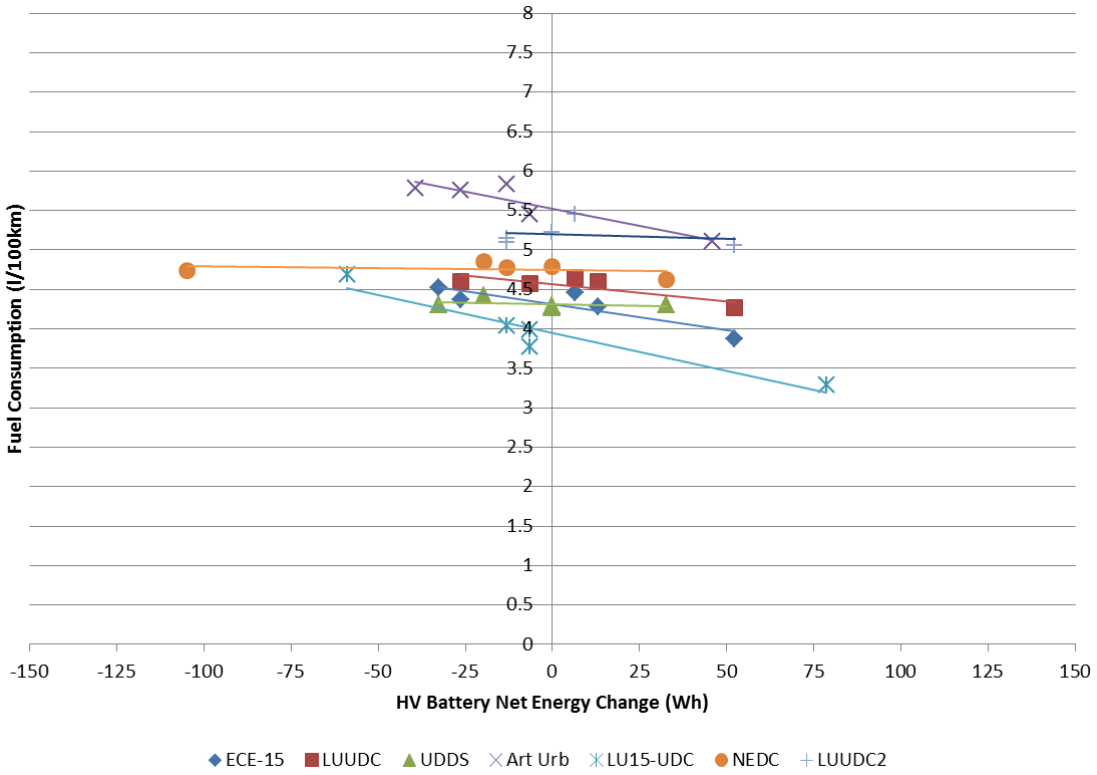

Figure 6.15: Post battery cell balancing chassis dynamometer drive cycle fuel consumption results SOC correction plot with enlarged scale

Table 6.10: Post battery cell balancing chassis dynamometer drive cycle SOC correction line equations

Drive Cycle	Equation
LUUDC	y = -0.0044x + 4.5691
LUUDC2	y = -0.0012x + 5.2030
ECE-15	y = -0.0066x + 4.3159
UDDS	y = -0.0007x + 4.3158
Artemis Urban	y = -0.0086x + 5.5211
LU15-UDC	y = -0.0097x + 3.9465
NEDC	y = -0.0005x + 4.7461

The charge corrected fuel consumption results are summarised in Table 6.11, with the results from before the battery balancing and the percentage differences between them.

Table 6.11: Chassis dynamometer drive cycle fuel consumption results comparison of before and after battery cell balancing

Drive Cycle	Fuel Consumption (l/100km)		Difference
	Before	After	
LUUDC	4.80	4.57	-4.9%
LU15 UDC	4.31	3.95	-8.5%
ECE-15	4.35	4.32	-0.7%
UDDS	4.42	4.32	-2.3%
Artemis Urban	5.54	5.52	-0.3%
NEDC	4.88	4.75	-2.7%

The results show that there were reductions in fuel consumption across all of the drive cycles due to the cell balancing. The size of the difference varies between drive cycles from 0.3% to 8.5%, with an average of 3.2%. The LU15-UDC stands out as having a larger fuel consumption change. For Artemis Urban it can be expected that the very small difference may have been greater. This is attributed to the point discussed in Section 4.2 regarding the discharging end of the SOC correction line possibly being lower than it should be, giving slightly lower original fuel consumption than it should have been. This in turn will lead to the difference between the two sets of tests being smaller.

The 4.9% decrease for the LUUDC shows that the battery capacity had a more significant effect than the simulations predicted, by a factor of over two. The charge and discharge resistance effect will still be in place in addition to the 4.9%, so to get an approximate quantification of this, simulations were carried out like in the previous section, but this time with just the charge and discharge resistances changed. On the LUUDC for each of the resistance increases tested, the fuel consumption and the percentage changes are shown in Table 6.12.

Table 6.12: HV battery increased charge and discharge resistance simulation fuel consumption results

Inc. in chg. & disch. Resistances	Fuel Cons. (l/100km)	Change
20%	3.71	0.8%
30%	3.75	2.0%
40%	3.77	2.6%

From this it can be estimated that for the test battery there would be an effect of approximately +2%, so it can be concluded that the battery has around a 7% total contribution to the vehicle degradation factor, but as seen with the battery capacity the percentage could be higher in reality.

Comparing the quoted combined fuel consumption (4.3 l/100km) to the new NEDC value of 4.75 l/100km recorded after the battery balancing, it is 10.5% higher. Therefore this is the overall vehicle degradation factor now excluding the battery imbalance effect.

6.2.4.2 New LUUDC2 Chassis Dynamometer Test Results

Following the work in Chapter 5 where a new drive cycle was developed, additional chassis dynamometer tests were carried out. This was to compare the energy consumption on the new LUUDC2 to the original LUUDC.

Figure 6.15 shows the new LUUDC2 energy consumption is higher than the original LUUDC, and the charge corrected fuel consumption value of 5.20 l/100km is 13.9% greater. This confirms that the drive cycle accuracy is very significant in the results it produces. Comparing the new cycle consumption to the ECE-15 in Table 6.11 (4.32 l/100km), the real-world driving is now 20.4% higher than the legislative cycle.

To compare the LUUDC2 result to the real-world security driving, the factor that the battery balancing has been carried out since then has to be taken into account. Because the style and statistics of the LUUDC2 are closest to the LUUDC out of the drive cycles tested, it can be expected that the change in fuel consumption due to the battery voltage balancing would be similar to that of the LUUDC. Therefore applying an equivalent percentage increase to the LUUDC2 test fuel consumption gives the estimated pre-battery balancing fuel consumption. The increase measured for the LUUDC is 5.1%, therefore using a factor of 5%:

$$\text{LUUDC2 fuel consumption} = 5.20 \times 1.05 = \mathbf{5.46}\ \text{l/100km}$$

The difference between this chassis dynamometer testing and the real-world driving (6.61 l/100km) is now reduced to 21.0%, for which the contributory factors to this are studied in the Section 6.3.

6.2.5 Section Conclusions

By making the results from Section 6.2 relative to the same reference point of the chassis dynamometer test, they can be made directly comparable. For the NEDC the difference from the manufacturer's quoted fuel consumption is -9.5% due to vehicle degradation. There is a further difference of -16.2% to the simulation result, making up the total -25.7%. The vehicle degradation factor would be an additional -2.4% with the reduced battery capacity before conditioning taken into account.

Therefore for the LUUDC2, using and applying the same proportion ratio for these two factors, the differences would be:

- Vehicle degradation: -7.4%
- Simulation model accuracy: -12.6%

Within the vehicle degradation factor the battery is estimated to contribute around -1.9%, so for real world driving the total effect of the battery including capacity reduction is estimated to be -6.8%.

The results from Section 6.2 are combined with the other results from this thesis in an overall summary diagram that can be seen in Chapter 7 in Figure 7.1.

6.3 Factors Affecting HEV Energy Consumption in Real-World Driving

6.3.1 Temperature and Auxiliary Usage

There is a significant discrepancy in the fuel consumption results for the real-world driving by university security in Chapter 4 and for the chassis dynamometer testing on the drive cycle derived from it, in Section 6.2.4.2. At 6.61 l/100km and 5.46 l/100km respectively, the real-world driving figure is 21.0% higher than the LUUDC2. After the accuracy of the cycle in representing the logged driving data, which is discussed in Section 5.1, has been taken into account the other main factor thought to contribute to this is the effect of variation in ambient temperature and the corresponding use of the heater or air conditioning.

6.3.1.1 Auxiliary Use Study Based on Literature

Due to resources available, this investigation has to be mainly based on existing literature in this area. Lohse-Busche et al. [84] carried out chassis dynamometer drive cycle fuel consumption tests in a thermal chamber at the Advanced Powertrain Research Facility (APRF) at Argonne National Laboratory at various ambient temperatures, with and without air conditioning and the heater running. Several cars including conventional, hybrid, and plug-in hybrid cars were tested, including a 2010 Toyota Prius. Tests were carried out on three drive cycles which included the UDDS. The authors carried out tests in the following three test conditions:

- 22°C (72°F) with no heater or air conditioning
- -6.5°C (20°F) with heater
- 36.3°C (95°F) with air conditioning

From this the data for the Toyota Prius on the UDDS was used, with this being an urban drive cycle. The data is shown in Table 6.13. Compared to the baseline case at 22°C with no auxiliaries on, they found that at -6.5°C with the heater on there was a 38% increase in fuel consumption on hot start and a 75% increase on cold start. With the air conditioning running in 36.3°C ambient temperature, large

increases in fuel consumption were seen with 56% on hot start and 61% on cold start.

Table 6.13: Various ambient temperature and auxiliary use fuel consumption test results from [84]

Amb. Temp (°C)	Cold start FC (l/100km)	Hot start FC (l/100km)
-6.5	6.3	4.7
22	3.6	3.4
36.3	5.8	5.3

To use the findings of Lohse-Busche et al., average temperature records were obtained for the real-world test data collection period. Monthly average temperatures for the Midlands were found from the Met Office [85], which can be seen in Table 6.14. By linearly interpolating between the fuel consumption data points from the literature, at each month's average temperature an estimated fuel consumption could be found. A copy of the code used to do this is in Appendix 11.

Table 6.14: Loughborough real-world driving test period monthly average temperatures from the Met Office [85] and corresponding interpolated estimated fuel consumptions

Month	Avg. temp (°C)	Interp. CS FC (l/100km)	Interp. HS FC (l/100km)
Apr	6.9	5.03	4.09
May	11.5	4.59	3.88
Jun	13.4	4.41	3.79
Jul	15.3	4.23	3.71
Aug	16.3	4.14	3.66
Sep	12.7	4.48	3.82
Oct	9.0	4.83	3.99
Nov	6.1	5.11	4.13
Dec	4.3	5.28	4.21
Avg.	10.61	4.68	3.92

A plot of the test data points from Table 6.13 are shown in Figure 6.16. The mean across the total period was taken to compare to the 22°C baseline, the values can be seen in Table 6.14.

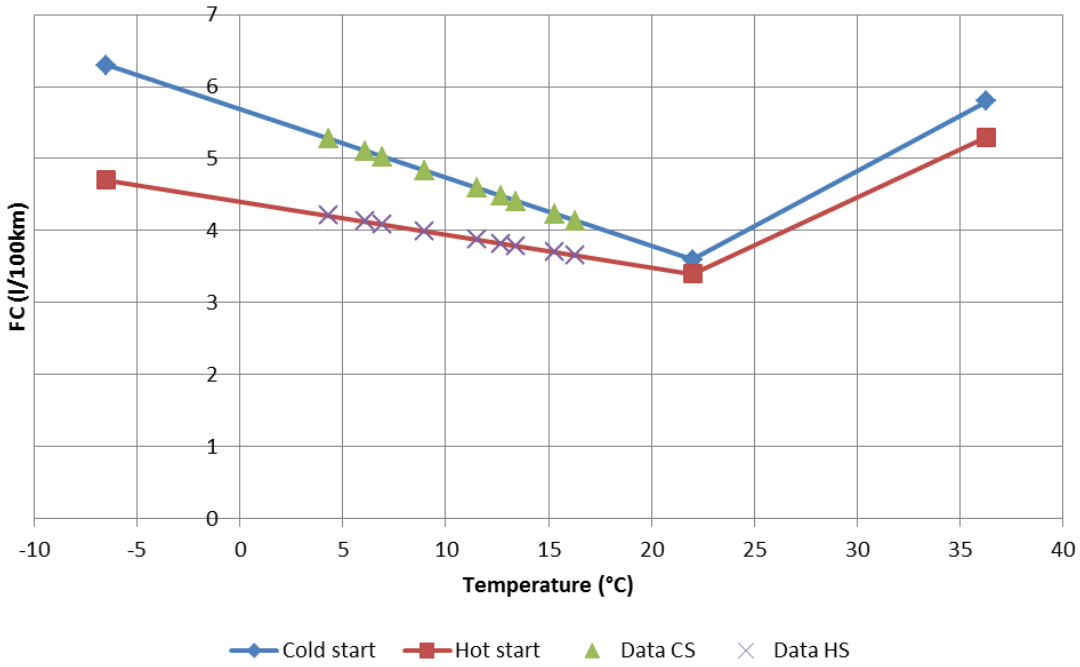

Figure 6.16: Various ambient temperature and auxiliary use test results from Lohse-Busche et al. [84] with Loughborough real-world driving test period monthly average temperature points

For cold start, fuel consumption of 4.68 l/100km with climate control is 29.9% higher than the 3.6 l/100km without, and on hot start 3.92 l/100km compared to 3.4 l/100km is 15.3% greater fuel consumption with the lower ambient temperature and heater in use. While the vehicle was in service with Security it was used 24 hours a day so the majority of the time it would have been running in hot start conditions, therefore the fuel use increase on hot start can be estimated as 15%. This therefore accounts for a large proportion of the difference between the real-world and the chassis dynamometer fuel consumptions. This result can be seen in an overall summary diagram in Figure 7.1 in the Conclusions.

In reality the percentage increase is likely to be higher than this due to the occasional cold start periods and frequent use of additional auxiliaries such as radio, lights and heated rear window. At low temperatures of less than approximately 5°C the Prius ICE is kept running more of the time to maintain the engine temperature, keeping it above 70°C. This will contribute to increased fuel consumption particularly during periods where the vehicle was stationary for a significant amount of time during a patrol with the ignition switched on. Additionally, the air conditioning system in the test vehicle switches on automatically when the ignition

is turned on, each time after it has been left off for a certain period of time. This is likely to have meant that users had the system switched on at times when it was not necessary, adding to the fuel consumed.

6.3.1.2 Auxiliaries Chassis Dynamometer Test

A limited comparison test was carried out with our test vehicle on the chassis dynamometer to measure the effect of using auxiliaries. For this test the headlights and radio were switched on along with the air conditioning, which was set to minimum temperature with maximum fan power, "Max Cold". The ambient temperature in the laboratory was 28-30°C and the LUUDC2 was used. Three runs were conducted in the same way as the last chassis dynamometer tests discussed in Section 6.2.4, and at the same time. The target for the battery was to have one run charge sustaining, one with a small discharge, and one with a small charge, in order to produce an SOC correction plot.

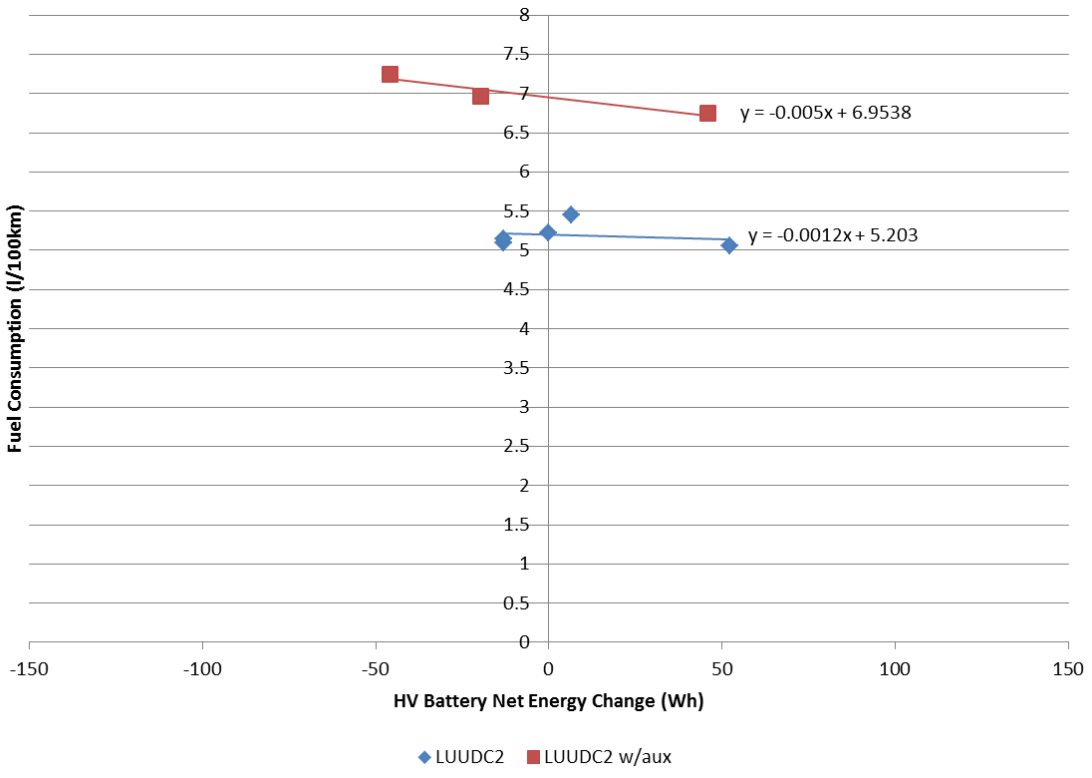

Figure 6.17: LUUDC2 with and without auxiliaries chassis dynamometer fuel consumption results SOC correction plot

From Figure 6.17 it can be seen that the energy consumption with auxiliaries is significantly higher than without. With an SOC corrected fuel consumption figure

of 6.95 l/100km, it is a 33.7% increase. When driving the car during these tests it was clearly noticeable that the engine was running much more of the time during the test, in fact almost all of the time when non-stationary. Although the air conditioning on the Prius is electronic so it does not require the engine to be operating like a conventional system, it adds to the fuel consumption in a different way. When the car is stationary with the air conditioning running it depletes the high voltage battery SOC, meaning when the vehicle starts moving it has to run the engine to drive the vehicle and/or charge the battery sooner than it would do had the battery not been depleted while stopped. This was also acknowledged during the testing when monitoring the SOC level during the stops in the drive cycle.

Using interpolation of the data from the literature shown in Table 6.13 and Figure 6.16, the estimated equivalent fuel consumption at 29°C is 4.33 l/100km, a 27.4% increase. This is lower than the measured test result due to three possible factors. Firstly, the air conditioning in this test was set with a higher demand on the "Max Cold" setting which could operate differently to the other settings and use more energy. In the literature as discussed in Chapter 2, El Khoury and Clodic [64] tested a Prius II with and without the air conditioning switched on. At 28°C with the air conditioning on, they found that the fuel consumption was increased by 0.7 l/100km, a 19.4% increase. This was with the air conditioning set at a controlled temperature of 20°C; however when it was set to the maximum cooling temperature and air flow setting "Max Cold" this difference doubled to 1.4 l/100km and 38.9%. This relates very well to the 15% and 34% results from this section of our study.

A second factor in the tests is the air conditioning is defective in our test car, the system performs weakly and does not blow particularly cold air, most likely because it requires re-gassing. This could mean that the system is working additionally hard to try to reduce the cabin temperature but not having a result due to the defect, meaning it is stuck in this cycle. Finally, a Prius III was used in the literature so some differences in operation and results to the Prius II would be expected.

6.3.2 Other Real-World Factors

The small remaining circa 6% difference between the laboratory test and real-world driving fuel consumption is likely to be made up of several other minor factors that occur in real-world driving and are not covered in the chassis dynamometer testing. In the US the Environmental Protection Agency applies a larger 9.5% increase to drive cycle fuel consumption to account for real-world factors not covered by their dynamometer testing [30].

Besides the temperature and auxiliaries factor potentially being larger, as discussed in the previous section, potential other factors could include:

- Tyre pressures
- Wind
- Vehicle loading
- Reduced motor-generator efficiency

Taking tyre pressures from this list as an example, some existing literature on the topic have been found. If tyre pressures are not regularly monitored they could drop below the recommended setting which increases the tyre distortion, increasing the contact area, therefore increasing rolling resistance which gives poorer fuel economy. From Brace et al. [86] it was found that reduced tyre pressures can have a 2.6% increase in fuel consumption. This was for a 0.5 bar (7.25 psi) reduction of pressure tested on the NEDC. The NEDC is a higher speed cycle so the effect is not likely to be as large as this in the urban driving conditions [82]. In Calwell et al. [82], in simulation modelling a 10% increase in rolling resistance gave over 2% increase in fuel consumption for motorway driving, however for urban driving it was 1%, so about half the amount. Linked to this, it was quoted that The Rubber Manufacturers Association state a 1 psi reduction in tyre pressure would give approximately 1.1% increase in rolling resistance.

Further investigation into tyre pressures and the other possible factors above to breakdown the 6% into its components would be recommended for further work in this area.

6.4 Chapter Conclusions

The effect of differing battery SOC was seen to have a large effect on the fuel consumption due to the battery energy utilisation. Simulations showed the energy usage and explain the trends seen. For the SOC correction plot trendlines, a clear relationship was found between the lines' gradient and the cycle distance. With increasing distance the gradient reduces until a point at which it becomes almost constant.

Chassis dynamometer testing of the new LUUDC2 gave fuel consumption 13.9% higher than the LUUDC, confirming the simulation results in the previous chapter. This makes the difference from the ECE-15 now 20.4%, which is almost double the difference seen earlier in Chapter 4 for the old cycle.

Factors affecting HEV energy consumption which account for the 20% difference between chassis dynamometer test and simulation results were studied. The Autonomie model inaccuracy was determined by using values for the NEDC, as official manufacturers' fuel consumption is available for this cycle. The same ratios for the factors were applied to the LUUDC2 results. This equates to the 20% being split with 7.4% as vehicle degradation and 12.6% as simulation model inaccuracy. The effect of the battery cell voltage imbalance is a further 4.9% on top of the vehicle degradation, which was determined after carrying out battery charge and discharge testing, plus rebalancing the cells.

The remaining main factor investigated as a contributor to the difference of 21% between the chassis dynamometer test and real-world driving was the use of climate control auxiliaries in low and high ambient temperatures. For this a study was carried out using data from the literature for testing carried out by others. It was concluded that this contributed 15% or more of the total, leaving 6% which is a sum of other small real-world factors.

These conclusions are discussed in more detail in Chapter 7.

7 Conclusions

In this project a Toyota Prius was put into an application carrying out on-road urban driving, collecting data in the process. A real-world drive cycle, the LUUDC2, was developed from the GPS data gathered, which was used for chassis dynamometer testing and carrying out simulations. During these tests existing drive cycles were tested for comparison, and in particular the ECE-15 was used as a benchmark due to it being the standard European legislative urban driving cycle.

The effect that the SOC of the HV battery at the start of test has was established. The main findings from this project include the drive cycle effect, of which the accelerations are of key importance. Plus, factors that contribute to the increased energy consumption in real-world driving have been determined and quantified by separating work into the following main parts:

1) Comparison of chassis dynamometer tests to simulation results – Laboratory based, eliminating on-road real-world influential factors
2) Comparison of dynamometer tests to real-world driving – Includes on-road testing with real-world factors involved

7.1 Findings

7.1.1 Battery SOC Effect

Analysis of how HV battery SOC at the start of a test affects energy consumption was carried out. There was found to be a 30% increase in fuel consumption on the LUUDC when running a test with a low SOC of 43%, compared to a high 77% SOC. This is due to the increased use of electrical power to drive the vehicle when a higher charge level is available, with therefore less use of the ICE so less fuel burnt. This is reflected in the net change in SOC over the tests, with the low initial SOC it was +12% whereas for the high initial SOC it was a -23% change. Analysis of corresponding simulation data signals showed higher energy usage from the battery and lower energy usage from the ICE when the start of test SOC was higher and vice versa.

Due to the proved significance of battery SOC, corrections were carried out on all test results of varying SOC changes to give an interpolated result corresponding to a zero net battery energy change. The fuel and battery energy relationship trendlines of test points showed different gradients for different cycles. This was investigated in relationship to drive cycle length. It was found that the gradient reduces as the cycle distance increases, to the point at which the gradient becomes zero and the cycle length increasing beyond this point has no further effect.

7.1.2 Drive Cycle Effect

The real-world cycle was found to give energy consumption 20.4% higher than the ECE-15 due to the cycle's more transient profile with a significantly larger number of accelerations per kilometre. The Artemis Urban, which is an existing real-world drive cycle, gave 6.2% higher fuel consumption than the LUUDC2. Again this was established to be due to the effect of the accelerations with it consisting of more high magnitude accelerations.

Another cycle was developed, the LU15-UDC, which is a low speed cycle with close to constant speed cruising at 15 mph and minimal acceleration or deceleration events and stops. In comparisons of the two developed cycles, the

LUUDC2 fuel consumption was found to be 32% higher in chassis dynamometer tests and simulations.

The contribution of cycle acceleration effect to this difference was studied through creating a set of synthetic drive cycles consisting of a series of constant rate accelerations and decelerations, with each cycle having a different acceleration rate. From this the finding was that the difference in acceleration rate contributed 13.6% of the 32% fuel consumption difference. Although it is envisaged that using additional comprehensive statistical analysis methods may show that it has a larger contribution.

A unique way of calculating accelerations and analysing them, rather than using how it is conventionally done elsewhere, was introduced for making the drive cycle comparisons. For the analysis, acceleration and deceleration distributions using counts of the calculated accelerations within specified ranges were produced. An important output of this work is that by using these acceleration distributions for the refinement of a driving cycle, it was found that significant improvement in the cycle's representativeness of the dataset could be made. This highlights the importance of creating a cycle accurately in order for it to give meaningful results.

Comparison was made with a pure electric vehicle which was tested on the same drive cycles as the HEV. The EV gave consistently lower energy consumption than the HEV in the range of 69-72%. This was normalised by mass due to significant difference between the two vehicles which reduced this difference to 59-63%. This difference will be mainly down to the high efficiency of electric motors compared to ICEs.

7.1.3 Comparison of Chassis Dynamometer Tests to Simulation Results

In this first of the two main areas of investigation, the simulation fuel consumption was found to be 20% lower than in the dynamometer tests for the LUUDC2 and LU15-UDC. One contributor is the simulation model was found to not give results entirely accurate of those of a real Prius. Using the NEDC, the simulation fuel

consumption could be compared to the manufacturer's quoted combined figure, which in theory should be the same. The simulation result from Section 6.2.1 was 18% lower, showing that this constitutes a large proportion of the total 25.7% difference between the simulation and chassis dynamometer tests for the NEDC. For the LUUDC2 it equates to 12.6% of the 20% total. However, simulation was still a useful tool to study the energy use of the powertrain at a component level.

Degradation of the test vehicle due to its age and mileage covered was found to be the other significant contributor to the fuel consumption difference, again based on the NEDC. The chassis dynamometer fuel consumption was 10.5% higher than the manufacturer's quoted figure. Relating this to the LUUDC2 this equates to the vehicle degradation giving 7.4% lower fuel consumption.

Prior to this, battery charge and discharge cycle tests were carried out in the laboratory to determine any reduction in capacity of the HV battery. It was found that the battery modules had 18% lower capacity on average, and up to 34% in the worst case for one module. The pack can only operate within the limits of the poorest module so it will have had a 34% reduced capacity compared to new. Carrying out repeated charging cycles balanced the cell voltages within the battery modules, bringing the capacity back up to their original rated level. Comparing drive cycle tests done after the battery balancing to those done previously, for the real-world LUUDC the fuel consumption was reduced by 4.9%, and on average for all the drive cycles tested there was a 3.2% reduction. By modification of the charge and discharge resistances in the simulation software's battery model it is estimated that the effect of the battery degradation is at least a further 2%, which is a component of the 7.4% for total vehicle degradation.

7.1.4 Comparison of Chassis Dynamometer Tests to Real-World Driving

The fuel consumption from the real-world driving carried out by Loughborough University Security was initially measured to be 38% higher than the dynamometer test on the original LUUDC. A cycle accuracy study was carried out, comparing

statistics of the driving dataset with the derived cycle. Due to the importance of accelerations towards the test results that a drive cycle will give, acceleration magnitude distributions were created and analysed. It was found that the cycle could be better matched to the dataset's statistics, so a sensitivity analysis was carried out with cycles produced with different software input settings to find the optimum. A new drive cycle, the LUUDC2, which much more closely matched the dataset was produced and tested. Its resulting higher fuel consumption, measured as +13.3% in simulations and +13.9% in chassis dynamometer tests, reduced the difference to the real-world driving by 17%, bringing it down to 21%.

Gradient was investigated as a contributor through the LU15-UDC cycle that was created primarily for this purpose. The cycle was produced from logged real-world driving carried out across the Loughborough University campus and was tested on the chassis dynamometer. Surveying of this main campus driving route was carried out to map the gradients. This was incorporated into simulation analysis to compare the cases of with and without gradients, alongside comparing the real-world driving with chassis dynamometer tests.

The resulting finding was that gradient had negligible effect on fuel consumption for a HEV in the case of a circuit route, returning to the same start point. Investigating the power and energy flow signals for each of the key components, it was confirmed that due to the engine-off time enabled by the downhill gradients along with energy recuperation, this balances with the additional energy consumption required to drive on uphill sections compared to without gradients.

A guideline comparison with a conventional diesel vehicle was made using a simulation model. For this, parameters for a Citroën Berlingo like that typically used by the university security were applied to inbuilt simulation model components. For this vehicle the fuel consumption was 5.8% higher with the gradients compared to with no gradients due to the continuously running ICE in both cases. This showed that the finding above is specific to HEV powertrains.

The main contributor to the real-world fuel consumption increase was found to be the use of auxiliaries, including using the air conditioning or heater in low or high ambient temperatures. A study was carried out using data from the literature for testing carried out on a Toyota Prius in a climatic chassis dynamometer chamber. These results were linked to local average temperature records, interpolating to give estimated fuel consumption results. This showed that the auxiliary use contributes 15% to the real-world difference. With our vehicle the air conditioning automatically comes on when the ignition is switched on so there is a high likelihood that at times when the air conditioning was not needed it will have been running due to this, adding further to the fuel consumption. Combined with the test car's air conditioning not performing correctly, the increase could easily be higher than 15%.

Additionally, chassis dynamometer testing was carried out with our test car on the LUUDC2 with the air conditioning running at "Max Cold" and the headlights and radio on which gave fuel consumption 33.7% higher than without auxiliaries. This agrees with results in the literature, and highlights the significance that the use of air conditioning can have on real-world energy consumption of a HEV.

The remaining 6% is made up of a collection of other small factors that can have an effect in real-world driving, such as wind, vehicle loading and tyre pressures.

7.2 Results Summary

The results from Section 7.1 are combined and presented in a diagram in Figure 7.1 linking them all together. In this diagram each of the red boxes represents a test and they are positioned on a proportional scale based around the chassis dynamometer test as the central reference point. Above this represents higher fuel consumption and below it represents lower fuel consumption. The numbers at the corners of the test boxes are the fuel consumption results for that test (in l/100km). All results in the blue shaded area are for the LUUDC and all results in the green shaded area are for the NEDC, which were used to determine the split of the vehicle deterioration and simulation accuracy components. For the chassis dynamometer test box there are numbers above and below it which represent before and after HV battery cell voltage balancing respectively. The percentage differences shown between these points therefore represent the fuel consumption reduction due to the battery balancing.

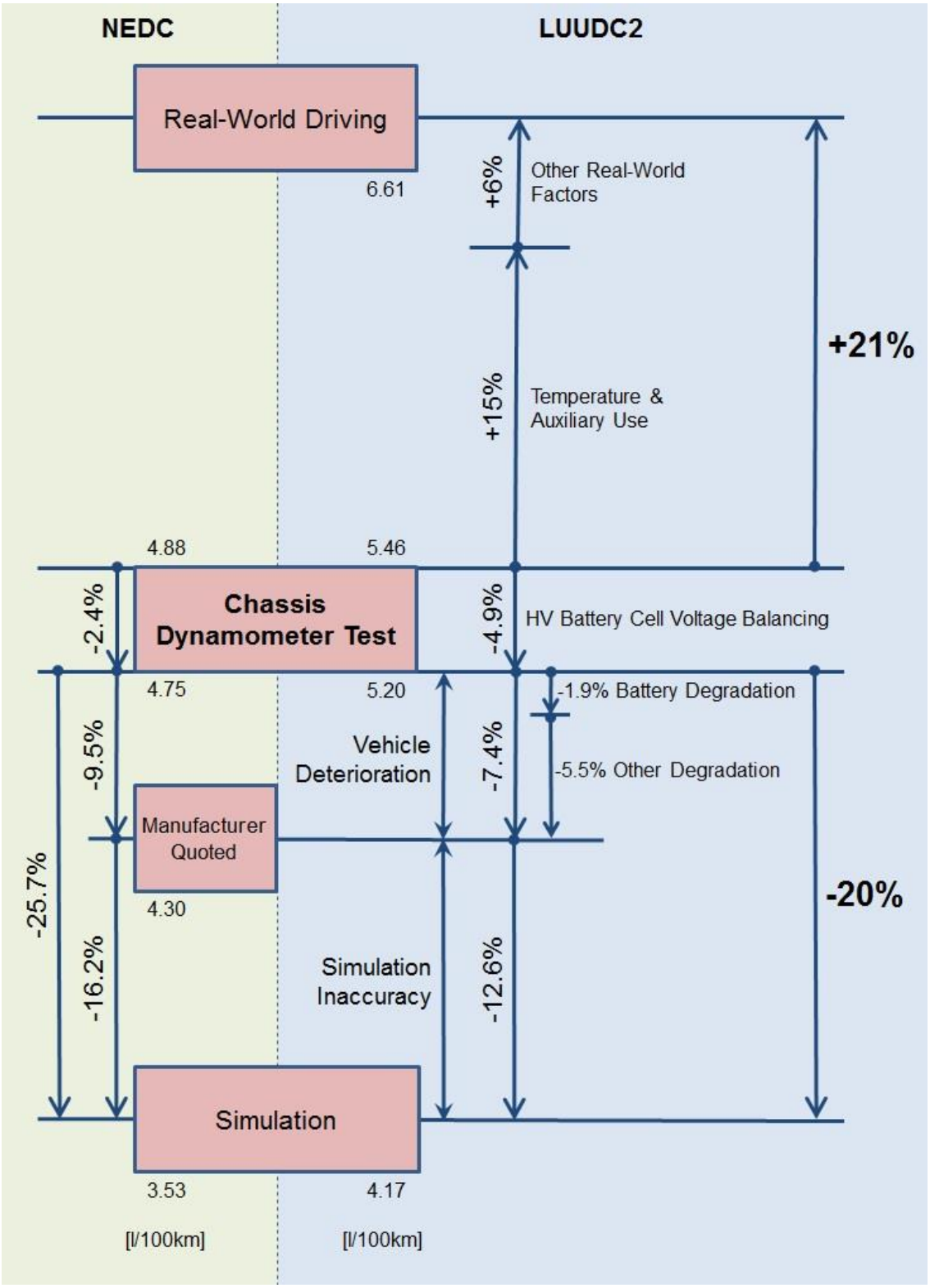

Figure 7.1: Results summary diagram of real-world energy consumption factors

7.3 Suggestions for Further Work

To take this work further, the suggested next stage would be to develop parts of the analysis in a different way, particularly for the effect of accelerations on the fuel consumption of a drive cycle. Investigation using a mathematical approach with a more complex statistical analysis of the drive cycle accelerations, by maybe using cluster analysis for example, is likely to show an increased contribution of accelerations to the energy consumption.

The work within this project was all based on urban driving, to develop it further other driving environments could be investigated, such as rural and motorway driving. By developing additional driving cycles for these other uses, investigations could be made into the other main driving types to find out if the factors contributing to fuel consumption are the same as those discovered for urban driving. Additionally, the drive cycle production could potentially be improved by writing the programme to create the cycles, rather than using existing software. This could then incorporate what has been learnt in this work about the importance of detailed acceleration metrics towards the accuracy of a cycle in representing the input dataset.

A new HV battery pack could be installed in the test car to further investigate battery degradation. By testing the car with the new battery the effect of this could be seen directly. Alternatively, comparative testing with another Toyota Prius would enable the work to be developed to further investigate the vehicle degradation including the motor-generators and ICE. By testing an equivalent new car against a highly used one, direct comparisons could be made.

An area of improvement to the existing methodology would be to have a more comprehensive vehicle instrumentation system installed. By monitoring the motor-generator's current, voltage, speed, and possibly torque, along with validated sensing of the HV battery, component energy use of the test vehicle could be studied alongside the data obtained from the simulations.

7.4 List of Publications

The following publications have been written to date:

- M.A. Lintern, R. Chen, S. Carroll and C. Walsh, *Simulation study on the measured difference in fuel consumption between real-world driving and ECE-15 of a hybrid electric vehicle*, IET Hybrid and Electric Vehicle Conference, 2013. HEVC 2013. London, UK
- S. Carroll, C. Walsh, C. Bingham, R. Chen and M.A. Lintern, *Electric Vehicle Efficiency Mapping*, IMechE Sustainable Vehicle Technologies 2012. SVT 2012. Gaydon, UK

References

[1] BP. *Statistical Review of World Energy 2014 - Oil Reserves.* 2014; Available at: http://www.bp.com/en/global/corporate/about-bp/energy-economics/statistical-review-of-world-energy/review-by-energy-type/oil/oil-reserves.html. Accessed August, 2014.

[2] BP. *BP Energy Outlook 2035.* January 2014.

[3] IPCC. *IPCC Fourth Assessment Report: Climate Change 2007.* 2007; Available at: http://www.ipcc.ch/publications_and_data/ar4/wg3/en/ch5s5-2.html. Accessed August, 2014.

[4] EPA. *Global Greenhouse Gas Emissions Data.* Available at: http://www.epa.gov/climatechange/ghgemissions/global.html. Accessed August, 2014.

[5] AA. *Petrol and diesel price archive.* 2010; Available at: http://www.theaa.com/motoring_advice/fuel/fuel-price-archive.html. Accessed August, 2014.

[6] Toyota UK. *Toyota Prius Marks Three Million Worldwide Sales.* 2013; Available at: http://media.toyota.co.uk/2013/07/toyota-prius-marks-three-million-worldwide-sales/. Accessed August, 2014.

[7] Toyota USA. *Worldwide Sales of Toyota Hybrids Top 6 Million Units.* 2014; Available at: http://corporatenews.pressroom.toyota.com/releases/worldwide+toyota+hybrid+sales+top+6+million.htm. Accessed August, 2014.

[8] Stansfield R. *Fuel economy: why your car won't match the official mpg.* 2012; Available at: http://www.telegraph.co.uk/motoring/green-motoring/9241054/Fuel-economy-why-your-car-wont-match-the-official-mpg.html. Accessed September, 2014.

[9] Truett R. *Why hybrids often deliver lower mpg than advertised.* 2013; Available at: http://www.autonews.com/article/20130816/OEM05/130819927/why-hybrids-often-deliver-lower-mpg-than-advertised. Accessed September, 2014.

[10] Kmiecik O. *Hybrid driving – Toyota's top tips for best fuel economy.* 2013; Available at: http://blog.toyota.co.uk/hybrid-driving-technique-toyotas-top-tips-for-achieving-the-best-fuel-economy-in-your-hybrid#.VDGRaPldV8F. Accessed September, 2014.

[11] European Commission. *Reducing CO2 emissions from passenger cars.* Available at: http://ec.europa.eu/clima/policies/transport/vehicles/cars/index_en.htm. Accessed February, 2015.

[12] Automotive Council. *Automotive Technology Roadmaps.* 2013; Available at: http://www.automotivecouncil.co.uk/2013/09/automotive-technology-roadmaps/. Accessed August, 2014.

[13] SAE. *Hybrid Electric Vehicle (HEV) & Electric Vehicle (EV) Terminology.* 2008; J1715.

[14] Koichiro Muta, Makoto Yamazaki and Junji Tokieda. *Development of New-Generation Hybrid System THS II - Drastic Improvement of Power Performance and Fuel Economy.* Paper no: 2004-01-0064. 2004 SAE World Congress; March 8-11, 2004; USA: SAE International; 2004.

[15] Plasmeier M. *Toyota Prius Cut-Away Engine.* 2006; Available at: https://www.flickr.com/photos/theplaz/508894633/. Accessed July, 2011. Reproduced under Creative Commons CC BY-NC-SA 2.0 licence: https://creativecommons.org/licenses/by-nc-sa/2.0/

[16] Matthew Zolot, Ahmad A. Pesaran and Mark Mihalic. *Thermal Evaluation of Toyota Prius Battery Pack.* Paper no: 2002-01-1962. 2002 Future Car Congress; June 3-5, 2002; USA: SAE International; 2002.

[17] Autoshop101. *Toyota Technical Training - Toyota Hybrid System: Section 4 - Engine.* Available at: www.autoshop101.com. Accessed August, 2014.

[18] Namwook Kim, Aymeric Rousseau and Eric Rask. *Autonomie Model Validation with Test Data for 2010 Toyota Prius.* Paper no: 2012-01-1040. 2012 SAE World Congress; April 24-26, 2012; USA: SAE International; 2012.

[19] Autoshop101. *Toyota Technical Training - Toyota Hybrid System: Section 3 - High-Voltage Battery.* Available at: www.autoshop101.com. Accessed August, 2014.

[20] K. J. Kelly, M. Mihalic and M. Zolot. *Battery usage and thermal performance of the Toyota Prius and Honda Insight during chassis dynamometer testing.* Battery Conference on Applications and Advances, 2002. The Seventeenth Annual; January 14-18, 2002; USA: U.S. Department of Energy; 2002.

[21] Toyota GB. *Prius Specifications.* Available at: http://www.toyotagb-press.co.uk/protected/vehicles/archived/press_packs/prius0305/pack.htm. Accessed July, 2011.

[22] Takuji Matsubara, Hideaki Yaguchi, Toshifumi Takaoka, et al. *Development of New Hybrid System for Compact Class Vehicles.* Paper no: 2009-01-1332. SAE International; 2009.

[23] Kim N, Rousseau A and Rask E. *Vehicle-level control analysis of 2010 Toyota Prius based on test data.* Proceedings of the Institution of Mechanical Engineers Part D-Journal of Automobile Engineering 2012; 226(D11):1483-1494.

[24] Staunton RH, Ayers CW, Marlino LD, et al. *Evaluation of 2004 Toyota Prius Hybrid Electric Drive System.* 2006.

[25] Tamsanya S, Chungpaibulpatana S and Limmeechokchai B. *Development of a driving cycle for the measurement of fuel consumption and exhaust emissions of automobiles in Bangkok during peak periods.* International Journal of Automotive Technology 2009 04/01; 10(2):251-264.

[26] Tong HY, Tung HD, Hung WT, et al. *Development of driving cycles for motorcycles and light-duty vehicles in Vietnam.* Atmospheric Environment 2011 9; 45(29):5191-5199.

[27] EPA. *Dynamometer Drive Schedules.* Available at: http://www.epa.gov/nvfel/testing/dynamometer.htm. Accessed February, 2014.

[28] DieselNet. *Emission Test Cycles: Worldwide engine and vehicle test cycles.* Available at: https://www.dieselnet.com/standards/cycles/. Accessed August, 2014.

[29] M. Kuhler and D. Karstens. *Improved Driving Cycle for Testing Automotive Exhaust Emissions.* Paper no: 780650. Passenger Car Meeting; June 5-9, 1978; USA: SAE International; 1978.

[30] Meyer M, Nelson D and Lohse-Busch H. *Battery Charge Balance and Correction Issues in Hybrid Electric Vehicles for Individual Phases of Certification Dynamometer Driving Cycles as Used in EPA Fuel Economy Label Calculations.* SAE International Journal of Alternative Powertrains 2012; 1(1):219-230.

[31] Tong HY, Hung WT and Cheung CS. *Development of a driving cycle for Hong Kong.* Atmospheric Environment 1999 7/1; 33(15):2323-2335.

[32] André M. *The ARTEMIS European driving cycles for measuring car pollutant emissions.* Science of The Total Environment 2004 12/1; 334–335(0):73-84.

[33] INRETS. *INRETS Publications: ARTEMIS Cycles.* Available at: http://www.inrets.fr/ur/lte/publi-autresactions/fichesresultats/ficheartemis/road3/method31/All_Cycles_in_Artemis_BD_092006.xls. Accessed May, 2013.

[34] André M. *Real-world driving cycles for measuring cars pollutant emissions – Part A: The ARTEMIS European driving cycles.* 2004.

[35] Tong HY and Hung WT. *A Framework for Developing Driving Cycles with On-Road Driving Data.* Transport Reviews 2010 09/01; 2014/09; 30(5):589-615.

[36] Lyons TJ, Kenworthy JR, Austin PI, et al. *The development of a driving cycle for fuel consumption and emissions evaluation.* Transportation Research Part A: General 1986 11; 20(6):447-462.

[37] Lin J and Niemeier D. *An exploratory analysis comparing a stochastic driving cycle to California's regulatory cycle.* Atmospheric Environment 2002 DEC; 36(38):5759-5770.

[38] Dai Z, Niemeier D and Eisinger D. *Driving Cycles: A New Cycle Building Method that Better Represents Real-World Emissions.* UC Davis-Caltrans Air Quality Project 2008; Task Order No 66.

[39] Ronald E. Kruse and Thomas A. Huls. *Development of the Federal Urban Driving Schedule.* Paper no: 730553. Automobile Engineering Meeting; May 14-18, 1973; USA: SAE International; 1973.

[40] Kamble SH, Mathew TV and Sharma GK. *Development of real-world driving cycle: Case study of Pune, India.* Transportation Research Part D: Transport and Environment 2009 3; 14(2):132-140.

[41] Nesamani KS and Subramanian KP. *Development of a driving cycle for intra-city buses in Chennai, India.* Atmospheric Environment 2011 10; 45(31):5469-5476.

[42] Mridul Gautam, Nigel Clark, Wesley Riddle, et al. *Development and Initial Use of a Heavy-Duty Diesel Truck Test Schedule for Emissions Characterization.* Paper no: 2002-01-1753. International Spring Fuels & Lubricants Meeting & Exhibition; May 6-9, 2002; USA: SAE International; 2002.

[43] Esteves-Booth A, Muneer T, Kirby H, et al. *The measurement of vehicular driving cycle within the city of Edinburgh.* Transportation Research Part D: Transport and Environment 2001 5; 6(3):209-220.

[44] Chen C, Huang C, Jing Q, et al. *On-road emission characteristics of heavy-duty diesel vehicles in Shanghai.* Atmospheric Environment 2007 8; 41(26):5334-5344.

[45] M. Montazeri-Gh and M. Naghizadeh. *Development of car drive cycle for simulation of emissions and fuel economy.* Proceedings 15th European Simulation Symposium; October 26-29, 2003; SCS European Council/SCS Europe BVBA; 2003.

[46] Michael Duoba, Theodore Bohn and Henning Lohse-Busch. *Investigating Possible Fuel Economy Bias Due To Regenerative Braking in Testing HEVs on 2WD and*

4WD Chassis Dynamometers. Paper no: 2005-01-0685. 2005 SAE World Congress; April 11-14, 2005; USA: SAE International; 2005.

[47] Burton J, Walkowicz K, Sindler P, et al. *In-Use and Vehicle Dynamometer Evaluation and Comparison of Class 7 Hybrid Electric and Conventional Diesel Delivery Trucks.* SAE International Journal of Commercial Vehicles 2013; 6(2):545-554.

[48] Hu Li, Gordon Andrews E., Adnan Khan A., et al. *Analysis of Driving Parameters and Emissions for Real World Urban Driving Cycles using an on-board Measurement Method for a EURO 2 SI car.* Paper no: 2007-01-2066. SAE International; 2007.

[49] Tong HY, Hung WT and Cheung CS. *On-Road Motor Vehicle Emissions and Fuel Consumption in Urban Driving Conditions.* Journal of the Air & Waste Management Association 2000 04/01; 2014/09; 50(4):543-554.

[50] Guido Lenaers. *Real Life CO2 Emission and Consumption of Four Car Powertrain Technologies Related to Driving Behaviour and Road Type.* Paper no: 2009-24-0127. 9th International Conference on Engines and Vehicles; September 13-18, 2009; Italy: Consiglio Nazionale delle Ricerche; 2009.

[51] Fontaras G, Pistikopoulos P and Samaras Z. *Experimental evaluation of hybrid vehicle fuel economy and pollutant emissions over real-world simulation driving cycles.* Atmospheric Environment 2008 JUN; 42(18):4023-4035.

[52] P. Sharer, R. Leydier and A. Rousseau. *Impact of Drive Cycle Aggressiveness and Speed on HEVs Fuel Consumption Sensitivity.* Paper no: 2007-01-0281. 2007 World Congress; April 16-19, 2007; USA: SAE International; 2007.

[53] Zhang S, Wu Y, Liu H, et al. *Real-world fuel consumption and CO2 (carbon dioxide) emissions by driving conditions for light-duty passenger vehicles in China.* Energy 2014 5/1; 69(0):247-257.

[54] Mock P, German J, Bandivadekar A, et al. *Discrepancies between type approval and "real-world" fuel consumption and CO2 values.* 2012.

[55] Mock P, German J, Bandivadekar A, et al. *From laboratory to road - A comparison of official and 'real-world' fuel consumption and CO2 values for cars in Europe and the United States.* 2013.

[56] Mock P, Tietge U, Franco V, et al. *From laboratory to road - A 2014 update of official and 'real-world' fuel consumption and CO2 values for passenger cars in Europe.* 2014.

[57] Zahabi SAH, Miranda-Moreno L, Barla P, et al. *Fuel economy of hybrid-electric versus conventional gasoline vehicles in real-world conditions: A case study of cold cities in Quebec, Canada.* Transportation Research Part D: Transport and Environment 2014 10; 32(0):184-192.

[58] Howey DA, Martinez-Botas RF, Cussons B, et al. *Comparative measurements of the energy consumption of 51 electric, hybrid and internal combustion engine vehicles.* Transportation Research Part D: Transport and Environment 2011 8; 16(6):459-464.

[59] Karner D and Francfort J. *Hybrid and plug-in hybrid electric vehicle performance testing by the US Department of Energy Advanced Vehicle Testing Activity.* Journal of Power Sources 2007 11/22; 174(1):69-75.

[60] EPA. *The official U.S. government source for fuel economy information.* Available at: http://www.fueleconomy.gov/feg/findacar.shtml. Accessed September, 2014.

[61] Duarte GO, Varella RA, Gonçalves GA, et al. *Effect of battery state of charge on fuel use and pollutant emissions of a full hybrid electric light duty vehicle.* Journal of Power Sources 2014 1/15; 246(0):377-386.

[62] Hu Li, Gordon E. Andrews, Basil Daham, et al. *Impact of Traffic Conditions and Road Geometry on Real World Urban Emissions Using a SI Car.* Paper no: 2007-01-0308. SAE International; 2007.

[63] Eric Wood, Evan Burton, Adam Duran, et al. *Contribution of Road Grade to the Energy Use of Modern Automobiles Across Large Datasets of Real-World Drive Cycles.* Paper no: 2014-01-1789. 2014 SAE World Congress; April 8-10, 2014; USA: SAE International; 2014.

[64] G. El Khoury and D. Clodic . *Method of Test and Measurements of Fuel Consumption Due to Air Conditioning Operation on the New Prius II Hybrid Vehicle.* Paper no: 2005-01-2049. Vehicle Thermal Management Systems Conference and Exhibition; May 10-12, 2005; USA: SAE International; 2005.

[65] Christenson M, Loiselle A, Karman D, et al. *The Effect of Driving Conditions and Ambient Temperature on Light Duty Gasoline-Electric Hybrid Vehicles (2): Fuel Consumption and Gaseous Pollutant Emission Rates.* 2007.

[66] US DOE. *2004 Toyota Prius-2721 Hybrid Battery Test Results.* 2007.

[67] US DOE. *2004 Toyota Prius-1052 Hybrid Battery Test Results.* 2008.

[68] Grey T and Shirk M. *2010 Toyota Prius VIN 0462 Hybrid Electric Vehicle Battery Test Results.* 2013; INL/EXT-13-28025.

[69] Grey T and Shirk M. *2010 Toyota Prius VIN 6063 Hybrid Electric Vehicle Battery Test Results.* 2013; INL/EXT-13-28026.

[70] PriusChat. *Gen2 Prius: Custom PIDs for Torque (Android App) with formulas.* 2011; Available at: http://priuschat.com/threads/gen2-prius-custom-pids-for-torque-android-app-with-formulas.95370/#axzz3FkTWl0is. Accessed August, 2013.

[71] Stone R. *Introduction to Internal Combustion Engines.* Third ed. UK: Macmillan Press Ltd; 1999.

[72] Google. *Google Maps.* 2014; Available at: https://www.google.co.uk/maps. Accessed September, 2014.

[73] survcentex. *Surveying in Central Texas.* 2011; Available at: https://www.flickr.com/photos/57683586@N02/5403122132/. Accessed April, 2015. Cropped image reproduced under Creative Commons CC BY 2.0 licence: https://creativecommons.org/licenses/by/2.0/

[74] Panasonic. *Ni-MH Handbook - Industrial Batteries.*

[75] EPA. *Emission Facts: Average Carbon Dioxide Emissions Resulting from Gasoline and Diesel Fuel.* 2005; EPA420-F-05-001.

[76] SAE. *Recommended Practice for Measuring the Exhaust Emissions and Fuel Economy of Hybrid-Electric Vehicles, Including Plug-in Hybrid Vehicles.* 2010; J1711.

[77] SAE. *Recommended Practice for Measuring Fuel Economy and Emissions of Hybrid-Electric and Conventional Heavy-Duty Vehicles.* 2002; J2711.

[78] UN ECE. *UN ECE Regulation No. 101 Revision 3.* 2013; E/ECE/324/Rev.2/Add.100/Rev.3−E/ECE/TRANS/505/Rev.2/Add.100/Rev.3.

[79] Ericsson E. *Independent driving pattern factors and their influence on fuel-use and exhaust emission factors.* Transportation Research Part D: Transport and Environment 2001 9; 6(5):325-345.

[80] A. Rousseau, J. Kwon, P. Sharer, et al. *Integrating Data, Performing Quality Assurance, and Validating the Vehicle Model for the 2004 Prius Using PSAT.* Paper no: 2006-01-0667. 2006 SAE World Congress; April 3-6, 2006; USA: SAE International; 2006.

[81] Rousseau A, Sharer P and Pasquier M. *Validation Process of a HEV System Analysis Model: PSAT.* 2004.

[82] Calwell C, Ton M, Gordon D, et al. *California State Fuel-Efficient Tire Report: Volume II.* 2003(600-03-001CR).

[83] Peter Leijen and Jonathan Scott. *Failure Analysis of Some Toyota Prius Battery Packs and Potential for Recovery.* Paper no: 2013-01-2561. 2013 SAE/KSAE International Powertrains, Fuels & Lubricants Meeting; October 21-23, 2013; USA: SAE International; 2013.

[84] Henning Lohse-Busch, Michael Duoba, Eric Rask, et al. *Ambient Temperature (20°F, 72°F and 95°F) Impact on Fuel and Energy Consumption for Several Conventional*

Vehicles, Hybrid and Plug-In Hybrid Electric Vehicles and Battery Electric Vehicle. Paper no: 2013-01-1462. SAE International; 2013.

[85] Met Office. *UK Midlands Monthly Temperature History 2012.* 2013; Available at: http://www.metoffice.gov.uk/climate/uk/. Accessed June 12, 2014.

[86] Brace CJ, Burke R and Moffa J. *Increasing accuracy and repeatability of fuel consumption measurement in chassis dynamometer testing.* Proceedings of the Institution of Mechanical Engineers, Part D: Journal of Automobile Engineering 2009 September 01; 223(9):1163-1177.

Appendices

Appendix 1 – Sample of Logged Driving Data

	A	K	Q	R	S	T
1	Date	Module[M-1	AI5	AI6	AI7	GPS Data(GPRMC)
2	20121008 064942	1	2.534	4.633	-5	$GPRMC,235955.037,V,,,,,0.00,0.00,050180,,,N*48
3	20121008 064943	1	2.534	4.627	-5	$GPRMC,235956.037,V,,,,,0.00,0.00,050180,,,N*4B
4	20121008 064944	1	2.538	4.535	-5	$GPRMC,235957.037,V,,,,,0.00,0.00,050180,,,N*4A
5	20121008 064945	1	2.564	4.602	-5	$GPRMC,235958.037,V,,,,,0.00,0.00,050180,,,N*45
6	20121008 064946	1	2.517	4.631	-5	$GPRMC,235959.037,V,,,,,0.00,0.00,050180,,,N*44
7	20121008 064947	1	2.426	4.696	-5	$GPRMC,054017.157,V,,,,,0.00,0.00,070180,,,N*47
8	20121008 064948	1	2.426	4.696	-5	$GPRMC,054018.157,V,,,,,0.00,0.00,070180,,,N*48
9	20121008 064949	1	2.456	4.692	-5	$GPRMC,054019.157,V,,,,,0.00,0.00,070180,,,N*49
10	20121008 064950	1	2.456	4.694	-5	$GPRMC,054020.157,V,,,,,0.00,0.00,070180,,,N*43
11	20121008 064951	1	2.464	4.693	-5	$GPRMC,054021.157,V,,,,,0.00,0.00,070180,,,N*42
12	20121008 064952	1	2.457	4.699	-5	$GPRMC,054022.157,V,,,,,0.00,0.00,070180,,,N*41
13	20121008 064953	1	2.471	4.675	-5	$GPRMC,054023.157,V,,,,,0.00,0.00,070180,,,N*40
14	20121008 064954	1	2.473	4.668	-5	$GPRMC,054024.157,V,,,,,0.00,0.00,070180,,,N*47
15	20121008 064955	1	2.477	4.674	-5	$GPRMC,054025.157,V,,,,,0.00,0.00,070180,,,N*46
16	20121008 064956	1	2.477	4.674	-5	$GPRMC,054026.157,V,,,,,0.00,0.00,070180,,,N*45
17	20121008 064957	1	2.47	4.667	-5	$GPRMC,054027.157,V,,,,,0.00,0.00,070180,,,N*44
18	20121008 064958	1	2.489	4.649	-5	$GPRMC,054028.157,V,,,,,0.00,0.00,070180,,,N*4B
19	20121008 064959	1	2.512	4.66	-5	$GPRMC,054029.157,V,,,,,0.00,0.00,070180,,,N*4A
20	20121008 065000	1	2.512	4.651	-5	$GPRMC,054030.157,V,,,,,0.00,0.00,070180,,,N*42
21	20121008 065001	1	2.548	4.662	-5	$GPRMC,054031.157,V,,,,,0.00,0.00,070180,,,N*43
22	20121008 065002	1	2.539	4.657	-5	$GPRMC,054032.157,V,,,,,0.00,0.00,070180,,,N*40
23	20121008 065003	1	2.542	4.651	-5	$GPRMC,054033.156,V,,,,,0.25,0.00,081012,,,N*43
24	20121008 065004	1	2.542	4.651	-5	$GPRMC,054033.156,V,,,,,0.25,0.00,081012,,,N*43
25	20121008 065005	1	2.554	4.651	-5	$GPRMC,054035.000,V,,,,,0.66,26.99,081012,,,N*74
26	20121008 065006	1	2.553	4.651	-5	$GPRMC,054036.000,V,,,,,0.21,26.99,081012,,,N*74
27	20121008 065007	1	2.553	4.636	-5	$GPRMC,054037.000,A,5246.1128,N,00113.6337,W,0.13,26.99,081012,,,A*48
28	20121008 065008	1	2.552	4.634	-5	$GPRMC,054038.000,A,5246.1121,N,00113.6337,W,0.09,26.99,081012,,,A*45
29	20121008 065009	1	2.55	4.635	-5	$GPRMC,054039.000,A,5246.1130,N,00113.6330,W,0.02,26.99,081012,,,A*48
30	20121008 065010	1	2.545	4.642	-5	$GPRMC,054040.000,A,5246.1132,N,00113.6328,W,0.02,26.99,081012,,,A*4D
31	20121008 065011	1	2.547	4.639	-5	$GPRMC,054041.000,A,5246.1134,N,00113.6325,W,0.02,26.99,081012,,,A*47
32	20121008 065012	1	2.543	4.634	-5	$GPRMC,054042.000,A,5246.1135,N,00113.6323,W,0.16,26.99,081012,,,A*46
33	20121008 065013	1	2.543	4.634	-5	$GPRMC,054043.000,A,5246.1140,N,00113.6318,W,0.38,26.99,081012,,,A*41
34	20121008 065014	1	2.538	4.638	-5	$GPRMC,054044.000,A,5246.1144,N,00113.6314,W,0.51,26.99,081012,,,A*41
35	20121008 065015	1	2.53	4.635	-5	$GPRMC,054045.000,A,5246.1144,N,00113.6316,W,0.55,26.99,081012,,,A*46
36	20121008 065016	1	2.528	4.637	-5	$GPRMC,054046.000,A,5246.1148,N,00113.6316,W,0.65,29.34,081012,,,A*42
37	20121008 065017	1	2.523	4.629	-5	$GPRMC,054047.000,A,5246.1150,N,00113.6316,W,0.63,29.56,081012,,,A*48
38	20121008 065018	1	2.52	4.632	-5	$GPRMC,054048.000,A,5246.1152,N,00113.6314,W,0.77,28.97,081012,,,A*4E
39	20121008 065019	1	2.519	4.64	-5	$GPRMC,054049.000,A,5246.1153,N,00113.6313,W,0.71,30.13,081012,,,A*4A
40	20121008 065020	1	2.525	4.642	-5	$GPRMC,054050.000,A,5246.1153,N,00113.6314,W,0.68,29.22,081012,,,A*47
41	20121008 065021	1	2.525	4.642	-5	$GPRMC,054051.000,A,5246.1155,N,00113.6314,W,0.74,29.62,081012,,,A*49
42	20121008 065022	1	2.529	4.645	-5	$GPRMC,054052.000,A,5246.1208,N,00113.6230,W,0.30,29.62,081012,,,A*46
43	20121008 065023	1	2.518	4.643	-5	$GPRMC,054053.000,A,5246.1260,N,00113.6122,W,0.28,29.62,081012,,,A*40
44	20121008 065024	1	2.522	4.646	-5	$GPRMC,054054.000,A,5246.1260,N,00113.6122,W,0.24,29.62,081012,,,A*4B
45	20121008 065025	1	2.524	4.642	-5	$GPRMC,054055.000,A,5246.1263,N,00113.6120,W,0.16,29.62,081012,,,A*4A
46	20121008 065026	1	2.523	4.638	-5	$GPRMC,054056.000,A,5246.1264,N,00113.6120,W,0.15,29.62,081012,,,A*4D
47	20121008 065027	1	2.53	4.643	-5	$GPRMC,054057.000,A,5246.1265,N,00113.6118,W,0.37,29.62,081012,,,A*46
48	20121008 065028	1	2.525	4.637	-5	$GPRMC,054058.000,A,5246.1266,N,00113.6117,W,0.16,29.62,081012,,,A*46
49	20121008 065029	1	2.525	4.637	-5	$GPRMC,054059.000,A,5246.1268,N,00113.6115,W,0.03,29.62,081012,,,A*4F
50	20121008 065030	1	2.526	4.633	-5	$GPRMC,054100.000,A,5246.1268,N,00113.6115,W,0.07,29.62,081012,,,A*46
51	20121008 065031	1	2.535	4.643	-5	$GPRMC,054101.000,A,5246.1269,N,00113.6116,W,0.04,29.62,081012,,,A*46
52	20121008 065032	1	2.527	4.639	-5	$GPRMC,054102.000,A,5246.1270,N,00113.6116,W,0.01,29.62,081012,,,A*48
53	20121008 065033	1	2.529	4.638	-5	$GPRMC,054103.000,A,5246.1272,N,00113.6115,W,0.01,29.62,081012,,,A*48
54	20121008 065034	1	2.528	4.643	-5	$GPRMC,054104.000,A,5246.1275,N,00113.6113,W,0.01,29.62,081012,,,A*4E
55	20121008 065035	1	2.532	4.643	-5	$GPRMC,054105.000,A,5246.1276,N,00113.6111,W,0.01,29.62,081012,,,A*4E
56	20121008 065036	1	2.526	4.634	-5	$GPRMC,054106.000,A,5246.1277,N,00113.6109,W,0.00,29.62,081012,,,A*44
57	20121008 065037	1	2.529	4.64	-5	$GPRMC,054107.000,A,5246.1278,N,00113.6107,W,0.01,29.62,081012,,,A*45
58	20121008 065038	1	2.529	4.64	-5	$GPRMC,054108.000,A,5246.1279,N,00113.6106,W,0.01,29.62,081012,,,A*4A

20121008_064942_1

Appendix 2 – Sample of Processed Driving Data

(a) Stage 1 – After Excel macro

	A	B
1	0	0
2	24607	0.24076
3	24608	0.16668
4	24609	0.03704
5	24610	0.03704
6	24611	0.03704
7	24612	0.29632
8	24613	0.70376
9	24614	0.94452
10	24615	1.0186
11	24616	1.2038
12	24617	1.16676
13	24618	1.42604
14	24619	1.31492
15	24620	1.25936
16	24621	1.37048
17	24622	0.5556
18	24623	0.51856
19	24624	0.44448
20	24625	0.29632
21	24626	0.2778
22	24627	0.68524
23	24628	0.29632
24	24629	0.05556
25	24630	0.12964
26	24631	0.07408
27	24632	0.01852
28	24633	0.01852
29	24634	0.01852
30	24635	0.01852
31	24636	0
32	24637	0.01852
33	24638	0.01852
34	24639	0.03704
35	24640	0
36	24641	0
37	24642	0
38	24643	0.01852
39	24644	0.01852
40	24645	0.01852
41	24646	0.01852
42	24647	0
43	24648	0
44	24649	0
45	24650	0.01852
46	24651	0.01852
47	24652	0.01852
48	24653	0.01852

(b) Stage 2 – After MATLAB programme

	A	B
168	167	0
169	168	0
170	169	0
171	170	0
172	171	0
173	172	0
174	173	0
175	174	0
176	175	1.7964
177	176	2.5002
178	177	2.9447
179	178	3.6484
180	179	3.5744
181	180	3.5929
182	181	3.7225
183	182	4.0188
184	183	3.2595
185	184	3.3521
186	185	3.2966
187	186	2.1113
188	187	0
189	188	1.0186
190	189	2.5928
191	190	4.5004
192	191	5.1856
193	192	5.7782
194	193	5.7042
195	194	5.1856
196	195	5.2597
197	196	4.204
198	197	3.8892
199	198	3.8707
200	199	5.2412
201	200	5.3152
202	201	4.2596
203	202	3.5744
204	203	3.667
205	204	4.5559
206	205	5.7412
207	206	6.2783
208	207	6.6672
209	208	9.76
210	209	11.575
211	210	13.446
212	211	16.131
213	212	19.205
214	213	21.483
215	214	22.965

Appendix 3 – MATLAB Programme to Process Driving Data CSV Files, Version 1

```
% Script file to format data after initial Excel processing to round nil
% speeds down to zero and filter out long zero speed periods, and to find
% unrealistic accelerations/decelerations due to GPS errors and smooth
% the speed trace prior to these

% Matthew Lintern 2013

clear all
close all

fprintf('~ ~ ~ ~ Drive Cycle Data Nil Speed Rounding & Filtering, and Speed Data↙
Smoothing ~ ~ ~ ~\n\n')

maxstop = 300;    % Set max stop time in secs

% Batch processing - Producing list of files to process
Filelist = dir('*.csv');
nooffiles = size(Filelist,1);

disp(['Max stop is currently set to ' num2str(maxstop) ' secs'])
progrun = input('Please press any key to run programme or Ctrl+C to abort\n','s');

for k = 1:nooffiles

    % Get the file name
    infilename = Filelist(k).name;
    disp(['File to be processed: ' infilename])

    % Define data from file
    data = csvread(infilename);

    % Define data columns
    time = data(:,1);
    speed = data(:,2);

    speed_size = size(speed);
    rows1 = speed_size(1);

    % Replace speeds < 1 with 0
    for p = 1:rows1
        if speed(p)<1
            speed(p)=0;
        end
    end

    % Form new data array with edited zero speeds
    moddata = [time, speed];

    % Check for periods at zero speed and reduce to max stop time
    zerosecs = 0;   % Set counter for stop time

    for q = 1:rows1
        if speed(q)== 0
            zerosecs = zerosecs+1;
            if zerosecs > maxstop
```

```
                moddata(q,:) = 999;     % To delete rows with zeros over maxstop↙
later
            end
            if q <= rows1-1 && speed(q+1)~= 0
                zerosecs = 0;
            end
        end
    end

    time = moddata(:,1);
    speed = moddata(:,2);

    % Find speed=999 in speed data then delete these rows
    cutzeros = find(speed==999);
    speed(cutzeros) =[];

    % Form new array with modified speed & time data
    modspeed = speed;

    % Check first speed value is 0 and insert 0 if not
    if modspeed(1)~=0
        modspeed = [0;modspeed];
    else
    end

    % Check last speed value is 0 and insert 0 if not
    rows2 = length(modspeed);
    if modspeed(rows2)~=0
        modspeed = [modspeed;0];
    else
    end

    rows = length(modspeed);

    % Check for non-real accelerations/decelerations and insert rows to smooth
    % them, formulated in a new array
    newspeed = [modspeed(1)];

    for n = 2:rows
        accel = modspeed(n)-modspeed(n-1);
        if accel >= -30 && accel <= 16
            newspeed = [newspeed ; modspeed(n)];
            rowno = length(newspeed);
        end
        if accel > 16 && accel <= 100
            m = modspeed(n-1)+3.35;
            newrows = [];
            while m < modspeed(n)
                newrows = [newrows ; m];
                m = m+3.35;
            end
            newspeed = [newspeed ; newrows ; modspeed(n)];
            rowno = length(newspeed);
        end
        if accel < -30 && accel >= -100
```

```
            m = modspeed(n-1)-3.40;
            newrows = [];
            while m > modspeed(n);
                newrows = [newrows ; m];
                m = m-3.40;
            end
            newspeed = [newspeed ; newrows ; modspeed(n)];
            rowno = length(newspeed);
        end
        if accel > 100
            m = modspeed(n-1)+3.35;
            newrows = [];
            while m < modspeed(n)
                newrows = [newrows ; m];
                m = m+3.35;
            end
            newspeed = [newspeed ; newrows ; modspeed(n)];
            rowno = length(newspeed);
            disp(['* * * * !!!! WARNING: Acceleration was > 100 at row ' num2str↙
(rowno) ', please check data !!!! * * * *'])
        end
        if accel < -100
            m = modspeed(n-1)-3.40;
            newrows = [];
            while m > modspeed(n);
                newrows = [newrows ; m];
                m = m-3.40;
            end
            newspeed = [newspeed ; newrows ; modspeed(n)];
            rowno = length(newspeed);
            disp(['* * * * !!!! WARNING: Deceleration was > 100 at row ' num2str↙
(rowno) ', please check data !!!! * * * *'])
        end
    end

    % Re-numbering time column
    newspeedlength = length(newspeed);
    newtime = [0:newspeedlength-1]';
    newdata = [newtime, newspeed];

    % Create output filename based on input filename
    fnamel = length(infilename);
    outfilename = [infilename(1:fnamel-4) '_s300processed.csv'];

    % Save file with new data array
    csvwrite(['*File directory here*                                    ↙
                                                                    ' outfilename], newdata)

    % Give message when data processing is complete
    fprintf(['Data processing complete for file ' infilename '\nThe output filename↙
is: ' outfilename '\n\n'])
    % disp(['Data processing of file ' infilename ' complete'])
    % disp(['The output filename is: ' outfilename])
end

fprintf('All data processing complete\n\n')

% ~~~~~~~~~~~~~~~~~~~~~~~~~~~~~~ END ~~~~~~~~~~~~~~~~~~~~~~~~~~~~~~
```

Appendix 4 – FCRT Drive Cycle Revised Settings Validation Cycle Simulation Results

Weekly Cycles with Varying Cycle Duration

No	Cycle	Input Duration (h)	Input Max Segment (h)	Max Segment % of Duration	Cycle Duration (h)	Fuel consumption (l/100km)	CO2 g/km	Mean	Sqrd diff	Variance	Std dev
	LUW1.0.5-0.17s300	0.5	0.17	34%	0.41	8.16	220.61	6.64	2.30	0.44	0.66
	LUW1.0.7-0.23s300	0.7	0.23	33%	0.56	6.55	177.14		0.01		
	LUW1.0.8-0.26s300	0.8	0.26	33%	0.65	6.25	169.04		0.16		
	LUW1.1.0-0.33s300	1.0	0.33	33%	0.82	7.11	192.20		0.22		
	LUW1.1.5-0.50s300	1.5	0.50	33%	1.22	6.68	180.70		0.00		
	LUW1.2.0-0.66s300	2.0	0.66	33%	1.63	6.00	162.21		0.41		
	LUW1.3.0-0.99s300	3.0	0.99	33%	2.39	6.09	164.62		0.31		
	LUW1.4.0-1.32s300	4.0	1.32	33%	3.22	6.31	170.63		0.11		
	LUW2.0.5-0.17s300	0.5	0.17	34%	0.42	8.22	222.48	7.07	1.33	0.27	0.52
	LUW2.0.7-0.23s300	0.7	0.23	33%	0.57	6.98	188.91		0.01		
	LUW2.0.8-0.26s300	0.8	0.26	33%	0.65	7.09	191.76		0.00		
	LUW2.1.0-0.33s300	1.0	0.33	33%	0.81	6.63	179.30		0.19		
	LUW2.2.0-0.66s300	2.0	0.66	33%	1.64	6.61	178.92		0.21		
	LUW2.3.0-0.99s300	3.0	0.99	33%	2.47	7.25	196.24		0.03		
	LUW2.4.0-1.33s300	4.0	1.33	33%	3.29	6.70	181.15		0.14		
	LUW3.0.5-0.17s300	0.5	0.17	34%	0.42	8.39	227.05	7.21	1.39	0.37	0.61
	LUW3.0.7-0.23s300	0.7	0.23	33%	0.58	7.37	199.44		0.03		
	LUW3.0.8-0.26s300	0.8	0.26	33%	0.65	7.11	192.29		0.01		
	LUW3.1.0-0.33s300	1.0	0.33	33%	0.82	7.24	195.74		0.00		
	LUW3.2.0-0.66s300	2.0	0.66	33%	1.64	6.55	177.19		0.44		
	LUW3.3.0-0.99s300	3.0	0.99	33%	2.47	6.60	178.49		0.37		

Weekly Cycles with Varying Maximum Segment Length

No	Cycle	Input Duration (h)	Input Max Segment (h)	Max Segment % of Duration	Cycle Duration (h)	Fuel consumption (l/100km)	CO2 g/km	Mean	Sqrd diff	Variance	Std dev
	LUW1.0.5-0.02s300	0.5	0.02	4%	0.53	6.69	181.06	7.50	0.66	0.37	0.61
	LUW1.0.5-0.05s300	0.5	0.05	10%	0.44	7.38	199.53				
	LUW1.0.5-0.07s300	0.5	0.07	14%	0.47	7.20	194.90		0.09		
	LUW1.0.5-0.10s300	0.5	0.10	20%	0.44	7.15	193.39		0.13		
	LUW1.0.5-0.13s300	0.5	0.13	26%	0.40	7.32	198.09		0.03		
	LUW1.0.5-0.15s300	0.5	0.15	30%	0.40	7.18	194.30		0.11		
	LUW1.0.5-0.17s300	0.5	0.17	34%	0.41	8.16	220.61		0.43		
	LUW1.0.5-0.20s300	0.5	0.20	40%	0.40	7.76	209.87		0.07		
	LUW1.0.5-0.25s300	0.5	0.25	50%	0.40	8.70	235.27		1.43		
	LUW2.0.5-0.02s300	0.5	0.02	4%	0.50	7.10	192.08	7.76	0.43	0.30	0.55
	LUW2.0.5-0.05s300	0.5	0.05	10%	0.50	7.55	204.21		0.04		
	LUW2.0.5-0.10s300	0.5	0.10	20%	0.44	8.74	236.55		0.97		
	LUW2.0.5-0.15s300	0.5	0.15	30%	0.42	7.54	203.85		0.05		
	LUW2.0.5-0.25s300	0.5	0.25	50%	0.49	7.85	212.45		0.01		
	LUW3.0.5-0.02s300	0.5	0.02	4%	0.50	8.00	216.43	7.93	0.00	0.79	0.89
	LUW3.0.5-0.05s300	0.5	0.05	10%	0.47	7.23	195.45		0.49		
	LUW3.0.5-0.10s300	0.5	0.10	20%	0.48	7.14	193.27		0.63		
	LUW3.0.5-0.15s300	0.5	0.15	30%	0.43	7.69	208.08		0.06		
	LUW3.0.5-0.25s300	0.5	0.25	50%	0.42	9.60	259.65		2.78		

Monthly Cycles with Varying Cycle Duration

No	Cycle	Input Duration (h)	Input Max Segment (h)	Max Segment % of Duration	Cycle Duration (h)	Fuel consumption (l/100km)	CO2 g/km	Mean	Sqrd diff	Variance	Std dev
	LUM1.0.5-0.17s300	0.5	0.17	34%	0.41	6.99	189.10	6.76	0.05	0.06	0.25
	LUM1.0.8-0.27s300	0.8	0.27	34%	0.64	6.77	183.09		0.00		
	LUM1.1.0-0.33s300	1.0	0.33	33%	0.80	6.71	181.41		0.00		
	LUM1.1.5-0.50s300	1.5	0.50	33%	1.22	6.93	187.44		0.03		
	LUM1.2.0-0.66s300	2.0	0.66	33%	1.64	7.02	189.92		0.07		
	LUM1.3.0-1.00s300	3.0	1.00	33%	2.44	6.68	180.58		0.01		
	LUM1.4.0-1.32s300	4.0	1.33	33%	3.25	6.22	168.14		0.29		
	LUM2.0.5-0.17s300	0.5	0.17	34%	0.41	8.22	222.46	7.56	0.44	0.65	0.81
	LUM2.0.8-0.26s300	0.8	0.26	33%	0.64	8.07	218.23		0.26		
	LUM2.1.0-0.33s300	1.0	0.33	33%	0.80	8.25	223.11		0.48		
	LUM2.2.0-0.66s300	2.0	0.66	33%	1.61	7.01	189.75		0.30		
	LUM2.3.0-1.00s300	3.0	1.00	33%	2.42	6.23	168.52		1.76		
	LUM3.0.5-0.17s300	0.5	0.17	34%	0.39	8.14	220.13	7.30	0.71	0.40	0.63
	LUM3.0.8-0.27s300	0.8	0.26	33%	0.63	7.10	191.95		0.04		
	LUM3.1.0-0.33s300	1.0	0.33	33%	0.80	7.91	214.08		0.37		
	LUM3.2.0-0.66s300	2.0	0.66	33%	1.61	6.88	186.17		0.18		
	LUM3.3.0-1.00s300	3.0	1.00	33%	2.39	6.47	174.98		0.69		

Appendix 5 – MATLAB Programme to Convert 10 Hz Drive Cycle Data Files to 1 Hz

```
% Programme to convert drive cycle files with 0.1s steps to 1s steps

% Matthew Lintern 2014

clear all
% clc

disp('Convert drive cycle files with 0.1s steps into 1s steps')
disp('NB. Check data file starts at 0 and ends on a whole sec at 0 km/h')

% Request filename input to load data from
infilename = input('Please enter a CSV drive cycle data filename to convert
(including extension): ', 's');
data = csvread(infilename);

% Specify columns from data
intime = data(:,1);
invel = data(:,2);

% Create new data array using every 10th line from input file
norows = length(intime);
outdata = [0 0];
for n = 11:10:norows
    timepoint = intime(n);
    velpoint = invel(n);
    newrow = [timepoint velpoint];
    outdata = [outdata;newrow];
end

% Create output filename based on input filename
fnamel = length(infilename);
outfilename = [infilename(1:fnamel-4) '_processed_1Hz.csv'];

% Save file with new data array
csvwrite(['*File directory here*
'' outfilename], outdata)

% Give message to show that processing has finished
fprintf(['Data processing complete for file ' infilename '\nThe output filename is: '
outfilename '\n\n'])


% ~ ~ ~ ~ ~ ~ ~ END ~ ~ ~ ~ ~ ~
```

Appendix 6 – Chassis Dynamometer Operating Test Procedure

Chassis Dynamometer Operating Guide

Version 2, 2014 *Matthew Lintern*

This guide is for use by persons that have been trained in the correct operation of the chassis dynamometer. It refers to the AAE Department chassis dynamometer in the Stewart Miller Building.

Health and Safety Measures
(Additional to those listed in the risk assessment)

- Ensure emergency stop button is put in vehicle in easy reach of the driver

Road Load Simulation (RLS) Tests

- An operator must be present in the control room when running tests with sustained periods of high speeds (>65 mph)
- Demonstration tests should only be run at low speeds (<25mph) when spectators are present in the chassis dyno area

Speed Control Tests

- An operator must be present in the control room when running tests in speed control mode with a driver

Operation Steps

The order of procedures is:

1. Model the vehicle in software
2. Switch on and setup dyno
3. Setup vehicle on rollers
4. Warm up dyno rollers
5. Carry out inertia, friction & windage calibration
6. Warm up vehicle on rollers
7. Carry out vehicle calibration (forced coastdown)
8. Vehicle coastdown
9. Testing

Instructions for carrying out the above steps are as follows.

Vehicle Modelling

Carry out: Once to set up your vehicle model

1. Open *DM_Vehicle_Management.exe* from the desktop or *All Programs* > *Dynamotive Ltd* > *Control*
2. Fill in the relevant new vehicle details in the cells of the blank row across the top then click on the list of vehicles below to enter the details onto the list
3. Click on *V-t Curve* on the *Offline Modelling* tab on the left hand side
4. Ensure that your correct vehicle is still selected in the list above then click *Clear Table* to remove any existing values
5. Click *Properties* to open the *Velocity Time Set Up* window
6. Enter the values for *Vehicle Mass*, *Start Speed*, *End Speed* and *Interval* to match those from the proving ground coastdown tests, then click *Ok*
7. Enter the gate times in the table
8. Click *Calculate* to calculate the coefficients then on the window that appears click *Close*. WARNING, DO NOT click *Save* as it will crash the system!
9. Click *Save to Vehicle File*

Switch on & Set up Dyno

Carry out: Every day of running the dyno

1. Switch on isolator T18-1A-D on wall
2. Switch on main switch on DynaMotive inverter
3. Press the red *System Fault/Reset* button on the DynaMotive control module under the desk, or red *Fault/Reset* button on the DynaMotive inverter
4. Open *ChassisDyno.exe* from the desktop or *All Programs* > *Dynamotive Ltd* > *Control*
5. On the *Dynamometer Configuration* window that opens click *Advanced…* to select the relevant flywheel required by clicking the check box next to *400 kg Flywheel* or *800 kg Flywheel* or none selected, then click *Close*
6. Click *Close*
7. Click *OK* on the *Warning: Could not load…* error message that appears
8. When the software opens if the dials are not shown on the screen go to *File* > *Open…* > *DynoDials.col* in the *C:/DMDyno/Displays folder*
9. Rearrange and/or reposition the dials to a suitable place in the GUI

AAE SM Chassis Dynamometer Operating Guide

Vehicle Setup

1. Remove roller covers
2. Position vehicle square to rollers
3. Raise wheel supports
4. Park vehicle on rollers
5. Lower vehicle into rollers
6. Attach lateral straps to vehicle tow eye(s) with the shackles, and the other ends to eye bolts on the floor with the hook end, leaving them quite slack. These should be at the front on a FWD vehicle and back on a RWD
7. Attach longitudinal strap to rear tow eye of vehicle with some slack to allow for any movement
8. Fit safety guards around rollers using hex head bolts
9. If applicable attach the exhaust gas extraction pipe to the vehicle exhaust pipe using a jubilee clip
10. If applicable enable vehicle for rolling road use (disable ABS)
11. If the vehicle is to be driven on the dyno, position the cooling fan in front of vehicle inline with its cooling intake(s)
12. Put vehicle in neutral
13. Apply handbrake if a FWD vehicle or release handbrake on RWD vehicle
14. Run dyno at 5 km/h with rate at 1 km/h/s to allow vehicle to centralise itself on the rollers. With FWD use a driver to deal with any steering input required
15. Tighten ratchet straps but without applying pressure on the vehicle, to allow for any small movements

Warm up Dyno Rollers

Carry out: Every session you run the dyno, i.e. whenever the rollers have been left not running for long enough to cool down

1. Ensure vehicle is lifted off the rollers
2. Switch on Auxiliaries by right clicking on the *Aux* light at the bottom of the screen and clicking *Yes*
3. Go to *Dynamometer* > *Speed Control*
4. Set *Upper* to 80 km/h and *Rate* to 5 km/h/s
5. Click *Start* to switch on the dyno
6. Click *Raise* to start the dyno running
7. Allow the warm up to run for 30-45 mins
8. With *Lower* set to 0 km/h click *Lower* to reduce the dyno speed to a stop
9. Click *Stop* to switch off the dyno

AAE SM Chassis Dynamometer Operating Guide

Inertia, Friction & Windage Calibration

Carry out: Before every testing period, e.g. at the start of a weeks' testing

1. Go to *Dynamometer > Inertia, Friction & Windage Calibration*
2. Click *Start Test…*
3. Repeat test

Warm up Vehicle on Rollers

Method 1

1. Lower vehicle onto rollers
2. Strap down vehicle with ratchet straps but without applying pressure on the vehicle to allow for any small movements
3. Ensure the vehicle is out of gear (in neutral) and parking brake (handbrake) is off
4. Run the dyno as detailed in Warm up Dyno above for 20-30 mins

Method 2

1. Lower vehicle onto rollers
2. Strap down vehicle with ratchet straps but without applying pressure on the vehicle to allow for any small movements
3. Sit somebody in the vehicle and ensure the vehicle is out of gear (in neutral) and parking brake (handbrake) is off
4. Check on the right of the status bar at the bottom of the screen that the correct vehicle model is loaded. If not go to *Vehicle > Load model / Edit Coefficients*, click *Load Vehicle*, select the correct vehicle in the list then click *Load*
5. Switch on Auxiliaries by right clicking on the *Aux* light at the bottom of the screen and clicking *Yes*
6. Go to *Dynamometer >RLS Control*
7. Click *Start*
8. Drive the vehicle for 10 mins at approx 70 km/h
9. Slow the vehicle down to a standstill
10. Click *Stop* to switch of the dyno

Vehicle Calibration (Forced Coastdown)

Carry out: Before every testing period, e.g. at the start of a weeks' testing, or at the start of each day's testing for added accuracy

1. Go to *Vehicle* > *Load model / Edit Coefficients*
2. If the correct vehicle model is not already displayed click *Load Vehicle*, select the correct vehicle in the list then click *Load*
3. Click *Calibration Test…*
4. In the *Vehicle Calibration* window click *Edit Test…*
5. Set *First Sample*, *Last Sample* and *Interval* for the start speed, end speed and step interval respectively. Typically these will be 100 km/h, 5 km/h and 5 km/h
6. Set the number of runs you wish to complete in *Num Runs*, typically 3, then click *OK*
7. Click *Start Test*

Vehicle Coastdown

Carry out: Before every testing period, e.g. at the start of a weeks' testing, or at the start of each day's testing for added accuracy

1. Go to *Vehicle* > *Vehicle Coastdown*
2. In the *Vehicle Coastdown Test* window click *Edit Test…*
3. Set *First Sample*, *Last Sample* and *Interval* to match those of the proving ground coastdown test data for the start speed, end speed and step interval respectively
4. Set the number of runs you wish to complete in *Num Runs* then click *OK*
5. Click *Start Test*

Testing

Speed Control Mode

1. Switch on Auxiliaries by right clicking on the *Aux* light at the bottom of the screen and clicking *Yes*
2. Go to *Dynamometer > Speed Control*
3. Set *Upper* to test speed and *Rate* typically to 5 km/h/s
4. Click *Start* to switch on the dyno
5. Click *Raise* to start the dyno running
6. Carry out test
7. With *Lower* set to 0 km/h click *Lower* to reduce the dyno speed to a stop
8. Click *Stop* to switch off the dyno

Road Load Simulation (RLS) Mode

1. Check on the right of the status bar at the bottom of the screen that the correct vehicle model is loaded. If not go to *Vehicle > Load model / Edit Coefficients*, click *Load Vehicle*, select the correct vehicle in the list then click *Load*
2. Switch on Auxiliaries by right clicking on the *Aux* light at the bottom of the screen and clicking *Yes*
3. Go to *Dynamometer >RLS Control*
4. Click *Start*
5. Carry out test
6. Slow the vehicle down to a standstill
7. Click *Stop* to switch of the dyno

Shutdown & Switch off Dyno

Carry out: Every day of running the dyno

1. Close the chassis dyno software
2. Log off the PC
3. Switch off main switch on DynaMotive inverter
4. Switch off isolator T18-1A-D on wall

Appendix 7 – MATLAB Battery Test Data Processing Programme

```
% Programme to process battery test data

% Calculates:
% - Total current charged or discharged (A). For charges the voltage data
% is smoothed to be used to find the max point, which is used as the cutoff
% point for summing the current
% - Battery capacity (Ah)
% - Percentage difference in capacity against rated 6.5Ah

% Matthew Lintern 2014

clear all
clc

tic
fprintf('~ ~ ~ ~ Battery Charge/Discharge Test Data Processing ~ ~ ~ ~\n\n')

% Batch processing - Produce list of files to process
Filelist = dir('*.txt');
nooffiles = size(Filelist,1);

progrun = input('Please press any key to run programme or Ctrl+C to abort\n','s');
filenametext = input('Please enter the output filename (without extension): ','s');

results = [];
newresults = [];
reflist = [];

% figure

for x = 1:nooffiles

    % Get the file name
    infilename = Filelist(x).name;
    disp(['File to be processed: ' infilename])

    % Define data from file
    battdata = dlmread(infilename);

    % Define variables from input data array
    Ch1_V_dir = battdata(:,2);
    Ch1_I_EL = battdata(:,3);
    Ch1_I_PSU = battdata(:,5);

    Ch2_V_dir = battdata(:,12);
    Ch2_I_EL = battdata(:,13);
    Ch2_I_PSU = battdata(:,15);

    datadims = size(battdata);
    norows = datadims(1);

    % Smooth V data to remove high frequency accuracy fluctuations
    Ch1_V_dir_sm = smooth(Ch1_V_dir, 0.025, 'lowess');
    Ch2_V_dir_sm = smooth(Ch2_V_dir, 0.025, 'lowess');
```

```
    % Plot original voltage data and smoothed voltage data
    % Comment out lines below when processing large batches of files
    figure
    plot(Ch1_V_dir, 'k')
    hold on
    plot(Ch2_V_dir, 'g')
%     plot(Ch1_V_dir_sm, 'g')
%     plot(Ch2_V_dir_sm, 'r')
    hold off

    toc

    % Find max V points
    Ch1_Max_V_posn = find(Ch1_V_dir_sm == max(Ch1_V_dir_sm), 1);
    Ch2_Max_V_posn = find(Ch2_V_dir_sm == max(Ch2_V_dir_sm), 1);

    % Calculate total charge or discharge
    Ch1_I_EL_tot = 0;
    Ch1_I_PSU_tot = 0;
    Ch2_I_EL_tot = 0;
    Ch2_I_PSU_tot = 0;

    for n = 1:norows-10
        if battdata(n,1) < 0
            Ch1_I_EL_tot = Ch1_I_EL_tot + Ch1_I_EL(n);
        elseif battdata(n,1) > 0 && n <= Ch1_Max_V_posn
            Ch1_I_PSU_tot = Ch1_I_PSU_tot + Ch1_I_PSU(n);
        else
        end
        if battdata(n,11) < 0
            Ch2_I_EL_tot = Ch2_I_EL_tot + Ch2_I_EL(n);
        elseif battdata(n,11) > 0 && n <= Ch2_Max_V_posn
            Ch2_I_PSU_tot = Ch2_I_PSU_tot + Ch2_I_PSU(n);
        else
        end
    end

    Ch1_I_EL_tot = Ch1_I_EL_tot/10;
    Ch1_I_PSU_tot = Ch1_I_PSU_tot/10;
    Ch2_I_EL_tot = Ch2_I_EL_tot/10;
    Ch2_I_PSU_tot = Ch2_I_PSU_tot/10;

    % Calculate battery capacities and capacity difference from rated 6.5Ah
    Ch1_Cap = Ch1_I_EL_tot/3600;
    Ch1_Cap_chg = (-6.5+Ch1_Cap)/6.5;

    Ch2_Cap = Ch2_I_EL_tot/3600;
    Ch2_Cap_chg = (-6.5+Ch2_Cap)/6.5;

    % Produce filename reference
    fnamel = length(infilename);
    filenameref = [infilename(1:fnamel-4)];

    % Form new output results array
    newresults = [Ch1_I_EL_tot, Ch1_I_PSU_tot, Ch1_Cap, Ch1_Cap_chg, Ch2_I_EL_tot,↙
```

```
Ch2_I_PSU_tot, Ch2_Cap, Ch2_Cap_chg];

    % Add new results to results array
    results = [results; newresults]

    % Add file ref to ref list
    reflist = [reflist; filenameref]

end

% Produce output filenames
outfilename = [filenametext '.csv'];
outreffilename = [filenametext '_file_refs.csv'];

% Save files with results array, and ref list
csvwrite(['*File directory here*
*File directory here*' outfilename], results)
csvwrite(['*File directory here*
*File directory here*' outreffilename], reflist)

toc

fprintf('All data processing complete\n\n')

% ~~~~~~~~~~~~~~~~~~~~~~~~~~~ END ~~~~~~~~~~~~~~~~~~~~~~~~~~~
```

Appendix 8 – Security Real-World Driving Results Table

Month	Date from	Date to	No. of Days	Miles	Km	Fuel Added (l)	Fuel Cons. (MPG)	Fuel Cons. (l/100km)	CO2 Emissions (g/km)	Cumulative dist. (km)	Cumulative fuel added (l)	Cumulative fuel cons (l/100km)
1	09/04/2012	06/05/2012	28	1269	2042	152.98	37.71	7.49	173.91	2042.26	152.98	7.49
2	07/05/2012	01/06/2012	26	1585	2551	149.64	48.15	5.87	136.19	4593.07	302.62	6.59
3	02/06/2012	28/06/2012	19	754	1213	79.89	42.91	6.58	152.85	5806.51	382.51	6.59
4	29/06/2012	29/07/2012	31	1532	2466	163.21	42.67	6.62	153.68	8272.03	545.72	6.60
5	30/07/2012	01/09/2012	33	1654	2662	142.5	52.77	5.35	124.29	10933.88	688.22	6.29
6	02/09/2012	27/09/2012	23	1266	2037	133.41	43.14	6.55	152.02	12971.31	821.63	6.33
7	28/09/2012	21/10/2012	24	836	1345	114.8	33.11	8.53	198.10	14316.72	936.43	6.54
8	22/10/2012	19/11/2012	29	1128	1815	106.15	48.31	5.85	135.75	16132.06	1042.58	6.46
9	20/11/2012	22/12/2012	29	1306	2102	162.99	36.43	7.75	180.04	18233.87	1205.57	6.61
Overall	09/04/2012	22/12/2012	242	11330	18234	1205.57	42.72	6.61	153.50			

Appendix 9 – MATLAB Programme to Process Driving Data CSV Files, Version 2

```
% Script file to process the VT data files
%
% Functions include:
% - Round fluctuations in speed logged at nil speeds down to zero
% - Find GPS delayed start up & cut the following section of data out until
% the next stop

% Matthew Lintern 2014

% clc
clear all
close all

fprintf('~ ~ ~ ~ VT Data Processing ~ ~ ~ ~\n\n')

% Batch processing - Producing list of files to process
Filelist = dir('*.csv');
nooffiles = size(Filelist,1);

progrun = input('Please press Enter to run programme or Ctrl+C to abort\n','s');

tic

for m = 1:nooffiles

    % Get the file name
    infilename = Filelist(m).name;
    disp(['File to be processed: ' infilename])

    % Define data from file
    data = csvread(infilename);

    % Define data columns
    time = data(:,1);
    speed = data(:,2);

    speed_size = size(speed);
    rows1 = speed_size(1);

    % Replace speeds < 1 with 0
    for p = 1:rows1
        if speed(p)<1
            speed(p)=0;
        end
    end

    % Check first speed value is 0 and insert 0 if not
    if speed(1)~=0
        speed = [0;speed];
    else
    end

    % Check last speed value is 0 and insert 0 if not
    rows2 = length(speed);
    if speed(rows2)~=0
```

```
        speed = [speed;0];
    else
    end

    rows = length(speed);

    % Check for GPS jumps from cold start
    newspeed = [speed(1)];
    cuttrip = 0;     % Set counter for microtrip with a GPS jump at start to be cut↙
out

    for n = 2:rows
        accel = speed(n)-speed(n-1);
        if speed(n-1) == 0 && accel >= 20
            speed(n) = 999;
            cuttrip = cuttrip+1;
            while speed(n+cuttrip)> 0
                speed(n+cuttrip,:) = 999;   % To delete these rows later
                cuttrip = cuttrip+1;
            end
            cuttrip = 0;
        end
    end

    % Find speed=999 in speed data then delete these rows
    cutposns = find(speed==999);
    speed(cutposns) =[];

    % Form new array with modified speed data
    modspeed = speed;

    % Re-numbering time column and form new data array
    newspeedlength = length(modspeed);
    newtime = [0:newspeedlength-1]';
    newdata = [newtime, modspeed];

    % Smooth speed data and form new data array
    smoothedspeed = smooth(modspeed, 'lowess');
    newsmoothdata = [newtime, smoothedspeed];

    % Create output filename based on input filename
    fname1 = length(infilename);
    outfilename = [infilename(1:fname1-4) '_Processed.csv'];
    csvwrite(['*File directory here*↙
' outfilename], newdata)

    % Create smoothed output file filename
    smoothedoutfilename = [infilename(1:fname1-4) '_Processed_Smoothed.csv'];
    csvwrite(['*File directory here*↙
' smoothedoutfilename],↙
newsmoothdata)

    % Give message when data processing is complete
    fprintf(['Data processing complete for file ' infilename '\nThe output filenames↙
are: ' outfilename ' and ' smoothedoutfilename '\n\n'])

end

% Give message when all data processing is complete
fprintf('All data processing complete\n\n')

timetaken = toc

% ~~~~~~~~~~~~~~~~~~~~~~~~~~~ END ~~~~~~~~~~~~~~~~~~~~~~~~~~~
```

Appendix 10 – MATLAB Drive Cycle Statistics and Acceleration Distribution Programme

```
% Program to calculate drive cycle statistics
%
% Calculates:
% - Distance
% - Max speed
% - Average speed
% - No of accelerations
% - No of decelerations
% - Accelerations per km
% - Decelerations per km
% - Maximum acceleration
% - Maximum deceleration
% - Average acceleration
% - Average deceleration
%
% Produces an acceleration and deceleration magnitude distribution and per
% km distribution
%
% Code checks the speed ends with 2 lines of 0 (zero) and adds one if necessary
% Input data with speed in km/h
%
% Matthew Lintern 2014

% clc
clear all
close all

% Load a drive cycle data file
infilename = input('Please enter a CSV drive cycle data filename to load data from↙
(including extension): ','s');

% Define data from file
data = csvread(infilename);

time = data(:,1);
speedkmh = data(:,2);
speedkms = speedkmh./3600;  % Convert speed into km/s to calculate distance
dist = sum(speedkms);       % Calculate cycle distance in km

% Check speed value ends in two 0s and insert 0 at end if not
% (For later code to run correctly)
rows1 = length(speedkmh);
if speedkmh(rows1 -1)~=0
    speedkmh = [speedkmh;0];
    time = [time; rows1];
    fprintf(['Extra 0 speed line added to end' '\n\n'])
else
end

speed = speedkmh*1000/3600; % Convert speed to m/s

rows = length(speed);

ovrlaccelsarray =[];
ovrldecelsarray =[];
```

```
n = 2;
while n < rows
    if speed(n)> speed(n-1)                                % Check if accelerating
        accelarray = [speed(n-1)];                         % Form speed array of this↙
single accel period starting with first point value
        while speed(n)> speed(n-1) && n <= rows
            accelarray = [accelarray ; speed(n)];          % Form speed array of this↙
single accel period
            n = n+1;
        end
        ovrlaccel = (accelarray(length(accelarray)) - accelarray(1))/(length↙
(accelarray)-1);    % Calculates average accel of this period
        ovrlaccelsarray = [ovrlaccelsarray; ovrlaccel]; % Form array of all accels
        accelarray = [];                                   % Clear speed array of this↙
single accel period ready for next iteration

    elseif speed(n)< speed(n-1)                            % Check if decelerating
        decelarray = [speed(n-1)];                         % Form speed array of this↙
single decel period starting with first point value
        while speed(n)< speed(n-1) && n <= rows
            decelarray = [decelarray ; speed(n)];          % Form speed array of this↙
single decel period
            n = n+1;
        end
        ovrldecel = (decelarray(length(decelarray)) - decelarray(1))/(length↙
(decelarray)-1);    % Calculates average decel of this period
        ovrldecelsarray = [ovrldecelsarray; ovrldecel]; % Form array of all decels
        decelarray = [];                                   % Clear speed array of this↙
single decel period ready for next iteration
    else n = n+1;
    end
end

% disp(ovrlaccelsarray)
% disp(ovrldecelsarray)

% Count no of accels and decels in the cycle
noofaccels = length(ovrlaccelsarray);
noofdecels = length(ovrldecelsarray);
accelsperkm = noofaccels/dist;
decelsperkm = noofdecels/dist;

% Find the maximum accel and deccel
cyclemaxaccel = max(ovrlaccelsarray);
cyclemaxdecel = min(ovrldecelsarray);

% Calculate the overall average accel and decel
cycleavrgaccel = mean(ovrlaccelsarray);
cycleavrgdecel = mean(ovrldecelsarray);

% Calculate the cycle average speed
cycleavrgspeed = mean(speed);       % in m/s
cycleavrgspeedkmh = cycleavrgspeed*3600/1000;   % Convert to km/h
cyclemaxspeed = max(speed);         % in m/s
```

```
cyclemaxspeedkmh = cyclemaxspeed*3600/1000;     % Convert to km/h

% Cycle accel distribution
accelband1 = sum(ovrlaccelsarray < 0.25);
accelband2 = sum(ovrlaccelsarray >= 0.25 & ovrlaccelsarray < 0.5);
accelband3 = sum(ovrlaccelsarray >= 0.5 & ovrlaccelsarray < 0.75);
accelband4 = sum(ovrlaccelsarray >= 0.75 & ovrlaccelsarray < 1);
accelband5 = sum(ovrlaccelsarray >= 1 & ovrlaccelsarray < 1.5);
accelband6 = sum(ovrlaccelsarray >= 1.5 & ovrlaccelsarray < 2);
accelband7 = sum(ovrlaccelsarray >= 2 & ovrlaccelsarray < 2.5);
accelband8 = sum(ovrlaccelsarray >= 2.5 & ovrlaccelsarray < 3);
accelband9 = sum(ovrlaccelsarray >= 3 & ovrlaccelsarray < 3.5);
accelband10 = sum(ovrlaccelsarray >= 3.5);

% Form cycle acceleration distribution
acceldistribution = [accelband1 accelband2 accelband3 accelband4 accelband5↙
accelband6 accelband7 accelband8 accelband9 accelband10];
acceldistributionperkm = acceldistribution./dist;

% Cycle decel distribution
decelband1 = sum(ovrldecelsarray > -0.25);
decelband2 = sum(ovrldecelsarray <= -0.25 & ovrldecelsarray > -0.5);
decelband3 = sum(ovrldecelsarray <= -0.5 & ovrldecelsarray > -0.75);
decelband4 = sum(ovrldecelsarray <= -0.75 & ovrldecelsarray > -1);
decelband5 = sum(ovrldecelsarray <= -1 & ovrldecelsarray > -1.5);
decelband6 = sum(ovrldecelsarray <= -1.5 & ovrldecelsarray > -2);
decelband7 = sum(ovrldecelsarray <= -2 & ovrldecelsarray > -2.5);
decelband8 = sum(ovrldecelsarray <= -2.5 & ovrldecelsarray > -3);
decelband9 = sum(ovrldecelsarray <= -3 & ovrldecelsarray > -3.5);
decelband10 = sum(ovrldecelsarray <= -3.5);

% Form cycle deceleration distribution
deceldistribution = [decelband1 decelband2 decelband3 decelband4 decelband5↙
decelband6 decelband7 decelband8 decelband9 decelband10];
deceldistributionperkm = deceldistribution./dist;

% Give message & results when data processing is complete
fprintf(['Data processing complete for file ' infilename '\n\n'])

fprintf(['The cycle distance is: ' num2str(dist) ' km \n\n'])
fprintf(['The cycle maximum speed is: ' num2str(cyclemaxspeedkmh) ' km/h \n\n'])
fprintf(['The cycle average speed is: ' num2str(cycleavrgspeedkmh) ' km/h \n\n'])

fprintf(['The number of acceleration periods is: ' num2str(noofaccels) ' \n'])
fprintf(['The number of deceleration periods is: ' num2str(noofdecels) ' \n\n'])
fprintf(['The number of accelerations per km is: ' num2str(accelsperkm) ' \n'])
fprintf(['The number of decelerations per km is: ' num2str(decelsperkm) ' \n\n'])

fprintf(['The cycle maximum acceleration is: ' num2str(cyclemaxaccel) ' m/s^2 \n'])
fprintf(['The cycle maximum deceleration is: ' num2str(cyclemaxdecel) ' m/s^2 \n'])
fprintf(['The cycle average acceleration is: ' num2str(cycleavrgaccel) ' m/s^2 \n'])
fprintf(['The cycle average deceleration is: ' num2str(cycleavrgdecel) ' m/s^2 \n'])

fprintf(['The cycle acceleration distribution is: ' num2str(acceldistribution) '\n'])
fprintf(['The cycle deceleration distribution is: ' num2str(deceldistribution) '\n'])
```

```
fprintf(['The cycle acceleration distribution per km is: ' num2str↙
(acceldistributionperkm) '\n'])
fprintf(['The cycle deceleration distribution per km is: ' num2str↙
(deceldistributionperkm) '\n'])

% Form cycle stats array and accel & deccel combined array
cyclestats = [dist, cyclemaxspeedkmh, cycleavrgspeedkmh, noofaccels, noofdecels,↙
accelsperkm, decelsperkm, cyclemaxaccel, cyclemaxdecel, cycleavrgaccel,↙
cycleavrgdecel]';
acceldeceldistribution = [acceldistribution; deceldistribution;↙
acceldistributionperkm; deceldistributionperkm];

% Create output file for cycle stats based on input filename
fnamel = length(infilename);
% outcyclestatsfilename = 'processed_cycle_stats.csv'; %*Temp alternative to lines↙
below
outcyclestatsfilename = [infilename(1:fnamel-4) '_processed_cycle_stats.csv'];
csvwrite(['*File directory here*↙
*File directory here*' outcyclestatsfilename], cyclestats)

% Create output file for cycle accel/deccel distributions based on input filename
outacceldistsfilename = [infilename(1:fnamel-4) '_processed_accel_distributions.↙
csv'];
csvwrite(['*File directory here*↙
*File directory here*' outacceldistsfilename], acceldeceldistribution)


fprintf('All data processing complete\n\n')

% ~~~~~~~~~~~~~~~~~~~~~~~~~~~ END ~~~~~~~~~~~~~~~~~~~~~~~~~~~
```

Appendix 11 – MATLAB Temperature and Auxiliary Use Fuel Consumption Interpolation Programme

```
% Programme to interpolate between FC data points at various temperatures
% from literature for chosen input temperature
%
% Matthew Lintern 2014

% Change value of intemp below to get desired output
intemp = input('Enter a temperature in deg C to find corresponding FC: ');

temps = [-6.5 22 36.3]';
FC_cS = [6.3 3.6 5.8]';
FC_hS = [4.7 3.4 5.3]';

FC_cSresult = interp1(temps, FC_cS, intemp)
FC_hSresult = interp1(temps, FC_hS, intemp)
```